PH5001: Nuclear and Particle Physics

Lecture Notes

Nuclear Size · SEMF · Deuteron · Shell Model · Radioactivity

Course lectures: Prof. Bharat Kumar

Expanded notes compiled from Dunlap, Demtröder, Krane,
Petrera, Terranova, D'Auria, and primary literature

Preface

These notes follow the PH5001 lecture sequence of Prof. Bharat Kumar and expand each topic into a self-contained chapter suitable for a graduate or advanced undergraduate course. The pedagogical stance is deliberately intuition first, formalism second: every major formula is motivated by a physical question (how large is a nucleus? why is B/A nearly constant? why does K_α shift between isotopes?) before the algebra is developed in detail.

The treatment draws on several modern textbooks that treat the same material from complementary angles:

- **Dunlap** (2023) for nuclear size, Woods–Saxon parameters ($a = 0.52 \pm 0.01\,\mathrm{fm}$, $R_0 = 1.2\,A^{1/3}\,\mathrm{fm}$), and the semi-empirical mass formula with explicit coefficients;
- **Demtröder** (2023) for electron scattering, form factors, and multi-energy diffraction systematics;
- **Krane** (1988) for isotope shifts, classical nuclear structure, and the K_α data tradition;
- **Petrera** (2019) for worked problems (uniform-sphere form factors, radius estimates);
- **Terranova** (2021) and **D'Auria** (2018) for broader particle/nuclear context and shell-model connections.

Primary papers (Hofstadter, Weizsäcker, Moseley, Yukawa, Woods–Saxon) are cited where the historical origin of a result matters.

Figures are taken from the original lecture slides where available. Historical portraits are from Wikimedia Commons (see `figures/scientists/SOURCES.txt`).

The SEMF material (binding energy and term-by-term derivations) is collected in a single Lecture 4. Later lectures cover mass parabolas, neutron stars, the deuteron/NN force, nucleon scattering, meson exchange, the nuclear shell model, and radioactivity (α and β decay).

Contents

Chapter 1

Nuclear Size and Charge

"Like the radius of an atom, the radius of a nucleus is not a precisely defined quantity."
K. S. Krane

1.1 Posing the problem: how big is a nucleus?

Nuclei are not hard spheres with sharp edges. The density of nucleons and the nuclear potential are relatively constant over short distances and then drop rapidly toward zero. It is therefore natural to characterise the nuclear shape with two parameters: a **mean radius**, where the density is half its central value, and a **skin thickness**, over which the density falls from near its maximum to near zero. A third parameter is needed later for nuclei that are not spherical [6].

A further subtlety is that the radius one measures depends on the experiment. Electromagnetic probes (electron scattering, muonic X rays, optical and X-ray isotope shifts) determine the distribution of *nuclear charge*, mainly the protons. Hadronic probes (α scattering, pionic atoms) determine the distribution of *nuclear matter*, all nucleons. The two distributions are similar but not identical, especially in heavy nuclei with neutron skins [6, 1].

The nuclear size scale is the femtometre (fermi),

$$1\,\mathrm{fm} = 10^{-15}\,\mathrm{m} = 10^{-13}\,\mathrm{cm}. \tag{1.1}$$

Empirically, charge radii satisfy

$$R \simeq r_0\,A^{1/3}, \qquad r_0 \approx 1.2\text{–}1.25\,\mathrm{fm}, \tag{1.2}$$

from electron scattering. That $A^{1/3}$ law is the geometric face of nearly constant central density: if $A/(\frac{4}{3}\pi R^3)$ is roughly constant, then $R \propto A^{1/3}$.

Definition

The constant r_0 depends on the surface definition. Common conventions give

$$r_0 \approx \begin{cases} 1.2 - -1.25\,\mathrm{fm} & \text{(charge / equivalent hard sphere)}, \\ 1.3 - -1.4\,\mathrm{fm} & \text{(strong interaction / } \alpha \text{ scattering)}. \end{cases}$$

Throughout this chapter, $r_0 \approx 1.2\,\text{fm}$ is used for charge radii unless stated otherwise.

Key idea

Wavelength criterion. To resolve a feature of size ℓ, a probe needs $\lambda \lesssim \ell$. For $\ell \sim 10\,\text{fm}$ one needs $p \gtrsim 100\,\text{MeV}/c$. High-energy electron beams (100 MeV–1 GeV) provide exactly that [6].

Before writing a single scattering amplitude, it helps to recall why ordinary light cannot answer the size question.

1.1.1 A classroom analogy: chalk and wavelengths

Imagine a stick of chalk, a few centimetres long (Figure 1.1). With the naked eye (that is, with visible light), one can estimate its diameter without effort. Sound waves of ordinary frequencies cannot do the same job. Both light and sound are waves; the difference is their wavelength relative to the object being examined.

Figure 1.1: Everyday chalk sticks. Visible light (400–700 nm) has a wavelength far smaller than the diameter of the chalk, so the eye can resolve its size. Audible sound does not.

Visible light spans roughly 400–700 nm, four to seven orders of magnitude smaller than a centimetre-scale object. Audible sound, by contrast, lives in a very different regime. The wavelength of a wave of speed v and frequency ν is

$$\lambda = \frac{v}{\nu}. \tag{1.3}$$

Taking $v \approx 340\,\text{m/s}$ for air and $\nu = 1\,\text{kHz}$ as a representative audible tone, one finds $\lambda \approx 0.34\,\text{m}$—about thirty times larger than the chalk. A wave that long cannot "see" structure on the scale of a centimetre; it simply diffracts around the obstacle as if the obstacle were a point.

Key idea

To resolve a feature of size ℓ, a probe needs wavelength $\lambda \lesssim \ell$. Visible light works for chalk because $\lambda_{\text{light}} \ll \ell_{\text{chalk}}$. Audible sound fails because $\lambda_{\text{sound}} \gg \ell_{\text{chalk}}$. The same criterion decides whether electrons can resolve a nucleus.

The same logic, applied to the nucleus, is unforgiving. Early estimates from α-particle scattering already indicated nuclear radii of order a few fermis (10^{-15}–$10^{-14}\,\text{m}$). Visible light ($\lambda \sim 10^{-7}\,\text{m}$) is hopelessly coarse. Even hard γ-rays fall short of the needed resolution. One needs

a probe whose de Broglie wavelength is itself of nuclear size (a few fermis or less). High-energy electrons provide precisely that.

Remark

Electrons are preferred over protons or α particles for precision *charge*-density work because the electron–nucleus interaction is electromagnetic and calculable to high accuracy. Strong-interaction probes, while useful for hadronic form factors and neutron distributions, introduce model dependence that electron scattering largely avoids [2, 7]. Mass and charge radii need not agree at the percent level: Coulomb repulsion tends to push protons slightly farther out than neutrons in heavy nuclei.

1.2 Historical path: from Rutherford to Hofstadter

1.2.1 Rutherford scattering and a first radius

Historical note: Ernest Rutherford (1871–1937)

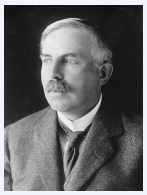

Ernest Rutherford was born in Brightwater, New Zealand, and trained at Canterbury College before moving to the Cavendish Laboratory under J. J. Thomson. After work on radioactivity in Montreal (where he classified α, β, and γ radiation and, with Soddy, formulated radioactive transformation), he took the chair at Manchester in 1907. There, with **Hans Geiger** and **Ernest Marsden**, he directed the α-particle scattering experiments that overthrew the Thomson "plum pudding" atom. In 1911 he proposed that essentially all the atomic mass and positive charge sit in a minute central *nucleus*, with electrons in the surrounding volume. He received the 1908 Nobel Prize in Chemistry for investigations into the disintegration of the elements and the chemistry of radioactive substances, ironically awarded just as his nuclear atom was taking shape. Later, at the Cavendish, he directed the laboratory in which Chadwick discovered the neutron (1932). Rutherford remains the founding figure of nuclear physics: every scattering formula in this chapter descends, conceptually, from his 1911 insight.

Rutherford's analysis of α-particle scattering established that the positive charge of the atom is concentrated in a tiny central nucleus. As long as the projectile remains outside the range of the nuclear force and samples only the Coulomb field of a point charge Ze, the classical differential cross section is

$$\left(\frac{\mathrm{d}\sigma}{\mathrm{d}\Omega}\right)_{\mathrm{R}} = \left(\frac{Z_1 Z_2 e^2}{8\pi\varepsilon_0\, m v_0^2}\right)^2 \frac{1}{\sin^4(\theta/2)} = \left(\frac{Z_1 Z_2 e^2}{16\pi\varepsilon_0\, E}\right)^2 \frac{1}{\sin^4(\theta/2)}. \tag{1.4}$$

The distance of closest approach for a head-on collision is

$$d_0 = \frac{Z_1 Z_2 e^2}{4\pi\varepsilon_0\, E}, \tag{1.5}$$

and for a general impact parameter the periapsis d and scattering angle are related by

$$d = \frac{d_0}{2}\left(1 + \frac{1}{\sin(\theta/2)}\right). \tag{1.6}$$

When d becomes smaller than a critical value d_N, the measured angular distribution begins

to deviate from Equation (1.4). That deviation has two physical origins: (i) the finite spatial extent of the nuclear charge (only charge inside radius d contributes fully to the deflection), and (ii) the onset of the short-range strong interaction.

Historical note: James Chadwick (1891–1974)

Sir James Chadwick studied under Rutherford at Manchester and later worked with Hans Geiger in Berlin before internment in Germany during World War I. Returning to Cambridge, he became Rutherford's close collaborator at the Cavendish. In 1920 he systematically analysed α-particle scattering from a range of targets and helped establish that nuclear radii scale roughly as $A^{1/3}$, the first quantitative size law for nuclei. His lasting fame, however, comes from 1932: interpreting the penetrating radiation that Bothe, Becker, Joliot and Curie had attributed to hard γ-rays, Chadwick showed that it consisted of neutral particles of roughly proton mass: the *neutron*. That discovery completed the proton–neutron picture of the nucleus and earned him the 1935 Nobel Prize in Physics. Without the neutron, the charge densities we extract from electron scattering could not be converted into nucleon densities via A/Z.

Chadwick and later workers analysed such deviations for a series of targets and established the empirical law

$$R_N \simeq r_0\, A^{1/3}, \tag{1.7}$$

with $r_0 \sim 1.3\,\mathrm{fm}$ from α scattering, slightly larger than the electromagnetic value, as expected when the strong force sets the scale [2].

Caution

As θ increases on $(0, \pi)$, $\sin(\theta/2)$ *increases*, so $\csc(\theta/2)$ *decreases*. The Rutherford cross section therefore falls with angle because of $1/\sin^4(\theta/2)$, not because $\sin(\theta/2)$ shrinks. A common slip in lecture notes reverses this statement.

1.2.2 Why electrons?

α particles and protons feel the poorly known nuclear force as soon as they penetrate the surface. Electrons do not: they couple only through the electromagnetic interaction, which is known to exquisite accuracy. High-energy electron scattering, pioneered by Robert Hofstadter and collaborators at Stanford in the 1950s, therefore became the definitive probe of nuclear charge distributions [7, 8, 2].

Historical note: Robert Hofstadter (1915–1990)

Robert Hofstadter was born in New York City and earned his Ph.D. at Princeton (1938) under Louis Ridenour and others, working on photoconductivity and infrared detectors. After wartime radar research and a period at Princeton, he joined Stanford University in 1950 as Associate Professor. There he seized the opportunity offered by the newly available high-energy electron beams from the Stanford linear accelerator (Mark III and related machines). From about 1953 onward, elastic and inelastic electron scattering became his principal research programme.

Directing a high-energy electron beam onto thin targets and measuring the angular distribution of scattered electrons, Hofstadter's group mapped the *charge form factors* of nuclei from light systems (carbon, oxygen) to heavy ones (gold, bismuth), and then of the proton and neutron themselves. The data revealed that nuclei have a roughly constant central density and a diffuse surface (the empirical basis of the Woods–Saxon profile), and that the proton is not a point particle but an extended object of rms radius $\sim 0.8\,\mathrm{fm}$. The term *fermi* (fm) for $10^{-15}\,\mathrm{m}$ entered common use in this community; Hofstadter himself used it in his 1961 Nobel lecture, "The electron-scattering method and its application to the structure of nuclei and nucleons" (11 December 1961).

He shared the 1961 Nobel Prize in Physics with Rudolf Mössbauer: Hofstadter "for his pioneering studies of electron scattering in atomic nuclei and for his consequent discoveries concerning the structure of nucleons." He remained at Stanford for the rest of his career, was elected to the U.S. National Academy of Sciences (1958), and later received the National Medal of Science (1986). The oxygen data we discuss below (Phys. Rev. **113**, 666, 1959, with Ehrenberg, Meyer-Berkhout, Ravenhall and Sobottka) are a canonical product of that Stanford programme [7, 8].

1.3 The de Broglie condition and the energies required

Historical note: Louis de Broglie (1892–1987)

Prince Louis-Victor de Broglie, of the French noble house of Broglie, was trained first in history before turning to theoretical physics under his brother Maurice and later Paul Langevin. In his 1924 doctoral thesis at the Sorbonne, he proposed that every material particle of momentum p is associated with a wave of wavelength $\lambda = h/p$, extending Einstein's wave–particle duality of light to matter. The idea seemed speculative until Davisson and Germer (1927), and independently G. P. Thomson, observed electron diffraction by crystals, confirming the de Broglie relation experimentally.

De Broglie received the 1929 Nobel Prize in Physics for the discovery of the wave nature of electrons. His relation is the conceptual starting point of this chapter: only when λ_{dB} is of nuclear size (a few fm) can an electron beam resolve the charge distribution inside a nucleus. High-energy electron accelerators are, in that sense, machines built to make de Broglie's wavelength short enough.

Quantum mechanics equips every particle of momentum p with a wavelength

$$\lambda = \frac{h}{p} = \frac{2\pi\hbar}{p} \equiv \lambda_{\mathrm{dB}}. \tag{1.8}$$

Large momentum means short wavelength. For electrons accelerated to kinetic energies well above their rest energy, the kinematics become ultra-relativistic, and the connection between energy and wavelength is especially simple.

1.3.1 Relativistic kinematics

The total energy E of an electron of rest mass m_e and momentum p is

$$E = \sqrt{p^2c^2 + m_e^2c^4}. \tag{1.9}$$

The kinetic energy controlled by the accelerator is the excess over rest energy:

$$K = E - m_ec^2 = \sqrt{p^2c^2 + m_e^2c^4} - m_ec^2. \tag{1.10}$$

Caution

The rest energy is $m_ec^2 \approx 511\,\mathrm{keV}$, *not* $m_e^2c^2$. The latter does not even have the dimension of energy. Always write $K = E - m_ec^2$.

For electrons, once $K \gg m_ec^2$—true already at a few tens of MeV—the rest mass may be neglected and

$$E \approx K \approx pc. \tag{1.11}$$

The de Broglie wavelength then collapses to

$$\lambda \approx \frac{hc}{E} = \frac{2\pi\,\hbar c}{E}. \tag{1.12}$$

In nuclear units the conversion constants

$$hc \approx 1240\,\mathrm{MeV\cdot fm}, \qquad \hbar c \approx 197.3\,\mathrm{MeV\cdot fm} \tag{1.13}$$

are indispensable. Thus, to resolve structure on the scale of $10\,\mathrm{fm}$,

$$E \approx \frac{1240\,\mathrm{MeV\cdot fm}}{10\,\mathrm{fm}} = 124\,\mathrm{MeV}. \tag{1.14}$$

Example: electrons at $500\,\mathrm{MeV}$

For $E = 500\,\mathrm{MeV}$ one has $\lambda_{\mathrm{dB}} \approx 0.4\,\mathrm{fm}$, already small compared with the diameter of a heavy nucleus [2]. Using Equation (1.12),

$$\lambda \approx \frac{1240\,\mathrm{MeV\cdot fm}}{500\,\mathrm{MeV}} = 2.5\,\mathrm{fm}$$

for the combination hc/E; the precise numerical factor depends on whether one quotes $\lambda = h/p$ or $\lambda = \hbar/p = hc/(2\pi E)$. What matters is the order of magnitude: hundreds of MeV put λ in the few-fermi range.

Key idea

To probe a length scale ℓ, choose $E \gtrsim hc/\ell$. For $\ell \sim 1\,\mathrm{fm}$ one needs $E \sim 1\,\mathrm{GeV}$. Modern facilities (Jefferson Lab, MAMI, formerly SLAC) operate comfortably in this regime.

1.4 Elastic electron scattering: the oxygen example

A classic data set is the elastic scattering of 420 MeV electrons from oxygen, shown in Figure 1.2 [8, 7].

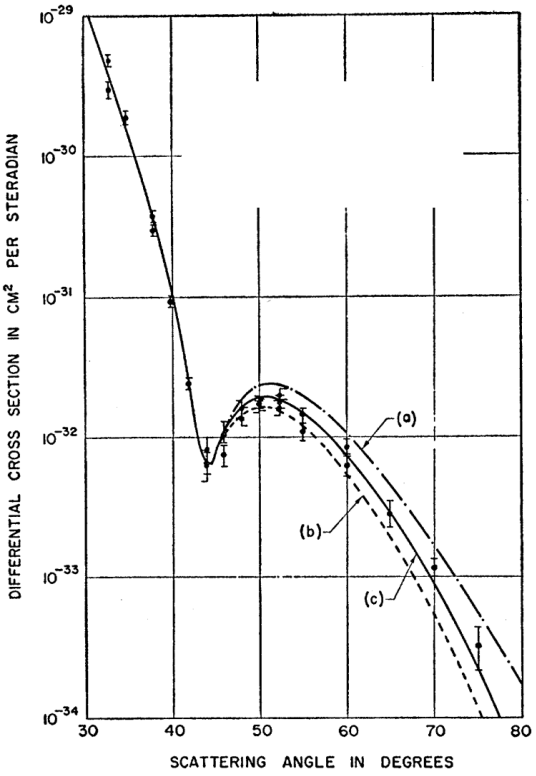

Figure 1.2: Differential cross section for elastic electron scattering from oxygen at 420 MeV, compared with harmonic-well charge distributions (a)–(c). The data display a clear diffraction minimum near 43°–44°. From Phys. Rev. **113**, 666 (1959).

What does one actually measure? A beam of monoenergetic electrons strikes a thin target. Detectors placed at laboratory angle θ count the scattered electrons. The observable is the differential cross section $\mathrm{d}\sigma/\mathrm{d}\Omega$, proportional to the number of electrons scattered into a solid angle $\mathrm{d}\Omega$ about θ.

Two features of Figure 1.2 are immediate.

1. **Overall fall-off.** The cross section drops by several orders of magnitude as θ increases from $\sim 30^\circ$ to $\sim 80^\circ$.

2. **Diffraction structure.** Superimposed on the fall-off is a deep minimum near 43°–44°, followed by a secondary maximum and a further decline.

The first feature is the relativistic generalisation of Rutherford scattering (Mott scattering for Dirac electrons). The second is the fingerprint of a finite nuclear size: diffraction of the electron wave by an extended charge distribution. Before developing that analogy, two experimental points deserve emphasis.

1.4.1 Selecting nuclear, not electronic, scattering

An oxygen target contains both a nucleus and eight atomic electrons. An incident electron can scatter from either. Scattering from an atomic electron transfers a large fraction of the beam energy (comparable masses in a nearly elastic collision), so the scattered electron emerges with substantially reduced energy. Scattering from the much heavier nucleus is essentially elastic: the recoiling nucleus takes little kinetic energy, and the scattered electron retains nearly its full beam energy.

Remark

In the laboratory one therefore applies an energy cut, retaining only events with $E' \approx E_{\text{beam}}$. That cut isolates elastic *nuclear* scattering and rejects the electron–electron background. The data of Figure 1.2 are of this elastic character.

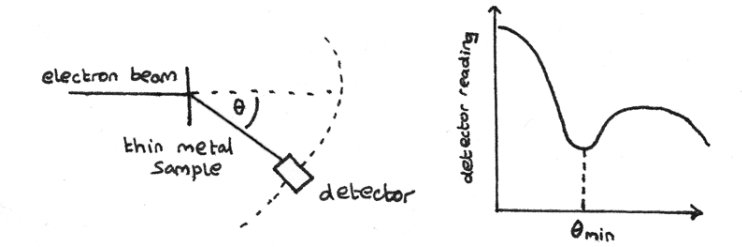

Figure 1.3: Left: schematic of an electron beam scattering from a thin sample into a detector at angle θ. Right: qualitative angular dependence of the detector reading, with a diffraction minimum at $\theta_{\min}$.

Even the Rutherford formula is not quantitatively applicable at 420 MeV. Electrons are ultra-relativistic ($E/m_e c^2 \sim 800$), so the proper point-charge baseline is the *Mott* cross section, the Dirac generalisation of Rutherford scattering. Finite nuclear size then multiplies the Mott result by the square of a form factor (Section 1.6).

Historical note: Nevill F. Mott (1905–1996)

Sir Nevill Francis Mott was one of the leading theoretical physicists of the twentieth century. Educated at Clifton College and St John's College, Cambridge, he worked in Copenhagen and Göttingen in the early years of quantum mechanics before returning to the United Kingdom. In 1929–1930, applying Dirac's relativistic theory of the electron to Coulomb scattering, he derived the cross section for a point charge that now bears his name: the *Mott formula*. It reduces to Rutherford scattering in the non-relativistic limit, but at high energy it includes spin and relativistic kinematics and becomes the natural baseline for electron–nucleus experiments.

Mott's career ranged far beyond nuclear scattering: he made foundational contributions to solid-state physics (metal–insulator transitions, the Mott insulator), shared the 1977 Nobel Prize in Physics with P. W. Anderson and J. H. Van Vleck for electronic structure of magnetic and disordered systems, and served as Cavendish Professor at Cambridge. In the present chapter, whenever we write $(\mathrm{d}\sigma/\mathrm{d}\Omega)_{\text{Mott}}$, we are using the point-charge Dirac result he obtained almost a century ago, the yardstick against which finite-size form factors are measured.

1.5 Diffraction analogy and a first estimate of the nuclear size

The diffraction minimum in Figure 1.2 is the nuclear counterpart of a familiar optical effect. Consider monochromatic, coherent light of wavelength λ incident on a single slit of width b (Figure 1.4). On a distant screen the intensity is

$$I(\theta) = I_0 \left(\frac{\sin \beta}{\beta} \right)^2, \qquad \beta = \frac{\pi b \sin \theta}{\lambda}. \tag{1.15}$$

The intensity vanishes whenever $\beta = m\pi$ for nonzero integer m, i.e. whenever

$$b \sin \theta = m\lambda, \qquad m = \pm 1, \pm 2, \ldots \tag{1.16}$$

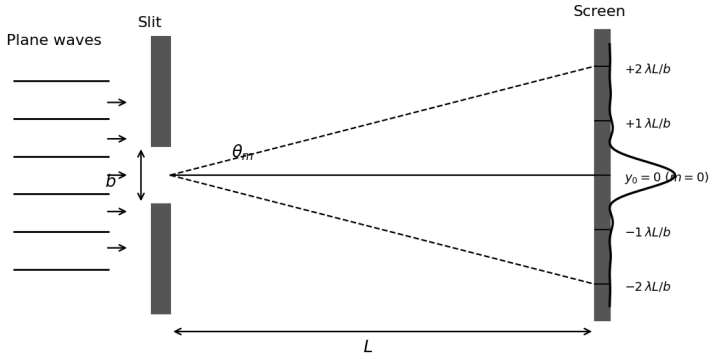

Figure 1.4: Geometry of single-slit diffraction. Plane waves of wavelength λ pass through a slit of width b and form an interference pattern on a distant screen ($L \gg b$). Intensity minima occur near $y_m = m\,\lambda L/b$ for integer $m \neq 0$.

For a *circular* aperture of diameter D, the first dark ring of the Airy pattern sits at

$$\sin \theta = \frac{1.22\,\lambda}{D}. \tag{1.17}$$

Treating the nucleus, very roughly, as a circular obstacle of diameter D, one may invert Equation (1.17) to estimate D from the observed diffraction minimum. Equivalently, the first minimum is often written condition as $\theta_{\min} \approx \lambda_{\mathrm{dB}}/D$ (in radians, for small angles), corresponding to a path difference of half a wavelength between opposite edges of the charge distribution [2].

Example: oxygen at 420 MeV

At $E = 420\,\mathrm{MeV}$,

$$\lambda \approx \frac{hc}{E} \approx \frac{1240\,\mathrm{MeV \cdot fm}}{420\,\mathrm{MeV}} \approx 3.0\,\mathrm{fm}.$$

The first minimum in the oxygen data lies near $\theta \approx 45^\circ$. Equation (1.17) then yields

$$D = \frac{1.22\,\lambda}{\sin\theta} \approx \frac{1.22 \times 3.0\,\mathrm{fm}}{\sin 45^\circ} = \frac{1.22 \times 3.0\,\mathrm{fm}}{1/\sqrt{2}} \approx 5.2\,\mathrm{fm}.$$

The corresponding radius, $R = D/2 \approx 2.6\,\mathrm{fm}$, is a respectable first estimate for ^{16}O. The empirical rule $R \approx 1.2\,\mathrm{fm}\,A^{1/3}$ with $A = 16$ gives $R \approx 3.0\,\mathrm{fm}$—the same order of magnitude.

Remark

This optical analogy is intentionally crude. The nucleus is not a hard disk with a sharp edge; the electron is a charged Dirac particle, not a scalar optical wave; and the Coulomb field extends beyond the nuclear surface. A proper treatment replaces the slit formula by a Fourier transform of the charge density (the form factor). The estimate nonetheless shows that the angular location of the first diffraction minimum is a direct ruler for the nuclear size. As the beam energy rises, λ falls and the first minimum moves to smaller angles [2], exactly as seen in multi-energy data for gold and other targets.

Why is only one minimum visible in the oxygen data? For a second minimum one would need $b \sin\theta = 2\lambda$, or $\sin\theta = 2\lambda/D$. With $D \approx 5.2\,\text{fm}$ and $\lambda \approx 3\,\text{fm}$ that ratio exceeds unity: no real angle exists. Heavier nuclei (larger D) or higher beam energies (smaller λ) push λ/D down and bring additional diffraction minima into the physical domain. Lead or gold at hundreds of MeV to GeV energies display a rich oscillatory pattern; the number of observed minima tracks the zeros of the form factor of a uniform sphere [3].

1.6 From diffraction to charge density: the form factor

Electron scattering can do more than estimate a single radius. Because the interaction is electromagnetic and weak compared with the nuclear binding scale (at moderate momentum transfers), the Born approximation is an excellent starting point for light nuclei. The scattering amplitude then becomes proportional to the Fourier transform of the nuclear charge density: the *charge form factor*.

1.6.1 Plane-wave Born picture

Write the initial and final electron waves as plane waves (Coulomb distortion is discussed below):

$$\psi_i(\boldsymbol{r}) = e^{i\boldsymbol{k}\cdot\boldsymbol{r}}, \qquad \psi_f(\boldsymbol{r}) = e^{i\boldsymbol{k}'\cdot\boldsymbol{r}}. \tag{1.18}$$

For elastic scattering $|\boldsymbol{k}| = |\boldsymbol{k}'| \equiv k$; only the direction changes. The three-momentum transfer is $\boldsymbol{q} = \boldsymbol{k} - \boldsymbol{k}'$. Squaring,

$$\begin{aligned} q^2 &= |\boldsymbol{k} - \boldsymbol{k}'|^2 = k^2 + k^2 - 2\boldsymbol{k}\cdot\boldsymbol{k}' = 2k^2(1 - \cos\theta) \\ &= 4k^2 \sin^2(\theta/2), \end{aligned} \tag{1.19}$$

where the last step uses the half-angle identity $1 - \cos\theta = 2\sin^2(\theta/2)$. Therefore

$$\boldsymbol{q} = \boldsymbol{k} - \boldsymbol{k}', \qquad q = |\boldsymbol{q}| = 2k\sin(\theta/2) \tag{1.20}$$

in the ultra-relativistic limit ($E \approx pc = \hbar c\, k$). In the literature one also meets $\Delta p = \hbar\Delta k = |\boldsymbol{p} - \boldsymbol{p}'|$; we use q for the magnitude of the three-momentum transfer.

The electron couples to the nuclear charge density $\rho(\boldsymbol{r}')$ through the Coulomb interaction.

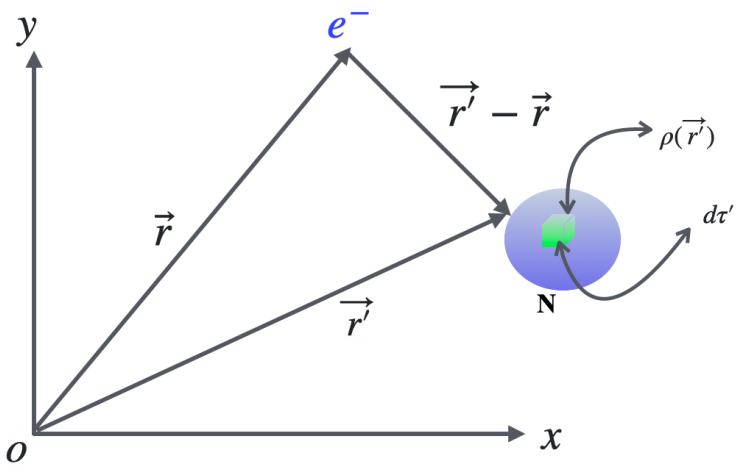

Figure 1.5: Geometry of the Coulomb interaction. An electron at $\boldsymbol{r}$ interacts with a nuclear charge element $\rho(\boldsymbol{r}')\,\mathrm{d}\tau'$ at $\boldsymbol{r}'$. The relative vector is $\boldsymbol{r}' - \boldsymbol{r}$; $\mathrm{d}\tau'$ is a nuclear volume element.

The perturbation may be written

$$H' = \int \rho(\boldsymbol{r}')\,\frac{-e}{4\pi\varepsilon_0\,|\boldsymbol{r}-\boldsymbol{r}'|}\,\mathrm{d}\tau'. \tag{1.21}$$

In first-order perturbation theory the transition amplitude is

$$\mathcal{M}_{fi} = \int \psi_f^*(\boldsymbol{r})\,H'\,\psi_i(\boldsymbol{r})\,\mathrm{d}\tau. \tag{1.22}$$

Substitute the plane waves and (1.21):

$$\begin{aligned}\mathcal{M}_{fi} &= \int \mathrm{d}\tau\, e^{-i\boldsymbol{k}'\cdot\boldsymbol{r}}\left[\int \mathrm{d}\tau'\,\rho(\boldsymbol{r}')\,\frac{-e}{4\pi\varepsilon_0\,|\boldsymbol{r}-\boldsymbol{r}'|}\right] e^{i\boldsymbol{k}\cdot\boldsymbol{r}} \\ &= \int \mathrm{d}\tau'\,\rho(\boldsymbol{r}')\left[\int \mathrm{d}\tau\,\frac{-e}{4\pi\varepsilon_0\,|\boldsymbol{r}-\boldsymbol{r}'|}\,e^{i\boldsymbol{q}\cdot\boldsymbol{r}}\right],\end{aligned} \tag{1.23}$$

with $\boldsymbol{q} = \boldsymbol{k} - \boldsymbol{k}'$. The inner integral is the Fourier transform of the Coulomb kernel. Shifting $\boldsymbol{s} = \boldsymbol{r} - \boldsymbol{r}'$ shows that it equals

$$e^{i\boldsymbol{q}\cdot\boldsymbol{r}'}\int \frac{-e}{4\pi\varepsilon_0\,s}\,e^{i\boldsymbol{q}\cdot\boldsymbol{s}}\,\mathrm{d}^3 s = e^{i\boldsymbol{q}\cdot\boldsymbol{r}'}\left(\frac{-e}{\varepsilon_0\,q^2}\right)$$

(in the convention where $\int e^{i\boldsymbol{q}\cdot\boldsymbol{s}}/s\,\mathrm{d}^3 s = 4\pi/q^2$). Thus

$$\mathcal{M}_{fi} = \underbrace{\left(-\frac{e}{\varepsilon_0\,q^2}\right)}_{\text{point Coulomb / Mott kinematics}} \int \rho(\boldsymbol{r}')\,e^{i\boldsymbol{q}\cdot\boldsymbol{r}'}\,\mathrm{d}\tau'. \tag{1.24}$$

The amplitude therefore factorises into a known kinematic piece times the Fourier transform of the charge density.

Definition: charge form factor

$$F(\boldsymbol{q}) = \frac{1}{Ze}\int \rho(\boldsymbol{r}')\, e^{i\boldsymbol{q}\cdot\boldsymbol{r}'}\,\mathrm{d}\tau', \qquad F(0) = 1. \tag{1.25}$$

For a spherical ground state $\rho = \rho(r)$ only, choose the polar axis along $\boldsymbol{q}$ so that $\boldsymbol{q}\cdot\boldsymbol{r}' = qr\cos\theta'$. Then

$$\begin{aligned} F(q) &= \frac{1}{Ze}\int_0^\infty \rho(r)\, r^2\,\mathrm{d}r \int_0^{2\pi}\mathrm{d}\phi' \int_{-1}^{1}\mathrm{d}(\cos\theta')\, e^{iqr\cos\theta'} \\ &= \frac{4\pi}{Ze}\int_0^\infty \rho(r)\,\frac{\sin(qr)}{qr}\, r^2\,\mathrm{d}r, \end{aligned} \tag{1.26}$$

because $\int_{-1}^{1} e^{ix\cos\theta}\,\mathrm{d}(\cos\theta) = 2\sin x/x$. Equivalently, writing the Fourier transform of a normalised charge density [2],

$$F(\Delta k) = \int \rho_e(\boldsymbol{r})\, e^{i\Delta k\cdot r}\,\mathrm{d}^3 r$$

(up to normalisation by the total charge Ze).

The measured cross section factors as

$$\frac{\mathrm{d}\sigma}{\mathrm{d}\Omega} = \left(\frac{\mathrm{d}\sigma}{\mathrm{d}\Omega}\right)_{\text{point}} |F(q)|^2, \tag{1.27}$$

where the point-charge baseline is the Rutherford (non-relativistic) or Mott (relativistic Dirac) formula. All information about the spatial distribution of charge resides in $F(q)$. The momentum transfer that enters the Fourier phase has magnitude

$$q = |\boldsymbol{q}| = 2p\sin(\theta/2) \tag{1.28}$$

for elastic scattering at beam momentum p [1].

Caution

The form factor is defined as the ratio of the full scattering amplitude to the point-charge (Rutherford/Mott) amplitude, so that the Coulomb $1/q^2$ factors cancel by construction [6, 1]. Do not confuse $F(q)$ with the full Born amplitude, which still contains the photon propagator. Also keep the matrix-element convention consistent: $\mathcal{M}_{fi} = \langle f|H'|i\rangle$ with the final wave conjugated, and a fixed sign for $\boldsymbol{q} = \boldsymbol{k} - \boldsymbol{k}'$.

Key idea

Measuring $\mathrm{d}\sigma/\mathrm{d}\Omega$ as a function of angle (hence of q) determines $|F(q)|$. One may then either (i) extract $\rho(r)$ by a model-independent numerical inversion, or (ii) assume a parametric Woods–Saxon shape and fit its parameters to the data [1]. Both routes are used in practice; the parametric form is convenient for nuclear-model calculations.

Example: uniform sphere

For a uniform charge distribution of radius R_A,

$$\rho(r) = \begin{cases} \dfrac{Ze}{\frac{4}{3}\pi R_A^3}, & r \le R_A, \\ 0, & r > R_A. \end{cases}$$

Equation (1.26) becomes

$$F(q) = \frac{4\pi}{Ze}\,\frac{Ze}{\frac{4}{3}\pi R_A^3}\int_0^{R_A}\frac{\sin(qr)}{qr}\,r^2\,\mathrm{d}r = \frac{3}{R_A^3}\int_0^{R_A} r^2\,\frac{\sin(qr)}{qr}\,\mathrm{d}r. \tag{1.29}$$

Integrate by parts (or use $j_1(x) = \sin x/x^2 - \cos x/x$) with $x = qR_A$:

$$F(q) = \frac{3}{(qR_A)^3}\left[\sin(qR_A) - qR_A\cos(qR_A)\right] = \frac{3j_1(qR_A)}{qR_A}. \tag{1.30}$$

The zeros of j_1 fix the diffraction minima. The first zero of $j_1(x) = 0$ solves $\tan x = x$ and lies at $x \approx 4.493$, so $q_1 R_A \approx 4.49$; counting zeros at fixed energy is a quick estimate of R_A [3].

For any spherical density the small-q expansion follows from $\sin(qr)/(qr) = 1 - (qr)^2/6 + \cdots$:

$$\begin{aligned} F(q) &= \frac{4\pi}{Ze}\int_0^\infty \rho(r)\left(1 - \frac{q^2r^2}{6} + \cdots\right)r^2\,\mathrm{d}r \\ &= 1 - \frac{q^2}{6}\langle r^2\rangle + \cdots, \end{aligned} \tag{1.31}$$

where $\langle r^2\rangle = (1/Ze)\int \rho(r)\,r^2\,\mathrm{d}^3r$. Thus the slope of $F(q)$ at the origin determines the rms charge radius without assuming a full density model. For the uniform sphere, $\langle r^2\rangle = \frac{3}{5}R_A^2$.

Coulomb distortion and heavy nuclei

At low energy, or for heavy nuclei ($Z\alpha$ not small), plane waves are a poor description of the electron in the nuclear Coulomb field. One then solves the Dirac equation in the electrostatic potential of a trial $\rho(r)$ (phase-shift / distorted-wave analysis) and adjusts ρ until the calculated cross section matches experiment. The qualitative content of Equation (1.27) survives; quantitative extractions for ^{208}Pb or ^{197}Au require this treatment [2].

1.7 Empirical charge densities: the Woods–Saxon profile

Once form-factor data are inverted, a remarkably simple picture emerges. Figure 1.6 shows proton (charge) densities for three representative nuclei: ^{16}O, ^{118}Sn, and ^{197}Au. Hofstadter's classic compilation for a broader range of nuclei (H through Bi) shows the same pattern [2]: a flat interior and a diffuse surface.

Several features are universal enough to deserve names.

1. **A flat interior.** From the centre out to a few fermis, $\rho_p(r)$ is roughly constant. Nuclei are

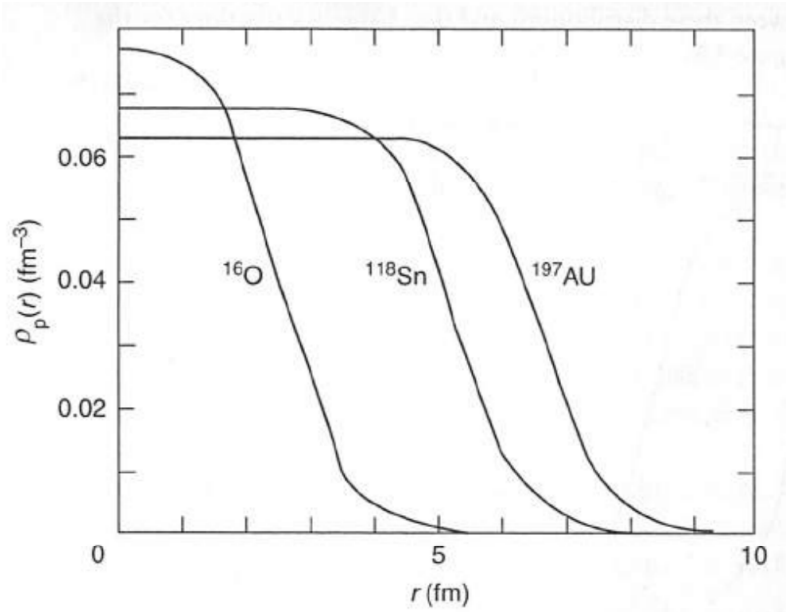

Figure 1.6: Woods–Saxon charge distributions for ^{16}O, ^{118}Sn, and ^{197}Au. The proton density $\rho_p(r)$ is nearly flat in the nuclear interior and falls smoothly through the surface. Heavier systems have larger half-density radii and slightly lower central charge densities.

not hollow; charge fills the volume.

2. **A diffuse surface.** The density does not terminate abruptly. It falls from $\sim 90\%$ to $\sim 10\%$ of its central value over a surface thickness of order 2.5 fm.

3. **Larger systems, larger radii.** The half-density radius grows with mass number, consistent with $R \propto A^{1/3}$.

4. **Mild A-dependence of the central charge density.** Lighter nuclei show a somewhat higher central ρ_p; heavier nuclei are slightly lower, consistent with Coulomb repulsion pushing protons outward. When one forms the *nucleon* density by scaling $\rho_A(r) \approx (A/Z)\,\rho_p(r)$, the central values collapse to a nearly universal $\rho_0 \approx 0.16 - -0.17\,1/\mathrm{fm}^3$.

Historical note: R. D. Woods and D. S. Saxon

The functional form that now bears their names was introduced in 1954 by **Roger D. Woods** and **David S. Saxon** at the University of California, Los Angeles, in a Physical Review paper on the elastic scattering of 20 MeV protons (Phys. Rev. **95**, 577, 1954). They needed a smooth, finite-range mean-field potential that was roughly constant in the nuclear interior and fell to zero over a surface of finite thickness: neither a pure square well nor an infinite oscillator. The form

$$V(r) = -\frac{V_0}{1 + \exp\big[(r - R)/a\big]}$$

did the job, and it quickly became the standard phenomenological optical and shell-model potential.
The same shape describes the empirical *charge density* extracted from electron scattering: a flat bulk and a diffuse surface. In the literature one meets both "Woods–Saxon" and "Saxon–Woods"; both refer to this two-parameter Fermi profile. Saxon later contributed broadly to nuclear reaction theory and computing in physics; the potential remains one of the most-cited phenomenological tools in nuclear structure.

Definition: Woods–Saxon (two-parameter Fermi) density

$$\rho(r) = \frac{\rho_0}{1 + \exp\big[(r - R)/a\big]}. \tag{1.32}$$

Here ρ_0 is the central density, R is the half-density radius ($\rho(R) = \rho_0/2$), and a is the diffuseness. The surface thickness t (distance from 90% to 10% of ρ_0) is related to a by

$$t = 4a \ln 3 \approx 4.40\, a. \tag{1.33}$$

A global analysis of scattering data finds that a is essentially independent of mass number,

$$a = 0.52\,\text{fm} \pm 0.01\,\text{fm}, \tag{1.34}$$

so the surface thickness is $t = 4a \ln 3 \approx 2.3\,\text{fm}$ [1]. The same functional form appears as the Woods–Saxon (or Saxon–Woods) mean field in the nuclear shell model [3, 4, 1].

What the charge densities show [1]

Comparing Woods–Saxon charge profiles for light and heavy nuclei one finds three regularities:

1. Larger nuclei have a larger half-density radius.
2. The surface width a (hence t) is nearly the same for all A.
3. The *central charge* density is higher in light nuclei than in heavy ones (Coulomb repulsion pushes protons outward as Z grows).

After rescaling to nucleon density by A/Z (Lecture 2), the central *nucleon* density becomes nearly universal.

Caution

Electrons couple to electric charge. What Figure 1.6 shows is therefore the *proton* (charge) density $\rho_p(r)$, not the full nucleon density. Neutrons are electromagnetically nearly invisible to ordinary (parity-conserving) electron scattering. The rescaling $\rho_A \approx (A/Z)\,\rho_p$ assumes similar proton and neutron profiles (reasonable for $N \approx Z$, increasingly questionable for heavy, neutron-rich systems).

1.7.1 Several definitions of "the" nuclear radius

Because the surface is diffuse, there is no unique nuclear radius. Three common definitions, following [2], are:

- R_m: radius at which the density has fallen to half its central value (the Woods–Saxon R).
- R_N: radius at which the density has essentially vanished (a practical outer edge).
- $R_{1/2}$: a half-density radius defined on a particular model of the edge.

They differ by $\sim 10 - -20\,\%$ and all scale roughly as $A^{1/3}$. The volume per nucleon implied by these radii lies in the range $\sim 4 - -9\,\mathrm{fm}^3$, corresponding to the saturation density above.

1.7.2 Charge radius and the $A^{1/3}$ law

Electron scattering determines not only the shape of $\rho(r)$ but also moments. The most frequently quoted is the root-mean-square (rms) charge radius,

$$\langle r^2 \rangle_{\mathrm{ch}}^{1/2} = \left(\frac{1}{Ze} \int r^2\, \rho(r)\, \mathrm{d}\tau \right)^{1/2}. \tag{1.35}$$

For a uniform sphere of radius R one has $\langle r^2 \rangle^{1/2} = \sqrt{3/5}\, R$; the Woods–Saxon surface corrects this at the few-percent level. From the low-q expansion Equation (1.31),

$$\langle r^2 \rangle = -6\, \frac{\mathrm{d}F}{\mathrm{d}(q^2)}\bigg|_{q=0}, \tag{1.36}$$

so a careful measurement of $F(q)$ near the origin yields the rms radius model-independently. Empirically, the half-density (or equivalent hard-sphere) radius follows [1]

$$R_0 = 1.2\,\mathrm{fm} \times A^{1/3}. \tag{1.37}$$

This is exactly what one expects for systems of different mass but the *same* bulk density: volume $\propto A$ implies radius $\propto A^{1/3}$. Equation (1.37) is a central input to the liquid-drop model developed in later chapters.

Example: ^{12}C radius from form-factor data [3]

Expanding $F(q)$ at low q and fitting measured cross sections for ^{12}C yields $\langle r^2 \rangle^{1/2} \approx 2.44\,\mathrm{fm}$ for a uniform-sphere equivalent radius, consistent with $r_0 A^{1/3}$ at $A = 12$.

1.7.3 Which feature of $F(q)$ constrains which property?

The form-factor programme answers three nested questions about $\rho_{\mathrm{ch}}(r)$:

Observable in $F(q)$	Density property	Typical scale
Low-q slope of F	$\langle r^2 \rangle_{\mathrm{ch}}$	$r_{\mathrm{rms}} \sim 2$–$6\,\mathrm{fm}$
Location of diffraction minima	Overall size R	$R \approx 1.2\,A^{1/3}\,\mathrm{fm}$
Depth / washing of minima	Surface diffuseness a (skin t)	$a \approx 0.52\,\mathrm{fm}$, $t \approx 2.3\,\mathrm{fm}$

A sharp sphere produces deep zeros of $j_1(qR)$; a diffuse Woods–Saxon surface softens those minima but does not erase the $A^{1/3}$ growth of R [6, 1, 7]. Lecture 2 will convert the same profiles into a saturated *matter* density.

Takeaway

The Woods–Saxon profile encodes two great empirical facts of nuclear bulk structure: **saturation** (a constant central density of order $0.16/\mathrm{fm}^3$) and a **surface of nearly universal thickness** ($t \approx 2.3\,\mathrm{fm}$). Both reappear in the liquid-drop model, the nuclear equation of state, and the neutron skins of heavy nuclei.

1.8 What electrons do not see: neutrons and skins

Electrons couple to electric charge. In a nucleus, charge resides on protons (up to small meson-exchange and spin-orbit contributions). The neutron distribution $\rho_n(r)$ is invisible to ordinary electron scattering.

In light, $N = Z$ nuclei one may reasonably assume $\rho_n \approx \rho_p$. In heavy nuclei, where $N > Z$, a neutron skin develops: the neutron distribution extends farther than the proton distribution. The skin thickness

$$\Delta r_{np} = \langle r^2 \rangle_n^{1/2} - \langle r^2 \rangle_p^{1/2} \tag{1.38}$$

is a laboratory observable with a direct link to the density dependence of the nuclear symmetry energy, and, through that link, to the radii of neutron stars. Measuring Δr_{np} requires either hadronic probes (with their attendant model dependence) or parity-violating electron scattering, in which the Z^0 boson couples preferentially to neutrons. That programme (PREX, CREX, and their successors) lies beyond this chapter, but the conceptual foundation has been laid: once the proton distribution is known, the neutron distribution becomes the next frontier.

Remark

Complementary probes of the charge distribution include muonic atoms: because $m_\mu \approx 207\,m_e$, the muonic Bohr radius is ~ 200 times smaller than the electronic one, so the muon wave function overlaps the nucleus strongly and level shifts are sensitive to $\langle r^2 \rangle_{\mathrm{ch}}$ [2]. Lecture 3 develops that finite-size spectroscopy in detail.

1.9 Summary and outlook

- Nuclear sizes are a few fermis. Probing them requires electron energies of hundreds of MeV so that $\lambda \lesssim R$.
- Rutherford/Chadwick α scattering first established $R \propto A^{1/3}$; Hofstadter electron scattering mapped the full charge density.
- Elastic electron scattering measures a diffraction pattern whose first minimum already yields a crude nuclear diameter, and whose full angular distribution determines the charge form factor $F(q)$.
- In the Born approximation, $\mathrm{d}\sigma/\mathrm{d}\Omega = (\mathrm{d}\sigma/\mathrm{d}\Omega)_{\mathrm{Mott}}\,|F(q)|^2$, with $F(q)$ the Fourier transform of $\rho(r)$.
- Empirical densities are well described by a Woods–Saxon profile: flat interior, diffuse surface of nearly universal thickness, and radius scaling as $A^{1/3}$.

- Electrons map protons. Neutrons (and with them the symmetry energy and the neutron-star connection) require additional probes.

Next. Lecture 2 converts charge density to mass density and explains saturation ($R \propto A^{1/3}$, short-range force). Lecture 3 then remeasures the same radii through atomic and muonic finite-size shifts.

1.10 Deeper physics: Mott baseline and reading $F(q)$

1.10.1 Rutherford / Mott baseline and finite-size reduction

For a point Coulomb centre the classical (and quantum) differential cross section is Rutherford's formula. One finds

$$\frac{\mathrm{d}\sigma}{\mathrm{d}\Omega} = \left(\frac{Zze^2}{8\pi\varepsilon_0 m v_0^2}\right)^2 \csc^4\frac{\theta}{2} \tag{1.39}$$

for non-relativistic projectiles of charge ze on a nucleus of charge Ze. A full quantum treatment of a pure $1/r$ potential reproduces the same formula. For relativistic electrons the point baseline is the Mott cross section (Dirac kinematics, same $1/\sin^4(\theta/2)$ angular skeleton with spin factors). Finite nuclear size multiplies this baseline by a form factor:

$$\left(\frac{\mathrm{d}\sigma}{\mathrm{d}\Omega}\right)_{\text{exp}} = \left(\frac{\mathrm{d}\sigma}{\mathrm{d}\Omega}\right)_{\text{point}} |F(\boldsymbol{q})|^2, \tag{1.40}$$

with $F(0) = 1$. At every nonzero angle, $|F|^2 < 1$: the nucleus is a softer scatterer than a point charge of the same Z [6, 1].

1.10.2 From $|F|^2$ back to $\rho_{\text{ch}}(r)$

In the plane-wave Born approximation,

$$F(q) = \frac{1}{Ze}\int \rho_p(\boldsymbol{r})\, e^{i\boldsymbol{q}\cdot\boldsymbol{r}/\hbar}\,\mathrm{d}^3 r, \qquad q = 2p\sin(\theta/2). \tag{1.41}$$

A practical inversion pipeline is:

1. Divide the measured $\mathrm{d}\sigma/\mathrm{d}\Omega$ by the Mott (point) prediction to obtain $|F(q)|^2$.
2. Fit a parametric density (Woods–Saxon, or a model-independent Fourier–Bessel expansion) so that its Fourier transform matches $F(q)$ over the measured q range.
3. Quote moments: $\langle r^2\rangle$ from the low-q curvature; R and a from the full pattern.

Diffraction minima at larger q constrain the surface diffuseness and possible shell oscillations in $\rho(r)$ [6, 1, 7].

Worked reading of a diffraction minimum

For a uniform sphere, the first zero of $j_1(qR)$ sits near $qR \approx 4.49$. With $q = 2p\sin(\theta/2)$ at fixed beam momentum, a measured first-minimum angle therefore returns R. Replacing

the sharp edge by a Woods–Saxon skin of thickness $t \approx 2.3\,\mathrm{fm}$ fills in the zero partially but hardly moves its angular location: size and diffuseness play distinct roles in $F(q)$, as in Section 1.7.3.

Key idea

What Hofstadter measured. Not a single radius, but a function $\rho_{\mathrm{ch}}(r)$: central plateau, surface of thickness $\sim 2.3\,\mathrm{fm}$, and $R \propto A^{1/3}$. Form-factor zeros move to smaller angles as beam energy rises (de Broglie wavelength shrinks), exactly as in optical diffraction from a larger aperture relative to λ.

1.11 Further physics: light nuclei, rms radii, and halos

Electron scattering does not give a single number "the radius." Heavy nuclei have nearly flat central charge densities that fall over a skin of thickness $\sim 2.3\,\mathrm{fm}$. Light nuclei ($A \lesssim 20$) often have densities peaked near $r = 0$, so a hard-sphere radius is less useful than the rms radius

$$\langle r^2 \rangle = \frac{\int r^2 \rho(r)\, \mathrm{d}^3 r}{\int \rho(r)\, \mathrm{d}^3 r}, \qquad r_{\mathrm{rms}} = \sqrt{\langle r^2 \rangle}. \tag{1.42}$$

For a uniform sphere of radius R, $r_{\mathrm{rms}} = \sqrt{3/5}\, R$. Typical values from electron scattering are $r_{\mathrm{rms}}(^{12}\mathrm{C}) \approx 2.4\,\mathrm{fm}$, $r_{\mathrm{rms}}(^{16}\mathrm{O}) \approx 2.7\,\mathrm{fm}$, $r_{\mathrm{rms}}(^{208}\mathrm{Pb}) \approx 5.5\,\mathrm{fm}$, while the deuteron is anomalously large, $r_{\mathrm{rms}}(^{2}\mathrm{H}) \approx 2.1\,\mathrm{fm}$ for only two nucleons [14, 6].

Some loosely bound systems form **halo nuclei**: one or two valence nucleons orbit a compact core at large distance. An example is ^{11}Be (one neutron outside ^{10}Be), where the valence neutron rms radius can reach $\sim 6\,\mathrm{fm}$ while the core is only $\sim 2.5\,\mathrm{fm}$. Such extremes underline that $R = r_0 A^{1/3}$ is a bulk average, not a universal law for every light species [14].

1.11.1 Quantitative rms radii

Selected rms charge radii from electron scattering [14] (approximate values):

Nucleus	r_{rms} (fm)	equiv. $R = \sqrt{5/3}\, r_{\mathrm{rms}}$	$R/A^{1/3}$
^{1}H	0.84–0.88	~ 1.1	—
^{2}H	2.1	2.7	~ 2.2 (anomalous)
^{4}He	1.7	2.1	~ 1.3
^{12}C	2.5	3.2	~ 1.3
^{16}O	2.7	3.5	~ 1.4
^{40}Ca	3.5	4.5	~ 1.3
^{208}Pb	~ 5.5	~ 7.1	~ 1.2

Heavy nuclei approach $R \approx 1.2\, A^{1/3}\,\mathrm{fm}$. The deuteron is an outlier because its wave function extends far beyond the range of the NN force (Lecture 8).

1.11.2 Skin thickness and constant central density

Electron-scattering charge densities for medium and heavy nuclei share two features [6, 1]:

1. the central density $\rho(0)$ is nearly independent of A (saturation of density);
2. the surface is diffuse: the **skin thickness** t, defined as the distance over which ρ falls from 90% to 10% of its central value, is roughly

$$t \approx 2.3\,\mathrm{fm},$$

almost independent of A.

A hard sphere would have $t = 0$. The finite t is the real-space counterpart of the gradual fall of the form factor $|F(q)|^2$ with momentum transfer. For a sharp sphere of radius R, the form factor involves spherical Bessel functions and has zeros at definite qR; a diffuse surface washes those minima out partially, but the diffraction pattern still fixes R [6, 7].

A fit of rms radii versus $A^{1/3}$ over the chart of the nuclides yields

$$R \approx R_0 A^{1/3}, \qquad R_0 \approx 1.2\text{–}1.25\,\mathrm{fm} \tag{1.43}$$

($R_0 \approx 1.23\,\mathrm{fm}$ is a common electron-scattering value) [6].

1.11.3 Borromean nuclei

A **Borromean** three-body system is bound, while every two-body subsystem is unbound. ^{6}He ($^{4}\mathrm{He}+n+n$) is the classic nuclear example: the two valence neutrons bind only in the presence of the α core. Halo and Borromean systems show that weak binding and extended wave functions are generic near the drip lines [14].

1.12 Problems with solutions

The numericals below follow the spirit of Petrera's problem book [3] and standard exercises on nuclear size [6, 1].

Problem 1.1 — Nuclear density (after Petrera 1.1.1)

Estimate the nuclear mass density in $\mathrm{g\,cm^{-3}}$, taking $R = r_0 A^{1/3}$ with $r_0 = 1.2\,\mathrm{fm}$ and neglecting binding energy ($m_p \approx m_n \approx 1.67 \times 10^{-24}\,\mathrm{g}$).

Solution 1.1

Volume $V = \tfrac{4}{3}\pi R^3$ with $R = r_0 A^{1/3}$ implies

$$\rho = \frac{A\,m_p}{\tfrac{4}{3}\pi (r_0 A^{1/3})^3} = \frac{3 m_p}{4\pi r_0^3}.$$

Insert $m_p = 1.67 \times 10^{-24}\,\mathrm{g}$ and $r_0 = 1.2 \times 10^{-13}\,\mathrm{cm}$:

$$\begin{aligned} r_0^3 &= (1.2)^3 \times 10^{-39} = 1.728 \times 10^{-39}\,\mathrm{cm}^3, \\ 4\pi r_0^3 &\approx 2.17 \times 10^{-38}\,\mathrm{cm}^3, \\ \rho &= \frac{3 \times 1.67 \times 10^{-24}}{2.17 \times 10^{-38}} \approx 2.3 \times 10^{14}\,\mathrm{g\,cm^{-3}}. \end{aligned}$$

Nuclear matter is about 10^{14} times denser than water. The result is independent of A once saturation and $R \propto A^{1/3}$ are assumed.

Problem 1.2 — Radius from the form factor (after Petrera 1.2.8)

At low momentum transfer the charge form factor admits

$$F(q^2) = 1 - \frac{q^2 \langle r^2 \rangle}{6\hbar^2} + \cdots .$$

Elastic electron scattering at 5° with $p = 720\,\mathrm{MeV}/c$ on $^{12}\mathrm{C}$ gives $\mathrm{d}\sigma/\mathrm{d}\Omega = 80\,\mathrm{mb/sr}$, while the Mott (point) cross section is about $99\,\mathrm{mb/sr}$. Estimate the rms charge radius of carbon.

Solution 1.2

The form factor is the ratio of measured to Mott cross sections:

$$|F|^2 = \frac{80}{99} \approx 0.808 \quad \Rightarrow \quad F \approx \sqrt{0.808} \approx 0.899$$

(positive at small q). Elastic kinematics give

$$q = 2p \sin(\theta/2) = 2 \times 720 \sin(2.5^\circ) = 1440 \times 0.0436 \approx 62.8\,\mathrm{MeV}/c.$$

From $F = 1 - q^2\langle r^2 \rangle/[6(\hbar c)^2] + \cdots$,

$$\begin{aligned} \langle r^2 \rangle &= \frac{6(\hbar c)^2}{(qc)^2}(1 - F) = \frac{6 \times (197\,\mathrm{MeV\,fm})^2}{(62.8\,\mathrm{MeV})^2}(0.101) \\ &\approx \frac{6 \times 38809}{3944} \times 0.101 \approx 59.0 \times 0.101 \approx 5.95\,\mathrm{fm}^2, \end{aligned}$$

so

$$\sqrt{\langle r^2 \rangle} \approx 2.44\,\mathrm{fm}.$$

For a uniform sphere, $R = \sqrt{5/3}\,\sqrt{\langle r^2 \rangle} \approx 3.15\,\mathrm{fm}$, consistent with $r_0 A^{1/3}$ at $A = 12$.

Problem 1.3 — Diffraction estimate of radius

Electrons of energy $E = 180\,\mathrm{MeV}$ scatter elastically from $^{197}\mathrm{Au}$. Treating the nucleus as a hard sphere of radius $R = (1.18A^{1/3} - 0.48)\,\mathrm{fm}$, how many diffraction minima are kinematically accessible (after Petrera 1.2.2)?

Solution 1.3

Uniform-sphere form-factor zeros solve $\tan x = x$ with $x = qR/\hbar$, near $x \approx 3\pi/2,\ 5\pi/2,\ 7\pi/2, \ldots$. Maximum $q \approx 2E/c$, so

$$x_{\max} = \frac{2E}{\hbar c} R \approx \frac{2 \times 180}{197} \times 6.4 \approx 11.7.$$

There are three zeros below $x_{\max}$ (up to $\sim 7\pi/2$). The angular distribution should show three clear minima.

Chapter 2

Mass Density and Saturation

"The central nuclear charge density is nearly the same for all nuclei. Nucleons do not congregate near the center."

K. S. Krane

2.1 From charge density to mass density

Electron scattering maps the proton (charge) density $\rho_p(r)$. A central empirical fact is that this density is nearly the same in the interior of all nuclei: nucleons do not pile up at the centre. Empirically one fits

$$\rho_p(r) = \frac{\rho_p(0)}{1 + \exp\big[(r - R)/a\big]}, \tag{2.1}$$

with a nearly universal surface diffuseness $a = 0.52\,\mathrm{fm} \pm 0.01\,\mathrm{fm}$ and a half-density radius $R_0 = 1.2\,\mathrm{fm} \times A^{1/3}$ [1, 6].

Electrons do not couple to neutrons. The full nucleon density, often called the mass or matter density, must be reconstructed from the charge density together with a model of how neutrons are distributed, or measured with hadronic probes. That matter density, and the near constancy of its central value, is the subject of this chapter. It is also the microscopic reason the strong force must be short ranged: if every nucleon attracted every other nucleon, neither the density nor the binding energy would scale as they do [6].

Here $\rho_p(r)$ denotes the *proton number density* (nucleons per fm^3), not the electromagnetic charge density $e\,\rho_p$. Electron scattering determines ρ_p because the charge density is $e\,\rho_p$ for point-like protons (up to small meson-exchange corrections). It is equally important to know the distribution of *all* nucleons (neutrons and protons), because nuclear binding, the equation of state, and the liquid-drop model all refer to the total nucleon number density $\rho(r)$. (The true mass density is $m_N\rho$; nuclear physics usually quotes number densities.)

Since neutrons are uncharged, ordinary Coulomb scattering does not observe them. Under a standard working assumption, however, one can still infer $\rho(r)$ from $\rho_p(r)$.

2.1.1 The constant N/Z assumption

A nucleus with N neutrons and Z protons has overall ratio N/Z and mass number $A = N + Z$. It is usually assumed that the local neutron-to- proton density ratio is the same everywhere

inside the nucleus:

$$\frac{\rho_n(r)}{\rho_p(r)} = \frac{N}{Z}. \tag{2.2}$$

The total nucleon density is the sum

$$\rho(r) = \rho_n(r) + \rho_p(r). \tag{2.3}$$

Eliminating ρ_n between these two equations gives immediately

$$\rho(r) = \rho_p(r)\left(1 + \frac{N}{Z}\right) = \rho_p(r)\,\frac{A}{Z}. \tag{2.4}$$

Definition: nucleon (mass) density from charge density

Under the assumption $\rho_n/\rho_p = N/Z$ everywhere,

$$\rho(r) = \frac{A}{Z}\,\rho_p(r).$$

Rescaling the measured proton density by A/Z converts a charge distribution into an estimate of the total nucleon density.

Caution

Equation (2.2) is an approximation, not a theorem. In heavy nuclei ($N > Z$) a *neutron skin* develops: $\rho_n(r)$ extends farther than $\rho_p(r)$. The constant-ratio assumption then fails in the surface. For the bulk and for light or near-symmetric nuclei it remains a useful first estimate; for precision neutron-skin physics one needs parity-violating electron scattering or hadronic probes (cf. Lecture 1).

2.1.2 What the rescaled densities look like

Figure 2.1 recalls the proton densities of ^{16}O, ^{118}Sn, and ^{197}Au. Applying Equation (2.4) produces the nucleon densities of Figure 2.2. Two features stand out at once.

1. The half-density radii and surface widths are essentially the same as in the charge densities: rescaling multiplies the vertical axis, not the radial shape.
2. All three nuclei now share virtually the *same central nucleon density*, $\rho_0 \approx 0.16 - -0.17\,1/\mathrm{fm}^3$.

Key idea

Saturation of nuclear matter: the central nucleon density is nearly independent of mass number [1]. Nuclei are not denser in the middle when they grow larger; they grow by adding a larger volume at fixed bulk density. This confirms the strong interaction is short ranged and dominated by nearest-neighbour nucleons.

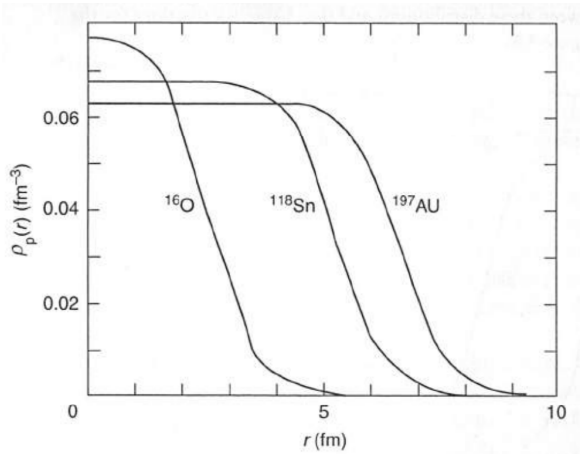

Figure 2.1: Proton densities $\rho_p(r)$ for ^{16}O, ^{118}Sn, and ^{197}Au.

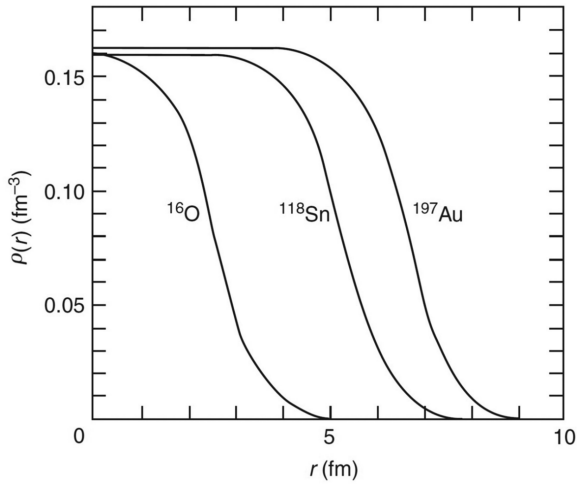

Figure 2.2: Nucleon densities $\rho = (A/Z)\rho_p$ with common central ρ_0.

2.2 Woods–Saxon parameters and the nuclear surface

The nucleon density is again described by a Woods–Saxon (two-parameter Fermi) profile,

$$\rho(r) = \frac{\rho_0}{1 + \exp\big[(r - R)/a\big]}, \tag{2.5}$$

where now ρ_0 is the central *nucleon* density, R is the half-density radius, and a is the diffuseness.

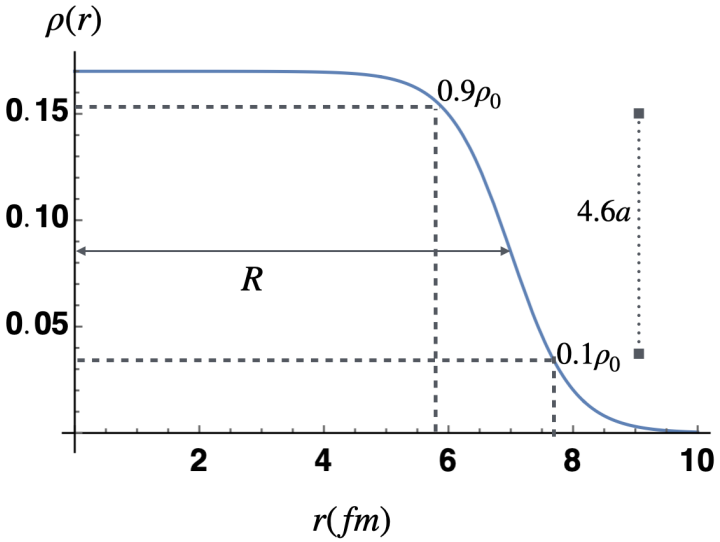

Figure 2.3: Geometry of the Woods–Saxon surface. The half-density radius R is the point where $\rho = \rho_0/2$. The surface thickness t, from $0.9\rho_0$ to $0.1\rho_0$, equals $4a \ln 3 \approx 4.4\,a$.

2.2.1 Surface thickness from first principles

To relate a to an observable surface thickness, evaluate the radii at which the density has fallen to 90% and 10% of ρ_0.

Setting $\rho = 0.9\rho_0$,

$$0.9\rho_0 = \frac{\rho_0}{1+e^{(r-R)/a}} \implies e^{(r-R)/a} = \frac{1}{9} \implies \frac{r-R}{a} = -\ln 9 = -2\ln 3. \tag{2.6}$$

Hence

$$r_{90} = R - a\ln 9 = R - 2a\ln 3 \approx R - 2.20\,a. \tag{2.7}$$

Setting $\rho = 0.1\rho_0$,

$$0.1\rho_0 = \frac{\rho_0}{1+e^{(r-R)/a}} \implies e^{(r-R)/a} = 9 \implies r_{10} = R + 2a\ln 3 \approx R + 2.20\,a. \tag{2.8}$$

The surface thickness is therefore

$$t \equiv r_{10} - r_{90} = 4a\ln 3 \approx 4.39\,a. \tag{2.9}$$

Remark

Lecture notes sometimes quote $t \approx 4.6a$ by approximating $\ln 9 \approx 2.3$. The exact factor is $4\ln 3 \approx 4.394$. A standard global fit gives $a = 0.52\,\text{fm} \pm 0.01\,\text{fm}$ [1], so

$$t = 4a\ln 3 \approx 4.39 \times 0.52\,\text{fm} \approx 2.28\,\text{fm}.$$

The nuclear "skin" is only a couple of fermis thick and is nearly independent of A. (The sketch in Figure 2.3 labels the thickness $4.6a$; we keep the exact $4\ln 3$.)

Example: surface of a heavy nucleus

With $a = 0.52\,\text{fm}$,

$$t \approx 2.3\,\text{fm}.$$

For ^{197}Au, $R_0 = 1.2\,\text{fm} \times 197^{1/3} \approx 7.0\,\text{fm}$ [1]. The density is essentially flat for $r \lesssim 5\,\text{fm}$ and has fallen to a few percent of ρ_0 by $r \approx 9 - -10\,\text{fm}$, matching Figure 2.2.

The central core is uniformly populated with nucleons up to $r \sim R$; beyond that the density decreases smoothly. The nucleus does not have a sharp boundary but a diffuse quantum surface.

2.2.2 The $A^{1/3}$ law for the half-density radius

The mean nuclear radius R_0 increases with mass number. Saturation already implies the functional form. If the central density is A-independent, the volume that holds A nucleons must grow as

$$A = \tfrac{4}{3}\pi R^3\,\rho_0 \quad \Rightarrow \quad R = \left(\frac{3}{4\pi\rho_0}\right)^{1/3} A^{1/3} \equiv r_0\,A^{1/3}. \tag{2.10}$$

With $\rho_0 \approx 0.16\,\text{fm}^{-3}$,

$$r_0 = \left(\frac{3}{4\pi \times 0.16}\right)^{1/3} \approx 1.14\,\text{fm}, \tag{2.11}$$

close to the conventional fit value. Analysis of electron-scattering data yields the empirical expression [1]

$$R_0 = 1.2\,\text{fm} \times A^{1/3}. \tag{2.12}$$

Combined with a constant central density, this is precisely the geometry of an incompressible liquid drop: volume $\propto A$, so radius $\propto A^{1/3}$. Equation (2.12) is a standard input to the liquid-drop model [1].

The mean inter-nucleon spacing at saturation follows from the same density:

$$d \sim \rho_0^{-1/3} \approx (0.16)^{-1/3}\,\text{fm} \approx 1.8\,\text{fm}, \tag{2.13}$$

comparable to the pion Compton wavelength that will appear in Lecture 11.

Takeaway

Three numbers characterise bulk nuclear matter as seen by electrons (rescaled to nucleons) [1]:

$$\rho_0 \approx 0.16/\text{fm}^3, \quad R_0 = 1.2\,\text{fm}\,A^{1/3}, \quad a = 0.52\,\text{fm} \pm 0.01\,\text{fm} \;\; (t \approx 2.3\,\text{fm}).$$

They will reappear in the liquid-drop model, the semi-empirical mass formula, and the nuclear equation of state.

2.3 What uniform density teaches about the strong force

The nucleus exists because a strong attractive force counters the Coulomb repulsion among protons. Without that force the nucleus would explode. Nuclear attraction is far stronger than Coulomb repulsion at fermi distances, yet the density profile is *flat*, not centrally peaked.

One might have expected the opposite. In a self-gravitating body such as the Earth, density is highest at the core and decreases toward the surface: every mass element attracts every other, so the equilibrium is centrally condensed. Why is the nucleus different?

Key idea

Nuclear forces are *short-ranged*. A given nucleon interacts significantly only with its nearest neighbours, not with all other nucleons in the system. There is therefore no long-range "pull toward the centre," and the equilibrium density is set locally by the balance of short-range attraction and short-range repulsion (the hard core / Pauli pressure). The result is a saturated, roughly constant bulk density.

Remark

The range of the strong force is of order the pion Compton wavelength, $\hbar/(m_\pi c) \approx 1.4\,\text{fm}$—comparable to the mean inter-nucleon spacing at saturation. Beyond two or three fermis the force has essentially died away. That is why adding nucleons increases the *volume* at fixed density rather than packing the centre more tightly, and why the surface thickness is a nearly universal few fermis set by the force range itself.

Historical note: Hideki Yukawa (1907–1981)

Hideki Yukawa, working in Osaka in 1934–1935, proposed that the short-range nuclear force is mediated by the exchange of a massive boson. The resulting potential,

$$V(r) \propto \frac{e^{-r/\lambda}}{r}, \qquad \lambda = \frac{\hbar}{mc},$$

falls exponentially with a range fixed by the mediator mass m. Yukawa estimated $m \sim 100\,\mathrm{MeV}/c^2$; the pion, discovered in 1947, has $m_\pi \approx 140\,\mathrm{MeV}/c^2$ and $\lambda \approx 1.4\,\mathrm{fm}$. He received the 1949 Nobel Prize in Physics, the first Nobel awarded to a Japanese scientist. Yukawa's insight is the microscopic reason the nuclear density saturates: the force simply does not reach across the whole nucleus.

2.4 A second method: nuclear size from atomic energy shifts

Electron scattering is not the only route to a nuclear radius. Atomic electrons themselves sample the nuclear interior: their wave functions are nonzero at $r = 0$, so a finite nuclear size shifts atomic energy levels relative to the point-nucleus idealisation. Measuring those shifts, in ordinary or more sensitively muonic atoms, provides an independent determination of $\langle r^2 \rangle_{\mathrm{ch}}$.

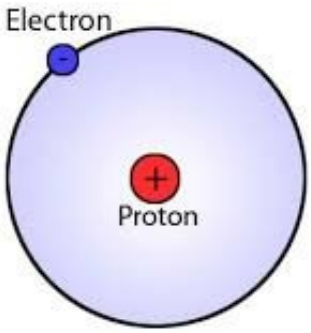

Figure 2.4: Schematic hydrogen-like atom: a single electron bound to a point-like positive charge. When the nucleus has finite size, the potential inside $r < R$ is modified and the bound-state energies shift.

2.4.1 Point nucleus: the Coulomb problem

For a hydrogen-like ion (one electron, nuclear charge Ze), the potential energy of the electron in the field of a *point* nucleus is

$$U(r) = -\frac{Ze^2}{4\pi\varepsilon_0\, r}. \tag{2.14}$$

The Hamiltonian is

$$H_0 = -\frac{\hbar^2}{2m_e}\nabla^2 - \frac{Ze^2}{4\pi\varepsilon_0\, r}, \tag{2.15}$$

and the ground-state energy of hydrogen ($Z = 1$) is the familiar

$$E_1 = -13.6\,\mathrm{eV}. \tag{2.16}$$

The corresponding ground-state wave function,

$$\psi_{100}(r) = \frac{1}{\sqrt{\pi}} \left(\frac{Z}{a_0} \right)^{3/2} e^{-Zr/a_0}, \tag{2.17}$$

with Bohr radius $a_0 = 4\pi\varepsilon_0\hbar^2/(m_e e^2) \approx 0.529\,\text{Å}$, is nonzero at the origin:

$$|\psi_{100}(0)|^2 = \frac{Z^3}{\pi a_0^3} \neq 0. \tag{2.18}$$

The electron therefore has a finite probability of being found inside the nuclear volume. If the nucleus is extended rather than point-like, the potential inside $r < R$ differs from Equation (2.14), and the energy levels shift.

Caution

Some lecture notes write $\psi_{100} \propto Z^3/(\pi a_0^3)\, e^{-Zr/a_0}$ without the square root. The correctly normalised ground state is Equation (2.17); what is proportional to $Z^3/(\pi a_0^3)$ is $|\psi(0)|^2$, not ψ itself.

Historical note: Niels Bohr (1885–1962)

Niels Bohr introduced the first quantum model of the hydrogen atom in 1913, postulating discrete orbits with angular momentum $n\hbar$ and explaining the Rydberg formula for spectral lines. The Bohr radius a_0 that appears in Equation (2.17) is the radius of the $n = 1$ orbit in that model; in modern quantum mechanics it sets the exponential scale of the ground-state wave function. Bohr received the 1922 Nobel Prize in Physics for his services to the investigation of the structure of atoms and of the radiation emanating from them. The finite-size corrections we derive below are small perturbations on the Bohr–Schrödinger spectrum, but they are measurable, and they encode the nuclear radius.

2.4.2 Finite nucleus: electrostatics of a uniformly charged sphere

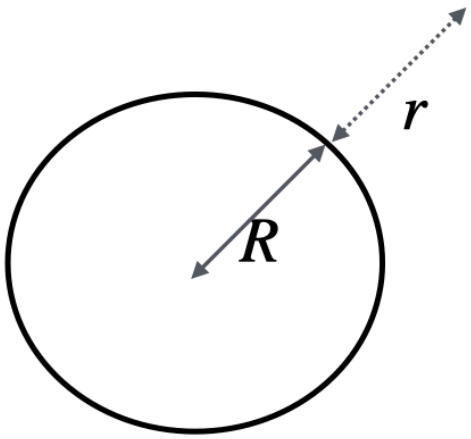

Figure 2.5: Spherical nucleus of radius R. Outside ($r > R$) the potential is identical to that of a point charge Ze. Inside ($r \leq R$) the field and potential must be recomputed for a uniform charge distribution.

Assume a spherical nucleus of radius R with charge Ze distributed uniformly. Gauss's law

gives the electric field.

Outside ($r > R$). All charge is enclosed, so

$$E(r) = \frac{1}{4\pi\varepsilon_0}\frac{Ze}{r^2}, \qquad V(r) = \frac{1}{4\pi\varepsilon_0}\frac{Ze}{r} \quad (r > R), \tag{2.19}$$

identical to the point-charge result (taking $V(\infty) = 0$).

Inside ($r \le R$). The charge enclosed within radius r is $Ze \cdot (r^3/R^3)$, so

$$E(r) = \frac{1}{4\pi\varepsilon_0}\frac{Ze\,r}{R^3}, \qquad r \le R. \tag{2.20}$$

The potential is continuous at $r = R$. Integrating inward from the surface,

$$\begin{aligned} V(r) &= V(R) - \int_R^r E(r')\,\mathrm{d}r' = \frac{1}{4\pi\varepsilon_0}\frac{Ze}{R} + \int_r^R \frac{1}{4\pi\varepsilon_0}\frac{Ze\,r'}{R^3}\,\mathrm{d}r' \\ &= \frac{1}{4\pi\varepsilon_0}\frac{Ze}{R} + \frac{1}{4\pi\varepsilon_0}\frac{Ze}{R^3}\cdot\frac{1}{2}(R^2 - r^2) \\ &= \frac{1}{4\pi\varepsilon_0}\frac{Ze}{2R^3}(3R^2 - r^2) = \frac{1}{4\pi\varepsilon_0}\frac{Ze}{2R}\left(3 - \frac{r^2}{R^2}\right). \end{aligned} \tag{2.21}$$

The potential energy of an electron (charge $-e$) inside the nucleus is therefore

$$U(r) = -e\,V(r) = -\frac{Ze^2}{8\pi\varepsilon_0\,R}\left(3 - \frac{r^2}{R^2}\right), \qquad r \le R. \tag{2.22}$$

Definition: electron potential energy for a uniform sphere

$$U(r) = \begin{cases} -\dfrac{Ze^2}{8\pi\varepsilon_0\,R}\left(3 - \dfrac{r^2}{R^2}\right), & r \le R, \\[2ex] -\dfrac{Ze^2}{4\pi\varepsilon_0\,r}, & r > R. \end{cases}$$

Outside, nothing changes. Inside, the potential is finite at $r = 0$ and shallower than the pure Coulomb singularity.

2.4.3 Perturbation theory for the finite-size shift

Write the full Hamiltonian as $H = H_0 + H_1$, where H_0 is the point-nucleus operator Equation (2.15) and H_1 is the difference between the finite-size and point-nucleus potentials. Since the two potentials agree for $r > R$,

$$H_1(r) = \begin{cases} U_{\text{finite}}(r) - U_{\text{point}}(r), & r \le R, \\ 0, & r > R. \end{cases} \tag{2.23}$$

Explicitly, for $r \le R$,

$$H_1(r) = -\frac{Ze^2}{8\pi\varepsilon_0\, R}\left(3 - \frac{r^2}{R^2}\right) + \frac{Ze^2}{4\pi\varepsilon_0\, r} = \frac{Ze^2}{8\pi\varepsilon_0}\left[\frac{2}{r} - \frac{1}{R}\left(3 - \frac{r^2}{R^2}\right)\right]. \tag{2.24}$$

Caution

A common slip is to write the first term of H_1 as $Ze^2/(8\pi\varepsilon_0 r)$ rather than $Ze^2/(4\pi\varepsilon_0 r)$. The point-nucleus potential energy is $-Ze^2/(4\pi\varepsilon_0 r)$; when one forms $U_{\text{finite}} - U_{\text{point}}$, the point piece contributes $+Ze^2/(4\pi\varepsilon_0 r) = +2\,Ze^2/(8\pi\varepsilon_0 r)$. Using the wrong factor of two spoils the cancellation that makes $H_1(R) = 0$ (continuity of the potential at the nuclear surface).

In first-order perturbation theory the energy shift of an unperturbed state $|\psi_0\rangle$ is

$$\Delta E = \langle \psi_0 | H_1 | \psi_0 \rangle = \int \psi_0^*(\boldsymbol{r})\, H_1(r)\, \psi_0(\boldsymbol{r})\, \mathrm{d}^3 r. \tag{2.25}$$

Because H_1 is supported only inside the tiny nuclear volume, and because s-state wave functions vary slowly on the scale of R, one may approximate $\psi_0(\boldsymbol{r}) \approx \psi_0(0)$ inside the integral. Then

$$\Delta E \approx |\psi_0(0)|^2 \int_{r<R} H_1(r)\, \mathrm{d}^3 r. \tag{2.26}$$

The radial integral can be evaluated in closed form. With $k \equiv Ze^2/(4\pi\varepsilon_0)$ one has $H_1(r) = k\big[1/r - 3/(2R) + r^2/(2R^3)\big]$ for $r \le R$, so

$$\int_{r<R} H_1\, \mathrm{d}^3 r = 4\pi k \int_0^R \left(r - \frac{3r^2}{2R} + \frac{r^4}{2R^3}\right)\mathrm{d}r = 4\pi k\left[\frac{R^2}{2} - \frac{R^2}{2} + \frac{R^2}{10}\right] = \frac{2\pi}{5}\, k\, R^2. \tag{2.27}$$

(The first two terms cancel; only the r^4 piece survives.) Hence

$$\Delta E \approx \frac{2\pi}{5}\frac{Ze^2}{4\pi\varepsilon_0} R^2 |\psi_0(0)|^2 = \frac{2\pi}{5}\frac{Ze^2}{4\pi\varepsilon_0} R^2 \frac{Z^3}{\pi a_0^3} \tag{2.28}$$

for the ground state (using Equation (2.18)).

More generally, for an arbitrary spherical charge distribution the leading finite-size shift depends only on the mean-square charge radius. To see why, expand the interior potential difference for r small compared with the atomic scale. Outside a spherical distribution the potential is pure Coulomb; inside, Gauss's law gives

$$E(r) = \frac{1}{4\pi\varepsilon_0}\frac{q(r)}{r^2}, \qquad q(r) = \int_0^r 4\pi r'^2 \rho_{\text{ch}}(r')\, \mathrm{d}r'.$$

Integrating from infinity and subtracting the point-nucleus potential yields, after one partial

integration,

$$\Delta E = \frac{2\pi}{3}\frac{Ze^2}{4\pi\varepsilon_0}\langle r^2\rangle_{\rm ch}|\psi(0)|^2 + \cdots , \tag{2.29}$$

with $\langle r^2\rangle_{\rm ch} = (1/Ze)\int \rho_{\rm ch}(r)\, r^2\, \mathrm{d}^3r$. For a uniform sphere $\langle r^2\rangle = \frac{3}{5}R^2$, and Equation (2.29) reduces exactly to Equation (2.28):

$$\frac{2\pi}{3}k\cdot\frac{3}{5}R^2|\psi(0)|^2 = \frac{2\pi}{5}kR^2|\psi(0)|^2.$$

This is the form used in precision atomic physics and muonic-atom analyses.

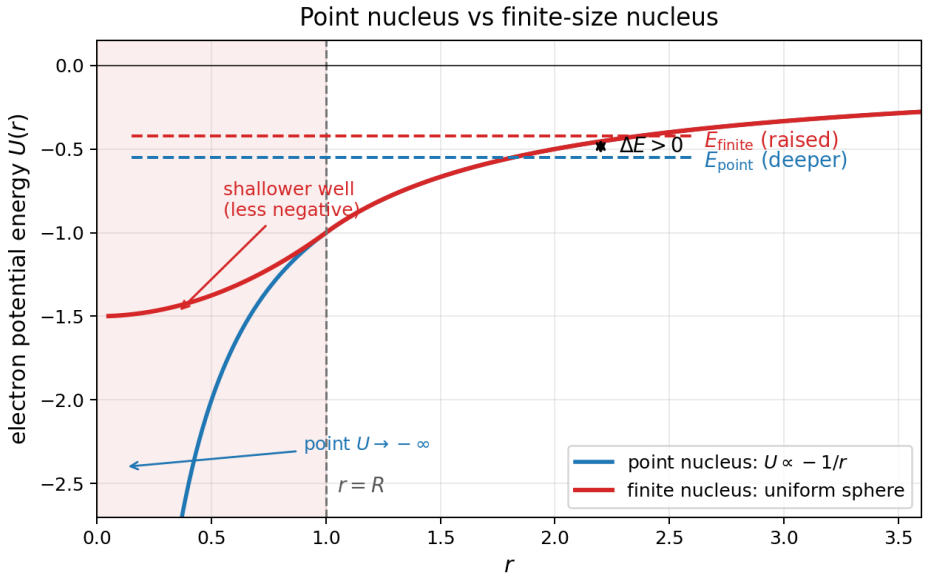

Figure 2.6: Point Coulomb well ($U \propto -1/r$, blue) versus a uniform sphere of radius R (red). Inside the nucleus the finite well is shallower. Dashed lines: schematic bound-state ($1s$) energies; the finite-size level lies higher by $\Delta E > 0$. Outside $r = R$ the potentials agree.

Remark

Because $H_1 > 0$ inside the nucleus (the finite-size well is shallower than pure Coulomb; Figure 2.6), one has $\Delta E > 0$: the **bound-state energy** E_{1s} moves *upward* (binding decreases). Only s waves have $|\psi(0)| \neq 0$ in the non-relativistic theory, so $p, d, \ldots$ states feel a much smaller finite-size effect at this order.

Key idea

A finite nuclear size *raises* the bound-state energy of s states (E_{1s} less negative; Figure 2.6), because the electron, when inside the nucleus, feels a shallower potential than the pure Coulomb well. The shift scales as Z^4R^2/a_0^3 for hydrogen-like ions and is largest for heavy nuclei and for muons (whose Bohr radius is ~ 200 times smaller).

Example: order of magnitude for hydrogen

For hydrogen, $Z = 1$, $R \sim 1\,\text{fm} = 10^{-5}\,a_0$, and $|\psi(0)|^2 = 1/(\pi a_0^3)$. Then

$$\frac{\Delta E}{|E_1|} \sim \left(\frac{R}{a_0}\right)^2 \sim 10^{-10}.$$

The shift is tiny in ordinary hydrogen (parts in 10^{10}) but becomes measurable in high-Z electronic atoms and is dramatic in muonic atoms, where the muon wave function overlaps the nucleus strongly [2].

Historical note: muonic atoms and the proton radius

Replacing the electron by a muon multiplies the reduced mass by $m_\mu/m_e \approx 207$, shrinks all Bohr radii by the same factor, and amplifies finite-size shifts by $\sim (207)^3$ in the wave-function density at the origin. Precision spectroscopy of muonic hydrogen at the Paul Scherrer Institute yielded a proton charge radius $r_p \approx 0.84\,\text{fm}$, about 4% smaller than the value long accepted from electronic hydrogen and early electron scattering: the so-called *proton radius puzzle*. The episode underlines both the power of atomic probes of nuclear size and the care required in comparing different experimental methods [2].

Historical note: Erwin Schrödinger (1887–1961)

Erwin Schrödinger formulated wave mechanics in 1926, writing the eigenvalue equation $H\psi = E\psi$ that underlies Equations (2.15) and (2.17). His treatment of the hydrogen atom recovered the Bohr levels and supplied the wave functions needed for perturbation theory. He shared the 1933 Nobel Prize in Physics with Paul Dirac. The finite-size analysis of this section is ordinary first-order perturbation theory on Schrödinger's hydrogen Hamiltonian, a direct descendant of that 1926 paper.

The finite-size shift derived here is the second experimental route to nuclear size: the same $\langle r^2\rangle_{\text{ch}}$ that Lecture 1 extracted from the low-q slope of $F(q)$ now appears as an atomic energy correction. Absolute shifts are hard to isolate because no point-nucleus reference sample exists; Lecture 3 shows how isotope differences cancel everything except ΔR.

2.5 Summary and outlook

- Electron scattering measures $\rho_p(r)$. Under $\rho_n/\rho_p = N/Z$, the nucleon density is $\rho = (A/Z)\,\rho_p$.
- Rescaled densities for different nuclei share a common central value $\rho_0 \approx 0.16/\text{fm}^3$: nuclear matter saturates.
- The Woods–Saxon surface thickness is $t = 4a\ln 3$ with the usual $a = 0.52\,\text{fm} \pm 0.01\,\text{fm}$ ($t \approx 2.3\,\text{fm}$); the half-density radius obeys $R_0 = 1.2\,\text{fm}\,A^{1/3}$ [1].
- A flat bulk density is the geometric signature of a short-range strong force: nucleons feel only their neighbours.
- Atomic electrons (and especially muons) provide a second radius measurement via the finite-size shift $\Delta E \propto Z\,|\psi(0)|^2\,\langle r^2\rangle_{\text{ch}}$.

Next. Lecture 3 specialises the finite-size shift to isotope differences and muonic atoms,

recovering the same $R_0 \approx 1.2\,\mathrm{fm}$ from spectroscopy. Lectures 4–5 then leave size for binding energy and the SEMF that encodes saturation as a volume term.

2.6 Deeper physics: saturation density and short-range force

2.6.1 Numerical saturation density

If the mass density is roughly uniform inside $R = r_0 A^{1/3}$ with $r_0 \approx 1.2\,\mathrm{fm}$, the mean nucleon density is

$$\rho_0 = \frac{A}{\frac{4}{3}\pi R^3} = \frac{3}{4\pi r_0^3} \approx 0.14\text{–}0.17\,\mathrm{fm}^{-3}, \tag{2.30}$$

depending on the precise radius definition (half-density vs equivalent uniform sphere vs rms). A representative value is $\rho_0 \approx 0.16\,\mathrm{fm}^{-3}$ [1, 2, 4]. In mass units this is

$$\bar{\rho} \sim 2.3 \times 10^{17}\,\mathrm{kg\,m}^{-3} \sim 2 \times 10^{14}\,\mathrm{g\,cm}^{-3}, \tag{2.31}$$

about 10^{14} times liquid water: the densest stable bulk matter on Earth is ordinary nuclear matter.

2.6.2 Why density saturation implies a short-range force

If every nucleon interacted attractively with every other nucleon (infinite-range two-body force), the binding energy would grow as $\binom{A}{2} \propto A^2$ and the equilibrium density would not be A-independent. Observed $B \propto A$ (Lecture 4) and $\rho \approx$ const together require that each nucleon feels only a fixed number of neighbours: the force range is of order the internucleon spacing $\sim$ 1–2 fm.

Light vs heavy surface fraction

With $t \approx 2.3\,\mathrm{fm}$ fixed and $R = 1.2\,A^{1/3}\,\mathrm{fm}$, a light nucleus ($R \sim 3\,\mathrm{fm}$) is mostly surface, while lead ($R \sim 7\,\mathrm{fm}$) is mostly bulk. That geometric fact foreshadows the SEMF: surface energy dominates the rise of B/A at low A; volume energy dominates the mid-mass plateau [1].

Remark

Mass vs charge distributions. Matter densities inferred from hadronic probes are similar in shape to charge densities, but not identical: neutron skins in heavy nuclei make the matter radius slightly larger than the charge radius. Lecture 1's electron probe measures charge; Lecture 2's saturation argument concerns the *matter* density that sets the SEMF volume term.

2.7 Further physics: saturation and the uncertainty principle

Constant central density and $B/A \sim$ const are two faces of the same fact: each nucleon interacts mainly with nearest neighbours (**saturation** of the nuclear force). A quantum link makes that

plausible. If A nucleons share a volume $\propto R^3$ with $R = r_0 A^{1/3}$, each occupies a linear size $\Delta x \sim r_0$. The uncertainty principle then gives a mean kinetic energy per nucleon of order

$$\langle T \rangle \sim \frac{\hbar^2}{2m_N r_0^2} \sim \text{tens of MeV}, \tag{2.32}$$

nearly independent of A. Because the kinetic energy per particle does not grow with system size, neither does the net binding per nucleon once nearest-neighbour attraction is fixed [14].

That argument fails for atoms: the long-range Coulomb field of the nucleus pulls electrons tighter as Z grows, so atomic size does not scale as $Z^{1/3}$ and the electron density rises with Z. Nuclear forces do not act that way: density saturates.

2.7.1 Saturation requires more than the Pauli principle

Nearest-neighbour counting explains why density and B/A do not grow with A, but a complete picture of saturation needs three ingredients [14]:

1. short-range attraction ($r \sim 1\,\text{fm}$);
2. a repulsive "hard core" at $r \lesssim 0.5\,\text{fm}$ (partly Pauli/quark structure);
3. the Pauli principle for nucleons as fermions.

Any pure power-law attraction would not saturate. The empirical Woods–Saxon density (flat interior, thin surface) is the geometric fingerprint of that three-part force.

2.7.2 Atoms vs nuclei

Atomic size does *not* grow as $Z^{1/3}$: the long-range Coulomb field of the nucleus increases electron density with Z. Nuclear density is approximately constant because the force is short-ranged and saturates. That contrast is the essential reason liquid-drop thinking works for nuclei and not for atoms [14, 5].

2.7.3 Fermi momentum and density at saturation

Treat protons and neutrons as independent Fermi gases in a volume $V = (4\pi/3)R^3$ with bulk density

$$n_0 \approx 0.15\text{–}0.17\,\text{fm}^{-3} \tag{2.33}$$

[14, 1]. For $N \approx Z \approx A/2$ the Fermi energy of each species is

$$\varepsilon_F = \frac{\hbar^2}{2m}(3\pi^2 n)^{2/3} \approx 35\,\text{MeV}, \tag{2.34}$$

corresponding to

$$p_F \approx 265\,\text{MeV}/c, \qquad k_F = p_F/\hbar \approx 1.33\,\text{fm}^{-1}. \tag{2.35}$$

The mean kinetic energy per nucleon in a free Fermi gas is $\frac{3}{5}\varepsilon_F \approx 21\,\text{MeV}$. Neutron-scattering and optical-model analyses place the depth of the mean field near $U \sim -40\,\text{MeV}$; the net volume

binding is then of order $a_V \sim |U| - \frac{3}{5}\varepsilon_F \sim 15$–$20\,\mathrm{MeV}$, consistent with the SEMF volume coefficient [14].

These numbers fix the density and energy scales that Lectures 4–6 carry into the liquid-drop formula and into compact-star estimates.

2.8 Problems with solutions

Problem 2.1 — Saturation density

Using $R = 1.2\,A^{1/3}\,\mathrm{fm}$, compute the mean nucleon number density $\rho_0 = A/(\frac{4}{3}\pi R^3)$ in fm^{-3} and in $\mathrm{g\,cm}^{-3}$ (take $m_N = 1.67 \times 10^{-24}\,\mathrm{g}$).

Solution 2.1

$$\rho_0 = \frac{3}{4\pi r_0^3} = \frac{3}{4\pi(1.2)^3} \approx 0.138\,\mathrm{fm}^{-3} \sim 0.14\text{–}0.17\,\mathrm{fm}^{-3}$$

depending on the precise radius definition. In mass units,

$$\rho_0 m_N \approx 2.3 \times 10^{14}\,\mathrm{g\,cm}^{-3},$$

as in Problem 1.1. This is the saturation density underlying the SEMF volume term.

Problem 2.2 — Neutron-star radius from density (Petrera 1.1.3)

A neutron star has mass $M \sim M_\odot = 2 \times 10^{30}\,\mathrm{kg}$ and density comparable to nuclear density $\rho \sim 2.3 \times 10^{14}\,\mathrm{g\,cm}^{-3}$. Estimate its radius.

Solution 2.2

$$\frac{4}{3}\pi R^3 \rho = M \quad \Rightarrow \quad R = \left(\frac{3M}{4\pi\rho}\right)^{1/3} \approx \left(\frac{3 \times 2 \times 10^{33}\,\mathrm{g}}{4\pi \times 2.3 \times 10^{14}\,\mathrm{g\,cm}^{-3}}\right)^{1/3} \approx 13\,\mathrm{km}.$$

Nuclear saturation density plus solar mass already yields the observed $R \sim 10\,\mathrm{km}$ scale (Lecture 7).

Problem 2.3 — Surface thickness

For a Woods–Saxon profile with $a = 0.52\,\mathrm{fm}$, compute the skin thickness t over which the density falls from 90% to 10% of its central value.

Solution 2.3

$$t = 4a \ln 3 \approx 4 \times 0.52 \times 1.099 \approx 2.3\,\mathrm{fm}.$$

The surface thickness is nearly independent of A, while $R \propto A^{1/3}$ grows: light nuclei are almost all surface; heavy nuclei have a thin skin on a large bulk.

Chapter 3

Finite Size and Isotope Shifts

"If we could only find a supply of atoms with 'point' nuclei we could measure ΔE and deduce R!"

K. S. Krane

3.1 Physical setup: what problem are we solving?

In solving the hydrogen atom one always assumes a point nucleus, $V = -Ze^2/(4\pi\varepsilon_0 r)$. Real nuclei are not points. Lectures 1–2 fixed the charge size from electron scattering: $R_0 \approx 1.2\,\mathrm{fm}\,A^{1/3}$ and a nearly universal skin $t \approx 2.3\,\mathrm{fm}$. The electron wave function penetrates to $r < R$, and inside the charge distribution the potential does *not* diverge as $1/r$. As a first approximation the nucleus may be taken as a uniformly charged sphere of radius R. Relative to a point nucleus, s-state energies then shift by an amount ΔE proportional to Z^4R^2 (derived below), which is precisely the finite-size correction introduced in Lecture 2.

No sample of point nuclei exists, so absolute finite-size shifts cannot be read off by simple subtraction. What can be measured cleanly is the difference between isotopes: same Z, different mass number and slightly different R. The isotope shift of K_α X-rays or optical lines then tests nuclear size, and in particular the $R \propto A^{1/3}$ law already suggested by electron scattering [6, 1]. Replacing the electron by a muon amplifies the same effect, because the muon Bohr orbit is about 207 times smaller.

3.2 Building the perturbation H_1 carefully

3.2.1 Point nucleus

For a hydrogen-like ion the electron (charge $-e$) in the field of a *point* nucleus (charge Ze) has potential energy

$$U_{\mathrm{point}}(r) = (-e)\cdot\left(\frac{1}{4\pi\varepsilon_0}\frac{Ze}{r}\right) = -\frac{Ze^2}{4\pi\varepsilon_0\, r}. \tag{3.1}$$

The minus sign means attraction: the energy is lowered when the electron approaches the nucleus. As $r \to 0$, $U_{\mathrm{point}} \to -\infty$. That infinite well is unphysical for a real nucleus of finite size.

3.2.2 Finite uniform sphere: field and potential

Assume a sphere of radius R with total charge Ze spread uniformly. Gauss's law gives the electric field $E(r)$ (radial, outward for $Z > 0$):

Outside ($r > R$). All charge is enclosed, so

$$E(r) = \frac{1}{4\pi\varepsilon_0}\frac{Ze}{r^2}, \qquad V(r) = \frac{1}{4\pi\varepsilon_0}\frac{Ze}{r} \quad (r > R), \tag{3.2}$$

exactly as for a point charge (with $V(\infty) = 0$).

Inside ($r \le R$). Only the charge fraction r^3/R^3 is enclosed:

$$E(r) = \frac{1}{4\pi\varepsilon_0}\frac{Ze\,r}{R^3}. \tag{3.3}$$

The electrostatic potential is continuous at $r = R$. Integrating inward from the surface,

$$\begin{aligned} V(r) &= V(R) + \int_r^R E(r')\,\mathrm{d}r' \\ &= \frac{1}{4\pi\varepsilon_0}\frac{Ze}{R} + \frac{1}{4\pi\varepsilon_0}\frac{Ze}{R^3}\int_r^R r'\,\mathrm{d}r' \\ &= \frac{1}{4\pi\varepsilon_0}\frac{Ze}{R} + \frac{1}{4\pi\varepsilon_0}\frac{Ze}{R^3}\cdot\frac{1}{2}(R^2 - r^2) \\ &= \frac{1}{4\pi\varepsilon_0}\frac{Ze}{2R}\left(3 - \frac{r^2}{R^2}\right). \end{aligned} \tag{3.4}$$

Check continuity at $r = R$

At $r = R$,

$$V(R) = \frac{1}{4\pi\varepsilon_0}\frac{Ze}{2R}(3 - 1) = \frac{1}{4\pi\varepsilon_0}\frac{Ze}{R},$$

which matches the exterior formula. At $r = 0$,

$$V(0) = \frac{1}{4\pi\varepsilon_0}\frac{3Ze}{2R},$$

finite (no singularity).

The electron potential energy is $U = -eV$:

$$U_{\text{finite}}(r) = \begin{cases} -\dfrac{Ze^2}{8\pi\varepsilon_0\,R}\left(3 - \dfrac{r^2}{R^2}\right), & r \le R, \\[2ex] -\dfrac{Ze^2}{4\pi\varepsilon_0\,r}, & r > R. \end{cases} \tag{3.5}$$

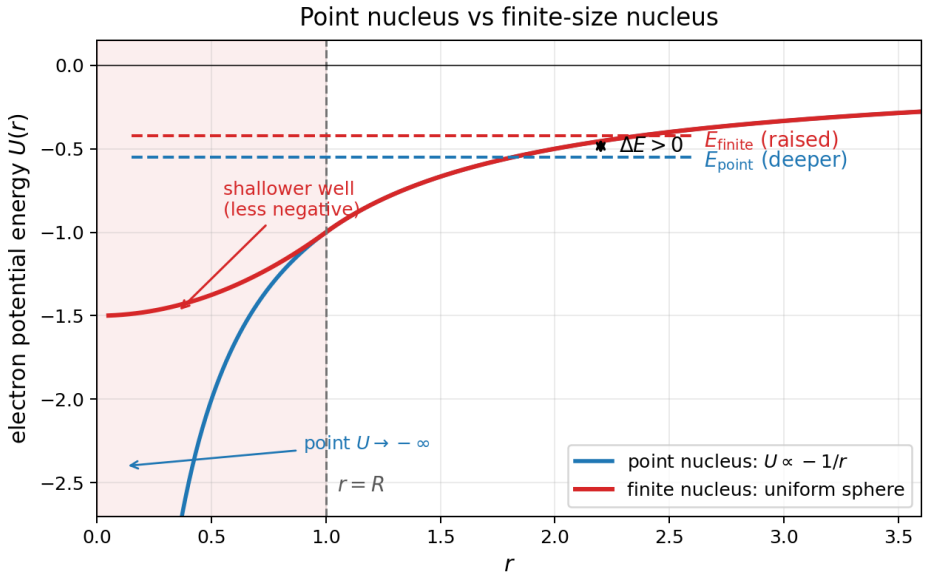

Figure 3.1: Electron potential energy for a point nucleus ($U \propto -1/r$, blue) and for a uniformly charged sphere of radius R (red). Outside the nucleus the two curves coincide. Inside, the finite-size well is shallower (less negative) because part of the nuclear charge lies outside the electron's position and attracts less strongly. The dashed lines are schematic $1s$ energies: raising the well raises the bound level from E_{point} to E_{finite} by $\Delta E > 0$ (weaker binding).

Remark

Compare U_{finite} and U_{point} at fixed $r < R$ in Figure 3.1. The finite-size well is *shallower* (less negative) because the electron, when inside the nucleus, does not feel the full Coulomb attraction of all the charge as if it were concentrated at a point. Raising the bottom of the well raises the **bound-state energy** of the electron, here the $1s$ energy E_{1s}. In the figure the dashed levels show this shift explicitly:

$$E_{\text{finite}} > E_{\text{point}} \qquad \text{(both negative; } |E_{\text{finite}}| < |E_{\text{point}}|\text{)},$$

so the finite-size correction is $\Delta E = E_{\text{finite}} - E_{\text{point}} > 0$.

Key idea

Reading Figure 3.1.

- At $r = 0$ the point potential dives to $-\infty$; the finite potential stays finite, $U(0) = -3Ze^2/(8\pi\varepsilon_0 R)$.
- For $0 < r < R$, red lies above blue: less attraction.
- For $r > R$, red = blue (all nuclear charge looks point-like).
- Bound-state energy E_{1s} (dashed) moves up with the well: weaker binding, $\Delta E > 0$.

3.2.3 Definition of the perturbation

Write the full Hamiltonian as $H = H_0 + H_1$, where H_0 is the usual point-nucleus hydrogen Hamiltonian and

$$H_1(r) \equiv U_{\text{finite}}(r) - U_{\text{point}}(r). \tag{3.6}$$

Outside the nucleus the two potentials agree, so $H_1 = 0$ for $r > R$. Inside,

$$\begin{aligned} H_1(r) &= -\frac{Ze^2}{8\pi\varepsilon_0 R}\left(3 - \frac{r^2}{R^2}\right) - \left(-\frac{Ze^2}{4\pi\varepsilon_0 r}\right) \\ &= -\frac{Ze^2}{8\pi\varepsilon_0 R}\left(3 - \frac{r^2}{R^2}\right) + \frac{Ze^2}{4\pi\varepsilon_0 r}. \end{aligned} \tag{3.7}$$

It is often convenient to factor $k \equiv Ze^2/(4\pi\varepsilon_0)$:

$$H_1(r) = k\left[\frac{1}{r} - \frac{3}{2R} + \frac{r^2}{2R^3}\right], \qquad r \le R. \tag{3.8}$$

Check $H_1(R) = 0$

At $r = R$,

$$\frac{1}{R} - \frac{3}{2R} + \frac{1}{2R} = \frac{2 - 3 + 1}{2R} = 0.$$

The perturbation vanishes smoothly at the nuclear surface. If a factor of two is dropped in the Coulomb term, this cancellation fails; that is a common algebraic trap.

Key idea

Only the interior region $r < R$ contributes to the energy shift. The entire calculation reduces to an integral of $H_1(r)$ weighted by the electron probability density inside the nucleus.

3.3 The $1s$ wave function, step by step

3.3.1 Normalised ground state

The hydrogen-like $1s$ wave function is

$$\psi_{1s}(r) = \frac{1}{\sqrt{\pi}}\left(\frac{Z}{a_0}\right)^{3/2} e^{-Zr/a_0}, \tag{3.9}$$

with

$$a_0 = \frac{4\pi\varepsilon_0\,\hbar^2}{m_e e^2} \approx 0.529\,\text{Å} = 5.29 \times 10^{-11}\,\text{m}. \tag{3.10}$$

Why these factors?

- The exponential e^{-Zr/a_0} is the solution of the radial Schrödinger equation for $n = 1$, $\ell = 0$. Larger Z pulls the cloud inward (effective Bohr radius a_0/Z).

- The prefactor is fixed by normalisation $\int |\psi|^2 \, \mathrm{d}^3 r = 1$. For a purely radial function, $\int_0^\infty 4\pi r^2 |\psi|^2 \, \mathrm{d}r = 1$.

Density at the origin. Set $r = 0$:

$$\psi_{1s}(0) = \frac{1}{\sqrt{\pi}} \left(\frac{Z}{a_0} \right)^{3/2}, \qquad |\psi_{1s}(0)|^2 = \frac{Z^3}{\pi a_0^3}. \tag{3.11}$$

The Z^3 dependence is crucial: heavier nuclei (larger Z) pack far more electron density near $r = 0$, so finite-size shifts grow rapidly with Z.

Caution

ψ_{1s} itself is proportional to $Z^{3/2}$, not Z^3. The quantity $Z^3/(\pi a_0^3)$ is $|\psi(0)|^2$, the probability density. Mixing the two is a frequent source of wrong powers of Z in ΔE.

3.3.2 First-order perturbation theory (what the formula means)

If the unperturbed eigenproblem is $H_0 \psi_n = E_n^{(0)} \psi_n$ and we add a small H_1, the first-order energy correction is

$$\Delta E_n = \langle \psi_n | H_1 | \psi_n \rangle = \int \psi_n^* \, H_1 \, \psi_n \, \mathrm{d}^3 r. \tag{3.12}$$

For the real $1s$ wave function this is simply the expectation value of H_1 in the unperturbed ground state:

$$\Delta E = \int |\psi_{1s}(r)|^2 H_1(r) \, \mathrm{d}^3 r. \tag{3.13}$$

Physical reading: average the extra potential energy H_1 with the probability density of finding the electron at each point. Since $H_1 = 0$ outside the nucleus, only the nuclear ball contributes.

3.4 Evaluating ΔE: full algebraic development

3.4.1 Write the integral in spherical coordinates

Because $|\psi_{1s}|^2$ and H_1 depend only on r,

$$\mathrm{d}^3 r = 4\pi r^2 \, \mathrm{d}r, \tag{3.14}$$

and

$$\Delta E = \int_0^R \underbrace{\frac{Z^3}{\pi a_0^3} e^{-2Zr/a_0}}_{|\psi_{1s}(r)|^2} H_1(r) \, 4\pi r^2 \, \mathrm{d}r. \tag{3.15}$$

(The factor e^{-2Zr/a_0} comes from $|e^{-Zr/a_0}|^2 = e^{-2Zr/a_0}$.)

3.4.2 Approximation: the exponential is almost 1

We must integrate only up to $r = R$. Compare length scales:

Quantity	Typical size	Comment
Nuclear radius R	$\sim 1 - -7\,\mathrm{fm}$	few fm
Bohr radius a_0	$5.29 \times 10^{-11}\,\mathrm{m}$	atomic scale
Ratio R/a_0	$\sim 2 \times 10^{-5}$	extremely small

For any $r \le R$,

$$\frac{2Zr}{a_0} \le \frac{2ZR}{a_0} \sim 2Z \times 10^{-5}. \tag{3.16}$$

Even for uranium ($Z = 92$),

$$\frac{2ZR}{a_0} \approx 1.8 \times 10^{-3} \ll 1. \tag{3.17}$$

Taylor expand:

$$e^{-2Zr/a_0} = 1 - \frac{2Zr}{a_0} + \cdots \approx 1, \tag{3.18}$$

with a relative error of order 10^{-3} or less for electronic atoms. Therefore, to an excellent approximation,

$$\Delta E \approx |\psi_{1s}(0)|^2 \int_0^R H_1(r)\, 4\pi r^2\, \mathrm{d}r = |\psi_{1s}(0)|^2 \int_{r<R} H_1\, \mathrm{d}^3 r. \tag{3.19}$$

Key idea

Because the nucleus is a speck on the atomic scale, the electron density hardly varies across it. Pull $|\psi(0)|^2$ out of the integral; only the volume integral of H_1 remains.

3.4.3 Volume integral of H_1 (line by line)

Start from Equation (3.8):

$$H_1(r) = k\left(\frac{1}{r} - \frac{3}{2R} + \frac{r^2}{2R^3}\right), \qquad k = \frac{Ze^2}{4\pi\varepsilon_0}. \tag{3.20}$$

Then

$$\begin{aligned} I &\equiv \int_{r<R} H_1\, \mathrm{d}^3 r = \int_0^R H_1(r)\, 4\pi r^2\, \mathrm{d}r \\ &= 4\pi k \int_0^R \left(r - \frac{3r^2}{2R} + \frac{r^4}{2R^3}\right) \mathrm{d}r. \end{aligned} \tag{3.21}$$

Integrate term by term:

$$\int_0^R r\, \mathrm{d}r = \frac{R^2}{2}, \tag{3.22}$$

$$\int_0^R \frac{3r^2}{2R}\, \mathrm{d}r = \frac{3}{2R} \cdot \frac{R^3}{3} = \frac{R^2}{2}, \tag{3.23}$$

$$\int_0^R \frac{r^4}{2R^3}\, \mathrm{d}r = \frac{1}{2R^3} \cdot \frac{R^5}{5} = \frac{R^2}{10}. \tag{3.24}$$

The first two contributions cancel:

$$\frac{R^2}{2} - \frac{R^2}{2} + \frac{R^2}{10} = \frac{R^2}{10}. \tag{3.25}$$

Therefore

$$I = 4\pi k \cdot \frac{R^2}{10} = \frac{2\pi}{5}\, k\, R^2 = \frac{2\pi}{5}\frac{Ze^2}{4\pi\varepsilon_0} R^2 = \frac{Ze^2 R^2}{10\,\varepsilon_0}. \tag{3.26}$$

Why the cancellation?

The $1/r$ and constant pieces of H_1 rearrange the Coulomb singularity into a finite well. Their weighted integrals over the ball cancel, leaving only the r^2 piece of the interior potential, which produces the factor $R^2/10$. That is why $\Delta E \propto R^2$, not R^3: after cancellation one power of R is lost relative to a naive volume estimate.

3.4.4 Assemble ΔE

$$\begin{aligned}\Delta E &= |\psi_{1s}(0)|^2\, I = \frac{Z^3}{\pi a_0^3} \cdot \frac{2\pi}{5} \cdot \frac{Ze^2}{4\pi\varepsilon_0} R^2 \\ &= \frac{Z^3}{\pi a_0^3} \cdot \frac{Ze^2 R^2}{10\,\varepsilon_0} \cdot \frac{2\pi}{2\pi} \\ &= \frac{Z^4 e^2 R^2}{10\pi\,\varepsilon_0\, a_0^3}.\end{aligned} \tag{3.27}$$

Final formula: $1s$ finite-size shift (uniform sphere)

$$\boxed{\Delta E_{1s} = \frac{Z^4 e^2 R^2}{10\pi\,\varepsilon_0\, a_0^3} > 0}$$

How to read the powers.

- $Z^4 = Z \cdot Z^3$: one Z from the Coulomb strength Ze^2, and Z^3 from $|\psi(0)|^2$.
- R^2: residual after the integral cancellation discussed above.
- $1/a_0^3$: denser electron cloud for smaller Bohr radius.
- Positive sign: the well is shallower, so the level moves *up* (less bound).

Example: scaling with Z and R

Compare hydrogen ($Z = 1$, $R \sim 1\,\text{fm}$) with mercury ($Z = 80$, $R \sim 7\,\text{fm}$):

$$\frac{\Delta E(\text{Hg})}{\Delta E(\text{H})} \sim 80^4 \times 7^2 \approx 4.1 \times 10^7 \times 49 \approx 2 \times 10^9.$$

Hydrogen's shift is $\sim 10^{-10}$ of $|E_{1s}|$; mercury's absolute shift is still only $\sim 0.1\,\text{eV}$, but that is measurable against a K_α energy of $\sim 100\,\text{keV}$.

3.4.5 Link to the mean-square radius

For a general spherical charge density (not necessarily uniform), the leading finite-size shift is obtained by expanding the Coulomb kernel for a localised charge and retaining the first correction beyond the monopole. With the electron density nearly constant across the nucleus,

$$\begin{aligned}\Delta E_{1s} &= |\psi_{1s}(0)|^2 \int [U_{\text{finite}}(\boldsymbol{r}) - U_{\text{point}}(\boldsymbol{r})]\,\mathrm{d}^3 r \\ &= \frac{2\pi}{3}\frac{Ze^2}{4\pi\varepsilon_0}\langle r^2\rangle_{\text{ch}}|\psi_{1s}(0)|^2,\end{aligned} \tag{3.28}$$

where the second line follows after one angular average and one radial partial integration (the same identity used in Lecture 2). For a uniform sphere,

$$\langle r^2\rangle = \frac{\int_0^R r^2 \cdot 4\pi r^2\,\mathrm{d}r}{\frac{4}{3}\pi R^3} = \frac{3}{5}R^2. \tag{3.29}$$

Inserting this into Equation (3.28) recovers Equation (3.27):

$$\frac{2\pi}{3}\,k\cdot\frac{3}{5}R^2\cdot\frac{Z^3}{\pi a_0^3} = \frac{2\pi}{5}\,kR^2\cdot\frac{Z^3}{\pi a_0^3} = \frac{Z^4e^2R^2}{10\pi\varepsilon_0 a_0^3}. \tag{3.30}$$

So the uniform-sphere calculation is a special case of a more general theorem: the leading shift measures $\langle r^2\rangle_{\text{ch}}$.

Writing E_{1s}^{point} for the unperturbed energy,

$$E_{1s} = E_{1s}^{\text{point}} + \Delta E_{1s}. \tag{3.31}$$

3.5 K_α X-rays: from levels to a measurable line

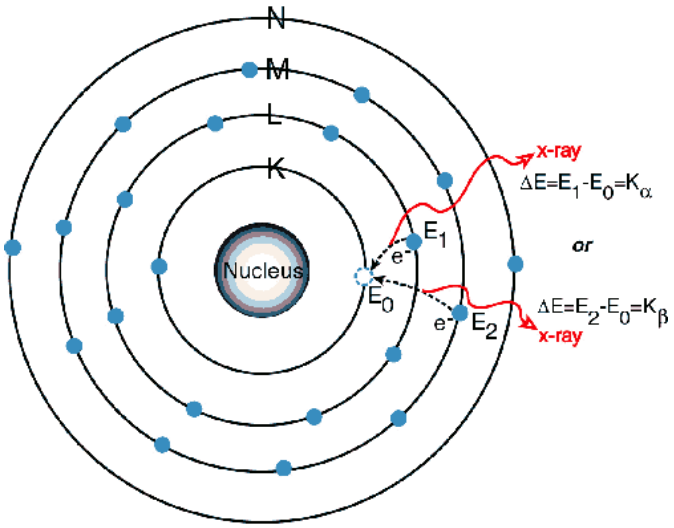

Figure 3.2: Atomic shells. A vacancy in the K shell ($1s$) is filled from a higher shell, emitting an X-ray. K_α corresponds mainly to $2p \to 1s$; K_β involves higher initial levels.

3.5.1 What is measured?

If a $1s$ electron is removed, an electron from a higher shell can drop into the vacancy. The energy difference is emitted as a characteristic X-ray (Figure 3.2). The K_α complex is dominated by $2p \to 1s$ transitions.

Historical note: Henry Moseley (1887–1915)

Henry Gwyn Jeffreys Moseley showed (1913–1914) that characteristic X-ray frequencies scale as $(Z-1)^2$, establishing Z as the true ordering parameter of the elements. That is why K_α energies are such a clean probe of nuclear charge and, through isotope shifts, of nuclear size.

3.5.2 Point-nucleus level energies

For a hydrogen-like ion,

$$E_n^{\text{point}} = -\frac{m_e Z^2 e^4}{8\varepsilon_0^2 h^2 n^2} = -\frac{Z^2}{n^2}\,\text{Ry}, \qquad \text{Ry} \approx 13.6\,\text{eV}. \tag{3.32}$$

Thus

$$E_{1s}^{\text{point}} = -Z^2\,\text{Ry}, \qquad E_2^{\text{point}} = -\frac{Z^2}{4}\,\text{Ry} \quad (\text{includes } 2p). \tag{3.33}$$

Photon energy for $2p \to 1s$. The electron falls from a less-bound level to a more-bound level. The photon energy is

$$\begin{aligned} E_{K_\alpha}^{\text{point}} &= E_2^{\text{point}} - E_{1s}^{\text{point}} \\ &= \left(-\frac{Z^2}{4} + Z^2\right)\text{Ry} = \frac{3}{4}\,Z^2\,\text{Ry}. \end{aligned} \tag{3.34}$$

(For real atoms, screening replaces Z by $\approx Z-1$, as in Moseley's law; the structure of the finite-size argument is unchanged.)

3.5.3 How ΔE_{1s} changes K_α

In non-relativistic theory, p-state wave functions vanish at $r = 0$, so their finite-size shifts are much smaller than that of $1s$. Keeping only ΔE_{1s},

$$\begin{aligned} E_{K_\alpha} &= E_2^{\text{point}} - (E_{1s}^{\text{point}} + \Delta E_{1s}) \\ &= (E_2^{\text{point}} - E_{1s}^{\text{point}}) - \Delta E_{1s} \\ &= E_{K_\alpha}^{\text{point}} - \Delta E_{1s}. \end{aligned} \tag{3.35}$$

Sign: why K_α softens

- Finite size raises E_{1s} (makes it less negative).
- E_2 is almost unchanged.
- The gap $E_2 - E_{1s}$ therefore shrinks.

- The emitted X-ray has slightly lower energy.

Key idea

$$E_{K_\alpha} = E_{K_\alpha}^{\text{point}} - \frac{Z^4 e^2 R^2}{10\pi\,\varepsilon_0\, a_0^3}.$$

Larger $R \Rightarrow$ smaller E_{K_α}.

3.6 Isotope shifts: cancelling everything except R

3.6.1 Why isotopes?

Two isotopes of the same element have:

- the *same* Z (same Coulomb strength, same electronic structure to an excellent approximation);
- *different* A, hence different nuclear radii $R(A)$.

All point-nucleus pieces of E_{K_α} cancel in a difference, and only the finite-size terms survive.

3.6.2 Algebra for two isotopes

Let the reference isotope have mass number A_0 and radius R_0, and another isotope have A and R. Then

$$E_{K_\alpha}(A_0) = E_{K_\alpha}^{\text{point}} - CR_0^2, \tag{3.36}$$
$$E_{K_\alpha}(A) = E_{K_\alpha}^{\text{point}} - CR^2, \tag{3.37}$$

where we abbreviated the positive constant

$$C \equiv \frac{Z^4 e^2}{10\pi\,\varepsilon_0\, a_0^3}. \tag{3.38}$$

Subtract:

$$\begin{aligned}\Delta E_{K_\alpha} &\equiv E_{K_\alpha}(A) - E_{K_\alpha}(A_0)\\ &= (E_{K_\alpha}^{\text{point}} - CR^2) - (E_{K_\alpha}^{\text{point}} - CR_0^2)\\ &= C(R_0^2 - R^2).\end{aligned} \tag{3.39}$$

Interpretation. If the second isotope is heavier, typically $R > R_0$, so $R_0^2 - R^2 < 0$ and $\Delta E_{K_\alpha} < 0$. The heavier isotope's K_α line lies at slightly lower energy. Experimental plots often display $-\Delta E_{K_\alpha}$ (a positive quantity that grows with A).

3.6.3 Insert $R_0 = 1.2\,\text{fm}\,A^{1/3}$

Electron-scattering systematics give the half-density radius [1]

$$R = R_0 = 1.2\,\text{fm} \times A^{1/3} \quad \Rightarrow \quad R^2 = (1.2\,\text{fm})^2\, A^{2/3}. \tag{3.40}$$

Then

$$\Delta E_{K_\alpha} = C\,(1.2\,\mathrm{fm})^2(A_0^{2/3} - A^{2/3}) = \frac{Z^4 e^2}{10\pi\,\varepsilon_0\,a_0^3}(1.2\,\mathrm{fm})^2(A_0^{2/3} - A^{2/3}). \tag{3.41}$$

Equivalently,

$$-\Delta E_{K_\alpha} = C\,(1.2\,\mathrm{fm})^2(A^{2/3} - A_0^{2/3}). \tag{3.42}$$

What to plot

Fix a reference isotope A_0. For each other isotope A, compute $-\Delta E_{K_\alpha}$ and plot it against $A^{2/3}$.

- **If the points fall on a straight line**, the data support $R \propto A^{1/3}$.
- **The slope** equals $C \times (1.2\,\mathrm{fm})^2$ if the R_0 law holds; a measured slope is a consistency check on that same coefficient.

Takeaway

Experimental checklist:

1. Measure E_{K_α} for several isotopes of one element.
2. Form shifts relative to a reference isotope.
3. Plot $-\Delta E$ versus $A^{2/3}$.
4. Linearity $\Rightarrow R \propto A^{1/3}$; slope checks $R_0 = 1.2\,\mathrm{fm}\,A^{1/3}$ from form-factor data [1].

3.6.4 Mercury data

Mercury ($Z = 80$) has several stable isotopes near $A \sim 200$. Figure 3.3 plots $-\Delta E$ against $A^{2/3}$ with ^{198}Hg as reference. The near-linearity is the experimental signature of $R \propto A^{1/3}$. Small odd–even staggering reflects pairing and slight deformation beyond the ideal spherical model.

Example: how small is the shift?

For mercury,

$$E_{K_\alpha} \sim 100\,\mathrm{keV} = 10^5\,\mathrm{eV}, \qquad |\Delta E| \sim 0.1\,\mathrm{eV} \text{ between nearby isotopes.}$$

The fractional change is

$$\frac{|\Delta E|}{E_{K_\alpha}} \sim 10^{-6}.$$

That is one part per million: tiny, but accessible to modern precision X-ray spectroscopy. The slope of the line, together with many other experiments, gives the standard $r_0 \approx 1.2\,\mathrm{fm}$.

3.7 Muonic atoms: the same maths with a heavy lepton

Electronic shifts are parts per million. Nature provides a louder version of the same calculation: replace the electron by a muon.

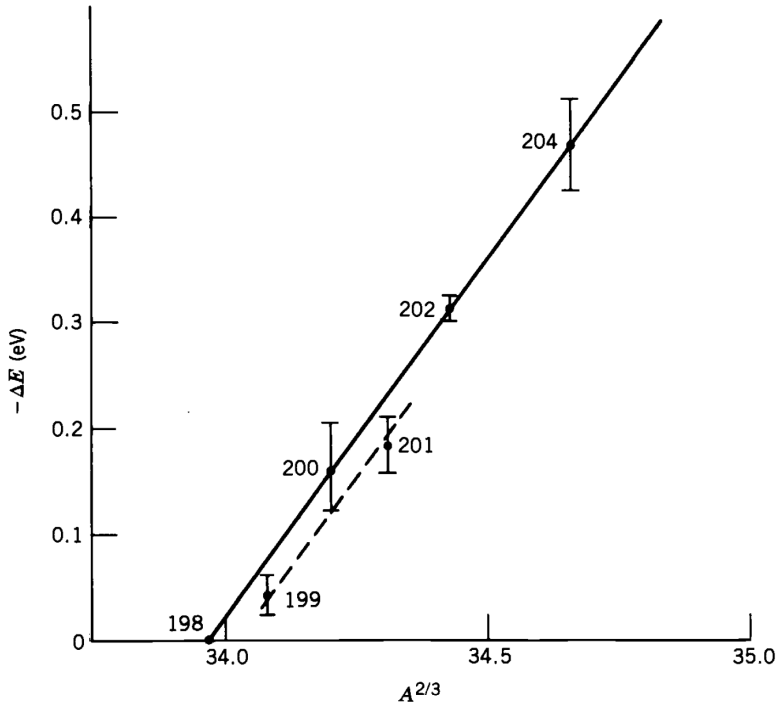

Figure 3.3: K_α isotope shifts in mercury ($Z = 80$), plotted as $-\Delta E$ versus $A^{2/3}$ relative to ^{198}Hg. Even and odd isotopes lie on nearly straight lines, as expected if $R \propto A^{1/3}$. After standard isotope-shift data, *Introductory Nuclear Physics*.

3.7.1 Muon basics

The muon μ^- has charge $-e$ and mass

$$m_\mu \approx 207\, m_e. \tag{3.43}$$

Lifetime $\tau_\mu \approx 2.2\,\mu\text{s}$ (rest frame), long enough to be captured into atomic orbits and emit X-rays before decaying ($\mu^- \to e^- \bar{\nu}_e \nu_\mu$).

Historical note: Carl D. Anderson (1905–1991)

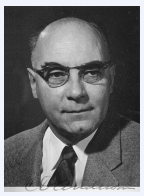

Carl David Anderson discovered the positron (1932) and the muon in cosmic rays (1936, with Neddermeyer). The muon was first mistaken for Yukawa's meson; it is in fact a heavy lepton. Anderson's particle is the probe behind modern muonic-atom determinations of nuclear charge radii.

3.7.2 How the Bohr radius scales

The Bohr radius comes from balancing Coulomb attraction against kinetic energy. With reduced mass μ of the orbiting lepton and the nucleus,

$$a_\mu = \frac{4\pi\varepsilon_0\,\hbar^2}{\mu e^2} = a_{\mathrm{B}}\,\frac{m_e}{\mu}. \tag{3.44}$$

For an electron on a heavy nucleus, $\mu \approx m_e$ and $a \approx a_\mathrm{B}$. For a muon, $\mu \approx m_\mu$ (still $\ll m_\mathrm{nucleus}$), so

$$a_\mu = a_0 \frac{m_e}{m_\mu} \approx \frac{a_0}{207}. \tag{3.45}$$

Caution

The mass ratio is ≈ 207, not 27. Hence $a_\mu = a_0/207$. Using 27 underestimates how tightly the muon is bound by almost an order of magnitude in linear size.

3.7.3 How ΔE scales for a muon

Repeat Equation (3.27) with $a_0 \to a_\mu$ and $m_e \to m_\mu$ in the wave function. The structure is unchanged:

$$\Delta E^{(\mu)} = \frac{Z^4 e^2 R^2}{10\pi\,\varepsilon_0\, a_\mu^3}. \tag{3.46}$$

Compared with the electronic shift,

$$\frac{\Delta E^{(\mu)}}{\Delta E^{(e)}} = \left(\frac{a_0}{a_\mu}\right)^3 = \left(\frac{m_\mu}{m_e}\right)^3 \approx 207^3 \approx 8.9 \times 10^6. \tag{3.47}$$

So muonic finite-size shifts are roughly *ten million times* larger in the naive scaling (before accounting for the fact that for heavy nuclei the muon orbit is so small that the constant-ψ approximation and non-relativistic theory both need upgrading).

Example: muon K-shell size in lead

Electron K radius $\sim a_0/Z$. Muon K radius $\sim a_\mu/Z = a_0/(207\,Z)$. For lead ($Z = 82$),

$$\frac{a_\mu}{Z} \approx \frac{0.529\,\text{Å}}{207 \times 82} \approx 3\,\text{fm},$$

comparable to the nuclear radius. The muon wave function overlaps the nuclear charge distribution strongly; precision $\langle r^2 \rangle$ follows from measured muonic X-ray energies.

Key idea

Same formulae, different mass: muonic atoms turn a parts-per-million electronic effect into a large, accurately measurable shift, at the price of a more careful (often relativistic, numerical) treatment for heavy Z.

Remark

For heavy nuclei one no longer pulls $|\psi(0)|^2$ out as a constant: the muon $1s$ state varies over nuclear dimensions. One then solves the Dirac equation in the electrostatic potential of a realistic $\rho(r)$ and adjusts $\langle r^2 \rangle$ (or a full density model) to match the observed transitions. The conceptual origin of the shift is still the same H_1 we built in Section 3.2.

3.8 Worked summary of the mathematics

One-page derivation map

1. $U_{\text{point}} = -\dfrac{Ze^2}{4\pi\varepsilon_0 r}$.
2. Uniform sphere $\Rightarrow U_{\text{finite}} = -\dfrac{Ze^2}{8\pi\varepsilon_0 R}(3 - r^2/R^2)$ for $r \le R$.
3. $H_1 = U_{\text{finite}} - U_{\text{point}}$ (zero outside).
4. $\Delta E = \int |\psi_{1s}|^2 H_1 \, \mathrm{d}^3 r$.
5. $e^{-2Zr/a_0} \approx 1$ on $r \le R$ because $R \ll a_0$.
6. $\Delta E \approx |\psi(0)|^2 \int H_1 \, \mathrm{d}^3 r$.
7. $\int H_1 \, \mathrm{d}^3 r = \dfrac{2\pi}{5} k R^2$ after cancellation of two terms in the radial integral.
8. $|\psi(0)|^2 = Z^3/(\pi a_0^3) \Rightarrow \Delta E = \dfrac{Z^4 e^2 R^2}{10\pi\varepsilon_0 a_0^3}$.
9. $E_{K_\alpha} = E_{K_\alpha}^{\text{point}} - \Delta E$.
10. Isotope difference $\propto (R_0^2 - R^2)$; with $R = 1.2\,\text{fm}\, A^{1/3}$, plot vs $A^{2/3}$.
11. Muon: replace $a_0 \to a_0/207$; shift grows as 207^3.

3.9 Three experimental routes to nuclear size

1. **Electron scattering** (Lectures 1–2). Maps $F(q)$ and $\rho_p(r)$; yields $R_0 = 1.2\,\text{fm}\, A^{1/3}$ and $a = 0.52\,\text{fm} \pm 0.01\,\text{fm}$ [1].
2. **Electronic K_α isotope shifts** (this lecture). $\Delta E_{1s} = Z^4 e^2 R^2/(10\pi\varepsilon_0 a_0^3)$ softens K_α; differences test $A^{1/3}$ via linearity in $A^{2/3}$.
3. **Muonic atoms**. Same maths with $a_\mu = a_0/207$; much larger shifts and precise $\langle r^2 \rangle_{\text{ch}}$.

Takeaway

The algebra is lengthy, but the physics is simple: a finite nucleus softens the Coulomb singularity, raises s-state energies by an amount $\propto Z^4 R^2$, and that shift is visible in X-rays once you compare isotopes or switch to muons. The same $R_0 = 1.2\,\text{fm}\, A^{1/3}$ that appears in electron scattering [1] reappears in the slope of the isotope-shift plot.

Next. Lecture 4 leaves size for *energy*: binding energy, the B/A curve, and the liquid-drop SEMF. Lecture 5 then turns the same mass formula into mass parabolas and β stability.

3.10 Deeper physics: comparing size probes

Lectures 1–3 measure nuclear size three ways. The results agree at the percent level only when each method quotes a carefully defined moment of ρ_{ch} [6, 1, 2].

3.10.1 Electron scattering vs atomic shifts

Probe	What is measured	Sensitivity
Elastic e^- scattering	$\lvert F(q)\rvert^2 \to \rho_{\mathrm{ch}}(r)$	Full radial profile; model-dependent at large q
Electronic K_α / optical isotope shift	$\Delta\langle r^2\rangle$ between isotopes	Relative radii; absolute scale needs calibration
Muonic atoms	Large finite-size shift $\propto m_\mu^3$	Absolute $\langle r^2\rangle_{\mathrm{ch}}$ for many Z

Muonic $1s$ levels are far more sensitive than electronic ones because the Bohr radius scales as $1/m$: $m_\mu/m_e \approx 207$ compresses the orbit by the same factor and boosts the overlap with the nucleus by $\sim 207^3$. That is why muonic X-rays became a precision tool for charge radii once muon beams were available [2, 6].

3.10.2 Mean-square radius as the universal intermediate

All three methods ultimately quote moments of ρ_{ch}. For a uniform sphere of radius R,

$$\langle r^2\rangle = \tfrac{3}{5}R^2, \tag{3.48}$$

so $R_{\mathrm{eq}} = \sqrt{5/3}\,\langle r^2\rangle^{1/2}$. Isotope-shift formulae depend on $\delta\langle r^2\rangle$, not on a model-dependent surface thickness. Electron scattering at low q measures the same $\langle r^2\rangle$ from the form-factor curvature (Lecture 1). Agreement among methods is a major empirical success of nuclear charge-density physics.

Order of magnitude for the $1s$ shift

For $Z \sim 80$ and $R \sim 7\,\mathrm{fm}$, the electronic finite-size correction to the $1s$ level is only of order eV–keV on a keV–MeV scale, yet modern X-ray and laser spectroscopy resolve isotope differences cleanly. The same algebra with $m \to m_\mu$ yields keV to MeV shifts: muonic spectroscopy is a nuclear, not atomic, measurement in disguise [6].

Key idea

Absolute shift vs isotope difference. The absolute finite-size correction $\Delta E(A,Z)$ is entangled with atomic-structure uncertainties. Differences $\Delta E(A,Z) - \Delta E(A',Z)$ cancel most of that background and isolate $\delta\langle r^2\rangle$. Electron scattering and muonic atoms calibrate the absolute scale that isotope shifts then track along a chain.

3.11 Further physics: separation energies and the isotope-shift ladder

Atomic size enters spectroscopy through level shifts; nuclear size also leaves fingerprints in the energies needed to remove a nucleon. The neutron and proton separation energies

$$S_n = [M(A-1,Z)+m_n-M(A,Z)]c^2, \qquad S_p = [M(A-1,Z-1)+m(^1\mathrm{H})-M(A,Z)]c^2 \tag{3.49}$$

are the nuclear analogues of ionisation energies: they probe valence nucleons. Sharp jumps in S_n or S_p at closed shells are shell signatures; smooth trends with A and Z follow the SEMF surface, Coulomb, and pairing terms (Lectures 4–5) [13, 6, 1].

Finite-size shifts of s levels and separation-energy systematics are complementary: both are sensitive to how tightly the outer nucleons (or the electron cloud near $r = 0$) feel the nuclear interior.

3.11.1 Mirror nuclei and a Coulomb-radius estimate

Binding-energy differences of mirror pairs provide an independent size check. For example,

$$B(^3\mathrm{H}) - B(^3\mathrm{He}) \approx 0.76\,\mathrm{MeV}$$

is largely the Coulomb energy of the two protons in ^{3}He. Writing

$$\Delta B \approx \frac{e^2}{4\pi\varepsilon_0}\left\langle\frac{1}{r_{12}}\right\rangle \sim \frac{e^2}{4\pi\varepsilon_0 R}$$

yields $R \sim 2\,\mathrm{fm}$, consistent with other light-nucleus radii [14]. Finite-size isotope shifts (this lecture) and mirror Coulomb differences are two faces of the same electrostatic physics.

3.11.2 Isotope-shift ladder: optical, K_α, and muonic

Three experimental ladders measure the same change of nuclear mean-square radius between isotopes A and A' [6, 1]:

1. **Optical isotope shifts** (valence transitions). The electron density at the nucleus is small, so shifts are tiny (parts in 10^6 of optical frequencies) but laser spectroscopy resolves them for long chains of radioactive isotopes.

2. K_α **X-ray isotope shifts.** The $2p \to 1s$ transition energy difference between isotopes is essentially the difference of $1s$ finite-size shifts, because p wave functions vanish at $r = 0$. A plot of ΔE_K versus $A^{2/3}$ is approximately linear for a sequence of isotopes [6].

3. **Muonic X rays.** The muon Bohr radius is $\sim m_e/m_\mu$ times smaller than the electronic one, so the muon spends a much larger fraction of its time inside the nucleus. Isotope shifts are correspondingly huge and dominate over many atomic-structure uncertainties.

For a uniform sphere the first-order $1s$ finite-size shift scales as

$$\Delta E_{1s} \propto Z^4\,R^2\,|\psi_{1s}(0)|^2, \tag{3.50}$$

so $\Delta E(A) - \Delta E(A') \propto R^2(A) - R^2(A')$. All three methods, after careful atomic-structure corrections, return R_0 consistent with electron scattering ($\sim 1.2\,\mathrm{fm}$).

3.11.3 Forward look: magic numbers in separation energies

Just as atomic ionisation energies jump at noble-gas Z, nuclear separation energies jump at magic N or Z:

$$N, Z = 2, 8, 20, 28, 50, 82, 126. \tag{3.51}$$

Lead isotopes show a clear discontinuity in S_n at $N = 126$ (^{208}Pb). The SEMF alone is smooth; the excess binding of magic and doubly magic nuclei relative to the liquid-drop fit is a shell-model signature that returns when single-particle potentials are discussed [14, 6]. For now it is enough that size probes and separation energies both organise the chart of nuclides before binding-energy systematics take over in Lecture 4.

3.12 Problems with solutions

Problem 3.1 — Finite-size shift for a uniform sphere

Show that for a hydrogen-like $1s$ electron and a uniform nuclear charge of radius $R \ll a_0/Z$, the first-order energy shift relative to a point nucleus is

$$\Delta E \approx \frac{2}{5}\frac{Z^4 e^2}{4\pi\varepsilon_0}\frac{R^2}{a_0^3}$$

(up to the standard hydrogenic normalisation constants; cf. Krane §3.1). Estimate ΔE for $Z = 80$, $R = 7\,\mathrm{fm}$.

Solution 3.1

Inside a uniform sphere the potential energy of an electron is

$$U_{\mathrm{finite}}(r) = -\frac{Ze^2}{8\pi\varepsilon_0 R}\left(3 - \frac{r^2}{R^2}\right), \qquad r \le R,$$

while $U_{\mathrm{point}} = -Ze^2/(4\pi\varepsilon_0 r)$. Their difference H_1 vanishes for $r > R$. With $|\psi_{1s}(0)|^2 = Z^3/(\pi a_0^3)$ nearly constant over the nucleus,

$$\int_{r<R} H_1\,\mathrm{d}^3r = \frac{2\pi}{5}\frac{Ze^2}{4\pi\varepsilon_0}R^2,$$

$$\Delta E = |\psi(0)|^2 \int H_1\,\mathrm{d}^3r = \frac{2}{5}\frac{Z^4e^2}{4\pi\varepsilon_0}\frac{R^2}{a_0^3}.$$

(The factor 2/5 is the uniform-sphere special case of the $\langle r^2\rangle = \frac{3}{5}R^2$ theorem.) For $Z = 80$, $R = 7\,\mathrm{fm} = 7\times10^{-15}\,\mathrm{m}$, $a_0 = 5.29\times10^{-11}\,\mathrm{m}$,

$$\frac{R^2}{a_0^3} \sim 4\times10^{-23}\,\mathrm{m}^{-1}, \qquad \Delta E \sim \text{eV–tens of eV}$$

on a K-shell scale of tens of keV: a small but measurable isotope-shift effect for electronic X rays, and a large effect for muons.

Problem 3.2 — Isotope shift and $A^{1/3}$

Two isotopes of the same element have mass numbers A and A' and radii $R = r_0 A^{1/3}$, $R' = r_0 (A')^{1/3}$. Argue that the difference of finite-size $1s$ shifts scales as

$$\Delta E(A) - \Delta E(A') \propto Z^4 (A^{2/3} - A'^{2/3}).$$

Why is a plot of K_α X-ray isotope shifts versus $A^{2/3}$ expected to be approximately linear?

Solution 3.2

From Problem 3.1, $\Delta E \propto Z^4 R^2$ and $R^2 \propto A^{2/3}$. Hence

$$\delta(\Delta E) \propto Z^4 (A^{2/3} - A'^{2/3}).$$

Plotting measured isotope shifts against $A^{2/3}$ (relative to a reference isotope) should be nearly linear with slope fixed by r_0. Deviations encode shell effects and deformation [6].

Problem 3.3 — Muonic enhancement

By what factor does the finite-size shift grow if the electron is replaced by a muon ($m_\mu / m_e \approx 207$), all else equal?

Solution 3.3

The Bohr radius scales as $1/\mu$, and $|\psi(0)|^2 \propto 1/a^3 \propto \mu^3$. Replacing m_e by m_μ therefore multiplies ΔE by

$$\Delta E_\mu = \left(\frac{m_\mu}{m_e} \right)^3 \Delta E_e \approx 207^3 \Delta E_e = 8.86 \times 10^6 \, \Delta E_e \sim 9 \times 10^6 \, \Delta E_e.$$

Caveat: for heavy nuclei the muon $1s$ orbit has size comparable to R, so the constant-$\psi(0)$ approximation and non-relativistic theory both need upgrading; the factor $\sim 10^7$ is the scaling estimate, not a precision prediction. Muonic K_α X-rays are a nuclear-size measurement, not an atomic one.

Chapter 4

Binding Energy and the SEMF

> *"Attempting to understand this curve of binding energy leads us to the semiempirical mass formula."*
>
> K. S. Krane

Lectures 1–3 fixed the nuclear *size*: charge densities, saturation, and finite-size shifts. This lecture turns to nuclear *energy*: how tightly nucleons stick together, and how that energy varies with A and Z. Binding energy is the mass defect of the nucleus written as an energy. The semi-empirical mass formula (SEMF) is a five-parameter model of $B(A, Z)$ that organises the chart of nuclides and the B/A curve [6, 1, 13, 14, 2].

Key idea

Binding energy is the mass defect of the nucleus written as an energy. The SEMF is a five-parameter model of $B(A, Z)$ that organises the chart of nuclides and the B/A curve.

4.1 Why not every (Z, N) combination is a nucleus?

Not every combination of protons and neutrons forms a stable (or even bound) nucleus. Ten free protons do not assemble into a long-lived $Z = 10$, $N = 0$ system; ten free neutrons do not form a stable droplet either. Here it is important to separate *existence* from *stability*. A nuclide may be bound against immediate nucleon emission yet radioactive against beta decay, alpha decay, or fission. The chart of nuclides is therefore a narrow ribbon in the (N, Z) plane: outside that ribbon, systems either beta decay toward lower-mass isobars or, beyond the drip lines, cannot bind the last nucleon at all [14, 6, 1].

Stability is a competition among three physical agents, each with a different range and different A, Z dependence:

- **short-range strong attraction** among nearest neighbours, which wants as many nucleons packed at saturation density as possible and scales roughly with the nuclear volume;
- **long-range Coulomb repulsion** among protons, which wants fewer protons at fixed A and grows roughly as Z^2/R;
- **quantum statistics and pairing**: the Pauli principle gives separate proton and neutron

Fermi seas and penalises a large imbalance $N - Z$, while an additional attractive pairing correlation favours even proton and neutron numbers.

No single force wins everywhere. Light nuclei hug $N = Z$ because asymmetry energy dominates Coulomb. Heavy nuclei drift to $N > Z$ because Coulomb grows faster with Z than the asymmetry cost of a moderate neutron excess. Far from the ribbon, the last neutron or proton is unbound: those loci are the neutron and proton drip lines predicted semi-quantitatively by the SEMF and mapped experimentally with radioactive beams [14, 1].

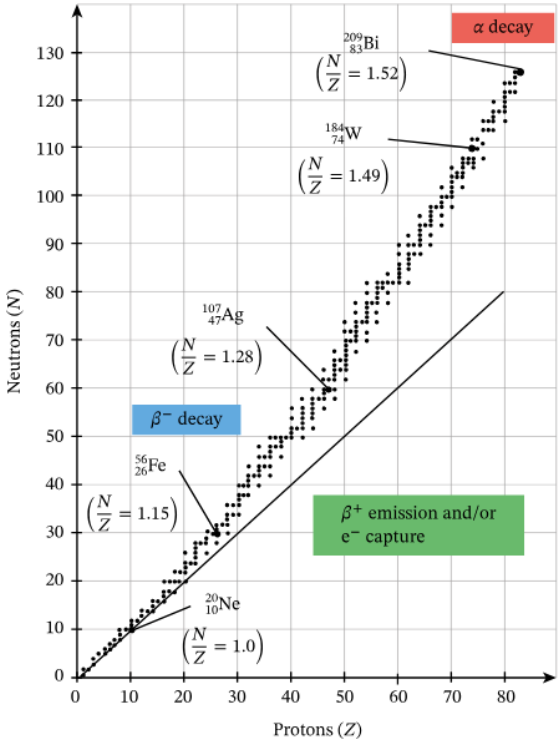

Figure 4.1: Chart of nuclides in the N–Z plane (valley of stability). Light nuclei prefer $N \approx Z$; heavy nuclei need $N > Z$. Nuclei off the valley return by $\beta^{\pm}$ (or electron capture) and, for heavy species, also by α emission; the drip lines mark where nucleon separation energies vanish.

Figure 4.1 is the experimental map we must eventually explain. Nuclei with a measured mass m are lighter than the free nucleons from which they are assembled. That mass defect is the **binding energy** B. A systematic study of $B(A, Z)$, and especially of the average B/A, leads to a few-parameter model of nuclear binding: the liquid-drop picture and the semi-empirical mass formula (SEMF) [6, 1, 2, 14]. The SEMF will not predict shell closures or spectroscopic details, but it organises why the valley exists, why $B/A \sim 8\,\mathrm{MeV}$, and why fusion and fission both release energy.

4.2 Total energy of a nucleus: derivation from rest masses

The preceding survey explains why energy comparison is the natural next step: a proposed (Z, N) combination can persist only when no allowed route leads to a lower-energy set of products. Before constructing the SEMF, we must therefore distinguish three energies that are often compressed into a single formula:

1. the rest energy of Z free protons and N free neutrons;

2. the smaller rest energy of the bound nucleus;

3. the rest energy of the neutral atom whose mass is actually tabulated.

The derivation below keeps all three ledgers explicit.

4.2.1 Separated nucleons versus a bound nucleus

Imagine first that every constituent is at rest and separated by arbitrarily large distances, so that their mutual interactions vanish. Taking this separated configuration as the reference threshold gives

$$E_{\text{free}} = Zm_pc^2 + Nm_nc^2. \tag{4.1}$$

The rest masses in Equation (4.1) already include each nucleon's internal quark and gluon energy. What is absent is the energy associated with their relative motion and their mutual nuclear and Coulomb interactions. For a nonrelativistic nuclear Hamiltonian this bookkeeping may be displayed schematically as

$$H = Zm_pc^2 + Nm_nc^2 + T_{\text{rel}} + V_{\text{strong}} + V_{\text{C}} + \cdots . \tag{4.2}$$

Here $T_{\text{rel}} > 0$, whereas the expectation value of the attractive part of V_{strong} is negative. Coulomb repulsion raises the energy. A bound state exists only when all contributions after the rest masses combine to a negative eigenvalue.

When the free nucleons assemble into a nucleus, energy is carried away by photons, emitted particles, or recoil. If the final nucleus is left in its ground state, the maximum released energy is the binding energy $B(A, Z)$. Conversely, precisely this energy must be supplied to reach the separated-nucleon threshold. Energy conservation may therefore be written

$$E_{\text{nuc}} + B = E_{\text{free}}. \tag{4.3}$$

Since the nucleus at rest has $E_{\text{nuc}} = M_{\text{nuc}}(A, Z)c^2$, it follows step by step that

$$M_{\text{nuc}}(A, Z)c^2 = Zm_pc^2 + Nm_nc^2 - B(A, Z), \tag{4.4}$$

$$B(A, Z) = \Big[Zm_p + Nm_n - M_{\text{nuc}}(A, Z)\Big]c^2. \tag{4.5}$$

Thus the *total internal-energy shift* of a bound nucleus is negative when the zero is chosen at separated nucleons:

$$E_{\text{internal}} = E_{\text{nuc}} - E_{\text{free}} = \langle T_{\text{rel}} + V_{\text{strong}} + V_{\text{C}} + \cdots \rangle = -B. \tag{4.6}$$

The binding energy B is quoted as a positive number, while the energy shift of the bound state is $-B$. These two sign conventions describe the same physics. It would be incorrect to identify $-B$ with the potential energy alone: confined nucleons have positive kinetic energy, so the attractive potential must be more negative than $-B$.

Why the minimum of total energy determines stability

At fixed $A = N + Z$, beta processes convert a neutron into a proton or a proton into a neutron. They therefore move between neighbouring isobars. The comparison must include every particle in the initial and final states. Neutral atomic masses do this bookkeeping conveniently:

$$Q_{\beta^-} = [M_{\rm at}(A,Z) - M_{\rm at}(A,Z+1)]c^2, \tag{4.7}$$

$$Q_{\beta^+} = [M_{\rm at}(A,Z) - M_{\rm at}(A,Z-1) - 2m_e]c^2, \tag{4.8}$$

$$Q_{\rm EC} \simeq [M_{\rm at}(A,Z) - M_{\rm at}(A,Z-1)]c^2, \tag{4.9}$$

apart from small electron-binding and recoil corrections. A channel is energetically open only when its Q value is positive. Thus the stable member of an isobaric chain lies at an allowed minimum of the *atomic* mass, subject also to selection rules. Lecture 5 develops this idea into the mass parabola $M(A,Z)$.

4.2.2 Binding is necessary but not sufficient for stability

Equation (4.5) answers one specific question: is the nucleus below the threshold of Z free protons plus N free neutrons? If $B > 0$, complete breakup into free nucleons costs energy. That does *not* prove that the nuclide is stable. A different partition, such as an α particle plus a daughter nucleus, may have a still lower total energy; a neighbouring isobar may be accessible through beta decay; and a heavy nucleus may lower its energy by fission. For any proposed decay

$$P \longrightarrow 1 + 2 + \cdots ,$$

the decisive quantity is

$$Q = \left(M_P - \sum_f M_f \right) c^2. \tag{4.10}$$

Positive Q means that energy conservation permits the decay, with Q becoming kinetic energy or radiation. Whether the decay is rapid then depends on the interaction involved, angular-momentum and parity selection rules, and possible barriers. Consequently:

- **bound** means below a specified breakup threshold;
- **energetically stable** means no allowed final state has lower total energy;
- **long-lived** may instead mean that a lower-energy channel exists but is strongly hindered, as in alpha decay or spontaneous fission.

4.2.3 Why experiments use atomic masses

Bare nuclear masses are less convenient experimentally than neutral atomic masses. Add the rest energy of Z free electrons to both sides of Equation (4.4):

$$M_{\rm nuc}c^2 + Zm_ec^2 = Z(m_p + m_e)c^2 + Nm_nc^2 - B. \tag{4.11}$$

Neither side is yet an atomic mass, because binding the electrons also lowers the energy. Let $B_e(Z, A) > 0$ denote the total electronic binding energy of the neutral atom. Its mass satisfies

$$M_{\text{at}}(A, Z)c^2 = M_{\text{nuc}}(A, Z)c^2 + Zm_e c^2 - B_e(Z, A). \tag{4.12}$$

For a ground-state hydrogen atom,

$$m(^1\text{H})c^2 = (m_p + m_e)c^2 - B_{\text{H}}, \qquad B_{\text{H}} = 13.6\,\text{eV}, \tag{4.13}$$

and hence

$$(m_p + m_e)c^2 = m(^1\text{H})c^2 + B_{\text{H}}. \tag{4.14}$$

Substitute Equations (4.12) and (4.13) into Equation (4.11). The exact atomic-mass relation is

$$\begin{aligned} M_{\text{at}}(A, Z)c^2 = {} & Zm(^1\text{H})c^2 + Nm_n c^2 - B(A, Z) \\ & + ZB_{\text{H}} - B_e(Z, A). \end{aligned} \tag{4.15}$$

Solving this equation for the nuclear binding energy gives

$$\begin{aligned} B(A, Z) = {} & \Big[Zm(^1\text{H}) + Nm_n - M_{\text{at}}(A, Z)\Big]c^2 \\ & + ZB_{\text{H}} - B_e(Z, A). \end{aligned} \tag{4.16}$$

This is the complete derivation of the nuclear binding energy from tabulated atomic masses. Notice that electron rest masses have not merely been discarded: they cancel because each proton on the separated side is paired with one electron to form a hydrogen atom. Only the much smaller difference between electronic *binding* energies remains.

4.2.4 Controlled approximation used in nuclear physics

The electronic correction in the second line of Equation (4.16) is small on a nuclear scale. The hierarchy is

$$\begin{aligned} & B_{\text{H}} = 13.6\,\text{eV}, \qquad B_e(Z, A) \sim \text{keV–1 MeV} \quad \text{(medium to very heavy atoms)}, \\ & B_{\text{nuc}} \sim \text{MeV–GeV}. \end{aligned} \tag{4.17}$$

Even a binding energy of tens of MeV is millions of times larger than the hydrogen ionisation energy. In heavy nuclei the nuclear binding is typically hundreds of MeV to more than a GeV, whereas total electronic binding remains at most of order MeV. Therefore, unless high-precision mass differences are required, one neglects $ZB_{\text{H}} - B_e$ and obtains

$$\boxed{B(A, Z) \simeq \Big[Zm(^1\text{H}) + Nm_n - M_{\text{at}}(A, Z)\Big]c^2.} \tag{4.18}$$

The approximation does not mean that electron binding is zero. It means that the difference of electronic binding terms is much smaller than the nuclear binding being extracted. Precision mass evaluations restore that correction when necessary.

4.3 Practical mass quantities

Section 4.2 has already established the physical meaning of B, the exact conversion between nuclear and atomic masses, and the approximation in Equation (4.18). We now use that result rather than derive it again. Throughout the remainder of this lecture, $M_{\mathrm{at}}(A, Z)$ denotes a neutral atomic mass, and $N = A - Z$.

4.3.1 Mass units and a numerical example

Atomic masses are normally quoted in unified atomic mass units. The mass–energy conversion is

$$1\,\mathrm{u}\,c^2 = 931.494\,\mathrm{MeV} \approx 931.5\,\mathrm{MeV}. \tag{4.19}$$

Thus a seemingly small mass defect of 10^{-2} u corresponds to nearly 10 MeV, which is a natural nuclear-energy scale. When the SEMF is converted into an atomic-mass formula in this lecture, we use

$$M_{\mathrm{at}}(A, Z) \simeq Zm(^1\mathrm{H}) + Nm_n - \frac{B(A, Z)}{c^2}.$$

This is an atomic-mass convention for applying the SEMF, with the electronic correction derived in Equation (4.16) neglected; the binding-energy formula itself is a model of the nucleus and does not depend on that bookkeeping choice [4].

Mass defect and B

For the α particle, the relevant mass defect is approximately $\Delta m = 0.0304\,\mathrm{u}$. Therefore

$$B = \Delta m\, c^2 \approx (0.0304\,\mathrm{u})(931.494\,\mathrm{MeV/u}) \approx 28.3\,\mathrm{MeV}.$$

Dividing by four gives $B/A \approx 7.07\,\mathrm{MeV}$, exceptionally large for so light a system. This strong binding helps explain the prominence of alpha clustering and alpha-decay products (see Problem 4.1) [6, 1, 2].

4.3.2 Mass excess

Many tables quote the **mass excess** (also called mass defect in some older tables)

$$\Delta(A, Z) \equiv [M_{\mathrm{at}}(A, Z) - A\,\mathrm{u}]c^2 \tag{4.20}$$

in MeV rather than the atomic mass itself [1, 6]. Because $A \cdot \mathrm{u}$ is an integer number of mass units, differences of mass excesses are differences of mass energies. Binding energies and Q values can be written entirely in terms of Δ's. For example, once $\Delta(^A X)$, $\Delta(^1\mathrm{H})$, and $\Delta(n)$ are known, (4.18) becomes an arithmetic combination of tabulated MeV values. We keep the mass form (4.18) in the main text for transparency.

4.3.3 Separation energies

Just as atomic ionisation energies probe the outermost electron, nucleon separation energies probe the outermost nucleon. The neutron and proton separation energies are

$$S_n(A,Z) = B(A,Z) - B(A-1,Z) = \big[M_{\mathrm{at}}(A-1,Z) + m_n - M_{\mathrm{at}}(A,Z)\big]c^2, \tag{4.21}$$

$$S_p(A,Z) = B(A,Z) - B(A-1,Z-1) = \big[M_{\mathrm{at}}(A-1,Z-1) + m(^1\mathrm{H}) - M_{\mathrm{at}}(A,Z)\big]c^2. \tag{4.22}$$

The atomic-mass bookkeeping is deliberate: $m(^1\mathrm{H})$ appears in S_p rather than m_p, so that electron masses cancel exactly as they do in B [6]. Odd–even staggering in S_n is direct evidence for pairing (pairing section below). Shell closures appear as jumps in separation energies (shell model, later). In the one-nucleon criterion, the neutron and proton drip lines occur when S_n or S_p reaches zero: adding one more nucleon no longer increases B, so the system is unbound against that emission channel. Pairing can make two-nucleon separation energies relevant as well [14, 1].

4.4 The curve of B/A: what must be explained

Because B grows roughly linearly with A, it is standard to plot the average binding energy per nucleon,

$$\frac{B}{A} = (\text{total binding energy})/(\text{number of nucleons}), \tag{4.23}$$

against A. This curve is the central experimental object of nuclear structure at the bulk level: it compresses thousands of measured masses into one smooth trend plus small ripples. Attempting to understand it leads to the SEMF, in which a few general parameters characterise how B varies with A and Z [6]. If B were strictly proportional to A, the plot would be a horizontal line at about 8 MeV; every deviation from that line is a clue about the nuclear force, nuclear geometry, or quantum statistics [1, 13].

4.4.1 Features of the experimental curve

Several remarkable features stand out on the experimental B/A curve [6, 1, 14, 13, 2, 5, 4]:

1. **Nearly constant B/A.** Except for the very lightest nuclei,

$$7.7\,\mathrm{MeV} \lesssim B/A \lesssim 8.8\,\mathrm{MeV}$$

   for stable species with $12 \lesssim A \lesssim 225$, or more loosely "between 7 and 9 MeV per nucleon." That is why one often says "about 8 MeV per nucleon." To within about 10%, most nuclei share this scale [6].

2. **Broad maximum in the iron–nickel region** ($A \sim 56$–62): the most tightly bound nuclei *per nucleon.* The smooth liquid-drop curve peaks near ^{56}Fe; precise atomic-mass data give the highest B/A at ^{62}Ni, with ^{58}Fe and ^{56}Fe only slightly lower [4, 14]. For energy release in stars and reactors, "iron peak" is the right mental picture even though the exact maximum nuclide is nickel-62.

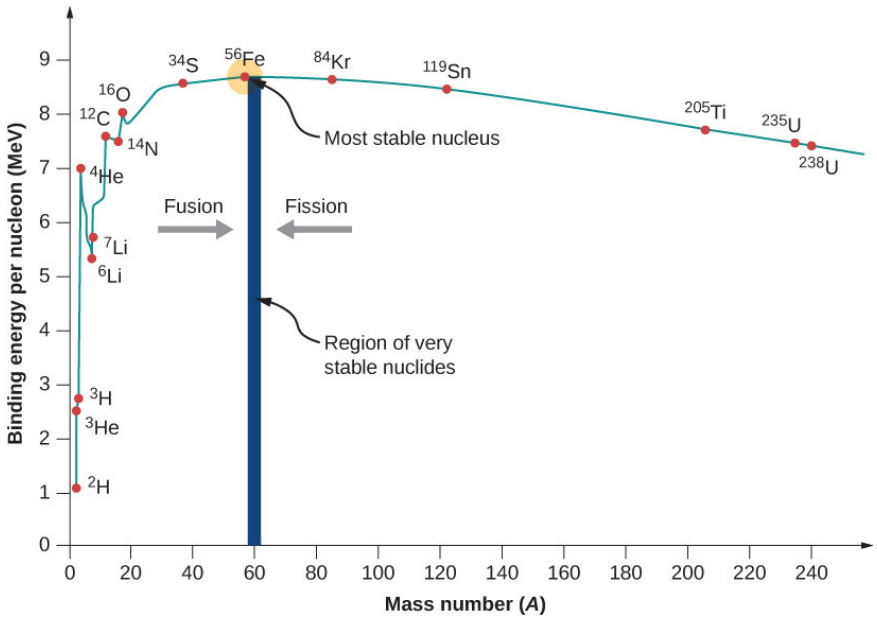

Figure 4.2: Binding energy per nucleon versus mass number. The curve is roughly flat near 8 MeV, peaks in the iron–nickel region, and falls slowly for heavy nuclei. Light $A = 4n$ species (^{4}He, ^{12}C, ^{16}O) sit above the smooth trend. Modern mass tables place the absolute maximum of B/A at ^{62}Ni, with ^{58}Fe and ^{56}Fe very close; the iron peak is the practical reference for fusion and stellar burning [6, 4].

3. **Rise at low A.** Light nuclei have a larger fraction of surface nucleons, so B/A climbs as A increases and the surface/volume ratio falls.

4. **Slow decline for heavy A.** Coulomb repulsion among many protons gradually wins; B/A falls toward uranium and beyond.

5. **Two ways to release energy.** Climbing the curve from below ($A \lesssim 56$) is fusion; climbing from above ($A \gtrsim 56$) is fission. Both increase B/A and therefore release energy. The light side of the curve is the domain of stellar nuclear burning; the heavy side is the domain of fission and α decay [14, 5, 13].

6. **Fine structure.** Odd–even staggering (pairing) and extra binding of light $A = 4n$ nuclei (α clustering: ^{4}He, ^{12}C, ^{16}O) sit on top of the smooth trend. Notably, ^{8}Be lies slightly *below* two α particles and therefore decays into them [2]. The SEMF captures the smooth part, not every shell or cluster peak.

4.4.2 Which SEMF term explains which feature?

The rest of this lecture builds the SEMF term by term. It helps to know in advance how each piece of the curve will be accounted for:

Feature on B/A	**SEMF term(s) responsible**
Nearly flat $\sim 8\,\text{MeV}$ for $12 \lesssim A \lesssim 225$	Volume $+a_V A$: short-range saturation gives $B \propto A$ and $B/A \sim a_V$ before corrections.
Rise from very light A	Surface $-a_S A^{2/3}$: at small A the surface/volume ratio is large, so $\lvert B_S\rvert/A \propto A^{-1/3}$ is a big penalty that falls as A grows.
Broad maximum near iron–nickel	Competition of surface (favours larger A) and Coulomb (favours smaller Z, hence limits growth of A for a given valley N/Z).
Slow decline past the peak	Coulomb $-a_C Z(Z-1)/A^{1/3}$: $\lvert B_C\rvert/A$ grows for heavy systems with many protons.
Valley of stability ($N \approx Z$ at light A, $N > Z$ at heavy A)	Coulomb plus asymmetry $-a_{\text{a}}(N-Z)^2/A$: Coulomb alone would push $Z \to 0$; asymmetry restores $N \sim Z$ when Coulomb is weak and permits controlled neutron excess when it is strong.
Odd–even ripples on B/A	Pairing δ: even–even nuclei gain a few hundred keV per nucleon; odd–odd lose a similar amount.
Spikes at ^{4}He, ^{12}C, ^{16}O	Beyond the SEMF: α clustering and shell structure (later chapters).

The liquid-drop model explains the *smooth* envelope. Shell and cluster effects are superimposed as corrections of order 1 MeV or less per nucleon on top of the $\sim 8\,\text{MeV}$ bulk scale [6, 1].

Key idea

First clue about the force. If every nucleon attracted every other nucleon with a long-range force, we would expect $B \propto A(A-1) \sim A^2$ and $B/A \propto A$. Experiment gives $B \propto A$ and $B/A \sim$ const. Therefore each nucleon interacts only with its nearest neighbours. Combined with constant density (Lecture 2), that is the signature of a short-range force of range comparable to the internucleon spacing [6, 1].

4.4.3 Why $B \propto A$ is surprising (and important)

A long-range force among A particles produces $\binom{A}{2} \sim A^2/2$ pairs. Gravity and Coulomb are of that type (every mass attracts every mass; every charge feels every charge). The strong residual force is not: saturated nuclear matter has fixed density and fixed coordination number, so the total binding scales with the number of particles, not the number of pairs [6, 1, 13].

From electron scattering we already know that the nuclear density is roughly constant, so each nucleon has about the same number of neighbours and contributes roughly the same amount to the binding energy [6]. The same linear behaviour is consistent with the short-range conclusions drawn from nucleon-density systematics in the previous chapters [1].

That observation is the starting point of the liquid-drop model.

4.5 The liquid-drop idea

The liquid-drop model is a *semi-empirical* model of $B(A, Z)$ [1, 6, 12, 14, 2]:

- **semi:** the algebraic form of each term is motivated by physics (geometry, electrostatics, quantum statistics);
- **empirical:** the numerical coefficients are fixed by fitting measured masses.

The idea goes back to Bohr (1935): the short range of nuclear forces, together with additivity of volumes and of binding energies, invites a liquid-drop description [14]. The same empirical fact drives the analogy from another direction: the nearly homogeneous mass density inside the nucleus suggests comparing the nucleus with a liquid drop in which the main part of the interaction is only between nearest neighbours [2]. In practice the model describes how the nuclear binding energy depends on neutron and proton number, and it is an effective way to organise the relative stability of nuclides [1].

Why a "drop"? Nuclei and classical liquid drops share

1. many constituents;
2. nearly constant interior density (incompressibility at leading order; volume $\propto A$);
3. a well-defined surface with surface tension;
4. short-range cohesion among neighbours (like molecules in a water droplet, or van der Waals cohesion in a classical liquid).

One must *not* identify the nuclear force with van der Waals forces; only the geometry of a saturating short-range interaction is borrowed [1]. The analogy is useful for energetics, not for microscopic dynamics.

The first three SEMF terms (volume, surface, Coulomb) would appear in the energy of any charged liquid droplet. The last two (asymmetry, pairing) are quantum and have no pure classical analogue: they encode Pauli filling of two fermion species and the tendency of like nucleons to form $J = 0$ pairs [6, 14, 13]. In that sense the SEMF is a first attempt to apply nuclear models to systematic behaviour: liquid-drop physics for the gross collective features, and shell/quantum ingredients for the last two terms [6].

Throughout we assume a spherical nucleus to leading order (a good approximation for most ground states near stability) and a nuclear volume directly related to A [1, 4]. Deformations and shell corrections refine that picture later; they are not needed to understand the smooth B/A curve.

4.5.1 Historical development: Gamow, Weizsäcker, Bethe

The picture of the nucleus as a charged liquid drop was developed in the early 1930s by **George Gamow**. The quantitative mass formula was written down by **Carl Friedrich von Weizsäcker** in 1935 ("Zur Theorie der Kernmassen") as the **semi-empirical mass formula**, and refined the same year by **Hans Bethe** and collaborators. The formula is therefore often called the **Bethe–Weizsäcker** (or SEMF) formula [12, 6, 1, 14, 4]. The numerical coefficients are chosen to

approximate observed ground-state binding energies; other than a_C (which is largely calculable from electrostatics), they are fixed empirically [14, 1].

Historical note: George Gamow (1904–1968)

George Gamow (born Georgiy Antonovich Gamov in Odessa) was a Soviet-American theoretical physicist and cosmologist. In the late 1920s he explained α decay as quantum tunnelling through the Coulomb barrier. In the early 1930s he developed the *liquid-drop* picture of the nucleus: nucleons packed at roughly constant density, held by a short-range attraction analogous to the cohesion of a liquid, with a surface and a Coulomb self-energy of the proton charge. That geometric intuition is the starting point of the SEMF volume, surface, and Coulomb terms. After leaving the Soviet Union he worked in the United States (George Washington University, later Colorado), co-authored the Alpher–Bethe–Gamow paper on Big Bang nucleosynthesis, and wrote celebrated popular books (*One, Two, Three... Infinity*, the Mr Tompkins series). The liquid-drop model of nuclear binding is one of his lasting contributions to nuclear physics.

Historical note: Carl Friedrich von Weizsäcker (1912–2007)

Carl Friedrich von Weizsäcker, German physicist and later philosopher, quantified Gamow's liquid-drop ideas in 1935 as the **semi-empirical mass formula**: binding energy written as a sum of volume, surface, Coulomb, and asymmetry contributions, with coefficients to be fixed by experiment [12]. His paper "Zur Theorie der Kernmassen" (Z. Phys. **96**, 431, 1935) established the algebraic structure still used today. He also worked on stellar energy generation (with Bethe) and, after the war, on the philosophy of science and the responsibility of scientists. In this course the SEMF is the Weizsäcker formula in modern notation, with standard numerical coefficients from global mass fits.

Historical note: Hans A. Bethe (1906–2005)

Hans Albrecht Bethe, German-American theoretical physicist, refined and popularised the mass formula in 1935 (hence *Bethe–Weizsäcker*). He received the 1967 Nobel Prize in Physics for the theory of energy production in stars (the CNO cycle and related work). Across a long career at Cornell he shaped nuclear and particle theory, nuclear astrophysics, and the theory of neutron stars. In the present lectures his name attaches both to the SEMF coefficients and to the stellar/compact-object applications of binding-energy systematics (Lectures 4–5).

4.6 SEMF terms derived in detail

The previous sections introduced the five SEMF terms and their historical origin. We now study each term in turn: packing for volume and surface, electrostatics for Coulomb, Fermi-gas (and shell) filling for asymmetry, and separation-energy systematics for pairing [13, 6, 1, 14, 2]. The A and Z dependence of each term reflects simple physical properties even though most numerical coefficients must be fitted [14].

4.7 Volume term: why $B_V = a_V A$

The volume term is the backbone of the B/A curve. If it were the only contribution, every nucleus would have $B/A \approx a_V/A \sim 15$–$16\,\mathrm{MeV}$ independent of A and Z. All other SEMF terms are corrections that pull the actual curve away from that flat ceiling.

4.7.1 Short-range force and nearest-neighbour counting

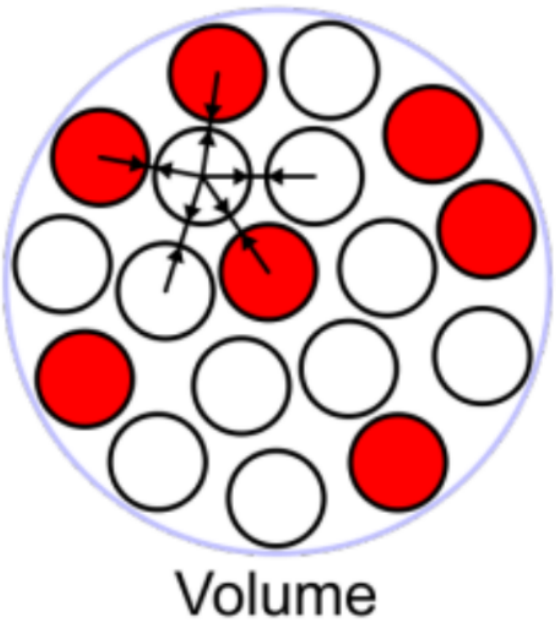

Figure 4.3: Volume (interior) nucleon. The open central circle is fully surrounded; black arrows show short-range attractive bonds to nearest neighbours (red).

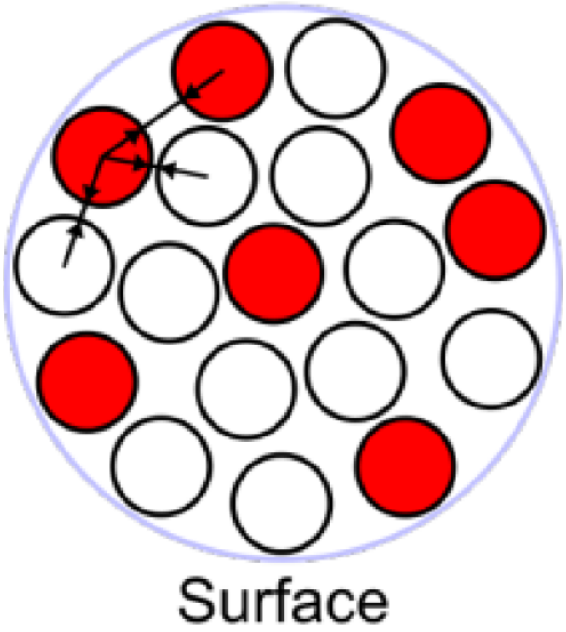

Figure 4.4: Surface nucleons (red). Some neighbour directions point outside the nucleus. Missing bonds reduce the binding energy.

Step 1 (range). The residual strong force has range $\sim$ 1–2 fm, comparable to the mean nucleon spacing but much smaller than the radius of a heavy nucleus. Therefore an interior nucleon interacts only with a fixed number of nearest neighbours, not with all other $A-1$ nucleons [6, 1, 13, 2].

Step 2 (saturated density). Electron scattering shows that the central density is nearly independent of A. Each interior nucleon therefore has roughly the *same* number of neighbours, call it n_{nn} (order ten). Constant nucleon density likewise implies $V \propto A$ and a binding contribution proportional to A for medium-to-heavy nuclei [2].

Step 3 (bond sharing). Let $U > 0$ be the attractive energy associated with one nearest-neighbour bond. Each bond is shared by two nucleons, so the contribution of bonds to the binding energy of one interior nucleon is

$$\frac{B}{A}\Big|_{\mathrm{bulk}} \approx \frac{1}{2}\, n_{\mathrm{nn}}\, U. \tag{4.24}$$

For A nucleons,

$$B_V = a_V\, A, \qquad a_V \equiv \tfrac{1}{2}\, n_{\mathrm{nn}}\, U. \tag{4.25}$$

Equivalently, without bond counting: nucleons are closely packed and the force is short ranged, so each nucleon contributes in the same way independently of the total number; the force is therefore proportional to A, not to $A(A-1)/2 \sim A^2$ [13].

In three-dimensional close packing of equal spheres, $n_{\mathrm{nn}} = 12$, so $a_V = 6U$. Fitting nuclear masses gives

$$a_V \approx 15.5\text{–}15.8\,\mathrm{MeV} \tag{4.26}$$

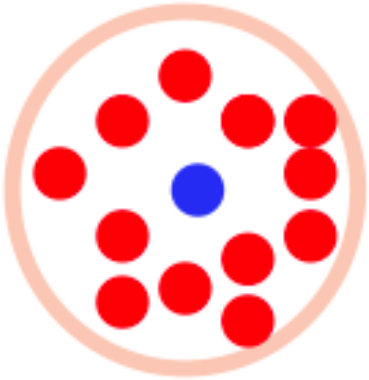

Figure 4.5: Idealised close packing: a central nucleon with twelve nearest neighbours (fcc/hcp coordination number 12).

[6, 1, 14, 13], hence a pedagogical bond scale $U \sim a_V/6 \sim 2.6\,\text{MeV}$. That U is an effective number after kinetic energy is subtracted (see below), not a bare NN potential depth. By itself the volume term would give a flat $B/A \sim 16\,\text{MeV}$; all other SEMF terms reduce that ceiling toward the observed $\sim 8\,\text{MeV}$ [14].

4.7.2 Why not A^2? (long-range would fail)

If every nucleon attracted every other, the number of pairs would be

$$\binom{A}{2} = \frac{A(A-1)}{2} \propto A^2, \tag{4.27}$$

so $B \propto A^2$ and $B/A \propto A$. Experiment shows B/A is nearly flat ($\sim 8\,\text{MeV}$) for medium-heavy nuclei. That single fact forces nearest-neighbour (volume) scaling and rules out long-range counting for the strong force [6, 1].

Checklist for the volume term

1. Force range $\ll R \Rightarrow$ only nearest neighbours.
2. Constant density $\Rightarrow$ fixed coordination number.
3. $B_V = a_V A$ (linear in A, not A^2).
4. a_V is the largest SEMF coefficient: bulk attraction sets the energy scale.

4.7.3 Why $a_V \sim 16\,\text{MeV}$, not $\sim 50\,\text{MeV}$

Scattering and few-body work suggest that the potential energy of a nucleon in nuclear matter is of order $U_{\text{pot}} \sim -40$ to $-50\,\text{MeV}$. The SEMF volume coefficient is much smaller. The resolution is that the fitted $a_V \approx 15.5\,\text{MeV}$ is smaller than the binding of a nucleon to its neighbours inferred from the strength of the nuclear interaction ($\sim 50\,\text{MeV}$): the total binding is the difference between that attraction and the kinetic energy of the nucleon itself [13]. Nucleons are fermions and fill Fermi levels up to $\varepsilon_F \sim 35\,\text{MeV}$. The mean kinetic energy per nucleon is $\frac{3}{5}\varepsilon_F \sim 21\,\text{MeV}$.

The *net* volume binding is

$$a_V \sim |U_{\text{pot}}| - \tfrac{3}{5}\varepsilon_F \sim 15\text{–}20\,\text{MeV}, \tag{4.28}$$

in agreement with the fitted a_V [13, 14]. Thus a_V already encodes the competition between short-range attraction and Fermi kinetic energy. A mean-potential estimate that yields $\sim 8\,\text{MeV}$ per nucleon after filling oscillator shells is the same physics in a shell-model language [14].

4.8 Surface term: why $-a_S A^{2/3}$

The surface term explains why B/A is *low* for the lightest nuclei and rises toward mid-mass (Section 4.4.2). Interior nucleons are fully coordinated; surface nucleons miss outward-pointing bonds. At small A almost every nucleon is a surface nucleon, so the fractional penalty $|B_S|/A \propto A^{-1/3}$ is large.

Step 1. Not every nucleon is an interior nucleon. Those on the surface (Figure 4.4) have fewer neighbours and are less tightly bound [1, 6, 13, 4]. In liquid-drop language: internal nucleons feel isotropic interactions, whereas nucleons near the surface feel forces coming only from the inside; the correction is therefore a surface-tension term [14]. Surface nucleons experience a smaller force, so the term is negative [4].

Step 2. Constant density $\Rightarrow R = r_0 A^{1/3}$. The surface area of a sphere is

$$S = 4\pi R^2 = 4\pi r_0^2\, A^{2/3} \propto A^{2/3}. \tag{4.29}$$

Equivalently, $S \propto V^{2/3}$ for a spherical nucleus [1]. The number of under-bound surface nucleons therefore scales as $A^{2/3}$.

Step 3. The volume term $a_V A$ *overcounts* the binding of surface nucleons (it pretends they have a full set of neighbours). One must subtract a correction proportional to the surface area:

$$B_S = -\,a_S\, A^{2/3}, \qquad a_S \approx 16.8\text{–}17.8\,\text{MeV}. \tag{4.30}$$

The coefficient a_S is of the same order as a_V, as expected if both come from the same short-range bonds; empirically $a_S \sim 13\text{–}18\,\text{MeV}$ [13, 14]. Together with Coulomb, the surface term limits the maximum A for which stable nuclei can exist: surface tension is literally what gives the model its name [5].

Effect on B/A.

$$\frac{B_S}{A} = -\frac{a_S}{A^{1/3}}. \tag{4.31}$$

At small A, almost all nucleons are on the surface, so B/A is strongly reduced. As A grows, surface/volume $\propto A^{-1/3}$ falls and B/A rises toward the volume ceiling. That is the main reason the experimental binding curve climbs through the light nuclei (Figure 4.10).

After volume and surface alone,

$$B \approx a_V A - a_S A^{2/3}. \tag{4.32}$$

Equation (4.32) depends only on A. It cannot explain Z dependence, the fall of B/A past iron,

or the valley of stability. Three more terms are required.

Remark

A Fermi-gas treatment of kinetic energy in a finite box also produces a surface piece $\propto A^{2/3}$ (missing states near free surfaces). The empirical a_S combines that kinetic surface correction with the missing-bond (potential) surface tension [14].

4.9 Coulomb term: why $-a_C Z(Z-1)/A^{1/3}$

Unlike the nuclear force, Coulomb repulsion is long range: every proton feels every other proton. That is why the Coulomb piece scales as $Z(Z-1)$, not as Z. It is also the main reason B/A *falls* slowly past the iron peak (Section 4.4.2) and why heavy stable nuclei need a neutron excess to dilute the proton charge [1, 6, 13, 2]. Basic electrostatics gives a potential energy for a uniform spherical distribution of Z charges proportional to $Z(Z-1)/R$; with $R \propto A^{1/3}$ this becomes the familiar SEMF Coulomb term [1]. The analytic coefficient for a sharp sphere with $r_0 = 1.2\,\text{fm}$ is $a_C = 0.72\,\text{MeV}$; one often still leaves a_C slightly free because the real charge density is diffuse near the nuclear surface [1, 6].

4.9.1 Combinatorial count of proton pairs

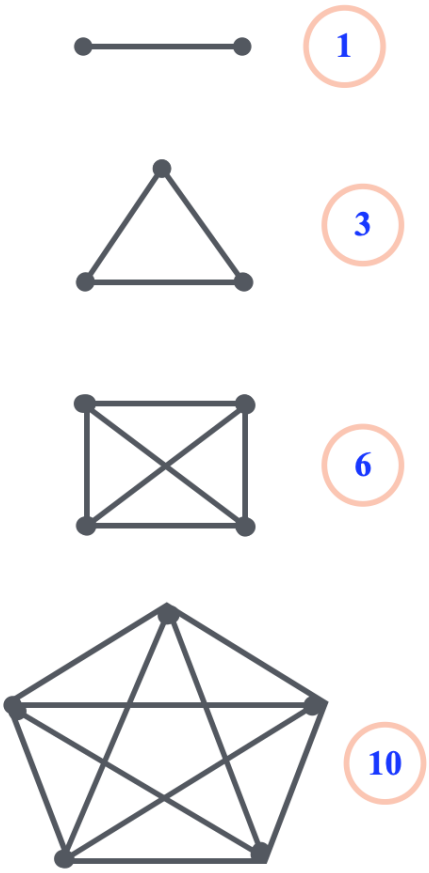

Figure 4.6: Pairwise interactions among Z protons: 2 protons $\to$ 1 link; 3 $\to$ 3; 4 $\to$ 6; 5 $\to$ 10. In general $\binom{Z}{2} = Z(Z-1)/2$. Because Coulomb is long range, every pair contributes.

Step 1 (long range). Number of distinct pp pairs:

$$\frac{Z(Z-1)}{2}. \tag{4.33}$$

Using $Z(Z-1)$ rather than Z^2 avoids counting a proton's self-repulsion [1, 6].

Step 2 (distance scale). Typical inter-proton distances scale with the nuclear radius $R \propto A^{1/3}$. Hence the Coulomb energy scales as

$$E_C \propto \frac{Z(Z-1)}{R} \propto \frac{Z(Z-1)}{A^{1/3}}. \tag{4.34}$$

4.9.2 Continuum formula: the factor $3/5$

A controlled calculation treats the nucleus as a uniformly charged sphere of charge Ze and radius R. Assemble the sphere by bringing in thin charged shells from infinity.

At intermediate radius $r \le R$, the charge already present is

$$q(r) = Ze\,\frac{r^3}{R^3}, \tag{4.35}$$

and the potential at the surface of that sphere is $q(r)/(4\pi\varepsilon_0 r)$. The work to add a shell of charge $\mathrm{d}q = Ze \cdot 3r^2\,\mathrm{d}r/R^3$ is

$$\mathrm{d}W = \frac{q(r)}{4\pi\varepsilon_0 r}\,\mathrm{d}q = \frac{1}{4\pi\varepsilon_0}\frac{Ze\,r^2}{R^3}\cdot Ze\cdot\frac{3r^2}{R^3}\,\mathrm{d}r = \frac{(Ze)^2}{4\pi\varepsilon_0}\frac{3r^4}{R^6}\,\mathrm{d}r. \tag{4.36}$$

Integrating from $r = 0$ to $r = R$,

$$\begin{aligned} E_C &= \frac{(Ze)^2}{4\pi\varepsilon_0}\frac{3}{R^6}\int_0^R r^4\,\mathrm{d}r = \frac{(Ze)^2}{4\pi\varepsilon_0}\frac{3}{R^6}\cdot\frac{R^5}{5} \\ &= \frac{3}{5}\frac{1}{4\pi\varepsilon_0}\frac{(Ze)^2}{R}. \end{aligned} \tag{4.37}$$

(The factor $3/5$ is pure geometry of a uniform sphere [13, 2, 1].)

With $R = r_0 A^{1/3}$ and $r_0 \approx 1.2\,\mathrm{fm}$,

$$\begin{aligned} a_C &= \frac{3}{5}\frac{e^2}{4\pi\varepsilon_0\, r_0} = \frac{3}{5}\frac{\hbar c\,\alpha}{r_0} \\ &\approx \frac{3}{5}\frac{197\,\mathrm{MeV\,fm}\times 1/137}{1.2\,\mathrm{fm}} \approx 0.72\,\mathrm{MeV}. \end{aligned} \tag{4.38}$$

In the SEMF one usually keeps the discrete-pair refinement

$$B_C = -\,a_C\,\frac{Z(Z-1)}{A^{1/3}}, \qquad a_C \approx 0.71\text{–}0.72\,\mathrm{MeV}. \tag{4.39}$$

(Replacing Z^2 by $Z(Z-1)$ subtracts the spurious self-energy of each proton.) Fits often leave a_C slightly free because the real charge density is not a sharp uniform sphere [1].

Physics consequences.

- $B_C < 0$: Coulomb always reduces binding relative to pure strong attraction.
- Along the valley, $Z \sim A/2$ to $A/2.5$, so $|B_C|/A$ grows roughly as $A^{2/3}$. That drives the slow *decline* of B/A for heavy nuclei.
- Coulomb alone favours $Z \to 0$ at fixed A. Nature does not: the asymmetry term restores $N \sim Z$.

Example: Coulomb cost for heavy nuclei

For $A \sim 238$, $Z \sim 92$,

$$\frac{B_C}{A} \sim -0.72 \cdot \frac{92 \cdot 91}{238^{4/3}} \sim -3\,\text{MeV},$$

a multi-MeV reduction of B/A compared with a light nucleus. Volume and surface alone cannot produce that heavy-end decline.

After volume, surface and Coulomb,

$$B = a_V A - a_S A^{2/3} - a_C \frac{Z(Z-1)}{A^{1/3}}. \tag{4.40}$$

Maximising B at fixed A still pushes $Z \to 0$. The next term stops that pathology.

4.10 Valley of stability: what Coulomb + asymmetry must explain

Figure 4.7 is the experimental map that Coulomb and asymmetry must jointly explain [6, 1, 13, 5, 14]:

1. **Light nuclei, $N \approx Z$.** Nuclear force is (approximately) charge independent. Pauli filling of two Fermi seas then prefers equal proton and neutron numbers when Coulomb is still weak. On the Segrè chart, stable nuclides hug $N \approx Z$ for $Z \lesssim 20$ [5].
2. **Heavy nuclei, $N > Z$.** Coulomb $\propto Z^2/A^{1/3}$ grows with Z. Extra neutrons dilute the proton density without adding Coulomb cost, so the valley bends above the $N = Z$ line ($N/Z \approx 1.15$ for Fe, ≈ 1.5 near Bi). Without an asymmetry term the SEMF would allow "stable isotopes of hydrogen with hundreds of neutrons" [6].
3. **Decay regions.** Neutron rich $\Rightarrow \beta^-$; proton rich $\Rightarrow \beta^+$ or EC. Very heavy systems also α decay when Coulomb has lowered B/A enough.

Without the asymmetry term, volume and surface alone place no restriction on N/Z, while Coulomb alone would drive every isobar toward $Z \to 0$. Nature does neither: the next term restores $N \sim Z$ at small A and permits only a controlled neutron excess at large A [1, 13].

Key idea

The valley is not a separate SEMF term. It is the observable balance of Coulomb (wants fewer protons) against asymmetry (wants $N = Z$).

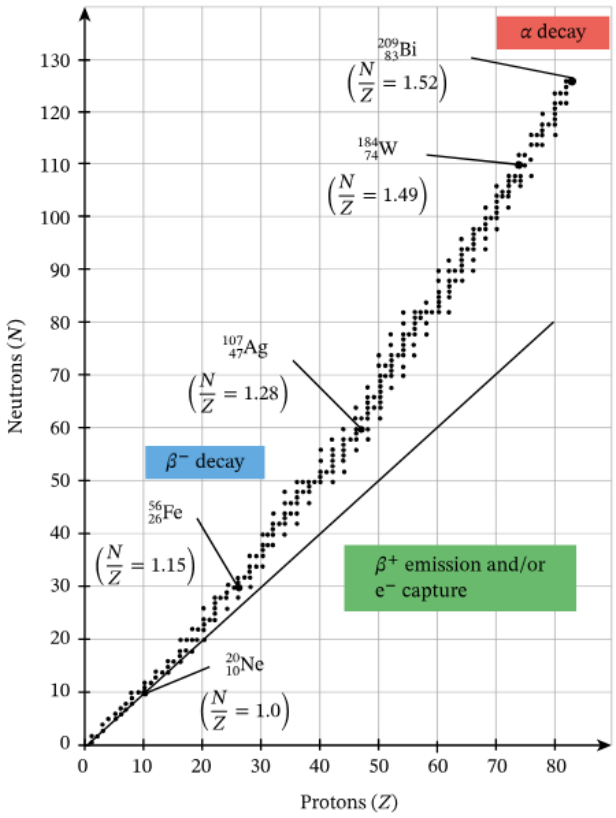

Figure 4.7: Chart of β-stable nuclides in the N–Z plane. Light systems hug $N = Z$. Heavier systems drift to $N > Z$ ($N/Z \approx 1.15$ for Fe, ≈ 1.28 for Ag, ≈ 1.49 for W, ≈ 1.52 for Bi). Neutron-rich: β^-. Proton-rich: β^+ / EC. Very heavy: α decay.

4.11 Asymmetry (symmetry) term: why $-a_{\mathrm{a}}(N-Z)^2/A$

Volume, surface, and Coulomb would allow any N/Z ratio at fixed A. Coulomb alone would drive $Z \to 0$. The asymmetry term restores $N \approx Z$ when Coulomb is weak and permits only a *controlled* neutron excess when Coulomb is strong. Together with Coulomb it shapes the valley of stability (Figure 4.7) and the mass parabolas of Lecture 5.

4.11.1 Physical picture

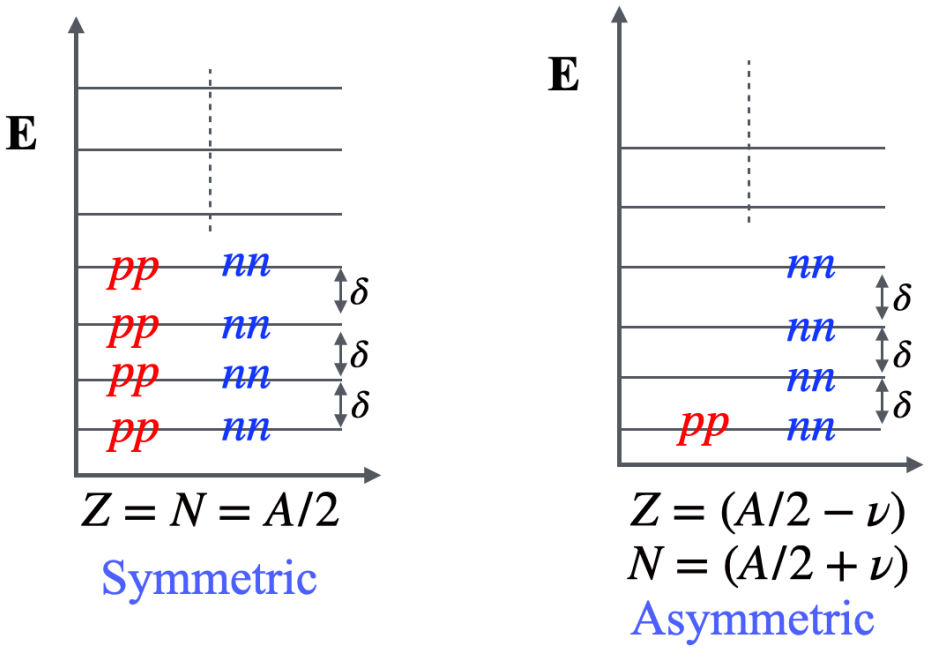

Figure 4.8: Left: symmetric filling $Z = N = A/2$. Right: asymmetric filling with extra neutrons. Excess neutrons must occupy higher single-particle levels, raising the total kinetic energy and lowering B.

Protons and neutrons are distinct fermions. Each species fills its own ladder of single-particle levels (Pauli principle) [6, 13, 14, 2, 4].

- If $N = Z$, both ladders are filled to the same height: minimal kinetic energy for given A.
- If $N > Z$, the neutron ladder is filled higher and the proton ladder lower. The extra neutrons sit in higher orbitals, so the total kinetic energy rises even though A is fixed.
- Higher energy of the system $\Rightarrow$ *smaller* binding energy B.

You cannot put excess neutrons into empty low proton levels: they are different particles. This correction (and pairing) go beyond a purely classical liquid drop: they require the quantum exclusion principle and, ultimately, the shell model [13]. A simple shell-level cartoon makes the scaling plausible: if adjacent shells are spaced by a constant δ, moving a proton up into a neutron orbital costs an energy that grows with the imbalance and yields the form $(N-Z)^2/A$ after averaging [4]. The same quadratic form follows from two Fermi gases (next subsection) [2].

4.11.2 Scaling: why $(N-Z)^2/A$

Define the neutron excess

$$\Delta \equiv N - Z = A - 2Z. \tag{4.41}$$

Two independent arguments give the same functional form.

(A) Toy ladder with spacing δ. Move $\Delta/2$ nucleons from the proton sea to the neutron sea. Each moved nucleon is raised by an energy of order $\delta \cdot (\Delta/2)$ relative to the Fermi surface, so the excess energy scales as

$$\Delta E \sim \delta \cdot \frac{\Delta^2}{4}. \tag{4.42}$$

In a large system the level density near the Fermi surface grows with A, so $\delta \sim 1/A$. Therefore

$$\Delta E \propto \frac{(N-Z)^2}{A}. \tag{4.43}$$

(B) Two Fermi gases (standard derivation). Let protons and neutrons be free Fermi gases in volume $V \propto A$, densities $\rho_p = Z/V$, $\rho_n = N/V$. The kinetic energy of one species is

$$E_{\mathrm{kin},\tau} = \frac{3}{5} N_\tau \frac{\hbar^2}{2m} (3\pi^2 \rho_\tau)^{2/3} = \frac{3}{5} N_\tau \, \varepsilon_{F,\tau}. \tag{4.44}$$

Write $N = (A/2)(1+x)$, $Z = (A/2)(1-x)$ with $x = (N-Z)/A = \Delta/A$. Because $\varepsilon_{F,\tau} \propto \rho_\tau^{2/3} \propto N_\tau^{2/3}$,

$$E_{\mathrm{kin}} = C' \left[\left(\frac{A}{2}\right)^{5/3} (1+x)^{5/3} + \left(\frac{A}{2}\right)^{5/3} (1-x)^{5/3} \right],$$

with C' fixed by the saturation Fermi energy. Expand $(1 \pm x)^{5/3} = 1 \pm \frac{5}{3}x + \frac{5}{9}x^2 + \cdots$: the odd powers cancel and

$$\begin{aligned} E_{\mathrm{kin}} &= 2C' \left(\frac{A}{2}\right)^{5/3} \left(1 + \frac{5}{9}x^2 + \cdots\right) \\ &= CA + \frac{C}{3} \frac{(N-Z)^2}{A} + \cdots, \end{aligned} \tag{4.45}$$

with $C = \frac{3}{5}\varepsilon_F$ at $N = Z$ ($\varepsilon_F \approx 35\,\mathrm{MeV}$ at saturation density). The linear (volume) piece is absorbed into a_V. The quadratic piece *raises* the energy of the nucleus and therefore *lowers* the binding:

$$B_{\mathrm{a}} = -\, a_{\mathrm{a}} \frac{(N-Z)^2}{A} = -\, a_{\mathrm{a}} \frac{(A-2Z)^2}{A}. \tag{4.46}$$

Empirical fits give

$$a_{\mathrm{a}} \approx 23\text{–}24\,\mathrm{MeV} \tag{4.47}$$

[6, 1, 14]. The pure kinetic estimate $C/3 \sim \varepsilon_F/3 \sim 12\,\mathrm{MeV}$ is only about half of the empirical value: the rest comes from isovector potential energy (the force also prefers $N = Z$). The *form* $(N-Z)^2/A$ is already fixed by the Fermi gas.

Caution

Some modern fits write $-a'(Z - A/2)^2/A$ with $a' \approx 94\,\text{MeV}$. Because $(Z - A/2)^2 = (N - Z)^2/4$, that is the same physics with a coefficient four times larger. Always check the algebraic form before copying a number [4].

Checklist for the asymmetry term

1. Vanishes when $N = Z$.
2. Grows as $(N - Z)^2$: quadratic cost of imbalance.
3. Falls as $1/A$: large systems tolerate imbalance more easily (so heavy nuclei can sit at $N > Z$).
4. Together with Coulomb, fixes N/Z along Figure 4.7.

Key idea

Asymmetry energy is mainly a kinetic (Pauli) penalty, reinforced by isovector mean fields. It is not a new fundamental force. Figure 4.8 is the picture to keep: extra neutrons climb the neutron ladder.

After Coulomb and asymmetry,

$$B = a_V A - a_S A^{2/3} - a_C \frac{Z(Z-1)}{A^{1/3}} - a_\text{a} \frac{(N-Z)^2}{A}. \tag{4.48}$$

4.11.3 Most stable Z at fixed A (preview; full derivation in Lecture 5)

Ignore pairing, treat A fixed, and minimise the atomic mass (or maximise B) with respect to Z. Balancing Coulomb against asymmetry yields the schematic result

$$Z^* \approx \frac{A/2}{1 + \kappa A^{2/3}}, \qquad \kappa \sim \frac{a_C}{4a_\text{a}} \approx 0.0075, \tag{4.49}$$

so $Z^* \approx A/2$ for light nuclei and $Z^* < A/2$ ($N > Z$) for heavy ones: the bend of Figure 4.7 [14, 1, 6, 13]. The same stationarity condition is the Z_min formula that Lecture 5 will derive carefully, including the small $m_n - m(^1\text{H})$ shift [6].

Remark

Lecture 5 starts from $M(A, Z)$, differentiates carefully with respect to Z (including $m_n - m(^1\text{H})$), obtains the working formula $Z \approx A/[2(1 + 0.0078\,A^{2/3})]$, and connects that minimum to mass-parabola figures for odd and even A.

4.12 Pairing term: why δ depends on even/odd N, Z

Pairing is the smallest of the five SEMF terms in magnitude (typically $\sim 1\,\text{MeV}$ total, or $\lesssim 0.1\,\text{MeV}$ per nucleon), but it has outsized consequences for stability. It produces the odd–even

staggering on B/A and, at fixed even A, splits the mass surface into two parabolas in Lecture 5.

4.12.1 Physical idea

Like nucleons (two protons or two neutrons) tend to form $J = 0$ pairs (opposite angular momenta). A paired configuration lies lower than an unpaired occupancy of the last orbital [6, 1, 13, 2]. Hence:

- even N (or Z): pairs complete $\Rightarrow$ extra binding;
- odd N (or Z): one unpaired nucleon $\Rightarrow$ less binding.

The odd–odd case is especially clear: when both Z and N are odd, one gains binding by converting one of the odd protons into a neutron (or vice versa) so that it can form a pair with its formerly odd partner [6]. With all other factors fixed, one must therefore *subtract* from B for odd–odd configurations and *add* for even–even ones [13]. Equivalently, two protons (or two neutrons) can occupy the same orbital with opposite spins, while an odd–odd nucleus always has an unpaired nucleon forced into the next higher level [2].

4.12.2 Experimental evidence: separation energies

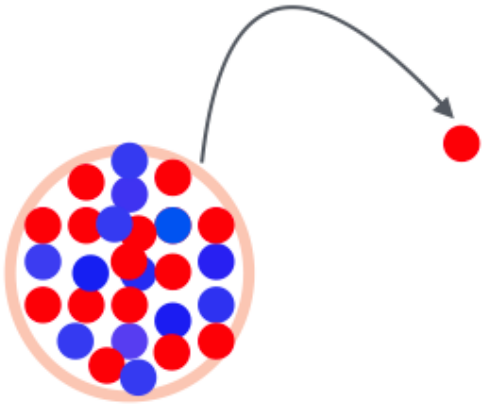

Figure 4.9: Schematic neutron separation: energy cost S_n. Even N: a pair must be broken. Odd N: the unpaired neutron is cheaper to remove.

$$S_n(A, Z) = [M(A-1, Z) + m_n - M(A, Z)]c^2, \tag{4.50}$$

$$S_p(A, Z) = [M(A-1, Z-1) + m_p - M(A, Z)]c^2. \tag{4.51}$$

Plotting S_n versus N shows a sawtooth: S_n is larger for even N (break a pair) than for odd N (remove the unpaired neutron). The same stagger appears in S_p versus Z [6, 1].

4.12.3 Census of stable nuclei

Configuration	Approx. number of β-stable nuclides
Even–even (Z even, N even)	~ 165–167
Odd A (exactly one of Z, N odd)	~ 100–110
Odd–odd (Z and N both odd)	only 4 (light)

The four stable odd–odd nuclei are ^{2}H, ^{6}Li, ^{10}B, and ^{14}N [6, 1]. Heavier odd–odd systems almost always β decay so that the unpaired proton and neutron become a like pair in an even–even daughter.

4.12.4 Pairing term in the SEMF

Taking odd-A nuclei as the baseline,

$$\delta = \begin{cases} +\,a_P\,A^{-3/4} & \text{even–even (more bound)}, \\ 0 & \text{odd } A, \\ -\,a_P\,A^{-3/4} & \text{odd–odd (less bound)}. \end{cases} \tag{4.52}$$

Typical $a_P \sim 12$–$34\,\mathrm{MeV}$ depending on whether one uses $A^{-3/4}$ or $A^{-1/2}$ [6, 1, 14, 13, 2, 4]. A common choice is $\delta = \pm 33.6\,A^{-3/4}$ for even–even / odd–odd [14]; another is $a_P A^{-1/2}\delta$ with $\delta = +1, 0, -1$ for ee / odd-A / oo [2]. The power of A is empirical; the sign pattern is not.

Caution

Sign conventions differ between sources (some write δ with the opposite overall sign in B vs M). Always verify that even–even nuclei gain binding and odd–odd nuclei lose it, and check whether a given formula fits B or M [1].

4.13 The full Weizsäcker / Bethe–Weizsäcker formula

Semi-empirical mass formula

$$B(A,Z) = a_V A - a_S A^{2/3} - a_C \frac{Z(Z-1)}{A^{1/3}} - a_{\mathrm{a}} \frac{(N-Z)^2}{A} + \delta, \tag{4.53}$$

with $N = A - Z$ and δ from Equation (4.52).

Equivalently, in atomic-mass form [4, 5, 6],

$$m(A,Z) = Z\,m(^{1}\mathrm{H}) + N\,m_n - B(A,Z)/c^2, \tag{4.54}$$

which connects the SEMF directly to tabulated masses. The Coulomb piece is sometimes written as $a_C Z^2/A^{1/3}$ (the large-Z approximation to $Z(Z-1)$); we keep $Z(Z-1)$ in (4.53) [14, 1, 6].

Coeff.	Typical value	Role	Derivation key
a_V	15.5–15.8 MeV	bulk nearest-neighbour net attraction	short range + saturation; net of Fermi KE
a_S	16.8–17.8 MeV	missing surface bonds	$S \propto R^2 \propto A^{2/3}$
a_C	≈ 0.72 MeV	proton self-energy	pairs $Z(Z-1)/2$; sphere 3/5
a_{a}	23–24 MeV	$N \neq Z$ kinetic (+ potential) penalty	two Fermi gases $\Rightarrow (N-Z)^2/A$
a_P	12–34 MeV	even–odd pairing	S_n stagger; even–even preference

A standard coefficient set that reproduces B/A well is [6, 1]

$$\begin{aligned} a_V &= 15.5\,\mathrm{MeV}, \quad a_S = 16.8\,\mathrm{MeV}, \qquad a_C = 0.72\,\mathrm{MeV}, \\ a_{\mathrm{a}} &= 23\,\mathrm{MeV}, \quad a_P = 34\,\mathrm{MeV} \qquad (\text{with } A^{-3/4}). \end{aligned} \tag{4.55}$$

Other widely used fits give $a_V = 15.75$, $a_S = 17.8$, $a_C = 0.71$, $a_{\mathrm{a}} = 23.7$ MeV [14], or nearly the same numbers (15.76, 17.81, 0.711, 23.7) [5], or $a_V \approx 15.8$, $a_S \approx 18.3$, $a_C \approx 0.71$ with pairing $\sim A^{-1/2}$ [4]. Differences of a few percent are fit choices (mass range, shell nuclei included or not), not new physics.

Remark

The SEMF is semi-empirical: the *forms* come from physics; the *numbers* are fixed by global fits to measured masses. It does not replace the shell model for magic numbers and spectroscopy, but it organises the bulk of the binding curve [6, 1]. Its importance is not that it predicts exotic new phenomena, but that it is a first successful application of nuclear models to a systematic nuclear property [6].

4.14 How the terms stack on B/A

Read Figure 4.10 from the top down at fixed A [2, 1, 13]:

How to read the B/A stack

1. **Volume (top).** Flat near $a_V \sim 15$–16 MeV. Independent of A if density and coordination number are fixed.
2. **Minus surface.** Large at small A; shrinks as $A^{-1/3}$. Explains the *rise* of net B/A from light nuclei toward iron.
3. **Minus Coulomb.** Grows with $Z^2/A^{4/3}$. Explains the *fall* of B/A past iron and the need for neutron excess.
4. **Minus asymmetry.** Extra cost when $|N-Z|$ is large. Moderate on the valley; large off it (drives β decay).
5. **Net B/A.** Peak near $A \sim 56$–62; fusion below the peak, fission above. Pairing is a small

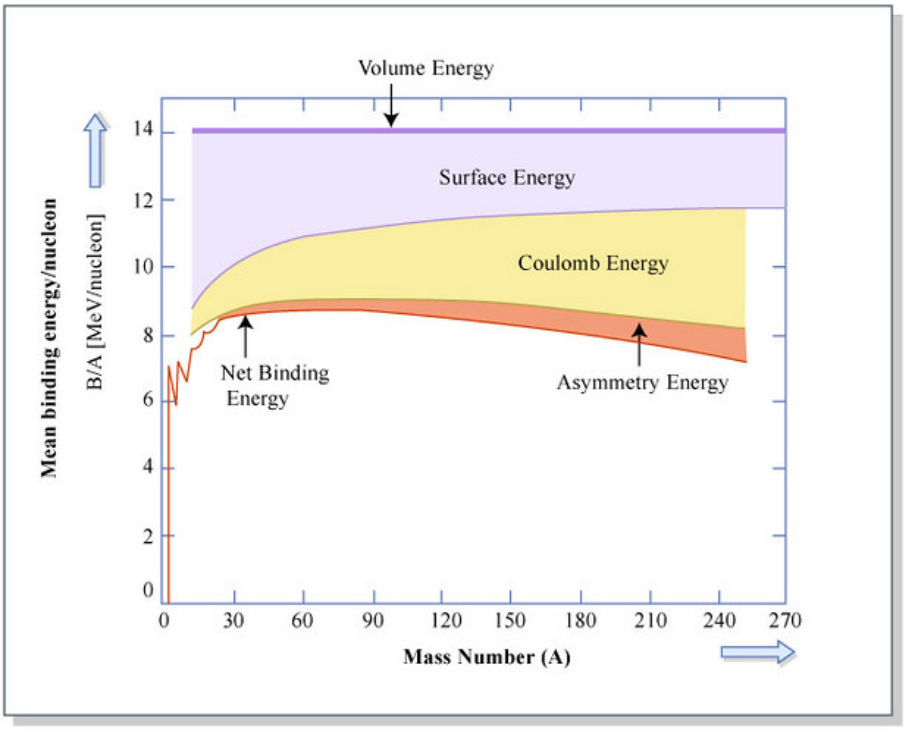

Figure 4.10: Decomposition of mean binding energy per nucleon. Top: volume ceiling. Subtract surface: rising light-A side. Subtract Coulomb: downward bend at large A. Asymmetry removes a further slice for neutron-rich heavy systems. Red: net B/A (pairing not drawn).

even–odd ripple on top.

Numerical sketch: ^{56}Fe

Use $a_V = 15.5$, $a_S = 16.8$, $a_C = 0.72$, $a_{\mathrm{a}} = 23$ (MeV) for ^{56}Fe ($A = 56$, $Z = 26$, $N = 30$):

$$\begin{aligned}
\frac{B_V}{A} &= 15.5, \\
\frac{B_S}{A} &= -\frac{16.8}{56^{1/3}} \approx -4.4, \\
\frac{B_C}{A} &= -0.72 \cdot \frac{26 \cdot 25}{56^{4/3}} \approx -1.7, \\
\frac{B_{\mathrm{a}}}{A} &= -23 \cdot \frac{(4)^2}{56^2} \approx -0.12.
\end{aligned}$$

Sum ≈ 9.3 MeV before pairing: the right order of magnitude compared with the experimental peak near 8.8 MeV. Coefficients are global fits, not exact for every nuclide.

Worked stacking: ^{100}Mo and ^{208}Pb

Take the same coefficients and valley charges $Z \approx A/[2(1 + 0.0078A^{2/3})]$: for $A = 100$, $Z \approx 43$; for $A = 208$, $Z \approx 82$.

Medium mass (^{100}Mo, $Z = 42$ for the stable isobar):

$$\frac{B_V}{A} = 15.5, \quad \frac{B_S}{A} = -\frac{16.8}{100^{1/3}} \approx -3.6, \quad \frac{B_C}{A} \approx -0.72 \cdot \frac{42 \cdot 41}{100^{4/3}} \approx -1.0,$$

$$\frac{B_\mathrm{a}}{A} \approx -23 \cdot \frac{16}{100} \approx -3.7 \quad \Rightarrow \quad B/A \approx 7.2\,\mathrm{MeV}.$$

The surface penalty is already moderate; Coulomb and asymmetry together remove $\sim 4.7\,\mathrm{MeV}$/nucleon from the volume ceiling.

Heavy nucleus (^{208}Pb, $Z = 82$, $N = 126$):

$$\frac{B_S}{A} \approx -\frac{16.8}{208^{1/3}} \approx -2.8, \quad \frac{B_C}{A} \approx -0.72 \cdot \frac{82 \cdot 81}{208^{4/3}} \approx -2.0,$$

$$\frac{B_\mathrm{a}}{A} \approx -23 \cdot \frac{44^2}{208} \approx -2.2 \quad \Rightarrow \quad B/A \approx 8.5\,\mathrm{MeV} \text{ (before pairing)}.$$

Surface is a smaller fraction of A, but Coulomb and asymmetry now dominate: the net B/A has fallen $\sim 0.3\,\mathrm{MeV}$ below the iron peak even though the volume term is unchanged. That is the liquid-drop reason heavy nuclei are less tightly bound per nucleon and why fission can release energy by moving toward mid-mass daughters.

Vertical slices at small and large A

At $A \sim 20$: surface slice is thick; Coulomb slice is thin; net B/A still climbing.
At $A \sim 200$: surface slice is thinner; Coulomb slice is thick; asymmetry is visible; net B/A has fallen below the iron maximum.
That is the physics of stellar fusion (building toward iron) and of fission reactors (splitting uranium toward the peak).

4.15 Term-by-term derivation summary

Term	Form	Why that form
Volume	$+a_V A$	short range + fixed neighbours $\Rightarrow$ linear in A, not A^2; net of Fermi KE.
Surface	$-a_S A^{2/3}$	surface nucleons under-bound; $S \propto R^2 \propto A^{2/3}$.
Coulomb	$-a_C Z(Z-1)/A^{1/3}$	long-range pairs $Z(Z-1)/2$; $R \propto A^{1/3}$; sphere factor 3/5.
Asymmetry	$-a_\mathrm{a}(N-Z)^2/A$	two Fermi seas; expand E_kin for $N \neq Z$; $\delta \sim 1/A$.
Pairing	$\delta(\mathrm{ee}/A/\mathrm{oo})$	like-nucleon pairs; S_n stagger; almost no stable odd–odd.

4.16 Deeper physics: SEMF coefficients and the B/A landscape

4.16.1 Standard coefficient sets

Fitting the liquid-drop formula to measured masses yields coefficient sets that agree at the 10% level. One convenient set is [1]

Coefficient	Typical value (MeV)	Role
a_V	15.5	volume attraction
a_S	16.8	surface deficit
a_C	0.72	Coulomb (3/5 sphere)
a_{a}	23.2	asymmetry / symmetry
a_P	34	pairing ($\pm A^{-3/4}$ or $\pm A^{-1/2}$)

A modern alternative quotes $a_V \approx 15.8$, $a_S \approx 18.3$, $a_C \approx 0.71$, $a_a \approx 23.2$–94.8 depending on the exact $(N-Z)^2/A$ normalisation, and $a_P \approx 11$–$12\,\mathrm{MeV}$ for an $A^{-1/2}$ pairing form [4]. One derives $a_C = 3e^2/(5 \cdot 4\pi\varepsilon_0 r_0)$ from the uniform-sphere Coulomb integral and recovers $a_C \sim 0.7\,\mathrm{MeV}$ for $r_0 \sim 1.2\,\mathrm{fm}$.

Caution

Coefficients are *fit parameters* to terrestrial masses near the valley of stability. Using them far from stability (drip lines) or at extreme A (neutron stars) is an extrapolation: useful for orientation, not a substitute for a microscopic EOS.

4.16.2 Features of the B/A curve that the SEMF must reproduce

1. **Rise at low A:** surface term $\propto A^{-1/3}$ dominates; light nuclei are surface-rich.
2. **Broad maximum near $A \sim 56$–62** (iron–nickel): competition of surface (wants larger A) and Coulomb (wants smaller Z, hence limits growth).
3. **Slow decline for heavy A:** Coulomb $\propto Z^2/A^{1/3}$ grows; fission becomes favourable.
4. **Odd–even staggering:** pairing; even–even nuclei sit higher in B/A.
5. **Light $A = 4n$ peaks:** α-clustering (^{4}He, ^{12}C, ^{16}O) exceeds the smooth SEMF; shell and cluster physics beyond the liquid drop [2, 6].

4.16.3 Mass defect and Q values

Any reaction or decay Q value is a difference of binding energies (or masses). Fusion of light nuclei and fission of heavy nuclei both move the system toward the iron peak and release energy:

$$Q = [B(\text{products}) - B(\text{reactants})] > 0 \tag{4.56}$$

when the products lie higher on the B/A curve. The SEMF thus organises not only stability but also the energetics of reactors and stars [1, 4].

4.17 Further physics: scales, drip lines, and limits of the SEMF

The main text derived each SEMF term. The notes below fix the *scales* of the coefficients and turn B/A into fusion, fission, and drip-line physics [6, 1, 14, 13, 2, 4, 5].

4.17.1 Coefficient sets

Coefficient	Set A	Set B	Set C
a_V (MeV)	15.5	15.75–15.76	≈ 15.8
a_S (MeV)	16.8	17.8	≈ 18.3
a_C (MeV)	0.72	0.71	≈ 0.71
a_{a} (MeV)	23	23.7	≈ 23
pairing form	$\pm a_P A^{-3/4}$	$\pm 33.6\, A^{-3/4}$	$\pm a_P A^{-1/2}$

[6, 1, 14, 5, 4]. Differences of a few percent are fit choices (which mass table, whether magic nuclei are weighted), not new physics. Always match the algebraic form of the asymmetry and pairing terms before copying a number: some fits write $(Z - A/2)^2/A$ with a coefficient four times larger than $(N - Z)^2/A$ [4, 5].

4.17.2 Fermi-gas origin of volume, surface, and asymmetry

At saturation density $n_0 \approx 0.16\,\mathrm{fm}^{-3}$ with $N \approx Z \approx A/2$ [14],

$$\varepsilon_F \approx 35\,\mathrm{MeV}, \qquad \tfrac{3}{5}\varepsilon_F \approx 21\,\mathrm{MeV}, \qquad p_F \approx 265\,\mathrm{MeV}/c. \tag{4.57}$$

A mean potential depth $U \sim -40\,\mathrm{MeV}$ then yields a net volume coefficient

$$a_V \sim |U| - \tfrac{3}{5}\varepsilon_F \sim 19\,\mathrm{MeV}, \tag{4.58}$$

close to the empirical 15–16 MeV. Expanding the kinetic energy of two Fermi gases for small $\delta = (N-Z)/A$ gives a kinetic asymmetry coefficient $\sim \varepsilon_F/3 \sim 12\,\mathrm{MeV}$; the empirical $a_{\mathrm{a}} \approx 23\,\mathrm{MeV}$ is roughly twice as large, so about half of asymmetry is potential (isovector) [14, 2].

Finite-size counting of states in a box also produces a kinetic surface term $\propto A^{2/3}$ of order 16 MeV, comparable to the empirical a_S [14]. The empirical surface coefficient therefore receives both this kinetic surface piece and the missing-bond (potential) surface tension of the liquid drop.

Thus the liquid-drop volume, surface, and asymmetry terms are not free inventions: they are the bulk, surface, and isovector pieces of a saturated Fermi liquid of nucleons.

4.17.3 Fermi-gas expansion for the asymmetry term

The kinetic energy of N_n neutrons and N_p protons in a common volume V is

$$E_K = \frac{3}{5}\,\varepsilon_F(N_n + N_p) \tag{4.59}$$

only when $N_n = N_p$. For $N_n \neq N_p$ one must use separate Fermi momenta. Setting $N_n = (A/2)(1+x)$ and $N_p = (A/2)(1-x)$ with $x = \Delta N/A$ and expanding $(1\pm x)^{5/3} = 1 \pm \frac{5}{3}x + \frac{5}{9}x^2 + \cdots$ yields [2]

$$E_K = CA + \frac{C}{3}\,\frac{(\Delta N)^2}{A} + \cdots, \tag{4.60}$$

with $C = \frac{3}{5}\varepsilon_F$ at symmetry. The first piece is absorbed into a_V; the second is precisely the asymmetry energy with a calculable kinetic coefficient. This is the derivation behind (4.46).

4.17.4 Fusion and fission Q values from B/A

Because B/A peaks near $A \sim 56$, energy is released when light nuclei fuse upward toward iron and when heavy nuclei fission downward toward iron [14, 5, 13, 6, 4]. For a reaction

$$X_1 + X_2 \to Y \qquad \text{or} \qquad X \to Y_1 + Y_2,$$

the Q value is the change in total binding energy (equivalently, the negative of the change in rest mass). The light side of the curve is the domain of stellar nuclear burning; the heavy side is the domain of fission and α decay (practically important mainly for $A \gtrsim 212$, because lifetimes are otherwise long) [14]. The SEMF, or measured mass excesses, turns the qualitative B/A argument into a number.

4.17.5 Drip lines from separation energies

Requiring the last added proton or neutron to be bound,

$$S_p > 0, \qquad S_n > 0,$$

defines the proton and neutron drip lines on the (N, Z) plane. Those lines are the boundary beyond which the last nucleon is unbound; most other combinations β or α decay toward long-lived species [14]. The SEMF predicts the drip lines semi-quantitatively; radioactive-beam experiments map the nucleus by nucleus [14, 1].

4.17.6 Pairing and mass parabolas (link to Lecture 5)

For even A, the pairing term splits the mass surface into two parabolas: even–even lower, odd–odd higher, separated by $\sim 2|\delta|$. That geometry is why some even–even nuclei can only decay by double β emission. For odd A, $\delta = 0$ and a single parabola remains [14, 6, 13, 5]. Lecture 5 makes those parabolas the main object of study.

4.17.7 What the SEMF cannot do

A few limitations should be kept in view:

- Magic numbers and shell gaps produce local spikes in B and in separation energies that the smooth SEMF misses [6, 14].
- Light $A = 4n$ cluster peaks (α, ^{12}C, ^{16}O) sit above the liquid-drop curve [2, 4].

- Coefficients fitted near the valley of stability are an extrapolation at the drip lines and a poor substitute for a microscopic EOS in neutron stars (Lecture 6) [4, 1].

The SEMF remains the right first model for the *smooth* landscape of nuclear binding.

4.18 Problems with solutions

Problem 4.1 — Binding energy of the α particle

Atomic masses (u): $m(^1\mathrm{H}) = 1.007825$, $m(n) = 1.008665$, $m(^4\mathrm{He}) = 4.002603$. Compute B and B/A for the α particle. Use $c^2 = 931.5\,\mathrm{MeV/u}$.

Solution 4.1

$$B = [2m(^1\mathrm{H}) + 2m(n) - m(^4\mathrm{He})]c^2 = (2\times 1.007825 + 2\times 1.008665 - 4.002603)\times 931.5 = 0.030377\times 931.5 \approx 28.3\,\mathrm{MeV}.$$

$$B/A \approx 7.07\,\mathrm{MeV}.$$

The α is exceptionally tightly bound for a light nucleus (cluster peak on the B/A curve) [6, 1].

Problem 4.2 — Coulomb coefficient a_C (Petrera 1.1.2)

Using classical electrostatics for a uniformly charged sphere of radius $R = r_0 A^{1/3}$ with $r_0 = 1.2\,\mathrm{fm}$, estimate the SEMF Coulomb coefficient in the term $a_C Z^2/A^{1/3}$. Take $\hbar c \approx 197\,\mathrm{MeV\,fm}$ and $\alpha \approx 1/137$.

Solution 4.2

$$E_C = \frac{3}{5}\frac{(Ze)^2}{4\pi\varepsilon_0 R} = \frac{3}{5}\frac{\alpha\,\hbar c}{r_0}\frac{Z^2}{A^{1/3}}.$$

$$a_C = \frac{3}{5}\frac{\alpha\,\hbar c}{r_0} \approx \frac{3}{5}\frac{197/137}{1.2} \approx 0.72\,\mathrm{MeV},$$

matching the usual fit [3, 6].

Problem 4.3 — B/A of ^{56}Fe from the SEMF

Use $a_V = 15.5$, $a_S = 16.8$, $a_C = 0.72$, $a_\mathrm{a} = 23\,\mathrm{MeV}$ (pairing neglected). Estimate B/A for ^{56}Fe ($Z = 26$).

Solution 4.3

$$\frac{B}{A} = a_V - \frac{a_S}{A^{1/3}} - a_C\frac{Z(Z-1)}{A^{4/3}} - a_\mathrm{a}\frac{(A-2Z)^2}{A^2}.$$

With $A = 56$, $Z = 26$, $A^{1/3} \approx 3.83$, $A - 2Z = 4$:

$$\begin{aligned} a_V &= 15.5, \\ a_S/A^{1/3} &\approx 4.39, \\ a_C Z(Z-1)/A^{4/3} &\approx 0.72 \times 650/(56 \times 3.83) \approx 2.18, \\ a_{\mathrm{a}}(A-2Z)^2/A^2 &\approx 23 \times 16/3136 \approx 0.12. \end{aligned}$$

$$B/A \approx 15.5 - 4.39 - 2.18 - 0.12 \approx 8.8\,\mathrm{MeV},$$

near the experimental iron-region maximum [6, 14].

Problem 4.4 — Volume vs surface for light and heavy nuclei

With $a_V = 15.5\,\mathrm{MeV}$ and $a_S = 16.8\,\mathrm{MeV}$, compare the volume and surface contributions to B/A for $A = 16$ and $A = 208$.

Solution 4.4

$B_V/A = a_V = 15.5\,\mathrm{MeV}$ (independent of A); $|B_S|/A = a_S A^{-1/3}$.

A	$a_S A^{-1/3}$ (MeV)	surface/volume
16	$16.8/2.52 \approx 6.7$	$\sim 43\%$
208	$16.8/5.92 \approx 2.8$	$\sim 18\%$

Light nuclei are surface-dominated; heavy nuclei are bulk-dominated [13].

Problem 4.5 — Coulomb energy of ^{208}Pb

Estimate the Coulomb self-energy of ^{208}Pb ($Z = 82$, $R = 1.2\,A^{1/3}\,\mathrm{fm}$) with the uniform-sphere formula. Give E_C in MeV and E_C/A.

Solution 4.5

$$R \approx 1.2 \times 5.92 \approx 7.1\,\mathrm{fm}, \quad E_C = a_C \frac{Z^2}{A^{1/3}} \approx 0.72 \frac{82^2}{5.92} \approx 820\,\mathrm{MeV}, \quad \frac{E_C}{A} \approx 3.9\,\mathrm{MeV}.$$

Coulomb is the main reason B/A falls for heavy nuclei [1, 6].

Problem 4.6 — Asymmetry energy of ^{208}Pb

For ^{208}Pb ($N = 126$, $Z = 82$) with $a_{\mathrm{a}} = 23\,\mathrm{MeV}$, compute the asymmetry contribution to B and to B/A.

Solution 4.6

$$E_{\mathrm{a}} = a_{\mathrm{a}}\frac{(N-Z)^2}{A} = 23\frac{44^2}{208} = 23\times 9.31 \approx 214\,\mathrm{MeV}, \qquad \frac{E_{\mathrm{a}}}{A} \approx 1.0\,\mathrm{MeV}.$$

Neutron excess costs hundreds of MeV in total binding, but only about 1 MeV per nucleon at lead [14].

Problem 4.7 — Q value for $d+d\to t+p$ (Petrera 1.3.3)

Binding energies: $B(^2\mathrm{H}) = 2.23\,\mathrm{MeV}$, $B(^3\mathrm{H}) = 8.48\,\mathrm{MeV}$. Compute the Q value of

$$^2\mathrm{H} + {}^2\mathrm{H} \to {}^3\mathrm{H} + p.$$

Also estimate the temperature needed for two deuterons to approach to 1.4 fm against Coulomb repulsion ($k_B = 8.6\times 10^{-5}\,\mathrm{eV/K}$).

Solution 4.7

Energy release equals the increase in total binding:

$$Q = B_t - 2B_d = 8.48 - 2\times 2.23 = 4.02\,\mathrm{MeV}.$$

Coulomb barrier in the rest frame of one deuteron (relative velocity $2v$):

$$4E_{\mathrm{kin}} = \frac{\alpha\,\hbar c}{R} \approx \frac{197/137}{1.4} \approx 1.0\,\mathrm{MeV} \quad\Rightarrow\quad E_{\mathrm{kin}} \approx 0.25\,\mathrm{MeV}$$

per deuteron. Scaling from $k_BT \sim 25\,\mathrm{meV}$ at 300 K,

$$T \sim 300\,\mathrm{K}\times\frac{0.25\times 10^6\,\mathrm{eV}}{25\times 10^{-3}\,\mathrm{eV}} \sim 3\times 10^9\,\mathrm{K}.$$

Fusion requires stellar temperatures [3].

Problem 4.8 — Both β modes of ^{64}Cu (Petrera 1.3.5)

Using the SEMF with $a_C = 0.697\,\mathrm{MeV}$, $a_{\mathrm{a}} = 23.3\,\mathrm{MeV}$, and $M_n - M_p - m_e = 0.782\,\mathrm{MeV}$, show that ^{64}Cu ($A = 64$, $Z = 29$) can β^- decay to ^{64}Zn and β^+ decay to ^{64}Ni. Estimate Q_{β^-} and Q_{β^+} (pairing: even–even final nuclei gain $\delta \approx 12/\sqrt{A}\,\mathrm{MeV}$ relative to odd–odd ^{64}Cu).

Solution 4.8

$$Q_{\beta^-} = (M_n - M_p - m_e) + [B(64,30) - B(64,29)],$$

$$Q_{\beta^+} = (M_p - M_n - m_e) + [B(64,28) - B(64,29)].$$

SEMF differences (Coulomb + asymmetry + pairing) give roughly [3]

$$B(64,30) - B(64,29) \approx 0, \quad B(64,28) - B(64,29) \approx 2.7\,\text{MeV},$$

so

$$Q_{\beta^-} \approx 0.78\,\text{MeV} > 0, \quad Q_{\beta^+} \approx 0.9\,\text{MeV} > 0.$$

Both branches are open; maximum $e^{\pm}$ kinetic energies equal the corresponding Q values. (Full coefficient arithmetic is in Petrera's solution key; the physics is the competition of Coulomb, asymmetry, and pairing on an odd–odd isobar.)

Chapter 5

Most Stable Z and Mass Parabolas

"For constant A, the mass formula represents a parabola of M vs Z."
K. S. Krane

5.1 Atomic mass from the SEMF

Lecture 4 constructed the binding energy $B(A, Z)$ and explained how its five terms shape the B/A curve. Stability against β decay is decided not by B alone but by the *atomic* mass $M(A, Z)$: at fixed mass number A, the isobar with the lowest mass cannot lower its energy by converting a neutron into a proton (or vice versa). Writing M as a function of Z at fixed A produces the mass parabolas of this lecture [6, 1, 14].

Key idea

From binding energy to atomic mass.

$$M(A, Z)\, c^2 = [Z\, m(^1\mathrm{H}) + (A - Z)\, m_n]c^2 - B(A, Z).$$

β decay changes Z by ± 1 at fixed A, so it moves along an isobaric slice of this surface. The SEMF turns that slice into a parabola in Z.

Key idea

Which SEMF terms matter at fixed A? When A is held constant, the volume term $a_V A$ and the surface term $a_S A^{2/3}$ are the same for every isobar and drop out of mass *differences*. What remains are:

- the free-nucleon mass piece, linear in Z through $Z\, m(^1\mathrm{H}) + (A - Z)\, m_n$;
- Coulomb, quadratic in Z;
- asymmetry, quadratic in Z through $(A - 2Z)^2$;
- pairing δ, constant on each even/odd Z ladder.

Lecture 4 fixed the bulk physics of B/A; Lecture 5 extracts the Z dependence that controls β stability.

The SEMF binding energy is

$$B(A,Z) = a_V A - a_S A^{2/3} - a_C \frac{Z(Z-1)}{A^{1/3}} - a_{\mathrm{a}} \frac{(N-Z)^2}{A} + \delta(A,Z), \tag{5.1}$$

with $N = A - Z$ and

$$\delta = \begin{cases} +a_P A^{-3/4} & \text{even–even,} \\ 0 & \text{odd } A, \\ -a_P A^{-3/4} & \text{odd–odd.} \end{cases} \tag{5.2}$$

The atomic mass energy is

$$M(A,Z)\,c^2 = \big[Z\,m(^1\mathrm{H}) + (A-Z)\,m_n\big]c^2 - B(A,Z). \tag{5.3}$$

(Using $m(^1\mathrm{H})$ rather than m_p folds the electron mass into the atomic ledger, which is what β energetics require.)

Substituting (5.1) into (5.3) makes the Z dependence explicit:

$$\begin{aligned} M(A,Z)\,c^2 =& \big[Z\,m(^1\mathrm{H}) + (A-Z)\,m_n\big]c^2 \\ & - a_V A + a_S A^{2/3} + a_C \frac{Z(Z-1)}{A^{1/3}} + a_{\mathrm{a}} \frac{(A-2Z)^2}{A} - \delta. \end{aligned} \tag{5.4}$$

Volume and surface depend only on A. Pairing is constant on each even/odd lattice of Z. The free nucleon (atomic) masses contribute a term linear in Z. Coulomb and asymmetry contribute quadratic pieces in Z.

5.2 Why $M(A,Z)$ is a parabola in Z

Expand the Z-dependent pieces at fixed A. With $N - Z = A - 2Z$,

$$\begin{aligned} a_{\mathrm{a}} \frac{(A-2Z)^2}{A} &= \frac{a_{\mathrm{a}}}{A}(A^2 - 4AZ + 4Z^2) \\ &= a_{\mathrm{a}} A - 4a_{\mathrm{a}} Z + \frac{4a_{\mathrm{a}}}{A}\,Z^2, \end{aligned} \tag{5.5}$$

and

$$a_C \frac{Z(Z-1)}{A^{1/3}} = \frac{a_C}{A^{1/3}}\,Z^2 - \frac{a_C}{A^{1/3}}\,Z. \tag{5.6}$$

The free-nucleon piece contributes $[m(^1\mathrm{H}) - m_n]c^2\,Z$. Collecting powers of Z,

$$M(A,Z)\,c^2 = \alpha(A) + \beta(A)\,Z + \gamma(A)\,Z^2 - \delta, \tag{5.7}$$

where

$$\beta(A) = \big[m(^1\mathrm{H}) - m_n\big]c^2 - 4a_{\mathrm{a}} - \frac{a_C}{A^{1/3}}, \tag{5.8}$$

$$\gamma(A) = \frac{a_C}{A^{1/3}} + \frac{4a_{\mathrm{a}}}{A} > 0. \tag{5.9}$$

(The linear asymmetry coefficient is $-4a_{\mathrm{a}}$, not $+4a_{\mathrm{a}}/A$: the latter belongs only to the quadratic piece.) The constant $\alpha(A)$ collects volume, surface, the $a_{\mathrm{a}}A$ piece, and the Am_nc^2 offset; it does not affect which Z is most stable. Because $\gamma > 0$, $M(Z)$ is a parabola opening *upward*: there is a unique minimum in Z, and nuclei far from that minimum have higher mass and can β decay toward it [6, 1].

Differentiating the quadratic form recovers the same stationarity condition used below: $\partial M/\partial Z = \beta + 2\gamma Z$, and setting that to zero with (5.8)–(5.9) reproduces (5.10).

Geometrically, Coulomb and asymmetry both contribute positive curvature ($\propto Z^2$). Coulomb raises the mass of proton-rich isobars; asymmetry raises the mass when $|N - Z|$ is large. The minimum is the compromise charge where those penalties balance, moderated by the small linear term $\beta(A)Z$ from nucleon mass differences and the linear piece of the Coulomb expansion.

The most stable isobar is the integer Z nearest the minimum of that parabola.

Key idea

At fixed A, Coulomb repulsion and asymmetry energy together make the mass a quadratic in Z. Minimising mass maximises stability against β decay.

5.3 Most stable Z: differentiation of the mass formula

5.3.1 Setting the derivative to zero

Ignore pairing for the moment (exact for odd A; for even A the pairing shifts two parallel parabolas but does not move their common $Z_{\min}$ at leading order). Start from (5.4) and differentiate with respect to Z at fixed A. Only the Z-dependent pieces contribute:

$$\frac{\partial}{\partial Z}\left[M(A,Z)\,c^2\right] = \underbrace{\left[m(^1\mathrm{H}) - m_n\right]c^2}_{\text{free-nucleon slope}} + \underbrace{a_C\frac{(2Z-1)}{A^{1/3}}}_{\text{Coulomb slope}} - \underbrace{a_{\mathrm{a}}\frac{4(A-2Z)}{A}}_{\text{asymmetry slope}}. \tag{5.10}$$

The asymmetry derivative uses $\partial(A-2Z)^2/\partial Z = -4(A-2Z)$. Setting the derivative to zero and rearranging so that positive mass-difference and Coulomb terms appear on the right-hand side,

$$\left[m_n - m(^1\mathrm{H})\right]c^2 + a_C\frac{(2Z-1)}{A^{1/3}} = 4a_{\mathrm{a}}\frac{(A-2Z)}{A}. \tag{5.11}$$

The left side favours more protons (neutrons are heavier than hydrogen atoms); the right side favours $N = Z$ through asymmetry. Coulomb enters with the $(2Z-1)$ factor from differentiating $Z(Z-1)$. Collecting terms that multiply Z,

$$Z\left(\frac{2a_C}{A^{1/3}} + \frac{8a_{\mathrm{a}}}{A}\right) = \left[m_n - m(^1\mathrm{H})\right]c^2 + \frac{a_C}{A^{1/3}} + 4a_{\mathrm{a}}, \tag{5.12}$$

and therefore the most stable charge

$$Z_{\min} = \frac{(m_n - m(^1\mathrm{H}))c^2 + a_C A^{-1/3} + 4a_{\mathrm{a}}}{2a_C A^{-1/3} + 8a_{\mathrm{a}}/A}. \tag{5.13}$$

This is the exact stationary condition for the SEMF mass parabola [6, 1]. The most stable nuclide is the integer Z closest to $Z_{\min}$.

5.3.2 Numerical size of the free-mass term

From atomic mass units,

$$m_n - m(^1\mathrm{H}) = 1.008665 - 1.007825 = 0.000840\,\mathrm{u}, \tag{5.14}$$

so

$$[m_n - m(^1\mathrm{H})]c^2 \approx 0.000840 \times 931.5 \approx 0.782\,\mathrm{MeV}. \tag{5.15}$$

With the usual coefficients $a_C = 0.72\,\mathrm{MeV}$ and $a_\mathrm{a} = 23\,\mathrm{MeV}$, for $A \sim 100$ one has

$$\frac{a_C}{A^{1/3}} \approx 0.16\,\mathrm{MeV}, \qquad \frac{4a_\mathrm{a}}{A} \approx 0.92\,\mathrm{MeV},$$

while $4a_\mathrm{a} = 92\,\mathrm{MeV}$ dominates the numerator of (5.13). The free-mass difference is not negligible next to $a_C/A^{1/3}$, but both are small compared with the asymmetry scale [6].

5.3.3 Working formula used in the lecture

Neglecting the small free-mass and linear-Coulomb pieces relative to $4a_\mathrm{a}$ in the numerator, and writing

$$Z_{\min} \approx \frac{4a_\mathrm{a}}{2a_C A^{-1/3} + 8a_\mathrm{a}/A} = \frac{A/2}{1 + \frac{1}{4}(a_C/a_\mathrm{a})\,A^{2/3}}, \tag{5.16}$$

one obtains with $a_C/a_\mathrm{a} = 0.72/23 \approx 0.0313$

$$Z_{\min} \approx \frac{A}{2(1 + 0.0078\,A^{2/3})}. \tag{5.17}$$

A closely related fit uses 0.0075 instead of 0.0078 in the denominator [14].

Key idea

Light vs heavy nuclei. For small A, $0.0078\,A^{2/3} \ll 1$, so $Z_{\min} \approx A/2$ ($N \approx Z$): oxygen, carbon, calcium. For large A the Coulomb correction grows, $Z_{\min} < A/2$, and long-lived nuclei become neutron rich ($N/Z \sim 1.5$ for lead). Equation (5.17) gives $Z/A \approx 0.41$ for heavy species, matching observation [6, 1].

A	$Z_{\min}$ (approx.)	Nearest stable Z	N/Z
16	7.6	8 (^{16}O)	1.0
40	18.3	20 (^{40}Ca)	1.0
56	25.1	26 (^{56}Fe)	1.2
125	52.3	52 (^{125}Te)	1.4
208	81.6	82 (^{208}Pb)	1.5

Values of $Z_{\min}$ come from (5.17); the nearest integer stable Z can differ by one when the parabola minimum falls between integers.

5.4 Odd A: one parabola and β decay toward the minimum

For odd A, $\delta = 0$. There is a *single* mass parabola. Nuclei with Z far from $Z_{\min}$ have large mass differences to their neighbours and decay by $\beta^{\pm}$ or electron capture; nuclei near the minimum are stable or long-lived.

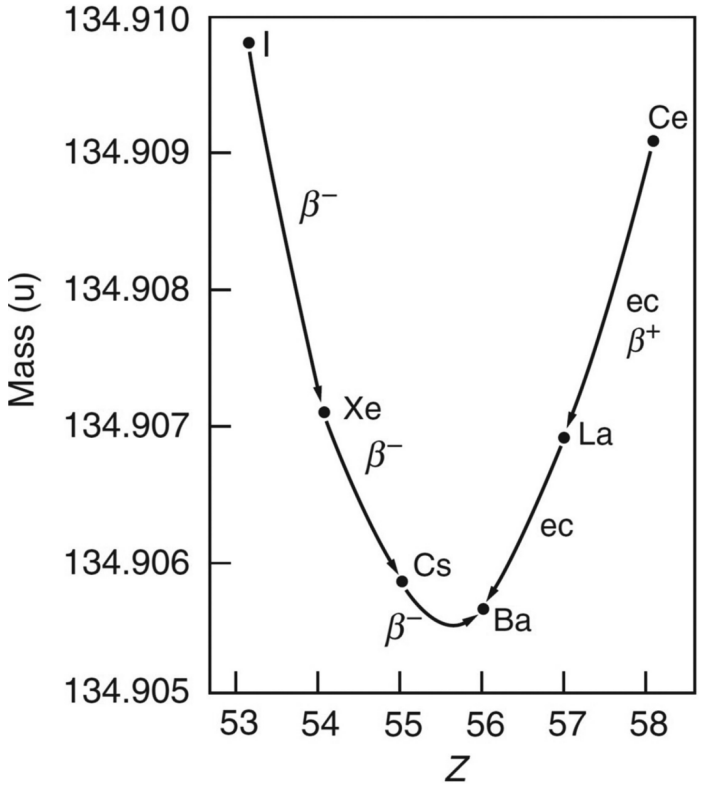

Figure 5.1: Mass parabola for odd $A = 135$ (lecture figure). One minimum near $Z = 56$; one (or few) β-stable isobar(s). Decay energy increases as one moves away from the minimum [1, 6].

5.4.1 β energetics on the parabola

Along an odd-A isobar the available energy for a single β step is the atomic mass difference of neighbouring isobars. For β^- ($Z \to Z+1$),

$$Q_{\beta^-} = [M(A,Z) - M(A,Z+1)]c^2. \tag{5.18}$$

For β^+ ($Z \to Z-1$),

$$Q_{\beta^+} = [M(A,Z) - M(A,Z-1)]c^2 - 2m_e c^2 \tag{5.19}$$

(the extra $2m_e c^2$ appears when atomic masses are used carefully for positron emission). Electron capture has a slightly lower threshold than β^+.

Because $M(Z)$ is parabolic, the mass difference between neighbours *grows* as one moves away from $Z_{\min}$. That is why β-decay Q values (and typically the decay rates) increase as one climbs the sides of the parabola [6, 1].

Key idea

Direction of β decay from geometry alone.

$Z < Z_{\min}$	neutron rich	β^- $(n \to p + e^- + \bar{\nu}_e)$,
$Z > Z_{\min}$	proton rich	β^+ or electron capture,
$Z \approx Z_{\min}$	stable / long-lived	no allowed single β.

The SEMF fixes the *direction* and approximate Q; Fermi theory fixes spectra and lifetimes.

5.5 Even A: pairing splits the mass surface into two parabolas

For even A, the pairing term shifts even–even nuclei *down* and odd–odd nuclei *up* by $|\delta| = a_P A^{-3/4}$ in the binding-energy convention of (5.1). Because $M c^2$ contains $-\delta$, the mass of an even–even isobar is lowered by $|\delta|$ and that of an odd–odd isobar is raised by $|\delta|$. The vertical separation between the two parabolas is therefore $2|\delta|$. The mass surface becomes two parallel parabolas sharing the same $Z_{\min}$ but offset in energy [6, 1, 14].

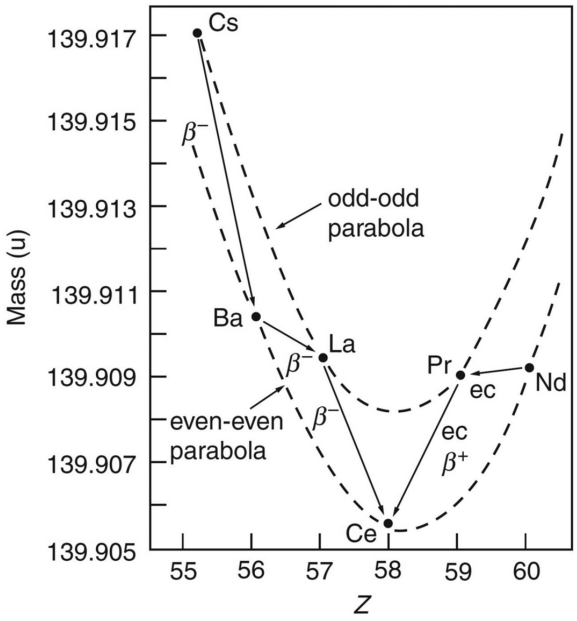

Figure 5.2: Even $A = 140$: pairing splits even–even (lower) and odd–odd (upper) chains. One β-stable even–even isobar near $Z = 58$.

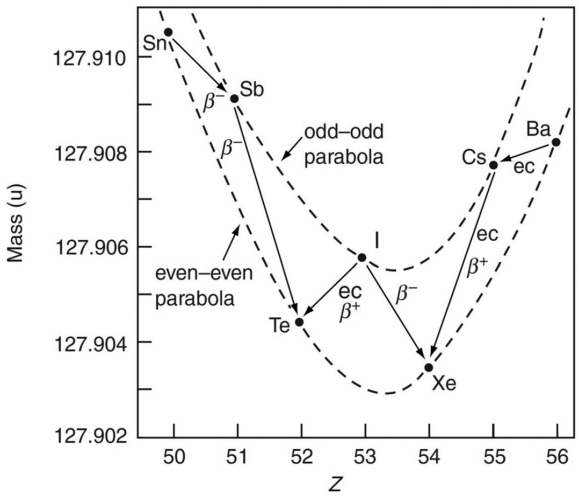

Figure 5.3: Even $A = 128$: two even–even isobars ($Z = 52, 54$) lie on the lower parabola; the odd–odd member can decay both ways. Some even–even chains are stable against *single* β but decay very slowly by double β (e.g. tellurium isotopes).

5.5.1 Two effects absent from odd-A chains

1. **Bidirectional β decay of odd–odd nuclei.** An odd–odd isobar near the minimum of the *upper* parabola can have both neighbours on the lower parabola at lower mass. Then both

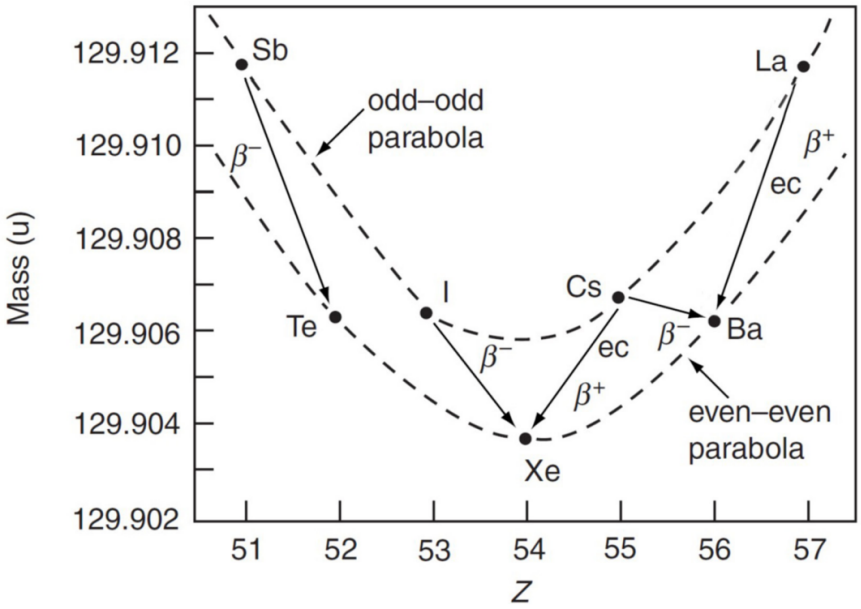

Figure 5.4: Even $A = 130$: three even–even nuclides ($Z = 52, 54, 56$) on the lower parabola can all be stable against single β decay relative to their odd–odd neighbours. Long-term evolution may still proceed by double β where $Q_{2\beta} > 0$.

β^- and β^+/EC are open. Classic example: ^{128}I can convert either a neutron or a proton to reach a more bound even–even neighbour [6, 1].

2. **Double β decay of even–even nuclei.** If single β from an even–even nucleus would land on a higher odd–odd isobar, that single step is energetically forbidden, yet a transition to a lower even–even neighbour two units of Z away can still be allowed. The nucleus may then decay only by **double beta decay** ($2\nu\beta\beta$, or the still-unseen $0\nu\beta\beta$). Candidates include ^{76}Ge, ^{128}Te, ^{130}Te, and ^{136}Xe, where single β is blocked by pairing but $Q_{2\beta} > 0$ [6, 1, 4]. Observationally, such nuclei can be extremely long lived: ^{128}Te has a $2\nu\beta\beta$ half-life of order 10^{24} yr.

Key idea

Pairing does not invent new forces; it rearranges which isobars are allowed to β decay. Odd A: one parabola, one valley. Even A: two parabolas, possible double-β and two-way decays.

5.5.2 Why light odd–odd nuclei can be stable

For small A the parabola is narrow (the coefficient $\gamma(A)$ is larger). The pairing offset can then place an odd–odd nucleus low enough to be stable against single β. The four stable odd–odd species ^{2}H, ^{6}Li, ^{10}B, ^{14}N live in that regime; heavier odd–odd nuclei almost always find an open β path to an even–even daughter [1, 6].

5.6 β Q values from the SEMF (worked structure)

Using atomic masses, the β^- energy release between neighbouring isobars is

$$Q_{\beta^-}(A,Z) = [M(A,Z) - M(A,Z+1)]c^2 = [m_n - m(^1\mathrm{H})]c^2 + B(A,Z+1) - B(A,Z) \quad (5.20)$$

(up to the usual atomic-mass bookkeeping). Substituting the SEMF, volume and surface cancel at fixed A, and one is left with Coulomb, asymmetry, and pairing differences, exactly the terms that shape the parabola [3, 14].

Similarly for β^+,

$$Q_{\beta^+}(A,Z) = [M(A,Z) - M(A,Z-1)]c^2 - 2m_e c^2, \quad (5.21)$$

so both Coulomb (fewer protons helps) and asymmetry (moving toward $N = Z$ or away from it) enter with opposite roles on the two sides of the valley.

Worked estimate: Q_{β^-} for ^{135}Cs

For odd $A = 135$, pairing vanishes and the SEMF gives a single parabola. With $a_C = 0.72$, $a_\mathrm{a} = 23$ (MeV), $Z_{\min} \approx 56$ so the valley sits near barium ($Z = 56$). Consider neutron-rich ^{135}Cs ($Z = 55$):

$$Q_{\beta^-} = [M(135,55) - M(135,56)]c^2.$$

Volume and surface cancel at fixed A. Using atomic masses in the SEMF,

$$Q_{\beta^-} \approx [m_n - m(^1\mathrm{H})]c^2 + a_C \frac{56\cdot 55 - 55\cdot 54}{135^{1/3}} + a_\mathrm{a} \frac{(135-110)^2 - (135-112)^2}{135}.$$

The free-mass piece is $+0.78\,\mathrm{MeV}$. The Coulomb piece is

$$0.72 \cdot \frac{56}{135^{1/3}} \approx 0.72 \cdot \frac{56}{5.13} \approx 7.9\,\mathrm{MeV}$$

(increasing Z costs Coulomb energy, which *reduces* Q when written as a mass difference favoring the daughter—equivalently the parent has smaller Coulomb energy). More carefully, the contribution to $M(Z) - M(Z+1)$ from Coulomb is

$$a_C A^{-1/3}[Z(Z-1) - (Z+1)Z] = -a_C A^{-1/3}(2Z) = -0.72 \cdot \frac{110}{5.13} \approx -15.4\,\mathrm{MeV}.$$

The asymmetry contribution to $M(Z) - M(Z+1)$ is

$$a_\mathrm{a} A^{-1}[(A-2Z)^2 - (A-2Z-2)^2] = a_\mathrm{a} A^{-1}[4(A-2Z) - 4] \approx 23 \cdot \frac{4\cdot 25 - 4}{135} \approx 16.6\,\mathrm{MeV}.$$

Altogether

$$Q_{\beta^-} \approx 0.78 - 15.4 + 16.6 \approx 2.0\,\mathrm{MeV}.$$

The measured value is $Q \sim 1.3\,\mathrm{MeV}$: the SEMF captures the direction and the MeV scale,

not every keV [6, 1]. The positive sign confirms β^- decay of neutron-rich ^{135}Cs toward ^{135}Ba.

Physics checklist for an isobar

1. Compute $Z_{\min}(A)$ from (5.17) (or (5.13)).
2. For odd A: one parabola; the integer Z nearest $Z_{\min}$ is stable; others β decay toward it with Q increasing up the sides.
3. For even A: draw two parabolas split by $\sim 2|\delta|$; identify even–even minima and any odd–odd bidirectional cases; mark possible double-β pairs.
4. Q_β follows from mass differences on that surface, with no weak matrix element required for the *sign* of the decay.

5.7 Connecting the valley of stability

Plotting the integer nearest to $Z_{\min}(A)$ for each A traces the valley of stability on the (N, Z) plane: $N \approx Z$ at low A, bending to $N > Z$ at high A. Lectures 4–5 therefore close the liquid-drop programme: binding energy and its Z landscape, including the β arrows that keep real nuclei near the valley [6, 1, 13].

5.8 Deeper physics: exact $Z_{\min}$ and isobar energetics

5.8.1 Complete mass formula in nuclear masses

The same parabola follows from writing the atomic mass with nuclear constituents,

$$M(A,Z) = (A-Z)m_n + Z(m_p+m_e) - \frac{a_V A}{c^2} + \frac{a_S A^{2/3}}{c^2} + \frac{a_C Z(Z-1)}{c^2 A^{1/3}} + \frac{a_{\mathrm{a}}(A-2Z)^2}{c^2 A} - \frac{\delta}{c^2}, \quad (5.22)$$

which differs from (5.4) only by the usual $m(^1\mathrm{H})$ versus m_p+m_e bookkeeping. Setting $\partial M/\partial Z = 0$ yields

$$Z_{\min} = \frac{(m_n - m_p - m_e)c^2 + a_C A^{-1/3} + 4a_{\mathrm{a}}}{2a_C A^{-1/3} + 8a_{\mathrm{a}}/A}, \quad (5.23)$$

equivalent to (5.13). The free-mass difference $(m_n - m_p - m_e)c^2 \approx 0.78\,\mathrm{MeV}$ is small next to $4a_{\mathrm{a}} \sim 90\,\mathrm{MeV}$; dropping it and the linear Coulomb piece recovers (5.17) [1].

Why heavy nuclei need extra neutrons

Coulomb pushes $Z_{\min}$ below $A/2$. Each missing proton relative to $A/2$ is replaced by a neutron, so $N - Z = A - 2Z_{\min}$ grows with A. The asymmetry term fights that growth; equilibrium is the compromise in (5.23). Without Coulomb, $Z_{\min} = A/2$ exactly (up to the tiny $m_n - m_p$ shift).

5.8.2 Parabola accuracy and Q_β residuals

At fixed A, the SEMF reproduces mass *differences* between neighbouring isobars to within a few hundred keV for medium-mass nuclei once the overall offset is fixed by the lowest isobar. Shell corrections and pairing details appear as residuals of order 0.5–1 MeV [14, 6]. Near $Z_{\min}$ the Q_β values are therefore small; far up the parabola they grow, setting the scale for Fermi-theory spectra in a later chapter.

5.9 Further physics: atomic minimum and chart systematics

5.9.1 Atomic mass minimum and the 0.78 MeV shift

Stability against β decay is decided by the *atomic* mass, not the bare nuclear mass. Minimising $M_{\text{atom}}(A, Z)$ includes the neutron–hydrogen mass difference $\delta_{nH} = (m_n - m(^1\text{H}))c^2 \approx 0.78\,\text{MeV}$ in $Z_{\min}$. Light nuclei slightly favour protons relative to a pure $N = Z$ Fermi-gas estimate, while Coulomb still forces $N > Z$ for heavy systems [14, 6].

5.9.2 Odd A one parabola; even A two

For odd A (pairing zero) masses follow one parabola in Z. For even A, even–even and odd–odd species form two parabolas split by $\sim 2|\delta|$. Double-β candidates sit on the even–even curve when single β would land on the higher odd–odd curve [14, 5, 13, 1].

A useful illustration is $A = 112$: ^{112}Sn and ^{112}Cd can both be stable against single β on the lower even–even parabola, while intermediate odd–odd ^{112}In lies higher and can decay both ways [14].

5.9.3 Systematics on the chart of nuclides

On the (N, Z) plane:

- nuclei *below* the valley (neutron excess) decay by β^-;
- nuclei *above* the valley (proton excess) decay by β^+ or electron capture;
- the valley bends toward $N > Z$ as A grows, as $Z_{\min}(A) < A/2$.

Plotting the integer nearest to $Z_{\min}(A)$ reproduces the valley curve seen on the chart of nuclides in Lecture 4.

5.10 Problems with solutions

Problem 5.1 — Evaluate $Z_{\min}$

Using $Z_{\min} = A/[2(1 + 0.0078\,A^{2/3})]$, compute $Z_{\min}$ for $A = 100$ and $A = 200$. For each, give N/Z at that charge.

Solution 5.1

For $A = 100$, $A^{2/3} \approx 21.54$,

$$Z_{\min} = \frac{50}{1 + 0.0078 \times 21.54} = \frac{50}{1.168} \approx 42.8 \quad \Rightarrow \quad \frac{N}{Z} \approx \frac{57.2}{42.8} \approx 1.34.$$

For $A = 200$, $A^{2/3} \approx 34.2$,

$$Z_{\min} = \frac{100}{1 + 0.0078 \times 34.2} = \frac{100}{1.267} \approx 78.9 \quad \Rightarrow \quad \frac{N}{Z} \approx \frac{121}{79} \approx 1.53.$$

Heavy nuclei are neutron rich [6].

Problem 5.2 — Free-mass difference

Show that $(m_n - m(^1\mathrm{H}))c^2 \approx 0.782\,\mathrm{MeV}$ using $m_n = 1.008665\,\mathrm{u}$, $m(^1\mathrm{H}) = 1.007825\,\mathrm{u}$, and $c^2 = 931.5\,\mathrm{MeV/u}$. Where does this number enter $Z_{\min}$?

Solution 5.2

$$(1.008665 - 1.007825) \times 931.5 = 0.000840 \times 931.5 \approx 0.782\,\mathrm{MeV}.$$

It appears in the numerator of the exact $Z_{\min}$ formula (5.13) as the free-mass drive toward protons; it is small compared with $4a_{\mathrm{a}} \approx 92\,\mathrm{MeV}$ [6, 14].

Problem 5.3 — Q_{β^-} sign on the parabola

At fixed odd A, $M(Z)$ is a parabola with minimum at $Z_{\min}$. Show that $Q_{\beta^-} = [M(Z) - M(Z+1)]c^2 > 0$ for all integers $Z < Z_{\min} - 1/2$, so neutron-rich isobars β^- decay toward the minimum.

Solution 5.3

Write $M(Z) = \alpha - \beta Z + \gamma Z^2$ with $\gamma > 0$. Then

$$M(Z) - M(Z+1) = \beta - \gamma(2Z + 1).$$

The minimum of M is at $Z_{\min} = \beta/(2\gamma)$, so

$$M(Z) - M(Z+1) = 2\gamma(Z_{\min} - Z - \tfrac{1}{2}).$$

For $Z \leq Z_{\min} - 1$ (integer steps below the vertex), this difference is positive: $Q_{\beta^-} > 0$. Geometry alone forces β^- on the neutron-rich side [6, 1].

Problem 5.4 — Pairing split and double β

Even–even and odd–odd mass parabolas at fixed even A are split by $2|\delta|$ with $|\delta| = a_P A^{-3/4}$. For $A = 128$ and $a_P = 34\,\mathrm{MeV}$, estimate the vertical split $2|\delta|$. Explain in one sentence

why an even–even nucleus can be stable against single β yet unstable against double β.

Solution 5.4

$$A^{3/4} = 128^{0.75} \approx (2^7)^{0.75} = 2^{5.25} \approx 38, \quad |\delta| \approx 34/38 \approx 0.9\,\text{MeV}, \quad 2|\delta| \approx 1.8\,\text{MeV}.$$

Single β would land on the higher odd–odd parabola, so $Q_\beta < 0$ for that step, while a jump of $\Delta Z = 2$ to a lower even–even neighbour can still have $Q_{2\beta} > 0$ [6, 1].

Problem 5.5 — Both β modes (Petrera-style)

For odd–odd ^{64}Cu near mid-mass, explain qualitatively why both β^- (to ^{64}Zn) and β^+ (to ^{64}Ni) can be open, using the two-parabola picture.

Solution 5.5

^{64}Cu sits on the upper (odd–odd) parabola. Both even–even neighbours ^{64}Ni and ^{64}Zn lie on the lower parabola and can be lower in mass than ^{64}Cu. Then both Q_{β^-} and Q_{β^+} are positive: bidirectional decay. Quantitative SEMF estimates give $Q \sim 1\,\text{MeV}$ for both branches [3, 6].

Chapter 6

SEMF and Neutron Stars

> *"The same short-range force that saturates $B/A \sim 8\,\mathrm{MeV}$ cannot bind pure neutrons; only gravity at stellar mass can."*
>
> after Weizsäcker; Bethe (SEMF)

6.1 The puzzle: pure neutrons fail on Earth

The SEMF was built for ordinary nuclei near the valley of stability. If one asks what happens for pure neutron matter, $Z = 0$, the volume and asymmetry terms no longer cancel in a favourable way: the nuclear terms alone leave pure neutrons unbound. Laboratory nuclei never form a stable drop of neutrons.

Nature nevertheless produces compact stellar remnants that are mostly neutrons in the bulk, with masses of order a solar mass and radii of order ten kilometres. Gravity, negligible on the fermi scale of a single nucleus, becomes the leading long-range attraction at $A \sim 10^{56}$–10^{57}. This chapter extrapolates the liquid-drop idea to that extreme and recovers the solar-mass, ten-kilometre scale of neutron stars as an order-of-magnitude estimate [1, 4, 6].

6.1.1 Nuclear landscape and the neutron drip line

Lecture 5 fixed the most stable Z at fixed A. The chart of nuclides (Figure 6.1; cf. Lectures 4–5) also shows, for each Z, a maximum N that still binds. Beyond that **neutron drip line**,

$$S_n(A, Z) = \big[M(A-1, Z) + m_n - M(A, Z)\big]c^2 \leq 0, \tag{6.1}$$

and the last neutron is unbound (Lecture 4 separation-energy language). Even the dineutron is unbound; few-neutron systems are unstable. Protons, and the Coulomb–asymmetry balance of Lectures 4–5, are essential for ordinary nuclei.

From the SEMF alone, pure neutron matter ($Z = 0$, $N = A$) has

$$\frac{B}{A} \approx a_V - a_\mathrm{a} \approx 15.5 - 23 \approx -7.5\,\mathrm{MeV} < 0 \tag{6.2}$$

(neglecting surface for large A). Asymmetry wins: liquid-drop nuclear physics alone *forbids* a stable pure-neutron drop of any laboratory size.

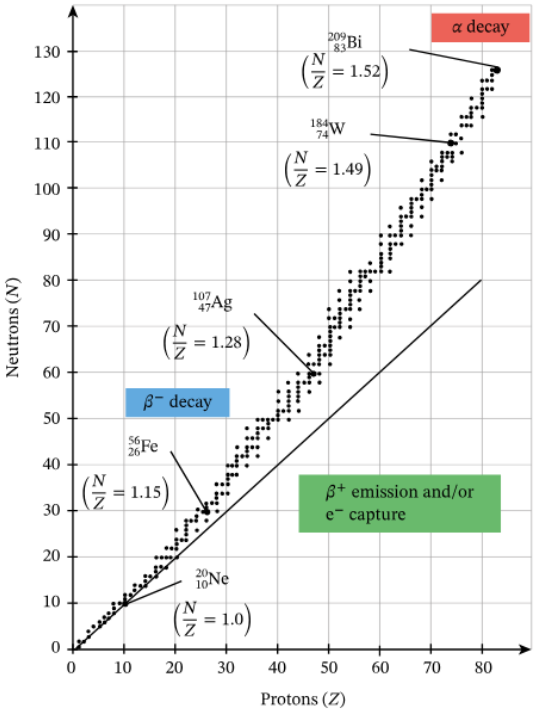

Figure 6.1: Nuclear landscape (valley of stability). For each Z only a limited band of N is bound. Beyond the neutron drip line, $S_n \leq 0$ and neutrons unbind. Laboratory nuclei never reach pure-neutron bulk matter.

6.1.2 Neutron stars exist anyway

Nature produces compact remnants that are mostly neutrons in the bulk (with a thin outer crust of nuclei and a small proton fraction in the core). Observed scales:

Quantity	Typical value
Mass	$\sim$ (1–2) $M_\odot$
Radius	$\sim$ 10–15 km
Mean density	$\sim$ (2–3) ρ_0 (nuclear saturation)
Nucleon number	$A \sim 10^{57}$ for $M \sim M_\odot$

That is $\sim 10^{55}$ times more nucleons than uranium, in a city-sized volume. The SEMF question: *how can such an object be bound when few neutrons are not?*

6.2 Birth of a neutron star

A compact sketch is enough for this nuclear course [4]:

1. Gas clouds collapse under gravity; fusion begins when the core is hot and dense (H $\rightarrow$ He in the Sun).

2. In stars several times heavier than the Sun, fusion proceeds through He, C, O, ... up to the iron-group peak of B/A (Lecture 4). Fusion past iron does not release net energy.

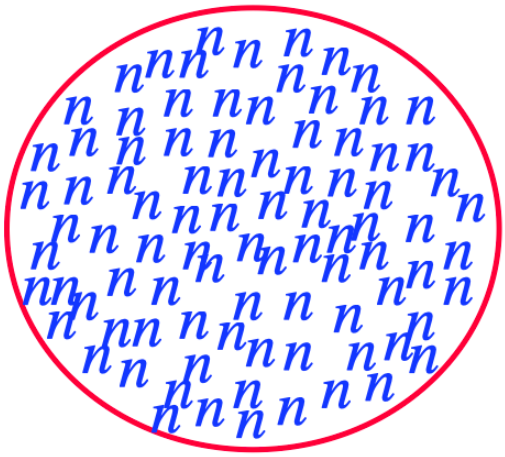

Figure 6.2: Schematic pure-neutron bulk (lecture cartoon). The star is not a giant laboratory nucleus: gravity and quantum degeneracy dominate the global energy and support balance.

3. When nuclear burning can no longer support the core, gravity wins: rapid collapse, bounce, and a core-collapse supernova that ejects the envelope.

4. In the residual core, electron Fermi energies become so high that inverse β decay (electron capture)

$$p + e^- \to n + \nu_e$$

converts most protons into neutrons. Neutrinos escape; the remnant cools into a neutron star.

Why inverse β wins at high density. In free space, $m_n c^2 - m_p c^2 \approx 1.3\,\mathrm{MeV}$ and free neutrons β^- decay. Inside a dense Fermi sea of electrons, capturing an electron from a high Fermi level can lower the total energy of the system even though the free n is heavier. The chemical potentials rearrange until β equilibrium

$$\mu_n = \mu_p + \mu_e \tag{6.3}$$

is reached, typically with a proton fraction of only a few percent in the core: *mostly* neutrons, not purely $Z = 0$.

6.3 Scales: density, number of neutrons, and forces

6.3.1 Number of nucleons

One solar mass is $M_\odot \approx 2 \times 10^{30}\,\mathrm{kg}$. With $m_n \approx 1.67 \times 10^{-27}\,\mathrm{kg}$,

$$A_\odot \approx \frac{M_\odot}{m_n} \approx \frac{2 \times 10^{30}}{1.67 \times 10^{-27}} \approx 1.2 \times 10^{57}. \tag{6.4}$$

A $1.4\,M_\odot$ neutron star therefore contains of order 10^{57} nucleons.

6.3.2 Mean density and the nuclear connection

Nuclear saturation density from Lectures 1–2 is

$$\rho_0 \approx 0.16\,\mathrm{fm}^{-3} \approx 2.7 \times 10^{17}\,\mathrm{kg\,m}^{-3}. \tag{6.5}$$

If a star of mass $M = 1.4\,M_\odot$ has radius $R = 12\,\mathrm{km}$,

$$\bar{\rho} = \frac{3M}{4\pi R^3} \sim (2\text{–}3)\,\rho_0. \tag{6.6}$$

Neutron stars are *nuclear-density objects* writ large: the same saturation that fixed $R = r_0 A^{1/3}$ for Pb reappears as a kilometre-scale radius for $A \sim 10^{57}$.

Radius from nuclear r_0

With $r_0 = 1.2\,\mathrm{fm}$ and $A = 10^{57}$,

$$R = r_0 A^{1/3} = 1.2\,\mathrm{fm} \times 10^{19} = 1.2\,\mathrm{km} \times 10^4 = 12\,\mathrm{km}.$$

Order-of-magnitude agreement with observed radii is not an accident: it is saturation density applied to a stellar baryon number.

6.3.3 Why gravity was dropped in Lectures 4–5

For two nucleons a fermi apart,

$$\frac{G m_n^2}{r} \sim 10^{-36}\,\mathrm{MeV} \qquad (r \sim 1\,\mathrm{fm}),$$

negligible next to a_V, a_C, or a_a. For $A \sim 10^{57}$ nucleons in a sphere of radius $\sim 10\,\mathrm{km}$, every nucleon feels the gravitational field of the whole star. Total gravitational self-energy scales as $GM^2/R \sim A^{5/3}$ at fixed density and can outweigh a fixed MeV-per-nucleon nuclear deficit.

Key idea

Laboratory nuclei: drop G. Neutron-star scale: keep G. The SEMF structure is reused as energy bookkeeping; gravity is the new long-range term.

6.4 Gravitational self-energy of a uniform sphere

6.4.1 Derivation (same logic as Coulomb 3/5)

Uniform density $\rho = M/(\frac{4}{3}\pi R^3)$. Enclosed mass at radius r:

$$m(r) = M\,\frac{r^3}{R^3}. \tag{6.7}$$

Shell mass:

$$\mathrm{d}m = 4\pi r^2\,\mathrm{d}r\,\rho = \frac{3M}{R^3}\,r^2\,\mathrm{d}r. \tag{6.8}$$

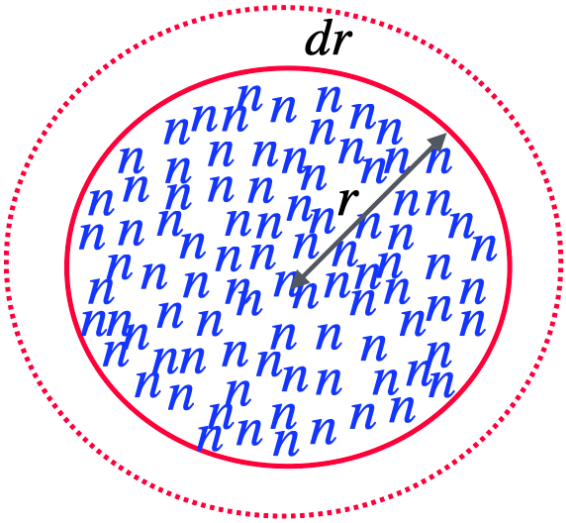

Figure 6.3: Assembly of a uniform sphere by thin shells. A shell of thickness dr at radius r feels the potential of the mass already inside r. Integrating gives $U_G = -3GM^2/(5R)$.

Potential of the interior on the shell:

$$\phi(r) = -\frac{G\,m(r)}{r} = -\frac{GM\,r^2}{R^3}. \tag{6.9}$$

Work to bring $\mathrm{d}m$ from infinity:

$$\mathrm{d}U = \phi\,\mathrm{d}m = -\frac{3GM^2}{R^6}\,r^4\,\mathrm{d}r. \tag{6.10}$$

Integrate $0 \to R$:

$$U_G = -\frac{3GM^2}{5R}. \tag{6.11}$$

Compare with the Coulomb self-energy of a uniform charged sphere (Lecture 4):

$$E_{\mathrm{C}} = \frac{3}{5}\frac{k_e(Ze)^2}{R}, \qquad U_G = -\frac{3}{5}\frac{GM^2}{R}.$$

Same geometric factor 3/5; opposite sign because gravity is attractive.

Binding language. $U_G < 0$ lowers the total energy relative to dispersed matter at infinity. In nuclear $B > 0$ language (Lecture 4), gravity contributes $+|U_G| = 3GM^2/(5R)$ to the binding budget.

Physics checklist for Figure 6.3

1. Shell-by-shell assembly: identical strategy to electrostatics.
2. Scaling: $U_G \propto M^2/R \propto A^{5/3}$ at fixed density.
3. Real stars are stratified; the GM^2/R scaling remains the right order of magnitude.

6.5 SEMF plus gravity for pure neutron matter

6.5.1 Modified binding energy

Start from the SEMF of Lectures 4–5 and add the magnitude of the Newtonian gravitational self-energy as an extra contribution to the *binding* energy (positive when the system is more tightly held together than free nucleons):

$$B = a_V A - a_S A^{2/3} - a_C \frac{Z(Z-1)}{A^{1/3}} - a_{\mathrm{a}} \frac{(N-Z)^2}{A} + \delta + \frac{3GM^2}{5R}. \tag{6.12}$$

In a total-energy ledger the gravitational self-energy is negative ($U_G = -3GM^2/5R$); writing $+|U_G|$ in B is the same physics packaged as binding. The pure-neutron SEMF exercise below uses this convention only as an order-of-magnitude cartoon.

6.5.2 Idealised pure-neutron limit

Take $Z = 0$, $N = A$, $M = m_n A$, $R = r_0 A^{1/3}$:

- Coulomb vanishes;
- asymmetry: $-a_{\mathrm{a}}(N-Z)^2/A = -a_{\mathrm{a}} A$;
- surface $\propto A^{2/3}$ negligible vs volume for huge A (surface/volume $\to 0$; same reason bulk beats surface in macroscopic matter);
- pairing $\propto A^{-3/4}$ negligible at $A \sim 10^{56}$.

Then

$$\frac{3GM^2}{5R} = \frac{3Gm_n^2}{5r_0} A^{5/3}, \tag{6.13}$$

and

$$B \approx (a_V - a_{\mathrm{a}})\, A + \frac{3Gm_n^2}{5r_0} A^{5/3}. \tag{6.14}$$

Nuclear piece alone is negative.

$$a_V - a_{\mathrm{a}} \approx -7.5\,\mathrm{MeV}.$$

That is the SEMF version of "you cannot build a stable nucleus from neutrons alone."

Gravity can reverse the sign. The second term grows as $A^{5/3}$. For large enough A it overcomes the 7.5 MeV per-nucleon deficit.

Caution

What this calculation is and is not. It is a pedagogical SEMF extrapolation: an existence argument for a bound pure-neutron system at stellar A. It is *not* modern neutron-star structure. Real support against collapse is neutron **degeneracy pressure** (and nuclear repulsion at short distance) balanced by gravity in general-relativistic hydrostatic equilibrium (Tolman–Oppenheimer–Volkoff equation). Gravity is attractive; degeneracy

provides the outward pressure. Here gravity enters only as extra binding in an energy ledger, good for order-of-magnitude A and M, not for precision $M(R)$ curves or the maximum mass.

6.6 Boundedness: critical A, mass, and numerical estimate

Require $B \geq 0$. Divide (6.14) by A:

$$(a_V - a_{\mathrm{a}}) + \frac{3Gm_n^2}{5r_0} A^{2/3} \geq 0. \tag{6.15}$$

With $a_V - a_{\mathrm{a}} \approx -7.5\,\mathrm{MeV}$,

$$A^{2/3} \geq \frac{7.5\,\mathrm{MeV}}{C}, \qquad C \equiv \frac{3Gm_n^2}{5r_0}. \tag{6.16}$$

Order of magnitude for C. In SI units,

$$\begin{aligned} G &= 6.67 \times 10^{-11}\,\mathrm{m^3\,kg^{-1}\,s^{-2}}, \\ m_n &= 1.67 \times 10^{-27}\,\mathrm{kg}, \\ r_0 &= 1.2\,\mathrm{fm} = 1.2 \times 10^{-15}\,\mathrm{m}. \end{aligned}$$

Then

$$\begin{aligned} \frac{Gm_n^2}{r_0} &= \frac{6.67 \times 10^{-11}\,(1.67 \times 10^{-27})^2}{1.2 \times 10^{-15}} \approx 1.55 \times 10^{-49}\,\mathrm{J} \\ &\approx 9.7 \times 10^{-37}\,\mathrm{MeV}, \end{aligned}$$

so

$$C = \frac{3}{5}\frac{Gm_n^2}{r_0} \sim 6 \times 10^{-37}\,\mathrm{MeV}.$$

Requiring $CA^{2/3} \gtrsim 7.5\,\mathrm{MeV}$ gives

$$A^{2/3} \gtrsim \frac{7.5}{6 \times 10^{-37}} \sim 1 \times 10^{37}, \qquad A \gtrsim 10^{56}.$$

Thus

$$A \gtrsim 10^{56} \tag{6.17}$$

(lecture estimate; the prefactor depends on the exact gap $a_{\mathrm{a}} - a_V$ and on r_0).

Mass.

$$M \approx m_n A \sim 10^{56} \times 1.67 \times 10^{-27}\,\mathrm{kg} \sim 1.7 \times 10^{29}\,\mathrm{kg} \sim 0.1\,M_\odot$$

for $A \sim 10^{56}$. Using $A \sim 10^{57}$ (closer to observed $1\,M_\odot$) matches solar-mass neutron stars. The SEMF+gravity argument recovers the *solar-mass order of magnitude*: that is its success [4].

Why $A = 2$, 100, or even 10^{10} still fail

For any laboratory or even planetary A, the gravity term per nucleon is far below 1 eV. Then

$$\frac{B}{A} \approx a_V - a_{\mathrm{a}} < 0 :$$

unbound. Only stellar A makes $CA^{2/3}$ competitive with 7.5 MeV.

Scale	A	Nuclear B/A	Gravity vs nuclear
Deuteron	2	$\sim +1.1$ MeV (needs $p+n$)	irrelevant
Lead	~ 200	$\sim +8$ MeV	irrelevant
"Neutron drop" (lab)	any small	~ -7.5 MeV if $Z = 0$	still unbound
Neutron star	$\sim 10^{57}$	nuclear $+ \mid U_G \mid$	gravity decisive

6.7 Physics beyond the SEMF cartoon

6.7.1 What actually supports a neutron star

In hydrostatic equilibrium, gravity pulls inward and a pressure gradient holds the star up. For white dwarfs the pressure is electron degeneracy; for neutron stars it is primarily **neutron degeneracy pressure** (Fermi gas of neutrons at nuclear density), stiffened at high density by repulsive nuclear forces. The SEMF calculation never writes that pressure: it only asks whether the total energy is lower than that of dispersed nucleons. Both viewpoints are useful; they answer different questions (global binding vs local force balance).

6.7.2 Internal structure (qualitative)

- **Atmosphere / outer crust:** ordinary (exotic) nuclei in a lattice with electrons; density rises from $\mathrm{g\,cm^{-3}}$ toward nuclear.
- **Inner crust:** neutron-rich nuclei coexist with a neutron fluid (past the drip density).
- **Outer core:** uniform *npe* matter (neutrons, protons, electrons) in β equilibrium; mostly neutrons.
- **Inner core:** uncertain (hyperons? deconfined quarks?): the regime where laboratory SEMF coefficients are least trustworthy.

6.7.3 Link back to asymmetry and the Fermi gas

The same Pauli filling that produced the asymmetry term $-a_{\mathrm{a}}(N-Z)^2/A$ (Lecture 4) is the microscopic origin of Fermi kinetic energy. In pure neutron matter the kinetic energy per nucleon is large; the SEMF packages that cost into a_{a}. Gravity does not cancel the Pauli principle: it adds a different energy scale that grows with system size.

Key idea

SEMF alone: pure neutrons unbound ($a_V < a_\mathrm{a}$). SEMF + gravity: a bound system appears only for $A \gtrsim 10^{56}$, with $M \sim M_\odot$ and $R \sim 10\,\mathrm{km}$ as order-of-magnitude scales. Few neutrons cannot form a star; a stellar number of neutrons can. Realistic stars are not pure neutron and are not held by this energy ledger: they are charge-neutral, β-equilibrated matter supported by an equation of state in hydrostatic (TOV) equilibrium.

6.8 Lessons and course connection

1. Asymmetry energy is real: unbound pure-neutron drops and the need for $N \sim Z$ in light nuclei share one SEMF term.
2. Coefficients a_V, a_a are terrestrial fits; using them at $A = 10^{57}$ is a bold but instructive extrapolation.
3. Gravity changes the ranking of terms: surface, Coulomb, and pairing drop out; volume, asymmetry, and GM^2/R remain.
4. Saturation density links fm and km: $R = r_0 A^{1/3}$ from electron scattering predicts neutron-star radii at the order-of-magnitude level.

Takeaway

Course arc (Lectures 1–6).

- **1–3:** Nuclear size and density (fm, saturation).
- **4–5:** Binding energy, SEMF, most stable Z, mass parabolas.
- **6:** Extreme SEMF: pure neutrons + gravity $\Rightarrow$ neutron-star mass/radius order of magnitude, with pointers to β equilibrium and TOV structure.

Next (Lecture 7). Leave the macroscopic star and return to the microscopic force that underlies a_V: the two-nucleon problem and the deuteron, the only bound NN system.

6.9 Deeper physics: from SEMF cartoon to realistic neutron stars

The pure-neutron SEMF+gravity estimate recovers solar-mass and ten-kilometre scales, but it is not a structure calculation. Three further layers make the cartoon honest without leaving the spirit of this course.

6.9.1 Chemical equilibrium and the proton fraction

In a neutron-star core, weak interactions maintain

$$n \leftrightarrow p + e^- + \bar{\nu}_e \tag{6.18}$$

in equilibrium with charge neutrality $n_p = n_e$ (and muons once $\mu_e > m_\mu c^2$). Chemical equilibrium requires

$$\mu_n = \mu_p + \mu_e. \tag{6.19}$$

Near saturation one may parameterise the energy per nucleon of asymmetric matter as

$$\frac{E}{A} = \varepsilon_0(\rho) + S(\rho)\,(1 - 2x_p)^2 + \cdots, \tag{6.20}$$

with proton fraction $x_p = n_p/n_b$ and symmetry energy $S(\rho)$. Differentiating and imposing (6.19) with ultra-relativistic electrons ($\mu_e = \hbar c\,(3\pi^2 n_e)^{1/3}$) yields a few-percent x_p near ρ_0: matter is neutron rich but not pure neutron. The SEMF $Z = 0$ exercise is therefore a pedagogical limit, not a literal composition. The asymmetry energy still sets the energy cost of that neutron richness: the same a_{a} (and its density dependence) that shaped the valley of stability controls the pressure of neutron-star matter [4, 1].

6.9.2 Fermi gas: momentum, energy, and degeneracy pressure

In a volume V the number of neutron spin states with momentum less than p_F is

$$N = 2 \cdot \frac{V}{(2\pi\hbar)^3} \cdot \frac{4\pi}{3} p_F^3 = \frac{V p_F^3}{3\pi^2\hbar^3}. \tag{6.21}$$

Hence

$$p_F = \hbar(3\pi^2 n)^{1/3}, \qquad n = N/V. \tag{6.22}$$

At nuclear saturation density $n \approx \rho_0 \approx 0.16\,\mathrm{fm}^{-3}$,

$$p_F c \approx \hbar c\,(3\pi^2\rho_0)^{1/3} \sim 300\,\mathrm{MeV},$$

so the neutrons are mildly relativistic. In the nonrelativistic limit the kinetic energy density and pressure of a Fermi gas are

$$\varepsilon_{\mathrm{kin}} = \frac{3}{5}\, n\, \frac{p_F^2}{2m_n}, \tag{6.23}$$

$$P = \frac{2}{3}\,\varepsilon_{\mathrm{kin}} = \frac{(3\pi^2)^{2/3}}{5}\,\frac{\hbar^2}{m_n}\, n^{5/3}. \tag{6.24}$$

That kinetic pressure supports the star against gravity (analogous to electron degeneracy in white dwarfs, but with the neutron mass and nuclear densities). Nuclear potentials modify both energy and pressure: attractive at low density, repulsive at high density. The SEMF volume and asymmetry terms are bulk averages of that physics near ρ_0; they are not a substitute for $P(\varepsilon)$. Pure neutron matter is not self-bound at zero pressure in realistic calculations: stellar gravity and the EOS together make the compact object.

6.9.3 Hydrostatic equilibrium: Newtonian then TOV

Global binding does not replace local force balance. In Newtonian gravity a spherical shell of thickness $\mathrm{d}r$ is in equilibrium when the pressure gradient balances the gravitational force on the

enclosed mass $m(r)$:

$$\frac{\mathrm{d}P}{\mathrm{d}r} = -\frac{Gm(r)\,\rho(r)}{r^2}, \qquad \frac{\mathrm{d}m}{\mathrm{d}r} = 4\pi r^2 \rho(r). \tag{6.25}$$

In general relativity the structure of a static spherical star obeys the Tolman–Oppenheimer–Volkoff (TOV) equations. With energy density $\varepsilon(r)$ (including rest mass) and pressure $P(r)$,

$$\frac{\mathrm{d}P}{\mathrm{d}r} = -\frac{G}{c^2}\frac{(\varepsilon + P)(m + 4\pi r^3 P/c^2)}{r^2(1 - 2Gm/(rc^2))}, \tag{6.26}$$

$$\frac{\mathrm{d}m}{\mathrm{d}r} = 4\pi r^2 \frac{\varepsilon}{c^2}. \tag{6.27}$$

Compared with (6.25), three relativistic corrections appear:

1. $\varepsilon + P$ replaces ρc^2 (pressure gravitates);
2. $m + 4\pi r^3 P/c^2$ replaces m (pressure contributes to the enclosed source);
3. the redshift factor $1 - 2Gm/(rc^2)$ in the denominator steepens the gradient near the Schwarzschild scale.

Boundary conditions: regular centre $m(0) = 0$, $P(0) = P_c$; the stellar surface is the radius R where $P(R) = 0$, and the gravitational mass is $M = m(R)$. The input is a cold equation of state $P(\varepsilon)$; the output is a mass–radius curve $M(R)$ and a maximum mass. Observed $M_{\max} \gtrsim 2\,M_\odot$ pulsars require a sufficiently stiff EOS at a few times ρ_0; GW170817 tidal deformability requires that the EOS not be too stiff near $2\rho_0$. The liquid-drop estimate $R \sim 10\,\mathrm{km}$, $M \sim M_\odot$ is the right order of magnitude; precision astrophysics needs the full EOS ladder [4].

Key idea

Three layers of understanding.

1. SEMF + gravity: order-of-magnitude A, M, R (this lecture).
2. Fermi gas + β equilibrium: composition and degeneracy pressure.
3. Realistic EOS + TOV: precision $M(R)$, maximum mass, tides.

This course develops layers 1–2 with honest pointers to layer 3.

6.9.4 Link to laboratory symmetry energy

The slope of the symmetry energy $S(\rho)$ at saturation,

$$L = 3\rho_0 \left.\frac{\mathrm{d}S}{\mathrm{d}\rho}\right|_{\rho_0}, \tag{6.28}$$

correlates with the neutron-skin thickness of ^{208}Pb and with neutron-star radii. Lecture 1's charge radii plus parity-violating electron scattering (PREX/CREX) therefore constrain the same physics that sets R_{NS} [1].

6.10 Further physics: nuclear density as the NS density scale

Electron scattering yields a bulk nucleon density

$$\rho_0 \approx 0.15\text{–}0.17\,\mathrm{fm}^{-3} \approx 2.3 \times 10^{14}\,\mathrm{g\,cm}^{-3} \tag{6.29}$$

[14, 1]. A self-gravitating ball of that density with mass $M \sim M_\odot$ has radius

$$R \sim \left(\frac{3M}{4\pi\rho_0}\right)^{1/3} \sim 10\text{–}15\,\mathrm{km}, \tag{6.30}$$

the same order obtained from $R = r_0 A^{1/3}$ with $A \sim 10^{57}$. Thus the laboratory saturation density is the bridge between fermi-scale nuclear physics and kilometre-scale compact stars. Realistic neutron-star models replace the pure-neutron SEMF cartoon by β-equilibrated matter and the TOV equation, but they still pass near ρ_0 in the outer core [14, 4].

6.10.1 Drip lines and pure neutrons

The neutron drip line is where $S_n = 0$. Pure neutron matter ($Z = 0$) lies far beyond that line for any laboratory A: the asymmetry energy costs $\sim a_\mathrm{a} \approx 23\,\mathrm{MeV}$ per nucleon relative to $N = Z$ matter, while volume attraction is only $\sim 16\,\mathrm{MeV}$ net. Gravity at $A \sim 10^{57}$ supplies an extra bulk binding $\propto A^{5/3}/R$ that laboratory nuclei never feel [14, 4].

Compact-star densities still pass near the laboratory saturation density $\rho_0 \sim 0.16\,\mathrm{fm}^{-3}$ in the outer core; that is why electron-scattering radii and neutron-star radii are conceptually linked.

6.10.2 Gravitational scale and Schwarzschild comparison

For $M = M_\odot$ the Schwarzschild radius is

$$R_\mathrm{S} = \frac{2GM}{c^2} \approx 3\,\mathrm{km}. \tag{6.31}$$

Observed neutron-star radii $\sim 10\text{–}14\,\mathrm{km}$ are only a few times R_S: general relativity is essential for the structure equations, even though the pedagogical SEMF+gravity estimate of this lecture is Newtonian. White dwarfs, supported by electron degeneracy at much lower density, have $R \sim R_\oplus$ and weaker relativity; the larger critical mass scale for neutron stars reflects the larger Fermi energy of nucleons compared with electrons at white-dwarf densities [14].

6.10.3 Asymmetry energy and the crust

In the outer crust of a neutron star, nuclei coexist with a degenerate electron gas; as density rises, nuclei become more neutron rich until free neutrons drip out ($S_n \to 0$). That threshold is the same drip-line physics as in the laboratory SEMF, now under pressure and in β equilibrium. The bulk asymmetry coefficient a_a and the density dependence of the symmetry energy control the proton fraction in the core and the thickness of the crust: links between nuclear mass fits and compact-star observables [14, 4].

6.10.4 Fermi energy in neutron matter

At $\rho \sim \rho_0$, a pure neutron gas would have a Fermi energy of order tens of MeV (comparable to the laboratory ε_F scale of Lecture 2). β equilibrium $n \leftrightarrow p + e + \bar{\nu}_e$ then fixes a small proton fraction so that $\mu_n = \mu_p + \mu_e$. The SEMF asymmetry term is a schematic way of writing the cost of $N \neq Z$; modern equations of state refine that cost as a function of density, but the order of magnitude is set by the same nuclear saturation physics measured on Earth.

6.11 Problems with solutions

Problem 6.1 — Nucleon number of a solar-mass neutron star

Estimate A for a neutron star of mass $M = 1.4\,M_\odot$ ($M_\odot = 2\times10^{30}\,\mathrm{kg}$, $m_n = 1.67\times10^{-27}\,\mathrm{kg}$).

Solution 6.1

$$A \approx \frac{M}{m_n} = \frac{1.4 \times 2 \times 10^{30}}{1.67 \times 10^{-27}} = \frac{2.8 \times 10^{30}}{1.67 \times 10^{-27}} \approx 1.7 \times 10^{57}.$$

Order of magnitude: $A \sim 10^{57}$.

Problem 6.2 — Radius from nuclear density (Petrera 1.1.3)

Using $\rho = 2.3 \times 10^{14}\,\mathrm{g\,cm^{-3}}$ and $M = M_\odot$, recompute R and compare with $R = r_0 A^{1/3}$ for $A = 10^{57}$, $r_0 = 1.2\,\mathrm{fm}$.

Solution 6.2

From density:

$$R = \left(\frac{3M}{4\pi\rho}\right)^{1/3} = \left(\frac{3 \times 2 \times 10^{33}\,\mathrm{g}}{4\pi \times 2.3 \times 10^{14}\,\mathrm{g\,cm^{-3}}}\right)^{1/3} \approx 13\,\mathrm{km}$$

(cf. Problem 2.2). From $A^{1/3}$:

$$R = 1.2\,\mathrm{fm} \times (10^{57})^{1/3} = 1.2 \times 10^{19}\,\mathrm{fm} = 1.2 \times 10^{4}\,\mathrm{m} = 12\,\mathrm{km}.$$

The two estimates agree: nuclear saturation density sets the kilometre scale of neutron stars.

Problem 6.3 — SEMF pure neutrons unbound

With $a_V = 15.5\,\mathrm{MeV}$ and $a_\mathrm{a} = 23\,\mathrm{MeV}$, show that pure neutron matter ($Z = 0$) has negative binding per nucleon from nuclear terms alone, and estimate the critical A at which $CA^{2/3}$ with $C = 3Gm_n^2/(5r_0) \sim 6 \times 10^{-37}\,\mathrm{MeV}$ can compensate.

Solution 6.3

For $Z = 0$, $N = A$,

$$\frac{B}{A} \approx a_V - a_{\rm a} = 15.5 - 23 = -7.5\,\text{MeV}$$

(unbound). Adding the gravity piece $+CA^{2/3}$ per nucleon and setting $CA^{2/3} = 7.5\,\text{MeV}$,

$$A^{2/3} = \frac{7.5}{6 \times 10^{-37}} \sim 1.3 \times 10^{37}, \qquad A \sim (1.3 \times 10^{37})^{3/2} \sim 10^{56}.$$

This is the stellar scale of Lecture 6. (The precise C comes from $3GM^2/(5R)$ with $M = Am_n$, $R = r_0 A^{1/3}$.)

Problem 6.4 — Fermi momentum at saturation

Using $p_F = \hbar(3\pi^2 n)^{1/3}$ and $n = \rho_0 = 0.16\,\text{fm}^{-3}$, compute $p_F c$ in MeV and comment on whether the neutrons are nonrelativistic.

Solution 6.4

$$(3\pi^2 n)^{1/3} = \left(3\pi^2 \times 0.16\right)^{1/3} \approx (4.74)^{1/3} \approx 1.68\,\text{fm}^{-1},$$
$$p_F c = \hbar c \cdot 1.68 \approx 197 \times 1.68 \approx 330\,\text{MeV}.$$

Since $m_n c^2 \approx 940\,\text{MeV}$, one has $p_F c/(m_n c^2) \sim 0.35$: mildly relativistic. The nonrelativistic pressure formula is a first estimate; a realistic EOS must include relativistic kinematics and nuclear interactions.

Chapter 7

The Deuteron and Nuclear Force

"For nuclear physicists, the deuteron should be what the hydrogen atom is for atomic physicists."

K. S. Krane

7.1 Why the deuteron is special

A deuteron is a bound proton–neutron system: the nucleus of deuterium (^{2}H). It is the simplest bound state of nucleons, and therefore an ideal laboratory for the nucleon–nucleon (NN) interaction.

In atomic physics, the hydrogen spectrum taught the Coulomb force and quantum electrodynamics. In nuclear physics one would like a similar study for the deuteron: measure transitions between excited states and read off the force. **Unfortunately there are no bound excited states of the deuteron.** The system is so weakly bound that any excitation puts the proton and neutron into the continuum. All information must therefore come from the ground-state binding energy and size, from ground-state multipoles (spin, magnetic moment, quadrupole moment), and from scattering of free nucleons [6, 2].

Key idea

The deuteron is the hydrogen atom of nuclear physics, with one crucial difference: it has only a ground state. Every number measured is a property of that single state, so the force must be extracted carefully and honestly.

7.2 Binding energy: three independent measurements

The binding energy B_d is known to high precision. Three independent methods agree [6].

7.2.1 Definition

Working always with *atomic* masses (as in Lectures 4–5),

$$B_d = [m(^1\mathrm{H}) + m(n) - m(^2\mathrm{H})]\,c^2. \tag{7.1}$$

With $c^2 = 931.50\,\mathrm{MeV/u}$, mass differences in atomic mass units convert directly to MeV.

7.2.2 Method 1: mass spectrometry

Mass doublets involving carbon and deuterium compounds fix $m(^2\mathrm{H})$ to better than $10^{-8}\,\mathrm{u}$. Combined with the hydrogen and neutron masses, one finds

$$B_d = 2.22463 \pm 0.00004\,\mathrm{MeV}. \tag{7.2}$$

7.2.3 Method 2: radiative capture

When a free proton and neutron form a deuteron,

$$p + n \to {}^2\mathrm{H} + \gamma, \tag{7.3}$$

the photon energy (minus a small recoil correction) equals B_d. The measured value is $2.224589 \pm 0.000002\,\mathrm{MeV}$, in excellent agreement with the mass-spectroscopic result.

7.2.4 Method 3: photodisintegration

The reverse process,

$$\gamma + {}^2\mathrm{H} \to p + n, \tag{7.4}$$

has a threshold equal to B_d (again corrected for recoil). Experiment gives $2.224 \pm 0.002\,\mathrm{MeV}$.

How weak is "weakly bound"?

Typical mid-mass nuclei have $B/A \sim 8\,\mathrm{MeV}$ (Lecture 4). The deuteron has $B/A \approx 1.11\,\mathrm{MeV}$. It sits far down on the rising part of the B/A curve: almost unbound. That single fact will control everything we calculate below.

For course work we adopt the rounded value used in the original lecture,

$$B_d \approx 2.225\,\mathrm{MeV}, \tag{7.5}$$

which is consistent with all three determinations at the level needed for the square-well analysis.

7.3 A simple model: the square well

7.3.1 Why a square well?

The true NN potential is complicated: a repulsive core at short distance, a strong attraction at $\sim 1\,\mathrm{fm}$, a pion-exchange tail at larger r, and spin- and tensor-dependent pieces (Lectures 7–9). To learn the *scale* of the force we represent the interaction by a three-dimensional square well in the relative coordinate $r = |\boldsymbol{r}_p - \boldsymbol{r}_n|$:

$$V(r) = \begin{cases} -V_0, & r < R, \\ 0, & r > R. \end{cases} \tag{7.6}$$

Here R is a measure of the range (roughly the "diameter" of the interaction region). The well depth V_0 is what we will fix from B_d.

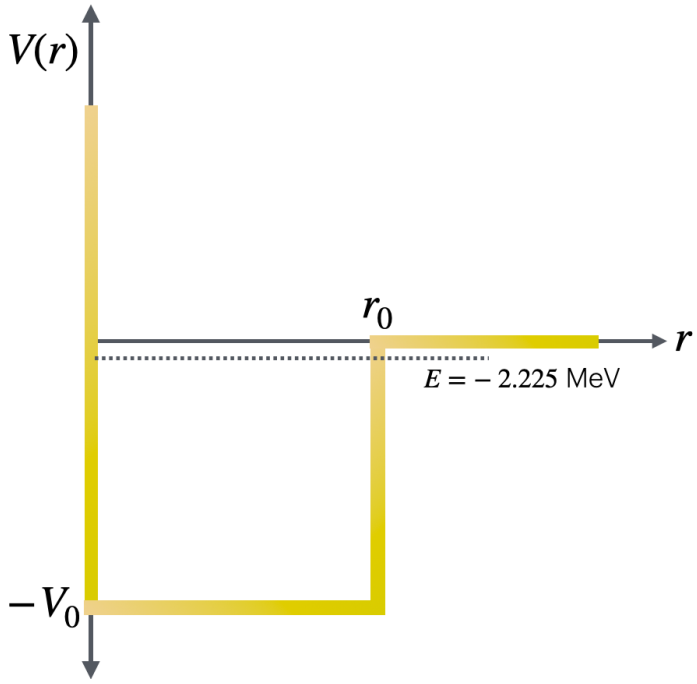

Figure 7.1: Square-well model of the NN potential (lecture figure). Inside $r < R$ the potential is $-V_0$; outside it vanishes. The deuteron energy $E = -B_d$ lies just below threshold.

7.3.2 Reduced mass and the radial equation

The two-body problem with equal masses $m_p \approx m_n \approx m_N$ reduces to a one-body problem with reduced mass

$$\mu = \frac{m_p m_n}{m_p + m_n} \approx \frac{m_N}{2}. \tag{7.7}$$

For a central potential we write the wave function as $\psi(\boldsymbol{r}) = Y_{\ell m}(\hat{r})\, u(r)/r$. The radial function $u(r)$ obeys

$$-\frac{\hbar^2}{2\mu}\frac{\mathrm{d}^2 u}{\mathrm{d}r^2} + \left[V(r) + \frac{\ell(\ell+1)\hbar^2}{2\mu r^2}\right] u = E u. \tag{7.8}$$

Assumption (to be checked later): the ground state has $\ell = 0$, by analogy with the hydrogen $1s$ state. Then the centrifugal term vanishes and (7.8) looks exactly like a one-dimensional Schrödinger equation on the half-line $r > 0$.

7.3.3 Interior and exterior solutions

With $E = -B_d < 0$, define

$$k = \frac{1}{\hbar}\sqrt{2\mu(V_0 - B_d)} \qquad (r < R), \tag{7.9}$$

$$\gamma = \frac{1}{\hbar}\sqrt{2\mu B_d} \qquad (r > R). \tag{7.10}$$

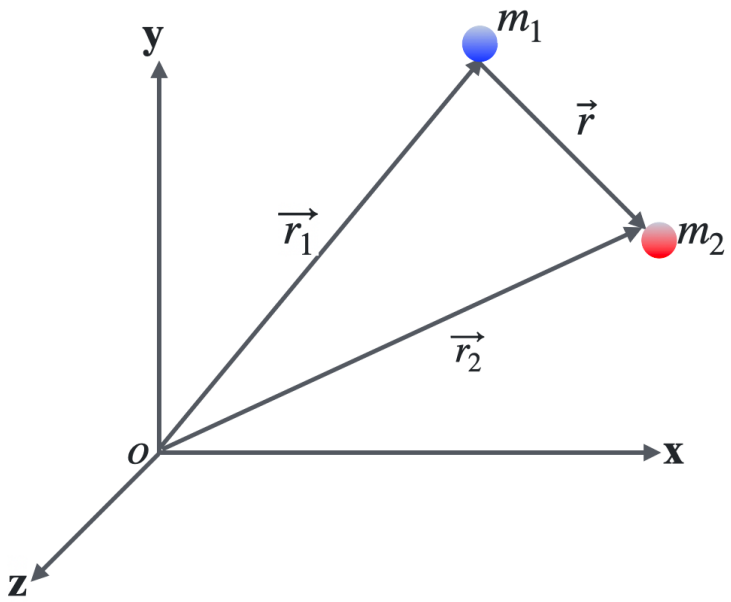

Figure 7.2: Relative coordinate of proton and neutron. The square well acts on this separation; the centre of mass moves freely.

(Equivalently $k = \sqrt{2\mu(V_0 + E)}/\hbar$ with $E = -B_d$. The lecture often writes $\hbar^2/2\mu \approx 41.3\,\text{MeV fm}^2$ for $\mu \approx m_N/2$.)

Inside the well the general solution is

$$u(r) = A\sin(kr) + B\cos(kr). \tag{7.11}$$

Boundary condition at the origin: ψ must remain finite, so $u(0) = 0$. That forces $B = 0$:

$$u(r) = A\sin(kr), \qquad r < R. \tag{7.12}$$

Outside the well,

$$u(r) = Ce^{-\gamma r} + De^{+\gamma r}. \tag{7.13}$$

Boundary condition at infinity: u must not explode, so $D = 0$:

$$u(r) = Ce^{-\gamma r}, \qquad r > R. \tag{7.14}$$

7.3.4 Matching: the transcendental condition

The physical content of the bound-state problem is fixed by the finite range of the force and by quantum mechanics. Outside the well there is no attraction, so a bound system ($E = -B_d < 0$) can exist only because the wave function tunnels under the continuum; the exterior solution must decay exponentially. Inside the well the nucleons feel a constant attraction $-V_0$, so the radial function oscillates. Matching the two regions at $r = R$ quantises the allowed (V_0, R) pairs that reproduce the measured binding energy [6, 13].

Write

$$V(r) = \begin{cases} -V_0 & r < R, \\ 0 & r > R, \end{cases} \qquad E = -B_d < 0.$$

For $r < R$ the radial Schrödinger equation becomes

$$-\frac{\hbar^2}{2\mu}\frac{\mathrm{d}^2u}{\mathrm{d}r^2} - V_0 u = Eu \quad \Rightarrow \quad \frac{\mathrm{d}^2u}{\mathrm{d}r^2} = -k^2 u,$$

with wave number

$$k = \frac{\sqrt{2\mu(V_0 - B_d)}}{\hbar} = \frac{\sqrt{2\mu(V_0 + E)}}{\hbar}, \tag{7.15}$$

where the second form uses $E = -B_d$ so that $V_0 - B_d = V_0 + E$ (not $V_0 + |E|$ written as a separate definition: since $E = -B_d$, one has $V_0 + E = V_0 - B_d$). Both expressions are identical; they are not two different physical definitions. The general interior solution is $u_{\mathrm{I}}(r) = A\sin(kr) + B\cos(kr)$. Because $\psi = u/r$ must remain finite at the origin, $u(0) = 0$, which forces $B = 0$:

$$u_{\mathrm{I}}(r) = A\sin(kr). \tag{7.16}$$

Physically this is the statement that there is no source of probability current at $r = 0$; the relative wave function vanishes at vanishing separation in the s-wave radial problem.

Outside the well, $V = 0$ and $E = -B_d$, so

$$\frac{\mathrm{d}^2u}{\mathrm{d}r^2} = \gamma^2 u, \qquad \gamma = \frac{\sqrt{2\mu B_d}}{\hbar}.$$

The exterior solution is $u_{\mathrm{II}}(r) = Ce^{-\gamma r} + De^{+\gamma r}$. The growing exponential is discarded so that the state is normalisable:

$$u_{\mathrm{II}}(r) = Ce^{-\gamma r}. \tag{7.17}$$

The decay length $1/\gamma$ is large when B_d is small: weak binding means the nucleons spend much of their time *outside* the range of the force, which is why the deuteron rms radius exceeds the naive well radius.

Continuity of ψ and of $\mathrm{d}\psi/\mathrm{d}r$ at the edge of a finite square well requires continuity of u and u' at $r = R$:

$$A\sin(kR) = Ce^{-\gamma R}, \tag{7.18}$$

$$Ak\cos(kR) = -C\gamma e^{-\gamma R}. \tag{7.19}$$

Dividing these two equations eliminates the unknown amplitudes A and C and yields the matching condition

$$k\cot(kR) = -\gamma. \tag{7.20}$$

Equation (7.20) is transcendental: once R and B_d are fixed, it determines the depth V_0 that can support the observed bound state. That is the quantitative link between the measured binding energy and the strength of the residual force.

7.4 Numerical result: $V_0 \approx 35$–$36\,\mathrm{MeV}$

Electron scattering gives an rms charge radius of the deuteron of about 2.1 fm. That number is *not* the force range: because the binding is weak, the wave function extends well beyond

the potential, so the matter/charge radius exceeds the interaction radius. Taking a force range $R \sim 2.0$–$2.1\,\text{fm}$ as a first estimate, with $B_d = 2.224\,\text{MeV}$ and $\hbar^2/(2\mu) \approx 41.5\,\text{MeV fm}^2$, one solves (7.20) as follows.

Define the dimensionless quantities

$$\xi \equiv kR, \qquad \eta \equiv \gamma R = R\sqrt{\frac{2\mu B_d}{\hbar^2}}. \tag{7.21}$$

For $R = 2.1\,\text{fm}$,

$$\eta = 2.1\sqrt{\frac{2.224}{41.5}} \approx 2.1 \times 0.231 \approx 0.486.$$

The matching condition $k\cot(kR) = -\gamma$ becomes $\xi\cot\xi = -\eta$, or

$$\xi\cot\xi = -0.486. \tag{7.22}$$

The relevant root in $(\pi/2, \pi)$ (the first bound state has $\xi > \pi/2$) is $\xi \approx 1.82$. Then

$$V_0 - B_d = \frac{\hbar^2 k^2}{2\mu} = \frac{\hbar^2}{2\mu}\frac{\xi^2}{R^2} = 41.5 \cdot \frac{(1.82)^2}{(2.1)^2} \approx 31.2\,\text{MeV}, \tag{7.23}$$

$$V_0 = 31.2 + 2.224 \approx 33.4\,\text{MeV}. \tag{7.24}$$

Varying R over 2.0–2.1 fm yields

$$V_0 \approx 33\text{–}35\,\text{MeV}. \tag{7.25}$$

(A shorter assumed range requires a deeper well, and conversely.) Equation (7.20) constrains a curve in the (R, V_0) plane, not a unique pair: one observable (B_d) cannot fix two potential parameters. Either way, the residual NN attraction sampled by the deuteron is tens of MeV deep on a fermi scale, barely enough to bind [6, 13].

(The section title quotes ≈ 35–$36\,\text{MeV}$ as a round classroom figure for $R \sim 2\,\text{fm}$; the explicit root above gives ≈ 33–$35\,\text{MeV}$ for the same range window.)

Key idea

Barely bound. The energy $E = -B_d$ lies just below the top of the well. If the force were slightly weaker, or the range slightly smaller, there would be no bound state at all. The wave function barely "turns over" inside the well so that it can match a decaying exponential outside [6].

Why this matters for the Sun and the early universe

Deuterium formation is the first step in the solar *pp* chain and in Big Bang nucleosynthesis. If no stable two-nucleon bound state existed, heavier nuclei would not form in the early universe and stellar hydrogen burning would not begin as it does. The weak binding of the deuteron is a threshold fact about the world we inhabit [6].

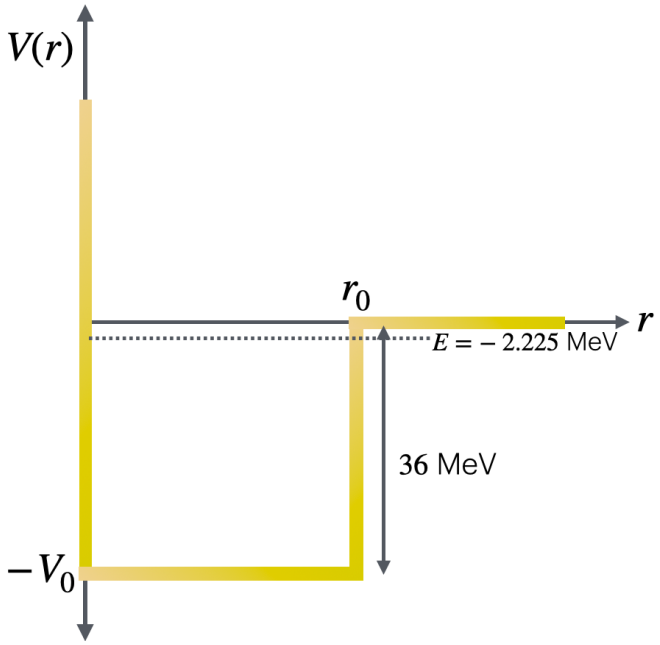

Figure 7.3: Lecture figure emphasising the depth V_0 needed to bind the deuteron. The bound level sits only $\sim 2.2\,\text{MeV}$ below the continuum, so most of the well depth is cancelled by kinetic energy of confinement.

Remark

Because the binding is weak, the probability of finding the nucleons *outside* the range R is large. The exponential tail extends far; low-energy NN scattering is correspondingly sensitive to the asymptotic normalisation. A large fraction of the time is spent outside the well [2].

7.5 Residual force: why nucleons attract at all

Before leaving the central model, place the force in a modern context. Nucleons are not elementary: $p = uud$, $n = udd$. The fundamental strong interaction (QCD) confines colour. Colour-neutral nucleons still interact at short distance through a residual force, much as neutral atoms form molecules through residual electromagnetic multipoles.

Yukawa's meson exchange (1935) explains the long-range tail: the force range is of order $\hbar/(m_\pi c) \sim 1.4\,\text{fm}$. The square well is a teaching caricature of that attraction plus short-range repulsion. Lectures 7–9 will show that even this picture is incomplete: the force depends on spin and contains a non-central (tensor) piece.

7.6 What we have learned, and what we have not

1. The deuteron binding energy is $B_d \approx 2.224\,\text{MeV}$, measured three independent ways.
2. There are no bound excited states: the system is barely bound.
3. A central square well with range $\sim 2\,\text{fm}$ requires depth $V_0 \sim 33$–$35\,\text{MeV}$ to bind; shorter range needs deeper V_0.

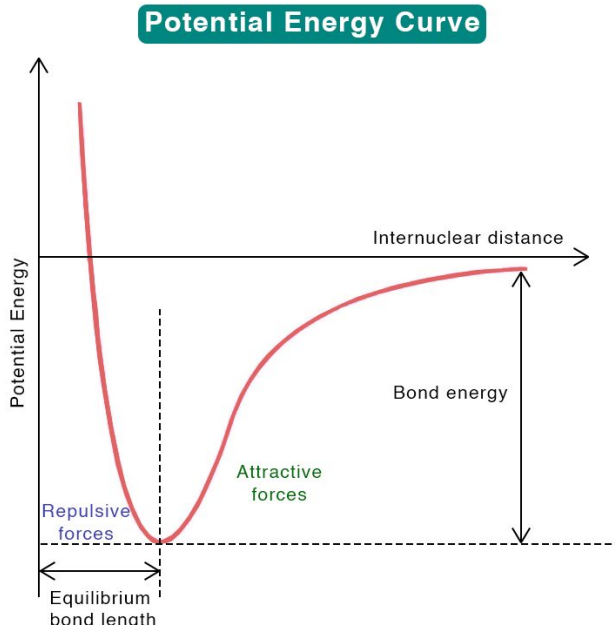

Figure 7.4: Molecular analogy: short-range repulsion, attractive well, finite range. Colour-neutral nucleons interact through residual colour forces on the fermi scale in a similar qualitative way.

4. That depth sets the scale of the NN attraction underlying the SEMF volume term a_V (Lecture 4).

5. We have *assumed* $\ell = 0$. Spin, magnetic moment, and quadrupole moment will test that assumption (Lectures 8–9).

Takeaway

In this lecture and the next.

- This lecture: binding energy and a central well ⇒ force range and depth.
- Next lecture: I^π and μ_d ⇒ spin dependence and a few-percent D-wave.
- Lecture after: $Q_d \neq 0$ ⇒ tensor (non-central) force.

Only after those three steps is the qualitative NN force complete for PH5001.

7.7 Deeper physics: weak binding and the asymptotic wave function

7.7.1 No bound excited states

Unlike the hydrogen atom, the deuteron has **no bound excited states**. Any excitation exceeds B_d and produces a free $p + n$ pair in the continuum. All structure information must therefore come from the ground-state multipoles (Lectures 8–9) and from scattering (phase shifts), not from a discrete spectrum [6, 2].

7.7.2 Wave function mostly outside the well

With $V_0 \sim 33$–$35\,\mathrm{MeV}$ and $R \sim 2\,\mathrm{fm}$, the matching condition $k\cot(kR) = -\gamma$ places the eigenenergy just below threshold. The exterior decay constant $\gamma = \sqrt{2\mu B_d}/\hbar$ is small ($\gamma^{-1} \approx 4.3\,\mathrm{fm}$), so the exponential tail extends far: the two nucleons spend a large fraction of the time *outside* the range of the force. That is why the rms charge radius ($\sim 2.1\,\mathrm{fm}$ from electron scattering) is not a direct measure of the force range, and why low-energy NN scattering is so sensitive to the asymptotic normalisation.

Range vs depth degeneracy

Fixing only B_d leaves a curve of allowed (R, V_0). Scattering lengths and effective ranges (Lecture 10) break that degeneracy by adding low-energy continuum information. A single bound-state energy never determines a unique potential.

7.7.3 Square well as a teaching potential

Realistic potentials (Yukawa one-pion tail, hard or soft core at short distance, tensor and spin–orbit terms) are more complex. The square well is retained because:

- it is analytically solvable for $L = 0$;
- it returns $V_0 \sim 33$–$40\,\mathrm{MeV}$ for $R \sim 2\,\mathrm{fm}$, the correct scale;
- it makes the near-threshold character of the bound state obvious.

Lectures 8–9 show why a pure central well is still incomplete: spin and quadrupole data demand a tensor component.

7.8 Further physics: only one bound NN state

There is only one bound $A = 2$ nucleus, the deuteron, and it has no bound excited states. Its binding energy is only $B_d \approx 2.225\,\mathrm{MeV}$, so any excitation puts the system into the $p + n$ continuum [14, 6, 13]. That single fact forces the entire multipole programme of Lectures 7–9: structure information must come from ground-state moments and from scattering, not from a discrete spectrum.

Modern NN potentials also include three-nucleon forces, which have no classical two-body analogue and are hard to fix from scattering alone [13, 4]. For PH5001 the two-body square well and the tensor force extracted from the deuteron remain the essential lessons.

At the QCD level, the residual nucleon–nucleon force is the long-distance face of a theory in which the strong coupling *grows* toward large distance (confinement) and becomes weak at short distance (asymptotic freedom) [15, 4]. Yukawa's pion sets the range ~ 1–$2\,\mathrm{fm}$ of the residual force used in this chapter.

7.8.1 Bound-state condition for a square well

For an s-wave square well of depth V_0 and range R,

$$V(r) = \begin{cases} -V_0 & r < R, \\ 0 & r > R, \end{cases} \tag{7.26}$$

the radial function $u(r) = r\psi(r)$ oscillates inside the well and decays as $e^{-\kappa r}$ outside, with

$$k = \frac{\sqrt{2\mu(V_0 + E)}}{\hbar}, \qquad \kappa = \frac{\sqrt{-2\mu E}}{\hbar}, \qquad E = -B_d < 0. \tag{7.27}$$

Matching u and u' at $r = R$ yields

$$k \cot(kR) = -\kappa. \tag{7.28}$$

The first bound state appears when the exterior decay constant vanishes, $\kappa \to 0^+$, so $\cot(kR) \to 0^-$ and

$$kR = \frac{\pi}{2} \qquad \text{(threshold)}. \tag{7.29}$$

At $E = 0$ one has $k = \sqrt{2\mu V_0}/\hbar$, hence at least one bound state requires

$$V_0 R^2 > \frac{\pi^2 \hbar^2}{8\mu} \approx 109\,\text{MeV fm}^2 \tag{7.30}$$

($\mu \approx m_N/2$). Fitting the deuteron gives approximately

$$V_0 R^2(s{=}1) \approx 140\,\text{MeV fm}^2, \tag{7.31}$$

while low-energy np scattering in the singlet channel yields

$$V_0 R^2(s{=}0) \sim 90\text{–}95\,\text{MeV fm}^2 \tag{7.32}$$

just *below* threshold. Typical phenomenological values are $V_0 \approx 47\,\text{MeV}$, $R \approx 1.7\,\text{fm}$ (triplet) and a shallower, wider singlet well [14, 6].

Because B_d is small, the exterior decay length $1/\kappa$ is long. Normalising the asymptotic wave $u(r) \sim A e^{-\kappa r}$ for $r > R$, the probability outside the well is

$$P_{>} = \frac{\displaystyle\int_R^\infty A^2 e^{-2\kappa r}\,\mathrm{d}r}{\displaystyle\int_0^\infty u^2\,\mathrm{d}r} \sim \frac{A^2 e^{-2\kappa R}/(2\kappa)}{\text{total norm}}, \tag{7.33}$$

which is of order 50%–70% for the deuteron: most of the probability density sits *outside* the range of the force, and the rms radius exceeds R.

7.8.2 No nn or pp bound states and charge independence

Charge independence of the strong force, together with the Pauli principle, explains why only pn binds: the $s = 1$, $\ell = 0$ state is allowed for pn but forbidden for identical nn or pp; the $s = 0$ channel is unbound for all three pairs [14]. Mirror binding differences such as ^{3}H vs ^{3}He are

then mostly Coulomb.

The naive reading "attractive in $s = 1$, repulsive in $s = 0$" is wrong: both channels are attractive; only the triplet is deep enough to bind [14, 6].

7.8.3 Yukawa potential and pion range

A more realistic long-range form is

$$V(r) = g\,\frac{\hbar c}{r}\,e^{-r/r_0}, \qquad r_0 = \frac{\hbar}{m_\pi c} \approx 1.4\,\text{fm}. \tag{7.34}$$

Yukawa predicted the pion mass from the force range [9, 14, 5]. In Born approximation the Fourier transform of the Yukawa potential is the propagator

$$M(q^2) \propto \frac{1}{q^2 + m_\pi^2 c^2}, \tag{7.35}$$

which reduces to a contact interaction when $m_\pi \to \infty$ (zero range). Short-range repulsion ("hard core") and multi-meson exchanges complete modern NN potentials [14, 15].

The same Yukawa logic, applied to the weak interaction with a heavy mediator, explains why the weak force looks feeble at low energy even though its underlying coupling is not tiny: $G_F \propto g^2/m_W^2$ [5]. For the strong residual force the light pion makes the range nuclear, not subnuclear.

7.8.4 Photodisintegration and the binding energy

The deuteron binding energy is measured to high precision from the threshold for

$$\gamma + {}^2\text{H} \to p + n, \tag{7.36}$$

and from the reverse radiative capture. The photon energy must supply at least $B_d \approx 2.224\,\text{MeV}$ (plus a small centre-of-mass correction). That B_d is only $\sim 0.1\%$ of the rest energy of the deuteron: the system is barely bound, which is why the wave function leaks so far outside the well [6, 14].

7.8.5 Why scattering is needed

With only one bound state, the deuteron samples the NN force mainly in the ${}^3S_1$–${}^3D_1$ channel at a fixed average separation. Nucleon–nucleon scattering (especially on hydrogen targets, to avoid multiple scattering inside a heavy nucleus) maps other partial waves, energies, and spin orientations. Phase shifts then constrain the full potential used in few-body and many-body calculations [6, 4].

7.8.6 Triplet vs singlet wells in numbers

Phenomenological square-well fits that also use low-energy scattering give distinct wells in the two spin channels [14]:

Channel	V_0 (MeV)	R (fm)	V_0R^2 (MeV fm^2)
Triplet $s=1$ (bound)	46.7	1.73	≈ 140
Singlet $s=0$ (unbound)	12.5	2.79	≈ 93.5
Threshold for one bound state			109

Both channels are attractive; only the triplet clears the quantum threshold $V_0R^2 > 109\,\text{MeV fm}^2$. That is the quantitative content of "spin-dependent nuclear force" at the square-well level.

7.9 Problems with solutions

Problem 7.1 — Binding energy of the deuteron

Atomic masses: $m(^1\text{H}) = 1.007825\,\text{u}$, $m(n) = 1.008665\,\text{u}$, $m(^2\text{H}) = 2.014102\,\text{u}$. With $c^2 = 931.5\,\text{MeV/u}$, compute B_d and B_d/A.

Solution 7.1

$$B_d = [m(^1\text{H}) + m(n) - m(^2\text{H})]c^2 = (1.007825 + 1.008665 - 2.014102) \times 931.5 = 0.002388 \times 931.5 \approx 2.224\,\text{MeV}.$$

$$B_d/A \approx 1.11\,\text{MeV},$$

much less than the mid-mass $\sim 8\,\text{MeV}$ per nucleon: the deuteron is barely bound [6, 14].

Problem 7.2 — Uncertainty estimate of V_0

For a square well of range $R = 2.1\,\text{fm}$ and reduced mass $\mu = m_N/2$, use $E_{\text{kin}} \sim 3\hbar^2/(2\mu R^2)$ with $\hbar^2/m_N \approx 41.5\,\text{MeV fm}^2$ and $B_d = 2.2\,\text{MeV}$ to estimate V_0.

Solution 7.2

Since $\hbar^2/(2\mu) = \hbar^2/m_N$,

$$E_{\text{kin}} \sim \frac{3 \times 41.5}{(2.1)^2} \approx 28\,\text{MeV}, \quad V_0 \sim E_{\text{kin}} + B_d \sim 30\,\text{MeV}.$$

Same tens-of-MeV scale as the matching solution $V_0 \approx 35\,\text{MeV}$ [6].

Problem 7.3 — Bound-state condition V_0R^2 (Basdevant)

For an s-wave square well, at least one bound state requires $V_0R^2 > \pi^2\hbar^2/(8\mu) \approx 109\,\text{MeV fm}^2$. (a) With $R = 1.73\,\text{fm}$ and $V_0 = 46.7\,\text{MeV}$ (triplet fit), compute V_0R^2 and compare with $109\,\text{MeV fm}^2$. (b) The singlet channel has $V_0R^2 \sim 93.5\,\text{MeV fm}^2$. What does that imply?

Solution 7.3

(a)

$$V_0 R^2 = 46.7 \times (1.73)^2 \approx 46.7 \times 2.99 \approx 140\,\text{MeV fm}^2 > 109\,\text{MeV fm}^2.$$

The triplet well is above threshold and binds the deuteron ($V_0 R^2 \approx 140\,\text{MeV fm}^2$ reproduces $B_d = 2.225\,\text{MeV}$) [14].

(b) $93.5 < 109$: the singlet well is just *below* threshold. There is no bound ${}^1S_0$ pn state; low-energy singlet scattering shows a virtual state [14, 6].

Problem 7.4 — Exterior decay length

With $B_d = 2.224\,\text{MeV}$ and $\hbar^2/m_N = 41.5\,\text{MeV fm}^2$, compute $\gamma = \sqrt{2\mu B_d}/\hbar = \sqrt{m_N B_d}/\hbar$ and the decay length $1/\gamma$. Compare with a typical well range $R \sim 2\,\text{fm}$.

Solution 7.4

$$\gamma = \sqrt{\frac{m_N B_d}{\hbar^2}} = \sqrt{\frac{B_d}{\hbar^2/m_N}} = \sqrt{\frac{2.224}{41.5}} \approx \sqrt{0.0536} \approx 0.231\,\text{fm}^{-1}.$$

$$\frac{1}{\gamma} \approx 4.3\,\text{fm} > R \sim 2\,\text{fm}.$$

Most of the probability density lies outside the range of the force: the deuteron is a loosely bound, extended system [6, 14].

Problem 7.5 — Thermal deuterons (Petrera 1.1.4)

Estimate the temperature at which two deuterons can approach to $r \sim 1\,\text{fm}$ against Coulomb repulsion. Use $k_B = 8.6 \times 10^{-5}\,\text{eV/K}$ and $\alpha\,\hbar c \approx 1.44\,\text{MeV fm}$.

Solution 7.5

In the rest frame of one deuteron the other approaches with relative velocity $2v$, so

$$4k_B T \sim \frac{\alpha\,\hbar c}{r} \approx \frac{1.44}{1} = 1.44\,\text{MeV}.$$

$$T \sim \frac{1.44 \times 10^6\,\text{eV}}{4 \times 8.6 \times 10^{-5}\,\text{eV/K}} \sim 4 \times 10^9\,\text{K}.$$

Nuclear contact among charged light nuclei requires stellar temperatures [3].

Problem 7.6 — Photodisintegration threshold

The $\gamma + {}^2\text{H} \to p + n$ threshold is essentially B_d plus a small centre-of-mass correction. If a photon of energy $E_\gamma = 2.50\,\text{MeV}$ breaks a deuteron at rest, what is the total kinetic energy of the $p + n$ system in the lab (neglect recoil of the compound system before breakup, to leading order)?

Solution 7.6

Energy conservation:

$$E_\gamma = B_d + T_p + T_n \quad \Rightarrow \quad T_p + T_n = 2.50 - 2.224 = 0.276\,\text{MeV}.$$

The excess photon energy above threshold appears as kinetic energy of the two nucleons [6].

Chapter 8

Deuteron Spin and Magnetic Moment

8.1 Nuclear spin and parity: careful definitions

The binding energy of the deuteron fixes the radial scale of a central NN well, under the assumption that the relative orbital angular momentum is $\ell = 0$. That assumption must now be tested with every other measured property of the ground state: the total angular momentum (nuclear spin), the parity, and the magnetic dipole moment [6, 2].

8.1.1 What "nuclear spin" means

Each nucleon carries orbital angular momentum $\boldsymbol{\ell}$ and intrinsic spin $\boldsymbol{s} = \frac{1}{2}\hbar$ (in units where we often set $\hbar = 1$ for quantum numbers). Their sum is

$$\boldsymbol{j} = \boldsymbol{\ell} + \boldsymbol{s}. \tag{8.1}$$

In a nucleus the total angular momentum is the vector sum of all nucleon contributions. Nuclear physicists call this total $\boldsymbol{I}$ and name it the **nuclear spin**, even though it includes orbital motion as well as spin. The usual quantum rules apply:

$$\boldsymbol{I}^2 \to I(I+1)\hbar^2, \qquad I_z \to M_I\hbar, \quad M_I = -I, \ldots, +I. \tag{8.2}$$

When two angular momenta j_1 and j_2 are coupled, the allowed total values follow the triangle rule

$$J = |j_1 - j_2|,\ |j_1 - j_2| + 1, \ldots,\ j_1 + j_2. \tag{8.3}$$

This rule will be applied twice: first $\boldsymbol{S} = \boldsymbol{s}_p + \boldsymbol{s}_n$, then $\boldsymbol{I} = \boldsymbol{L} + \boldsymbol{S}$.

8.1.2 Parity

Parity is the behaviour of the spatial wave function under $\boldsymbol{r} \to -\boldsymbol{r}$. If $\psi(-\boldsymbol{r}) = +\psi(\boldsymbol{r})$ the parity is even ($\pi = +$); if $\psi(-\boldsymbol{r}) = -\psi(\boldsymbol{r})$ it is odd ($\pi = -$). A central-potential wave function

separates as

$$\psi_{\ell m}(\boldsymbol{r}) = R_\ell(r) Y_{\ell m}(\theta, \phi). \tag{8.4}$$

Inversion leaves $r = |\boldsymbol{r}|$ unchanged but sends $(\theta, \phi) \to (\pi - \theta, \phi + \pi)$. Spherical harmonics obey

$$Y_{\ell m}(\pi - \theta, \phi + \pi) = (-1)^\ell Y_{\ell m}(\theta, \phi). \tag{8.5}$$

Therefore

$$\psi_{\ell m}(-\boldsymbol{r}) = (-1)^\ell \psi_{\ell m}(\boldsymbol{r}), \qquad \pi = (-1)^\ell. \tag{8.6}$$

Even ℓ gives even parity; odd ℓ gives odd parity.

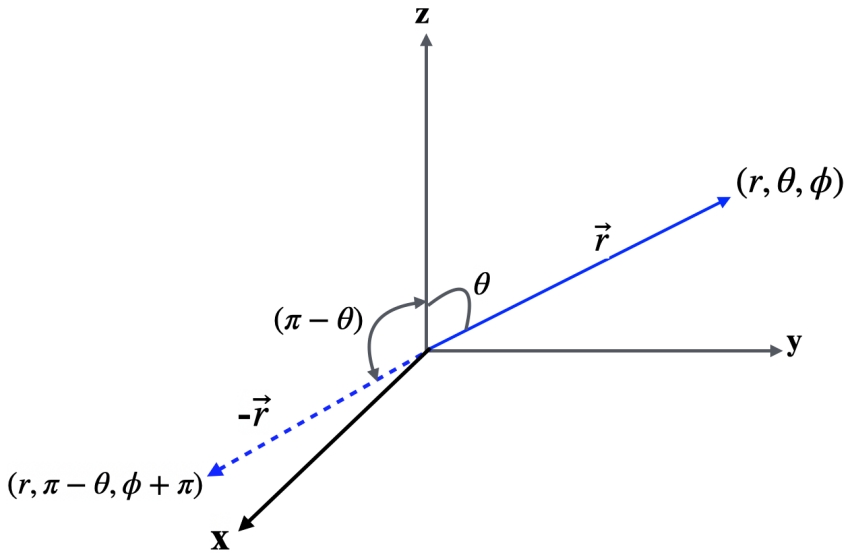

Figure 8.1: Inversion $\boldsymbol{r} \leftrightarrow -\boldsymbol{r}$. Nuclear states have definite parity when the Hamiltonian conserves parity.

8.1.3 Experimental assignment for the deuteron

Experiment gives

$$I^\pi(^2\mathrm{H}) = 1^+. \tag{8.7}$$

That single label will eliminate most of the angular-momentum possibilities we might have imagined.

8.2 Coupling two spins: four ways to make $I = 1$

The deuteron total angular momentum is

$$\boldsymbol{I} = \boldsymbol{s}_p + \boldsymbol{s}_n + \boldsymbol{L}, \tag{8.8}$$

where $\boldsymbol{L}$ is the relative orbital angular momentum. Each nucleon has $s = \frac{1}{2}$, so the total spin $\boldsymbol{S} = \boldsymbol{s}_p + \boldsymbol{s}_n$ obeys

$$S = \left|\tfrac{1}{2} - \tfrac{1}{2}\right|, \ldots, \tfrac{1}{2} + \tfrac{1}{2} = 0,\ 1. \tag{8.9}$$

For fixed S and L, the second application of Equation (8.3) gives

$$|L - S| \leq I \leq L + S. \tag{8.10}$$

We require $I = 1$:

- If $S = 0$, then $I = L$, so only $L = 1$ works.
- If $S = 1$, then $|L - 1| \leq 1 \leq L + 1$, which permits $L = 0, 1, 2$.

Thus there are exactly four couplings [6]:

(a) spins parallel ($S = 1$) with $L = 0$;

(b) spins antiparallel ($S = 0$) with $L = 1$;

(c) spins parallel ($S = 1$) with $L = 1$;

(d) spins parallel ($S = 1$) with $L = 2$.

Parity decides among them. The deuteron has *even* parity, and orbital parity is $(-1)^L$. Therefore L must be even: $L = 1$ is ruled out. Cases (b) and (c) drop. We are left with

$$^3S_1 \quad (L = 0,\ S = 1) \qquad \text{and} \qquad ^3D_1 \quad (L = 2,\ S = 1). \tag{8.11}$$

The bound state is **100% spin triplet**. There is no bound singlet pn state.

The notation $^{2S+1}L_I$ now follows directly. The superscript is the spin multiplicity $2S+1$, the letter denotes $L = 0, 1, 2, \ldots \to S, P, D, \ldots$, and the subscript is the total angular momentum I. Hence the two even-parity possibilities are $^3S_1$ and $^3D_1$.

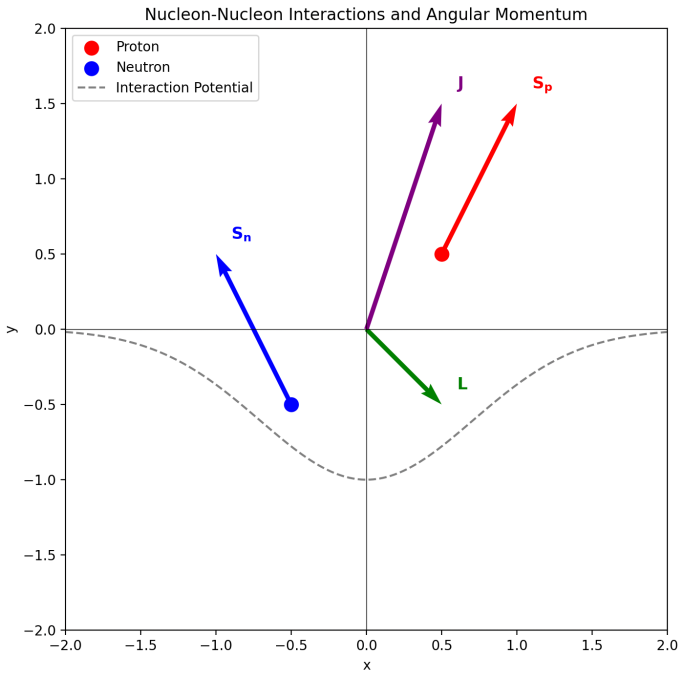

Figure 8.2: Schematic spins and orbital angular momentum in the NN system. The deuteron ground state is dominated by parallel spins and $L = 0$, with a small $L = 2$ admixture.

Key idea

Spin dependence of the nuclear force. Nature binds the triplet channel and not the singlet. The NN force depends on the relative orientation of the nucleon spins. A spin-independent central well would not explain that fact.

8.2.1 Triplet and singlet spin states

Start with the unique highest-projection product state,

$$|1,1\rangle = |\uparrow\uparrow\rangle. \tag{8.12}$$

Apply the total lowering operator $S_- = s_{p-} + s_{n-}$. Since $S_-|1,1\rangle = \hbar\sqrt{2}\,|1,0\rangle$,

$$S_-|\uparrow\uparrow\rangle = \hbar|\downarrow\uparrow\rangle + \hbar|\uparrow\downarrow\rangle, \tag{8.13}$$

$$\therefore \quad |1,0\rangle = \frac{1}{\sqrt{2}}\left(|\uparrow\downarrow\rangle + |\downarrow\uparrow\rangle\right). \tag{8.14}$$

A second lowering gives $|1,-1\rangle = |\downarrow\downarrow\rangle$. The three triplet states ($S=1$) are therefore

$$|1,1\rangle = |\uparrow\uparrow\rangle, \qquad |1,0\rangle = \tfrac{1}{\sqrt{2}}(|\uparrow\downarrow\rangle + |\downarrow\uparrow\rangle), \qquad |1,-1\rangle = |\downarrow\downarrow\rangle. \tag{8.15}$$

The remaining normalized $M_S = 0$ combination must be orthogonal to $|1,0\rangle$; it is the singlet

$$|0,0\rangle = \tfrac{1}{\sqrt{2}}(|\uparrow\downarrow\rangle - |\downarrow\uparrow\rangle). \tag{8.16}$$

A useful operator that distinguishes them is $\boldsymbol{s}_p \cdot \boldsymbol{s}_n$. Square $\boldsymbol{S} = \boldsymbol{s}_p + \boldsymbol{s}_n$:

$$\boldsymbol{S}^2 = \boldsymbol{s}_p^2 + \boldsymbol{s}_n^2 + 2\boldsymbol{s}_p \cdot \boldsymbol{s}_n, \tag{8.17}$$

$$\therefore \quad \boldsymbol{s}_p \cdot \boldsymbol{s}_n = \frac{1}{2}\left(\boldsymbol{S}^2 - \boldsymbol{s}_p^2 - \boldsymbol{s}_n^2\right). \tag{8.18}$$

Because $s_p = s_n = \frac{1}{2}$, $\boldsymbol{s}_p^2 = \boldsymbol{s}_n^2 = \frac{3}{4}\hbar^2$. Thus

$$\langle \boldsymbol{s}_p \cdot \boldsymbol{s}_n \rangle = \frac{\hbar^2}{2}\left[S(S+1) - \frac{3}{4} - \frac{3}{4}\right] = \begin{cases} +\dfrac{\hbar^2}{4}, & S = 1, \\ -\dfrac{3\hbar^2}{4}, & S = 0. \end{cases} \tag{8.19}$$

A potential containing $\boldsymbol{\sigma}_p \cdot \boldsymbol{\sigma}_n$ can therefore deepen the triplet well relative to the singlet. That is why the square-well depth of Lecture 7 applies to the *triplet* channel; the singlet well is shallower and does not bind.

Caution

The singlet value is not zero. It is negative ($-3\hbar^2/4$). Saying the singlet product "vanishes" is a common slip; the correct eigenvalues matter when one writes $V_\sigma(r)$.

8.3 Magnetic moments: from classical orbits to g-factors

8.3.1 Nuclear magneton

Consider a charge e moving with speed v in a circular orbit of radius r. Its period, current, and loop area are

$$T = \frac{2\pi r}{v}, \qquad \mathcal{I} = \frac{e}{T} = \frac{ev}{2\pi r}, \qquad \mathcal{A} = \pi r^2. \tag{8.20}$$

The magnetic dipole moment is current times area,

$$\mu = \mathcal{I}\mathcal{A} = \frac{evr}{2}. \tag{8.21}$$

Since the orbital angular momentum is $L = mvr$, this becomes

$$\boldsymbol{\mu}_\ell = \frac{e}{2m}\boldsymbol{L}. \tag{8.22}$$

For a proton, set $m = m_p$ and factor out one quantum $\hbar$. This defines the **nuclear magneton**

$$\mu_N = \frac{e\hbar}{2m_p} \approx 3.1525 \times 10^{-8}\,\text{eV/T}. \tag{8.23}$$

It is smaller than the Bohr magneton by $m_e/m_p \approx 1/1836$. Ordinary magnetism of matter is electronic; nuclear magnetism is a delicate probe [6].

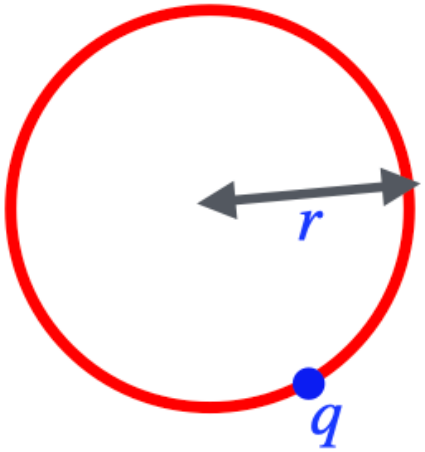

Figure 8.3: Classical orbital current: charge on a loop produces $\mu \propto qL/(2m)$. Neutrons have $q = 0$ and no orbital moment from net charge.

8.3.2 Orbital and spin contributions

We write

$$\mu_\ell = g_\ell\,\mu_N\,\frac{\ell_z}{\hbar}, \qquad \mu_s = g_s\,\mu_N\,\frac{s_z}{\hbar}. \tag{8.24}$$

For proton orbital motion $g_\ell = 1$; for the neutron $g_\ell = 0$. For free nucleon *spins*, experiment finds anomalous g-factors far from the Dirac value $g_s = 2$:

$$g_p = 5.5856912, \tag{8.25}$$

$$g_n = -3.8260837. \tag{8.26}$$

Equivalently, $\mu_p = +2.7928\,\mu_N$ and $\mu_n = -1.9130\,\mu_N$. The neutron's nonzero moment and the proton's large g_p are early evidence that nucleons are composite (meson clouds; today, quarks) [6, 2].

8.4 Deuteron magnetic moment: pure S-wave calculation

If the orbital angular momentum vanishes, there is no orbital magnetic moment: only the intrinsic spins of the proton and neutron contribute. With $I^\pi = 1^+$ and a pure ${}^3S_1$ configuration, the stretched state $M_I = 1$ has both spins aligned ($s_z = +\hbar/2$). The deuteron moment is then simply the sum of the free-nucleon moments [6],

$$\mu_d(L{=}0) = \mu_p + \mu_n = \frac{g_p + g_n}{2}\,\mu_N = \frac{5.5857 - 3.8261}{2}\,\mu_N = 0.8798\,\mu_N. \tag{8.27}$$

Experiment finds

$$\mu_d^{(\mathrm{exp})} = 0.8574376(4)\,\mu_N, \tag{8.28}$$

about $0.022\,\mu_N$ ($\sim 2.5\%$) below the pure S-wave value. The agreement is already striking: most of μ_d is indeed $\mu_p + \mu_n$. The residual deficit, however, is a genuine structural effect. Meson-exchange currents and relativistic corrections can shift the moment, but within the nonrelativistic NN picture the natural explanation is a small admixture of $L = 2$ in the ground-state wave function [6].

Key idea

Physics of the discrepancy. A pure s-wave deuteron would have $\mu_d = \mu_p + \mu_n$. The measured moment is slightly smaller, signalling a few-percent D-wave component and, with it, a non-central piece of the force.

8.5 D-wave admixture from μ_d

Write the ground state as a coherent mixture of even orbital waves allowed by $I^\pi = 1^+$,

$$|\psi\rangle = a_S\,|L{=}0\rangle + a_D\,|L{=}2\rangle, \qquad |a_S|^2 + |a_D|^2 = 1. \tag{8.29}$$

8.5.1 Expectation value of the magnetic-moment operator

The numerical D-state moment should not simply be quoted; it follows from an angular-momentum expectation value. In the centre-of-mass frame, and neglecting exchange currents,

the z-component of the two-nucleon magnetic-moment operator is

$$\frac{\hat{\mu}_z}{\mu_N} = \frac{1}{2}\frac{\hat{L}_z}{\hbar} + g_p\frac{\hat{s}_{pz}}{\hbar} + g_n\frac{\hat{s}_{nz}}{\hbar}. \tag{8.30}$$

Only the proton contributes an orbital magnetic moment. For nearly equal nucleon masses its orbital angular momentum about the centre of mass can be obtained explicitly. Let $M = m_p + m_n$, $\boldsymbol{r} = \boldsymbol{r}_p - \boldsymbol{r}_n$, and let $\boldsymbol{p}$ be the relative momentum in the centre-of-mass frame. Then

$$\boldsymbol{r}_p = \frac{m_n}{M}\boldsymbol{r}, \qquad \boldsymbol{p}_p = \boldsymbol{p}, \tag{8.31}$$

so

$$\boldsymbol{L}_p = \boldsymbol{r}_p \times \boldsymbol{p}_p = \frac{m_n}{M}\,\boldsymbol{r}\times\boldsymbol{p} = \frac{m_n}{M}\boldsymbol{L} \simeq \frac{1}{2}\boldsymbol{L}. \tag{8.32}$$

This produces the first term of Equation (8.30). Within the spin-triplet state the proton and neutron share the total spin symmetrically. Equivalently, the antisymmetric operator $\boldsymbol{s}_p - \boldsymbol{s}_n$ has zero diagonal matrix element between symmetric triplet spin states, and therefore

$$\langle s_{pz}\rangle = \langle s_{nz}\rangle = \frac{1}{2}\langle S_z\rangle. \tag{8.33}$$

The projection theorem itself follows in two steps. First, $\boldsymbol{J} = \boldsymbol{L} + \boldsymbol{S}$ implies

$$\boldsymbol{L}\cdot\boldsymbol{J} = \boldsymbol{L}\cdot(\boldsymbol{L}+\boldsymbol{S}) = \boldsymbol{L}^2 + \boldsymbol{L}\cdot\boldsymbol{S}, \tag{8.34}$$

$$\boldsymbol{J}^2 = \boldsymbol{L}^2 + \boldsymbol{S}^2 + 2\boldsymbol{L}\cdot\boldsymbol{S}. \tag{8.35}$$

Eliminating $\boldsymbol{L}\cdot\boldsymbol{S}$ gives

$$\boldsymbol{L}\cdot\boldsymbol{J} = \frac{1}{2}\left(\boldsymbol{J}^2 + \boldsymbol{L}^2 - \boldsymbol{S}^2\right). \tag{8.36}$$

In a state $|LSJM\rangle$, rotational symmetry says that the expectation value of $\boldsymbol{L}$ can point only along $\boldsymbol{J}$. Its z-projection is consequently

$$\langle L_z\rangle = \frac{\langle \boldsymbol{L}\cdot\boldsymbol{J}\rangle}{J(J+1)\hbar^2}\,\langle J_z\rangle. \tag{8.37}$$

Using $\langle J_z\rangle = M\hbar$ and the eigenvalues of the squared angular momenta in Equation (8.36) gives

$$\langle L_z\rangle = M\hbar\,\frac{J(J+1) + L(L+1) - S(S+1)}{2J(J+1)}, \tag{8.38}$$

$$\langle S_z\rangle = M\hbar\,\frac{J(J+1) + S(S+1) - L(L+1)}{2J(J+1)}. \tag{8.39}$$

The second line can be obtained either by interchanging L and S or from $\langle S_z\rangle = M\hbar - \langle L_z\rangle$. The observable deuteron moment is evaluated in the stretched state $J = M = 1$.

For ${}^3S_1$, $L = 0$ and $S = 1$, so

$$\frac{\langle L_z \rangle}{\hbar} = 1\,\frac{1(1+1)+0(0+1)-1(1+1)}{2(1)(1+1)} = \frac{2+0-2}{4} = 0, \tag{8.40}$$

$$\frac{\langle S_z \rangle}{\hbar} = 1\,\frac{1(1+1)+1(1+1)-0(0+1)}{2(1)(1+1)} = \frac{2+2-0}{4} = 1. \tag{8.41}$$

Equation (8.30) therefore reproduces

$$\begin{aligned}\mu({}^3S_1) &= \left[\frac{1}{2}(0) + \frac{g_p+g_n}{2}(1)\right]\mu_N \\ &= \frac{g_p+g_n}{2}\,\mu_N = \mu_p + \mu_n = 0.8798\,\mu_N.\end{aligned} \tag{8.42}$$

For ${}^3D_1$, $L = 2$, $S = 1$, and $J = M = 1$. Equations (8.38)–(8.39) give, step by step,

$$\frac{\langle L_z \rangle}{\hbar} = 1\,\frac{1(1+1)+2(2+1)-1(1+1)}{2(1)(1+1)} = \frac{2+6-2}{4} = \frac{3}{2}, \tag{8.43}$$

$$\frac{\langle S_z \rangle}{\hbar} = 1\,\frac{1(1+1)+1(1+1)-2(2+1)}{2(1)(1+1)} = \frac{2+2-6}{4} = -\frac{1}{2}. \tag{8.44}$$

The orbital and spin angular momenta are therefore partly antiparallel in the D state. Substitution into (8.30) yields

$$\begin{aligned}\mu({}^3D_1) &= \left[\frac{1}{2}\left(\frac{3}{2}\right) + \frac{g_p+g_n}{2}\left(-\frac{1}{2}\right)\right]\mu_N \\ &= \frac{1}{4}(3-g_p-g_n)\,\mu_N \approx 0.310\,\mu_N.\end{aligned} \tag{8.45}$$

This is the expectation-value derivation of the smaller pure-D magnetic moment [6, 2].

In the one-body operator approximation, $\langle {}^3S_1|\hat{\mu}_z|{}^3D_1\rangle = 0$: the angular functions with $L = 0$ and $L = 2$ are orthogonal, and the operator in (8.30) does not change L. The mixed-state expectation value can be expanded before the cross terms are discarded:

$$\begin{aligned}\langle\psi|\hat{\mu}_z|\psi\rangle &= |a_S|^2\langle {}^3S_1|\hat{\mu}_z|{}^3S_1\rangle + |a_D|^2\langle {}^3D_1|\hat{\mu}_z|{}^3D_1\rangle \\ &\quad + a_S^* a_D\langle {}^3S_1|\hat{\mu}_z|{}^3D_1\rangle + a_D^* a_S\langle {}^3D_1|\hat{\mu}_z|{}^3S_1\rangle \\ &= P_S\mu_S + P_D\mu_D.\end{aligned} \tag{8.46}$$

Therefore

$$\mu_d = P_S\,(0.880\,\mu_N) + P_D\,(0.310\,\mu_N), \qquad P_S + P_D = 1. \tag{8.47}$$

To obtain the commonly used form, substitute $P_S = 1 - P_D$ and $\mu_D = \frac{1}{4}(3 - g_p - g_n)\mu_N$:

$$\begin{aligned}\mu_d &= (1-P_D)(\mu_p+\mu_n) + P_D\frac{3-g_p-g_n}{4}\mu_N \\ &= (\mu_p+\mu_n) + P_D\left[\frac{3}{4}\mu_N - \frac{3}{2}(\mu_p+\mu_n)\right] \\ &= (\mu_p+\mu_n) - \frac{3}{2}\left[\mu_p+\mu_n-\frac{1}{2}\mu_N\right]P_D.\end{aligned} \tag{8.48}$$

Finally, requiring $\mu_d = 0.8574\,\mu_N$ and retaining the displayed rounded moments gives

$$\begin{aligned} 0.8574 &= 0.8798(1 - P_D) + 0.310 P_D \\ &= 0.8798 - (0.8798 - 0.310) P_D, \end{aligned} \tag{8.49}$$

$$(0.8798 - 0.310) P_D = 0.8798 - 0.8574,$$

$$P_D = \frac{0.8798 - 0.8574}{0.8798 - 0.310} = 0.0393 \approx 0.039, \qquad P_S = 1 - P_D \approx 0.961. \tag{8.50}$$

This classroom estimate suggests a few-percent D-wave. It is *not* a model-independent measurement of P_D: meson-exchange currents and relativistic corrections also shift μ_d. Independent NN scattering analyses still find a few-percent D-state probability, so the qualitative conclusion is robust: the force cannot be purely central. Only a tensor interaction can mix $L = 0$ with $L = 2$ in a single eigenstate. The electric quadrupole moment $Q_d \neq 0$ (Lecture 9) establishes that mixing far more cleanly than the magnetic-moment deficit alone [6].

Caution

Do not promote $P_D \approx 4\%$ to an observable. Treat it as a pedagogical estimate that motivates looking for a tensor force; the decisive geometric evidence is the nonzero quadrupole moment.

Key idea

What Lectures 7–9 establish together. Weak binding fixes the depth and range of the residual force. Spin and parity fix the channel as mostly ${}^3S_1$. The magnetic-moment deficit *suggests* a small D-wave; the quadrupole moment *requires* one, and with it a tensor force.

8.6 Preview of heavier nuclei

In odd-A nuclei, pairing often cancels the moments of all but the last unpaired nucleon. Plotting μ versus I produces the Schmidt lines. Real nuclei fall between those lines because of configuration mixing, the many-body cousin of the deuteron's D-wave. The deuteron is the cleanest few-body example of the same idea: free moments first, then a small admixture [6, 1].

Takeaway

Takeaways (Lecture 8).

- $I^\pi = 1^+$: even parity forces even L; the bound state is spin triplet.
- Spin-dependent force: triplet binds, singlet does not.
- Pure S-wave $\mu_d = 0.880\,\mu_N$; experiment $0.857\,\mu_N$.
- Mixture $\sim 96\%$ $S + \sim 4\%$ D is a classroom estimate of the magnetic deficit; quadrupole data (next lecture) establish the D-wave and the tensor force.

8.7 Deeper physics: magnetic moments beyond the deuteron

8.7.1 How μ is measured (Rabi and NMR)

Place a state of angular momentum I in a uniform field $\boldsymbol{B} = B\hat{\boldsymbol{z}}$. With $\hat{\mu}_z = g_I \mu_N \hat{I}_z/\hbar$, the Zeeman Hamiltonian is

$$\hat{H}_Z = -\hat{\boldsymbol{\mu}} \cdot \boldsymbol{B} = -g_I \mu_N B \frac{\hat{I}_z}{\hbar}. \tag{8.51}$$

Because $\hat{I}_z|I, M_I\rangle = M_I \hbar |I, M_I\rangle$,

$$E_{M_I} = -g_I \mu_N B M_I. \tag{8.52}$$

Adjacent substates therefore differ by

$$|\Delta E| = g_I \mu_N B = h\nu. \tag{8.53}$$

The Rabi molecular-beam method and nuclear magnetic resonance detect the frequency ν at which a radiofrequency field drives $\Delta M_I = \pm 1$ transitions. Since B is known, the resonance gives g_I, and the stretched-state moment is $\mu = g_I I \mu_N$. Free-nucleon moments $\mu_p = +2.7928\,\mu_N$ and $\mu_n = -1.9130\,\mu_N$ are among the most accurately known quantities in nuclear physics [2, 1].

8.7.2 Schmidt lines (preview of the shell model)

For odd-A nuclei the magnetic moment is often dominated by the last unpaired nucleon. Plotting μ versus I produces the Schmidt lines: two limiting curves for $j = \ell \pm \frac{1}{2}$. Real nuclei fall between the lines because of configuration mixing and meson-exchange currents. The deuteron is the few-body cousin of that story: free $\mu_p + \mu_n$ is the extreme independent-particle limit; a few-percent D-wave admixture is the simplest configuration mixing [6, 1]. The two Schmidt formulae are derived, rather than merely quoted, in Section 8.8.2.

8.7.3 Isospin language

Proton and neutron form an isospin doublet $t = \frac{1}{2}$. The deuteron has total isospin $T = 0$, and this assignment follows from exchange symmetry. For two nucleons, the spatial, spin, and isospin factors acquire under exchange the signs

$$(-1)^L, \qquad (-1)^{S+1}, \qquad (-1)^{T+1}, \tag{8.54}$$

respectively. Their product must be -1 for fermions, so

$$(-1)^{L+S+T} = -1. \tag{8.55}$$

The deuteron has even L and $S = 1$. Hence $L + S + T$ is odd only when $T = 0$. Explicitly, its isospin wave function is the antisymmetric combination

$$|T = 0, T_z = 0\rangle = \frac{1}{\sqrt{2}} \left(|pn\rangle - |np\rangle \right). \tag{8.56}$$

The $T = 1$, $S = 0$ pn partner of the virtual ${}^1S_0$ state is unbound, as are free nn and pp (after Coulomb). Charge independence of the strong force organises NN scattering lengths into a nearly universal pattern once Coulomb is removed. Lecture 10 develops this NN spin–isospin structure through phase shifts [4].

Remark

Quarks and anomalous moments. Dirac particles with charge e and mass m have $g = 2$. The proton's $g_p \approx 5.59$ and the neutron's nonzero moment are direct evidence of composite structure (charged quark currents and meson clouds), already anticipated in Lecture 7's residual-force discussion [2, 4].

8.7.4 Beyond the one-body magnetic operator

For the one-body operator derived in Section 8.5.1, the S–D cross term vanishes: $\hat{L}_z$, $\hat{s}_{pz}$, and $\hat{s}_{nz}$ do not change L, and the $L = 0$ and $L = 2$ angular functions are orthogonal. This gives the probability-weighted expectation value in Equation (8.48).

A precision calculation must add two-body meson-exchange currents, relativistic corrections, and small nucleon-structure effects. Those contributions alter the magnetic moment without being equivalent to a change in P_D. Modern potentials still find a few-percent D-state probability, so the classroom estimate is useful, but P_D itself is model dependent [6].

8.8 Further physics: magnetic moments and the nuclear magneton

To each angular momentum is associated a magnetic dipole

$$\boldsymbol{\mu} = g\,\mu_N \frac{\boldsymbol{j}}{\hbar}, \qquad \mu_N = \frac{e\hbar}{2m_p}. \tag{8.57}$$

For orbital motion of a proton, $g_\ell = 1$; for a neutron, $g_\ell = 0$. Spin g-factors of free nucleons are anomalous ($g_p \approx 5.59$, $g_n \approx -3.83$), a signal of internal structure [13, 6, 2, 5].

In odd-A nuclei a first approximation attributes μ to the last unpaired nucleon (Schmidt estimate). The deuteron is the clean two-body limit of the same idea: free moments first, then a small configuration admixture (D-wave) to match experiment. Exact g-factors of complex nuclei require interactions among many nucleons; the deuteron isolates the few-body physics.

8.8.1 Spin dependence from the deuteron alone

From $I^\pi = 1^+$ and $\mu_d \approx \mu_p + \mu_n$ one concludes that the ground state is mostly ${}^3S_1$. The absence of a bound ${}^1S_0$ pn state shows that the force is spin-dependent: both channels are attractive, but only the triplet is deep enough to bind [14, 6]. The small quadrupole moment and the μ_d deficit then require a few-percent ${}^3D_1$ admixture (tensor force; Lecture 9).

8.8.2 Schmidt lines for odd-A nuclei

For a single valence nucleon with orbital angular momentum ℓ and spin $s = \frac{1}{2}$, the one-body magnetic operator is

$$\frac{\hat{\mu}_z}{\mu_N} = g_\ell \frac{\hat{\ell}_z}{\hbar} + g_s \frac{\hat{s}_z}{\hbar}. \tag{8.58}$$

The measured moment is the expectation value in the stretched state $|j, m = j\rangle$. Since $j_z = \ell_z + s_z$, it is useful to write

$$\frac{\mu}{\mu_N} = g_\ell j + (g_s - g_\ell)\frac{\langle s_z \rangle}{\hbar}. \tag{8.59}$$

The projection theorem derived in Section 8.5.1, with $L \to \ell$, $S \to s$, and $M = j$, gives

$$\frac{\langle s_z \rangle}{\hbar} = j\,\frac{j(j+1) + s(s+1) - \ell(\ell+1)}{2j(j+1)}. \tag{8.60}$$

For aligned spin, $j = \ell + \frac{1}{2}$, so $\ell = j - \frac{1}{2}$ and $s(s+1) = \frac{3}{4}$. Substitution into Equation (8.60) gives

$$\begin{aligned} \frac{\langle s_z \rangle}{\hbar} &= \frac{j(j+1) + \frac{3}{4} - (j - \frac{1}{2})(j + \frac{1}{2})}{2(j+1)} \\ &= \frac{j^2 + j + \frac{3}{4} - (j^2 - \frac{1}{4})}{2(j+1)} = \frac{j+1}{2(j+1)} = \frac{1}{2}. \end{aligned} \tag{8.61}$$

Equation (8.59) then yields the upper Schmidt line,

$$\boxed{\frac{\mu}{\mu_N} = g_\ell j + \frac{1}{2}(g_s - g_\ell), \qquad j = \ell + \frac{1}{2}.} \tag{8.62}$$

Equivalently, $\mu/\mu_N = g_\ell \ell + g_s/2$: in the stretched state the orbital and spin projections are simply ℓ and $1/2$.

For anti-aligned spin, $j = \ell - \frac{1}{2}$, so $\ell = j + \frac{1}{2}$. Now

$$\begin{aligned} \frac{\langle s_z \rangle}{\hbar} &= \frac{j(j+1) + \frac{3}{4} - (j + \frac{1}{2})(j + \frac{3}{2})}{2(j+1)} \\ &= \frac{j^2 + j + \frac{3}{4} - (j^2 + 2j + \frac{3}{4})}{2(j+1)} = -\frac{j}{2(j+1)}. \end{aligned} \tag{8.63}$$

The lower Schmidt line is therefore

$$\boxed{\frac{\mu}{\mu_N} = g_\ell j - (g_s - g_\ell)\frac{j}{2(j+1)}, \qquad j = \ell - \frac{1}{2}.} \tag{8.64}$$

For an unpaired proton one inserts $g_\ell = 1$ and $g_s = g_p$; for an unpaired neutron, $g_\ell = 0$ and $g_s = g_n$. These are independent particle limits, not exact predictions. Experimental moments of odd-A nuclei generally lie between the Schmidt lines, shifted toward smaller $|\mu|$ by configuration mixing and meson-exchange currents [6, 2, 13]. The deuteron is the few-body prototype of that programme: start from free g-factors, then correct for orbital admixtures.

8.8.3 Nuclear magneton vs Bohr magneton

Because $m_p \approx 1836\, m_e$,

$$\begin{aligned}\mu_N &= \frac{m_e}{m_p}\,\mu_B \\ &= \frac{m_e}{m_p}\left(\frac{e\hbar}{2m_e}\right) = \frac{e\hbar}{2m_p} \\ &\approx \frac{1}{1836}\,\mu_B. \end{aligned} \tag{8.65}$$

Nuclear moments are therefore three orders of magnitude smaller than electronic moments, which is why nuclear magnetism is a precision hyperfine effect in atoms and a separate experimental industry (NMR, atomic beams, ion traps) [5, 2].

8.9 Problems with solutions

Problem 8.1 — Pure S-wave magnetic moment

Using $g_p = 5.5857$ and $g_n = -3.8261$, compute the pure ${}^3S_1$ prediction for μ_d and the fractional difference from the experimental value $0.8574\,\mu_N$.

Solution 8.1

$$\mu_d(L{=}0) = \frac{g_p + g_n}{2}\,\mu_N = \frac{5.5857 - 3.8261}{2}\,\mu_N = 0.8798\,\mu_N.$$

$$\Delta\mu = 0.8798 - 0.8574 = 0.0224\,\mu_N, \qquad \frac{\Delta\mu}{\mu_d(L{=}0)} \approx 2.5\%.$$

Most of μ_d is $\mu_p + \mu_n$; the small deficit is structural [6].

Problem 8.2 — D-wave probability from μ_d

Assume

$$\mu_d = P_S\,(0.8798\,\mu_N) + P_D\,(0.310\,\mu_N), \quad P_S + P_D = 1,$$

and $\mu_d = 0.8574\,\mu_N$. Find P_D.

Solution 8.2

$$0.8574 = 0.8798(1 - P_D) + 0.310\,P_D = 0.8798 - 0.5698\,P_D,$$

$$P_D = \frac{0.8798 - 0.8574}{0.5698} \approx 0.039 \approx 4\%, \quad P_S \approx 96\%.$$

[6, 14].

Problem 8.3 — Why $L = 1$ is excluded

List (S, L) combinations that can give $I = 1$ for pn and show which survive the experimental parity $\pi = +$.

Solution 8.3

Coupling the two spin-$\frac{1}{2}$ nucleons first gives

$$S = \left|\tfrac{1}{2} - \tfrac{1}{2}\right|, \ldots, \tfrac{1}{2} + \tfrac{1}{2} = 0,\ 1.$$

Angular-momentum addition then requires

$$|L - S| \leq I \leq L + S.$$

For $S = 0$, this reduces to $I = L$, so $I = 1$ requires $L = 1$. For $S = 1$, requiring $I = 1$ gives

$$|L - 1| \leq 1 \leq L + 1,$$

which is satisfied by $L = 0, 1, 2$. Thus the four possibilities are

$$(S, L) = (0, 1),\ (1, 0),\ (1, 1),\ (1, 2).$$

Parity is $\pi = (-1)^L$. The measured $\pi = +$ eliminates both $L = 1$ cases, leaving $(S, L) = (1, 0)$ and $(1, 2)$, or ${}^3S_1$ and ${}^3D_1$. Both have $S = 1$, so the bound state is entirely spin triplet even though it is not entirely S-wave [6].

Problem 8.4 — Nuclear magneton scale

Compute $\mu_N = e\hbar/(2m_p)$ in MeV/T using $e\hbar/(2m_e) = \mu_B = 5.788 \times 10^{-11}\,\text{MeV/T}$ and $m_p/m_e = 1836$. Why is nuclear magnetism hard to measure compared with electronic magnetism?

Solution 8.4

$$\mu_N = \frac{m_e}{m_p}\,\mu_B = \frac{5.788 \times 10^{-11}}{1836} \approx 3.15 \times 10^{-14}\,\text{MeV/T}.$$

Nuclear moments are ~ 2000 times smaller than electronic ones, so they appear only as tiny hyperfine shifts or require specialised methods (Rabi beams, NMR) [5, 2].

Problem 8.5 — Derive the ${}^3D_1$ magnetic moment

For a pure ${}^3D_1$ state, use the projection theorem to calculate $\langle L_z \rangle$ and $\langle S_z \rangle$ in the stretched state $J = M = 1$. Then evaluate

$$\frac{\hat{\mu}_z}{\mu_N} = \frac{1}{2}\frac{\hat{L}_z}{\hbar} + \frac{g_p + g_n}{2}\frac{\hat{S}_z}{\hbar}$$

and obtain the numerical moment using the g-factors of Problem 8.1.

Solution 8.5

For $L = 2$, $S = 1$, and $J = M = 1$,

$$\begin{aligned}\frac{\langle L_z\rangle}{\hbar} &= M\frac{J(J+1)+L(L+1)-S(S+1)}{2J(J+1)}\\ &= \frac{2+6-2}{4} = \frac{3}{2},\\ \frac{\langle S_z\rangle}{\hbar} &= M\frac{J(J+1)+S(S+1)-L(L+1)}{2J(J+1)}\\ &= \frac{2+2-6}{4} = -\frac{1}{2}.\end{aligned}$$

The magnetic moment is therefore

$$\begin{aligned}\frac{\mu(^3D_1)}{\mu_N} &= \frac{1}{2}\left(\frac{3}{2}\right) + \frac{g_p+g_n}{2}\left(-\frac{1}{2}\right)\\ &= \frac{3}{4} - \frac{g_p+g_n}{4} = \frac{1}{4}(3-g_p-g_n).\end{aligned}$$

Numerically,

$$\begin{aligned}3-g_p-g_n &= 3-5.5857-(-3.8261)\\ &= 3-5.5857+3.8261 = 1.2404,\\ \therefore\qquad \mu(^3D_1) &= \frac{1.2404}{4}\,\mu_N = 0.3101\,\mu_N.\end{aligned}$$

[6].

Problem 8.6 — Charge independence and no bound nn

Explain why charge independence of the strong force, together with the Pauli principle, is consistent with a bound pn ($s = 1$) deuteron and no bound nn or pp systems.

Solution 8.6

For two nucleons the exchange sign is

$$(-1)^L(-1)^{S+1}(-1)^{T+1} = (-1)^{L+S+T},$$

and Fermi statistics require this sign to be -1. In an S-wave, $L = 0$, so $S+T$ must be odd. The deuteron channel has $S = 1$, hence $T = 0$. Its isospin state

$$\frac{1}{\sqrt{2}}(|pn\rangle - |np\rangle)$$

has no nn or pp member: two identical nucleons necessarily have $T = 1$. For nn or pp with $L = 0$ and $T = 1$, antisymmetry therefore forces $S = 0$. Charge independence relates that channel to the unbound $T = 1$, $^1S_0$ pn channel, apart from electromagnetic and small charge-dependent effects. Thus the bound $T = 0$, $^3S_1$ channel exists only for pn, while the

allowed nn and pp S-wave channel does not bind [14, 6].

Chapter 9

Quadrupole Moment and Tensor Force

"The mixing of ℓ values in the deuteron is the best evidence we have for the noncentral (tensor) character of the nuclear force."

K. S. Krane

9.1 Electric quadrupole moment from the multipole expansion

The magnetic moment of the deuteron is close to, but not equal to, the sum of the free nucleon moments. That small discrepancy already suggests a few percent D-wave admixture. A sharper geometric probe is the electric quadrupole moment: it reports the *shape* of the charge distribution. The definition used in nuclear physics follows from the multipole expansion of the electrostatic potential of a localised charge density, exactly as in the original lecture (Fig. 1 below) [6, 1, 2].

9.1.1 Potential of a nuclear charge distribution (Fig. 1)

Let $\rho(\boldsymbol{r}')$ be the charge density of the nucleus. The electric potential at an exterior point $\boldsymbol{r}$ is

$$\Phi(\boldsymbol{r}) = \frac{1}{4\pi\varepsilon_0}\int \frac{\rho(\boldsymbol{r}')}{|\boldsymbol{r}-\boldsymbol{r}'|}\,\mathrm{d}^3 r', \tag{9.1}$$

where $\boldsymbol{r}'$ labels a charge element inside the nucleus (Figure 9.1).

9.1.2 Multipole expansion far from the nucleus

Far from the nucleus one expands the Coulomb kernel in Legendre polynomials. Write

$$|\boldsymbol{r}-\boldsymbol{r}'| = r\left(1 - 2\frac{r'}{r}\cos\theta + \left(\frac{r'}{r}\right)^2\right)^{1/2},$$

with θ the angle between $\boldsymbol{r}$ and $\boldsymbol{r}'$. For $r > r'$ the generating function of Legendre polynomials is

$$\frac{1}{|\boldsymbol{r}-\boldsymbol{r}'|} = \frac{1}{r}\sum_{\ell=0}^{\infty}\left(\frac{r'}{r}\right)^{\ell} P_\ell(\cos\theta). \tag{9.2}$$

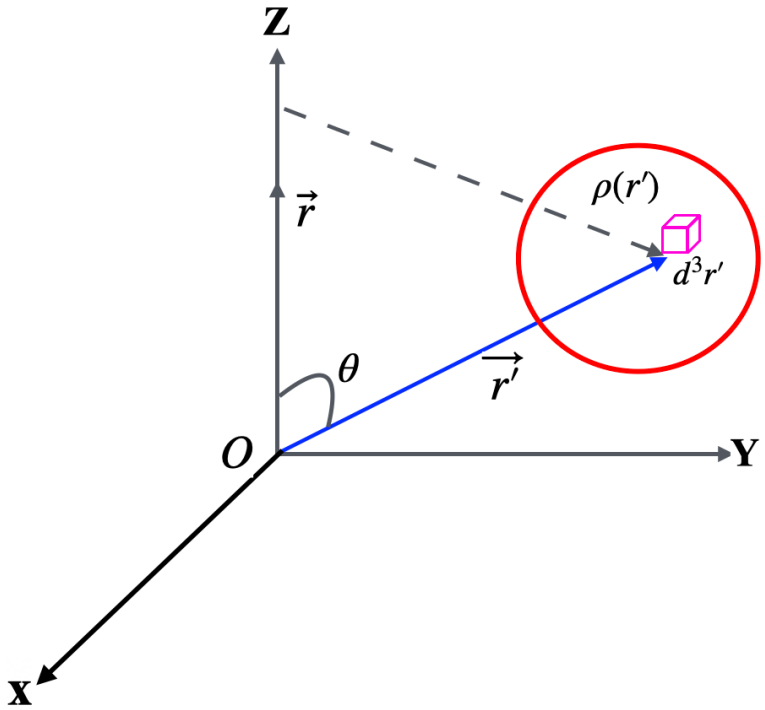

Figure 9.1: Charge distribution $\rho(\boldsymbol{r}')$ inside a nucleus (Fig. 1 of the lecture). An infinitesimal charge element occupies volume d^3r' at $\boldsymbol{r}'$. The field point $\boldsymbol{r}$ lies outside the distribution; θ is the angle between $\boldsymbol{r}$ and $\boldsymbol{r}'$.

The first three polynomials are $P_0 = 1$, $P_1(\cos\theta) = \cos\theta$, and $P_2(\cos\theta) = \tfrac{1}{2}(3\cos^2\theta - 1)$, so

$$\frac{1}{|\boldsymbol{r} - \boldsymbol{r}'|} = \frac{1}{r}\left(1 + \frac{r'}{r}\cos\theta + \frac{r'^2}{2r^2}(3\cos^2\theta - 1) + \cdots\right). \tag{9.3}$$

The quadrupole term is precisely the $\ell = 2$ piece of this expansion: it is of order $(r'/r)^2$ and must be retained if one wishes to discuss Q. (Omitting r'^2/r^2 would truncate before the quadrupole appears.)

Substitute (9.3) into (9.1):

$$\Phi(\boldsymbol{r}) = \frac{1}{4\pi\varepsilon_0}\int \rho(\boldsymbol{r}')\frac{1}{r}\left(1 + \frac{r'}{r}\cos\theta + \frac{r'^2}{2r^2}(3\cos^2\theta - 1) + \cdots\right)\mathrm{d}^3r'. \tag{9.4}$$

Collecting powers of $1/r$ and writing the integrated moments in standard form,

$$\Phi(\boldsymbol{r}) = \frac{e}{4\pi\varepsilon_0 r}\left(Z\,P_0 + \frac{D}{r}\,P_1(\cos\theta) + \frac{Q}{r^2}\,P_2(\cos\theta) + \cdots\right), \tag{9.5}$$

where

- the **monopole** Z is the total charge (in units of e);
- D is the **electric dipole** moment;
- Q is the **electric quadrupole** moment.

Nuclear ground states of definite parity have vanishing static electric dipole. The first multipole

that can report a permanent deformation is therefore the quadrupole.

9.1.3 Definition of the quadrupole tensor

The Cartesian quadrupole tensor associated with the third term of the expansion is

$$Q_{ij} = \int \rho(\boldsymbol{r})(3x_i x_j - r^2\delta_{ij})\,\mathrm{d}^3r, \tag{9.6}$$

with $i, j = x, y, z$ and δ_{ij} the Kronecker symbol. Examples:

$$Q_{xx} = \int \rho(\boldsymbol{r})\,(3x^2 - r^2)\,\mathrm{d}^3r, \tag{9.7}$$

$$Q_{xy} = \int \rho(\boldsymbol{r})\,(3xy)\,\mathrm{d}^3r. \tag{9.8}$$

There are nine components, but only five are independent (the tensor is symmetric and traceless). In nuclear spectroscopy the component measured in the stretched state is almost always

$$Q \equiv Q_{zz} = \int \rho(\boldsymbol{r})\,(3z^2 - r^2)\,\mathrm{d}^3r = e\langle 3z^2 - r^2\rangle \tag{9.9}$$

(when ρ is written so that eQ has the dimension of charge times area; tables often quote Q in barns). Classically, $Q > 0$ for a prolate (cigar-like) distribution along z, and $Q < 0$ for an oblate (flattened) one.

9.1.4 Spherical symmetry forces vanishing quadrupole

If the charge density is spherically symmetric, $\rho = \rho(r)$ only, then by symmetry

$$\int z^2\rho\,\mathrm{d}^3r = \int x^2\rho\,\mathrm{d}^3r = \int y^2\rho\,\mathrm{d}^3r = \frac{1}{3}\int r^2\rho\,\mathrm{d}^3r. \tag{9.10}$$

Hence $3z^2 - r^2$ averages to zero and

$$Q_{zz} = \int \rho(\boldsymbol{r}')\,(3z^2 - r^2)\,\mathrm{d}^3r' = 0. \tag{9.11}$$

Equivalently, on a sphere $x^2 = y^2 = z^2$ so $r^2 = 3z^2$ and $3z^2 - r^2 = 0$ pointwise in the average sense of (9.11). **A spherical charge distribution has no electric quadrupole moment.**

9.2 Deuteron quadrupole moment

9.2.1 Pure S-wave implies vanishing Q_d

Free protons and neutrons have vanishing electric quadrupole moments. Any nonzero Q of the deuteron must come from the *orbital* distribution of the proton's charge about the centre of mass.

If the NN potential were purely central, the ground state would be pure $L = 0$. The spatial wave function is then proportional to the spherical harmonic Y_{00}, which is angle-independent. The charge density is therefore spherically symmetric, and the multipole argument of Section 9.1.4

applies at once:

$$Q_d(L{=}0) = 0. \tag{9.12}$$

A pure s-wave deuteron would look electromagnetically spherical.

9.2.2 The measured value

Experiment finds a small but clearly nonzero moment for the bound deuteron [6]:

$$Q_d = Q_{zz} = 2.88 \times 10^{-27}\,\mathrm{cm}^2 = 0.00288\,\mathrm{b} = 0.288\,\mathrm{e}\cdot\mathrm{fm}^2. \tag{9.13}$$

(The unit is area, as required by (9.9); one barn $= 10^{-28}\,\mathrm{m}^2 = 100\,\mathrm{fm}^2$.) The value is tiny compared with collective rare-earth rotors (several barns), but it is not zero. That single experimental fact rules out a pure $L = 0$ ground state and, with it, a purely central NN potential.

A geometric scale eR^2 with $R \sim 2\,\mathrm{fm}$ is a few $e\cdot\mathrm{fm}^2$; the measured $Q_d \sim 0.3\,e\cdot\mathrm{fm}^2$ is smaller, consistent with a mild deformation from a few-percent D-wave rather than a strongly deformed rotor.

9.2.3 Mixed wave function and the D-state

Using the mixed ground state of Lecture 8,

$$|\psi\rangle = a_S|S\rangle + a_D|D\rangle, \qquad |a_S|^2 + |a_D|^2 = 1,$$

the spectroscopic quadrupole moment in the stretched state is

$$Q_d = \langle\psi|\hat{Q}_{zz}|\psi\rangle = |a_S|^2 Q_{SS} + 2\,\mathrm{Re}(a_S^* a_D)\,Q_{SD} + |a_D|^2 Q_{DD}. \tag{9.14}$$

The pure-S matrix element vanishes by spherical symmetry, $Q_{SS} = 0$. The interference and pure-D pieces may be written in terms of the radial functions $u(r) = rR_S(r)$ and $w(r) = rR_D(r)$ (standard Blatt–Weisskopf / Reid normalisation) as

$$Q_d = \frac{\sqrt{2}}{10}\int_0^\infty r^2\,(uw - \tfrac{w^2}{\sqrt{8}})\mathrm{d}r \quad \text{(in units of } e\text{)}, \tag{9.15}$$

up to an overall conventional factor of e when Q is quoted in $e\cdot\mathrm{fm}^2$. Equivalently, the dominant contribution is the S–D interference term $\propto a_S a_D$; the pure D–D piece is smaller because P_D itself is small. Evaluating the radial integrals requires a model for $u(r)$ and $w(r)$. Realistic potentials fitted to NN scattering reproduce $Q_d \approx 0.286\,e\cdot\mathrm{fm}^2$ with a few-percent D-state probability, consistent with the magnetic-moment estimate of Lecture 8 once exchange currents are acknowledged [6]. The positive sign of Q_d means a prolate (cigar-like) charge distribution along the spin axis.

Key idea

Two multipoles, one structure.

Observable	Pure S prediction	Experiment
μ_d/μ_N	0.880	0.857
Q_d	0	0.00288 b

Both point to a small D-wave. The quadrupole moment is an on/off signal of nonsphericity; the magnetic moment is a percent-level correction to an already large spin moment.

Caution

Extracting P_D from Q_d alone is model dependent because the D-state radial wave function is not measured directly. Potentials that produce a few-percent D-state also produce the observed Q_d, and scattering analyses agree. The qualitative need for a tensor force does not rest on a single fitted percentage [6].

9.3 Non-central force and the tensor operator

9.3.1 Why a central potential cannot mix L

In a purely central potential $V(r)$, orbital angular momentum is a constant of the motion: $[\boldsymbol{L}^2, H] = 0$. Energy eigenstates may therefore be chosen with definite L. A single eigenstate cannot be a coherent superposition of $L = 0$ and $L = 2$. Experiment, however, requires precisely that mixture: $Q_d \neq 0$ and the magnetic-moment deficit. The residual NN interaction therefore cannot be purely central; it must contain a piece that does not commute with $\boldsymbol{L}^2$.

Spin–spin forces of the form $V_\sigma(r)\,\boldsymbol{\sigma}_1 \cdot \boldsymbol{\sigma}_2$ still depend only on the relative distance: they split triplet from singlet but do not mix different L. The operator that couples S and D must involve the orientation of the relative vector $\boldsymbol{r}$ with respect to the nucleon spins.

9.3.2 Magnetic-dipole analogy and the tensor operator

A familiar non-central interaction is the force between two magnetic dipoles. At fixed separation the energy depends on how the moments are oriented relative to $\hat{\boldsymbol{r}}$: collinear and sideways arrangements are not equivalent.

Classically,

$$U \propto \frac{3(\boldsymbol{m}_1 \cdot \hat{r})(\boldsymbol{m}_2 \cdot \hat{r}) - \boldsymbol{m}_1 \cdot \boldsymbol{m}_2}{r^3}.$$

Replacing magnetic moments by nucleon spin operators yields the **tensor operator**

$$S_{12} = 3(\boldsymbol{\sigma}_1 \cdot \hat{r})(\boldsymbol{\sigma}_2 \cdot \hat{r}) - \boldsymbol{\sigma}_1 \cdot \boldsymbol{\sigma}_2, \tag{9.16}$$

and a potential piece $V_T(r)\,S_{12}$. In the coupled ${}^3S_1$–${}^3D_1$ subspace the angular matrix elements of S_{12} are standard:

$$\langle {}^3S_1|S_{12}|{}^3S_1\rangle = 0, \quad \langle {}^3S_1|S_{12}|{}^3D_1\rangle = \sqrt{8}, \quad \langle {}^3D_1|S_{12}|{}^3D_1\rangle = -2. \tag{9.17}$$

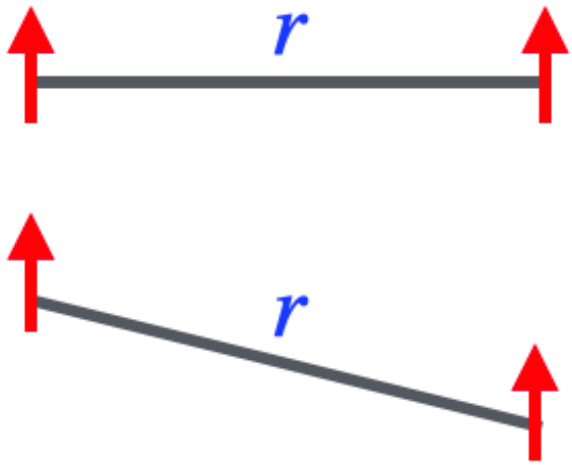

Figure 9.2: Two dipoles at fixed r: collinear versus tilted. The force depends on orientation, so it is non-central.

(The vanishing S–S diagonal shows that a pure central spin–spin force cannot mix L; only the off-diagonal tensor matrix element does.) Writing the radial wave as $\psi = u(r)Y_S + w(r)Y_D$, the coupled radial Schrödinger equations in the deuteron channel become

$$-\frac{\hbar^2}{m}\frac{\mathrm{d}^2 u}{\mathrm{d}r^2} + V_C u + \sqrt{8}\,V_T w = E u, \tag{9.18}$$

$$-\frac{\hbar^2}{m}\left(\frac{\mathrm{d}^2 w}{\mathrm{d}r^2} - \frac{6w}{r^2}\right) + (V_C - 2V_T - 3V_{LS})w + \sqrt{8}\,V_T u = E w, \tag{9.19}$$

where V_C collects central (including spin–spin) pieces and V_{LS} is the spin–orbit term. The off-diagonal $\sqrt{8}\,V_T$ is precisely what mixes u and w and generates $Q_d \neq 0$.

One-pion exchange produces exactly this tensor structure at long range, with radial factors $e^{-m_\pi r}/r$ and polynomials in $1/(m_\pi r)$ [6, 2, 4, 9]. In the deuteron channel V_T mixes ${}^3S_1$ with ${}^3D_1$, generates $Q_d \neq 0$, and shifts μ_d by a few percent. That mixing is the clearest bound-state evidence for the tensor character of the residual nuclear force [6].

Definition

Tensor force. The non-central NN potential contains $V_T(r)S_{12}$. In the deuteron it is responsible for S–D mixing, for $Q_d \neq 0$, and for the small correction to μ_d.

9.3.3 The full NN potential is richer

Phenomenological potentials include central, spin–spin, tensor, spin–orbit, and short-range terms, with isospin dependence. The deuteron bound state has taught us the first three. Scattering (all partial waves, both singlet and triplet, as functions of energy) fixes the rest. When the bound state runs out of information, the continuum (scattering) takes over.

9.4 Quadrupole moments of heavier nuclei (context)

Tables of quadrupole moments place the deuteron in perspective. Many nuclei have $|Q|$ of order eR^2 (single-particle scale). Rare-earth nuclei reach several barns: the whole proton distribution is collectively deformed. Closed-shell nuclei have $Q \approx 0$. For deformed heavy nuclei one distinguishes the **intrinsic** quadrupole moment Q_0 in the body-fixed frame from the **spectroscopic** moment measured in the laboratory; they differ by a projection factor depending on I. The deuteron is the few-body extreme: weak binding, small spectroscopic Q, tensor-driven rather than collective [6, 1].

9.5 Synthesis: Lectures 7–9

Lecture	Observable	Lesson
7	$B_d \approx 2.224\,\text{MeV}$	Range $\sim 2\,\text{fm}$, depth $\sim 35\,\text{MeV}$; barely bound
8	$I^\pi = 1^+$, $\mu_d = 0.857\,\mu_N$	Triplet; $\sim 96\%$ S + $\sim 4\%$ D; spin-dependent force
9	$Q_d = 0.00288\,\text{b}$	Nonspherical; tensor force $V_T S_{12}$

Takeaway

Physics of Lecture 9.

- $Q = \langle 3z^2 - r^2 \rangle$: vanishes for spherical charge distributions.
- $Q_d = 0.00288\,\text{b} \neq 0$: the deuteron is not a pure S-state.
- Consistent few-percent D-wave from μ_d and Q_d.
- Tensor operator S_{12} encodes the non-central force; pion exchange is its long-range origin.
- Lectures 7–9 define the qualitative NN force; Lectures 10–11 develop scattering phase shifts and meson exchange for the course.

9.6 Deeper physics: spectroscopic Q, shells, and one-pion tensor force

9.6.1 Intrinsic vs spectroscopic quadrupole moment

For deformed heavy nuclei one distinguishes the **intrinsic** quadrupole moment Q_0 in the body-fixed frame from the **spectroscopic** moment Q measured in the lab. They are related by a Clebsch–Gordan projection factor depending on I. For the deuteron $I = 1$ there is no collective rotor picture: Q_d is a few-body matrix element of $r^2 Y_{20}$ between S and D components. Standard values are

$$Q_d \approx +0.286\,\text{e} \cdot \text{fm}^2 \tag{9.20}$$

and stresses that free nucleons have $Q = 0$, so any nonzero deuteron Q is purely orbital / deformation physics [6].

9.6.2 Shell-model systematics of Q

The plot of quadrupole moments versus Z shows sign changes near magic numbers: closed shells are spherical ($Q \approx 0$); a valence proton hole just below a shell tends to give prolate $Q > 0$, while a particle just above tends toward oblate $Q < 0$ in the single-particle picture. Collective mid-shell nuclei have Q many times the single-particle estimate. The deuteron sits at the opposite extreme: no shells, weak binding, small Q generated by tensor-driven D-wave admixture [1].

9.6.3 One-pion exchange and S_{12}

The long-range NN force is one-pion exchange (Yukawa). The pseudoscalar pion coupling produces a potential containing the tensor operator S_{12} with radial dependence

$$V_T(r) \propto \frac{e^{-m_\pi r}}{r}\left(1 + \frac{3}{m_\pi r} + \frac{3}{(m_\pi r)^2}\right) \tag{9.21}$$

(up to spin–isospin factors). The angular matrix elements (9.17) then feed into the coupled equations (9.18)–(9.19), so pion exchange is the microscopic origin of the magnetic-dipole analogy in the lecture: it is non-central and mixes ${}^3S_1$–${}^3D_1$. Short-range repulsion, spin–orbit forces, and multi-pion / contact terms complete modern potentials (Argonne, CD-Bonn, chiral EFT). The deuteron Q_d and η_D (D/S asymptotic ratio) are primary constraints on V_T [6, 4, 2].

Key idea

Tensor force checklist.

- Operator: $S_{12} = 3(\boldsymbol{\sigma}_1 \cdot \hat{r})(\boldsymbol{\sigma}_2 \cdot \hat{r}) - \boldsymbol{\sigma}_1 \cdot \boldsymbol{\sigma}_2$.
- Bound-state signals: $Q_d \neq 0$, $\mu_d \neq \mu_p + \mu_n$, few-percent D-state probability (model dependent).
- Continuum signals: mixing parameters in NN phase-shift analyses (ε_1, etc.).
- Microscopic origin: one-pion exchange at long range.

9.6.4 What remains for scattering

Bound-state multipoles fix the deuteron channel. Scattering states access all partial waves, both singlet and triplet, as functions of energy. Phase shifts $\delta_{^1S_0}(E)$, $\delta_{^3S_1}(E)$, P- and D-wave phase shifts, and mixing angles complete the NN interaction and feed into many-body nuclear structure. That programme is the natural continuation of Lectures 7–9 [2, 6].

9.7 Further physics: multipoles beyond the quadrupole

Outside a localised charge distribution the electrostatic potential admits a multipole expansion: monopole (total charge), dipole (vanishes for definite-parity ground states), quadrupole, octupole, ... At large distance the lowest non-vanishing multipole dominates [13, 1, 6].

The same logic applies to magnetic multipoles and to radiation. In γ decay, multipole selection rules (angular momentum and parity of the photon field) organise transition rates (a topic for later lectures). For the deuteron ground state the essential static multipoles are already in hand: magnetic dipole μ_d and electric quadrupole Q_d. Together they require a tensor force and a few-percent D-wave, completing the qualitative NN picture of Lectures 7–9.

9.7.1 Deformation and quadrupole moments of heavier nuclei

Nuclei near closed (magic) shells are nearly spherical and have small Q. Nuclei far from magic numbers are often permanently deformed and can have large spectroscopic quadrupole moments; rotational bands appear in the spectrum [14, 6, 13]. The deuteron is the opposite extreme: few-body, weakly deformed, with Q_d generated by a small D-wave rather than collective rotation.

Static multipoles (monopole, dipole, quadrupole, ...) also organise electromagnetic radiation: γ transitions carry multipolarity $E1, M1, E2, \ldots$ with selection rules fixed by angular momentum and parity [13], the dynamical counterpart of the static moments used here.

9.7.2 Deuteron quadrupole moment in numbers

The free neutron and proton have vanishing electric quadrupole moments, so any $Q_d \neq 0$ must come from orbital structure. Experiment gives

$$Q_d = +0.00288\,\mathrm{b} = +0.286\,\mathrm{fm}^2, \tag{9.22}$$

small compared with heavy deformed nuclei but definitely nonzero [6]. A pure ${}^3S_1$ wave function would yield $Q_d = 0$. A mixed $S{+}D$ wave function produces

$$Q_d \propto a_S a_D \,\langle r^2 \rangle_{SD} + a_D^2 \,\langle r^2 \rangle_{DD}, \tag{9.23}$$

so Q_d is linearly sensitive to the S–D interference. Realistic potentials that fit scattering and B_d reproduce Q_d with a_D^2 of a few percent, consistent with the magnetic-moment estimate [6, 14].

The positive sign of Q_d corresponds to a prolate (cigar-like) deformation: more charge along the symmetry axis than in the equatorial plane.

9.7.3 Single-particle vs collective quadrupole moments

For a single valence proton in an orbit of mean-square radius $\langle r^2 \rangle \sim R^2 \sim r_0^2 A^{2/3}$, one expects

$$|Q| \lesssim e\,R^2 \sim 0.06\text{–}0.5\,e \cdot \mathrm{b} \tag{9.24}$$

from light to heavy nuclei. Many odd-A moments fall in that range, but rare-earth and actinide nuclei reach several $e \cdot \mathrm{b}$: the entire charged core is permanently deformed, so many protons contribute coherently [6, 2]. Even–even nuclei have vanishing spectroscopic Q in the laboratory frame if $I = 0$, but large *intrinsic* quadrupole moments show up in rotational spectra and in Coulomb excitation.

9.7.4 Tensor operator S_{12} and noncentral force

The simplest scalar operator that couples spin and relative coordinate is

$$S_{12} = 3(\boldsymbol{\sigma}_1 \cdot \hat{\boldsymbol{r}})(\boldsymbol{\sigma}_2 \cdot \hat{\boldsymbol{r}}) - \boldsymbol{\sigma}_1 \cdot \boldsymbol{\sigma}_2. \tag{9.25}$$

A potential $V_T(r)\, S_{12}$ is the tensor force. It vanishes when averaged over a spherically symmetric s-wave alone, but it mixes ${}^3S_1$ and ${}^3D_1$ and generates Q_d. In heavier nuclei the same tensor force contributes to the spin-orbit splitting and to few-nucleon binding, though its expectation value is partially averaged by many-body motion [14, 6].

One-pion exchange naturally produces a tensor potential of Yukawa range $r_0 \approx 1.4\,\mathrm{fm}$; that is the long-range reason the deuteron is not a pure s-wave state [9, 14].

9.7.5 Parity and multipole selection

A static electric multipole of order ℓ has parity $(-1)^\ell$; a magnetic multipole has parity $(-1)^{\ell+1}$. Nuclear ground states of definite parity therefore forbid static electric dipoles: the lowest allowed electric deformation is the quadrupole. That is why Q is the first multipole beyond the monopole in the structural discussion of the deuteron and of deformed heavy nuclei [1, 6].

9.8 Problems with solutions

Problem 9.1 — $Q = 0$ for a sphere

Show that $Q_{zz} = \int \rho(3z^2 - r^2)\,\mathrm{d}^3r$ vanishes for any spherically symmetric $\rho(r)$.

Solution 9.1

Spherical symmetry $\Rightarrow \int x^2\rho = \int y^2\rho = \int z^2\rho = \tfrac{1}{3}\int r^2\rho$. Hence

$$\int (3z^2 - r^2)\rho = 3 \cdot \tfrac{1}{3}\int r^2\rho - \int r^2\rho = 0.$$

A pure $L = 0$ deuteron would have $Q_d = 0$ [6].

Problem 9.2 — Units of Q_d

The deuteron quadrupole moment is $Q_d = 0.00288\,\mathrm{b}$ and also $2.88 \times 10^{-27}\,\mathrm{cm}^2$. Convert the barn value to $\mathrm{e}\cdot\mathrm{fm}^2$ ($1\,\mathrm{b} = 100\,\mathrm{fm}^2$) and verify consistency with $10^{-27}\,\mathrm{cm}^2$.

Solution 9.2

$$0.00288\,\mathrm{b} = 0.00288 \times 100 = 0.288\,\mathrm{fm}^2 = 0.288\,\mathrm{e}\cdot\mathrm{fm}^2$$

(charge e understood in nuclear tables). Also $1\,\mathrm{b} = 10^{-28}\,\mathrm{m}^2 = 10^{-24}\,\mathrm{cm}^2$, so

$$0.00288\,\mathrm{b} = 0.00288 \times 10^{-24}\,\mathrm{cm}^2 = 2.88 \times 10^{-27}\,\mathrm{cm}^2,$$

matching the lecture value. Compared with eR^2 for $R \sim 2\,\mathrm{fm}$ ($\sim 4\,e\cdot\mathrm{fm}^2$), the deformation is mild [6].

Problem 9.3 — Far-field expansion coefficient

Starting from

$$\frac{1}{|\boldsymbol{r}-\boldsymbol{r}'|} = \frac{1}{r}\left(1 - 2\frac{r'}{r}\cos\theta\right)^{-1/2}$$

(for $r \gg r'$), expand to order $(r'/r)^2$ and identify the $P_2(\cos\theta)$ term that defines the quadrupole contribution to Φ.

Solution 9.3

Binomial expansion $(1-x)^{-1/2} = 1 + \frac{1}{2}x + \frac{3}{8}x^2 + \cdots$ with $x = 2(r'/r)\cos\theta$:

$$\begin{aligned}\frac{1}{|\boldsymbol{r}-\boldsymbol{r}'|} &= \frac{1}{r}\left[1 + \frac{r'}{r}\cos\theta + \frac{3}{2}\left(\frac{r'}{r}\right)^2\cos^2\theta + \cdots\right] \\ &= \frac{1}{r}\left[1 + \frac{r'}{r}\cos\theta + \frac{r'^2}{2r^2}(3\cos^2\theta - 1) + \frac{r'^2}{2r^2} + \cdots\right].\end{aligned}$$

The angular piece $(3\cos^2\theta - 1) = 2P_2(\cos\theta)$ multiplies r'^2/r^3 in Φ and defines the quadrupole multipole after integration against $\rho(\boldsymbol{r}')$ [6, 1].

Problem 9.4 — Why a tensor force is required

Given $I^\pi = 1^+$, $\mu_d \neq \mu_p + \mu_n$, and $Q_d \neq 0$, explain why a purely central NN potential is ruled out.

Solution 9.4

A central potential conserves L, so each energy eigenstate has definite L. Even parity and $I = 1$ allow $L = 0$ and $L = 2$ separately, but not a coherent mixture in one eigenstate. Nonzero Q_d requires nonsphericity (D-wave), and the μ_d deficit requires the same mixture. The tensor force $V_T(r)S_{12}$ is the non-central operator that mixes ${}^3S_1$ and ${}^3D_1$ [6, 14].

Problem 9.5 — Tensor operator on a pure S-wave

The tensor operator is $S_{12} = 3(\boldsymbol{\sigma}_1\cdot\hat{r})(\boldsymbol{\sigma}_2\cdot\hat{r}) - \boldsymbol{\sigma}_1\cdot\boldsymbol{\sigma}_2$. Argue why $\langle S_{12}\rangle = 0$ in a pure ${}^3S_1$ state with spherical average, yet S_{12} can still mix S and D waves.

Solution 9.5

In a pure s-wave the orbital density is isotropic. Averaging $(\boldsymbol{\sigma}_1\cdot\hat{r})(\boldsymbol{\sigma}_2\cdot\hat{r})$ over angles reduces it to $\frac{1}{3}\boldsymbol{\sigma}_1\cdot\boldsymbol{\sigma}_2$, so $\langle S_{12}\rangle = 0$. Off-diagonal matrix elements between $L = 0$ and $L = 2$ need not vanish: S_{12} transforms as a rank-2 tensor and connects $\Delta L = 2$. That is how a

small D-wave is generated even though the pure-S diagonal expectation is zero [14, 6].

Problem 9.6 — Geometric scale of Q

Estimate the single-particle quadrupole scale eR^2 for $R = r_0 A^{1/3}$ with $r_0 = 1.2\,\mathrm{fm}$ at $A = 2$ and at $A = 160$. Compare with $Q_d = 0.288\,e\cdot\mathrm{fm}^2$ and with rare-earth moments of several $e\cdot\mathrm{b}$.

Solution 9.6

$$R(A{=}2) \approx 1.2 \times 1.26 \approx 1.5\,\mathrm{fm}, \quad eR^2 \approx 2.3\,e\cdot\mathrm{fm}^2;$$

$$R(A{=}160) \approx 1.2 \times 5.4 \approx 6.5\,\mathrm{fm}, \quad eR^2 \approx 42\,e\cdot\mathrm{fm}^2 = 0.42\,e\cdot\mathrm{b}.$$

Q_d is $\ll eR^2(A{=}2)$ (weak D-wave deformation). Collective rare-earth $Q \sim$ few b exceed the single-particle scale by an order of magnitude (coherent core deformation) [6, 2].

Chapter 10

Scattering of Nucleons

"Although the study of the deuteron gives us a number of clues about the nucleon–nucleon interaction, the total amount of information available is limited... To study the nucleon–nucleon interaction in different configurations, we can perform nucleon–nucleon scattering experiments."

K. S. Krane

The deuteron (Lectures 7–9) is the only bound two-nucleon system. It samples the residual NN force in a single channel, mostly ${}^3S_1$ with a few-percent D-wave, at a fixed average separation fixed by weak binding. That is not enough to reconstruct the full force. There are no bound excited states to explore other partial waves or spin orientations, and the continuum is invisible from multipole moments alone [6].

Scattering supplies what the bound state cannot: controllable energy, access to $\ell = 0, 1, 2, \ldots$, and both spin channels. In this lecture the experimental definition of the cross section is tied to partial-wave analysis. Phase shifts δ_ℓ become the language in which theory and experiment meet for a short-range central potential [6, 1, 2, 14].

10.1 Why scatter neutrons on protons?

A scattering experiment uses a monoenergetic **projectile** beam and a **target** with many scattering centres. For n–p scattering the projectiles are neutrons of chosen kinetic energy and the target is hydrogen: each scattering centre is a free proton (bound only in the atom, irrelevant at nuclear energies). A detector at polar angle θ relative to the beam axis counts scattered particles. For a central force the yield does not depend on the azimuthal angle ϕ.

Hydrogen is essential for a clean NN measurement. On a heavy nucleus an incident nucleon would scatter from several target nucleons within the force range, so the observed yield would mix many-body effects. On hydrogen each encounter is a single np collision; multiple scattering from different atoms is rare if the target is thin [6]. The same philosophy motivates electron scattering on thin foils when one wants the elementary charge form factor (Lecture 1): isolate one interaction per projectile.

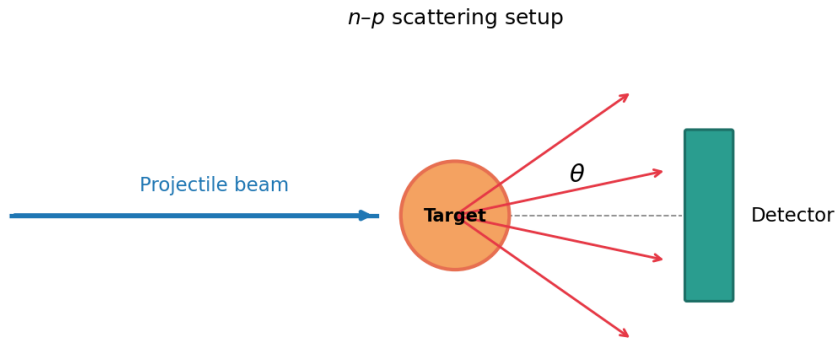

Figure 10.1: Schematic n–p scattering setup: monoenergetic projectile beam, hydrogen target, and detector at angle θ.

10.2 Differential and total cross sections

The number $\mathrm{d}N$ of particles recorded in time t into solid angle $\mathrm{d}\Omega$ grows with exposure time, detector acceptance, beam intensity I (particles per unit area per unit time), and the number of target centres N_t (or areal density n_a times the illuminated area). These experimental knobs are factored out by defining the **differential scattering cross section** $\mathrm{d}\sigma/\mathrm{d}\Omega$ through

$$\mathrm{d}N = \frac{\mathrm{d}\sigma}{\mathrm{d}\Omega}\, t\, \mathrm{d}\Omega\, I\, N_t. \tag{10.1}$$

Equivalently,

$$\frac{\mathrm{d}\sigma}{\mathrm{d}\Omega} = \frac{\mathrm{d}N}{\mathrm{d}\Omega\, n_a\, N_p}, \qquad N_p = tIA, \tag{10.2}$$

with A the beam area. The cross section has dimensions of area; the historical unit is the barn,

$$1\,\mathrm{b} = 10^{-28}\,\mathrm{m}^2 = 100\,\mathrm{fm}^2.$$

Nuclear NN cross sections at low energy are tens of barns, huge compared with the geometric size of a nucleon ($\sim 1\,\mathrm{fm}^2$), a quantum enhancement characteristic of low-energy s-wave scattering [6, 1].

Physically, $\mathrm{d}\sigma/\mathrm{d}\Omega$ is the effective area that the target presents for scattering into $\mathrm{d}\Omega$. It packages all of the unknown dynamics into a measurable quantity: once $\mathrm{d}\sigma/\mathrm{d}\Omega$ is known, one can compare theories without redoing the experiment for every proposed potential.

Angles and energies may be quoted in the laboratory or centre-of-mass (CM) frame. Partial-wave formulae below are written in the CM frame; converting to laboratory angles for equal-mass np scattering is a standard kinematic exercise. The **total** elastic cross section is the angular integral

$$\sigma_{\mathrm{tot}} = \int \frac{\mathrm{d}\sigma}{\mathrm{d}\Omega}\, \mathrm{d}\Omega. \tag{10.3}$$

For pure s-wave scattering, $\mathrm{d}\sigma/\mathrm{d}\Omega$ is isotropic in the CM frame and $\sigma_{\mathrm{tot}} = 4\pi\,(\mathrm{d}\sigma/\mathrm{d}\Omega)$.

10.3 Central potential, plane waves, and partial waves

A **central** potential $V(r)$ depends only on the nucleon–nucleon separation. Angular momentum about the force centre is then conserved, so eigenstates of definite orbital angular momentum ℓ are useful. In the absence of interaction the incident beam is a plane wave along z,

$$\psi_{\text{inc}} = e^{ikz}, \qquad k = \frac{p}{\hbar} = \frac{\sqrt{2\mu E}}{\hbar}, \tag{10.4}$$

where $\mu \approx m_N/2$ is the reduced mass of the NN system and E is the centre-of-mass kinetic energy. Multiplying by $e^{-iEt/\hbar}$ makes the wave travel in the $+z$ direction: toward the target for $z < 0$ and away from it for $z > 0$ [6].

A plane wave has definite energy and momentum along z, but it is *not* an eigenstate of $\boldsymbol{L}^2$. It is a coherent superposition of all orbital angular momenta. Because of axial symmetry about the beam, only projections $m = 0$ appear. The expansion in spherical waves (partial waves) reads

$$e^{ikz} = \sum_{\ell=0}^{\infty} i^{\ell}(2\ell+1)\, j_{\ell}(kr)\, P_{\ell}(\cos\theta), \tag{10.5}$$

where j_ℓ are spherical Bessel functions and P_ℓ Legendre polynomials. Each term $\ell = 0, 1, 2, \ldots$ is an s, p, d, … wave with a definite impact-parameter character in the semiclassical picture.

10.4 Phase shifts: what a short-range potential can do

Detectors sit centimetres from the target, while the nuclear force acts only for $r \lesssim$ a few fm. Outside the force range the wave is free again; the potential cannot change its wavelength there. What it *can* do is shift the phase of each outgoing partial wave relative to the free solution.

Free spherical waves have the asymptotic form

$$j_{\ell}(kr) \sim \frac{\sin(kr - \ell\pi/2)}{kr} \qquad (kr \to \infty). \tag{10.6}$$

In the presence of a short-range central potential the radial function $u_\ell(r) = rR_\ell(r)$ for r larger than the force range becomes

$$u_{\ell}(r) \sim \sin\!\big(kr - \ell\pi/2 + \delta_{\ell}\big), \tag{10.7}$$

where $\delta_\ell(E)$ is the **phase shift** in channel ℓ [6, 2]. Attractive potentials typically pull nodes of u_ℓ toward the origin (positive δ_ℓ); repulsive potentials push nodes outward (negative δ_ℓ).

All information about $V(r)$ that elastic scattering at energy E can provide is encoded in the set $\{\delta_\ell(E)\}$. Solving the radial Schrödinger equation for a model potential and reading δ_ℓ is the theoretical route; measuring $\mathrm{d}\sigma/\mathrm{d}\Omega$ and fitting δ_ℓ is the experimental route. Phase shifts themselves are not directly observed: they are a convenient parameterisation of the measured cross sections (and polarisations). The two routes meet in (10.11) below.

For $\ell = 0$ one may write the exterior wave as a combination of incoming and outgoing spherical waves $e^{\pm ikr}/r$. Scattering does not create or destroy particles in elastic scattering, so it cannot change the *amplitudes* of those waves; it can only change the relative phase of the

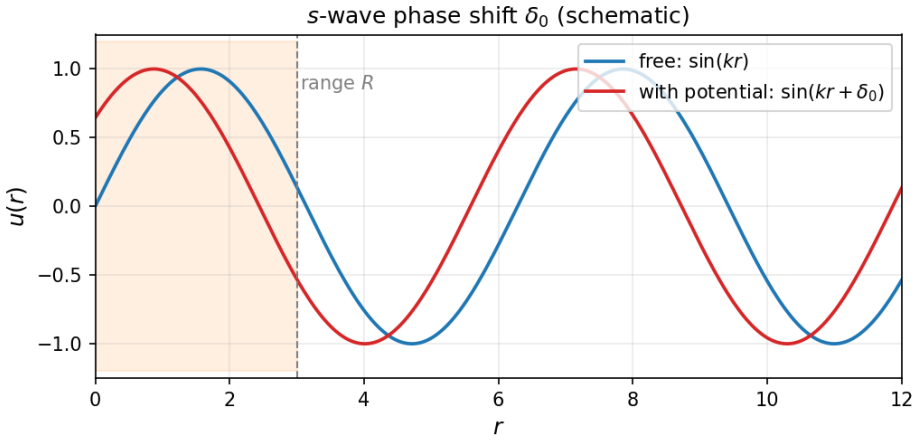

Figure 10.2: Schematic s-wave radial wave $u(r)$. Inside the force range the potential distorts the wave; outside, the free oscillation is shifted by the phase δ_0.

outgoing piece. That single phase is δ_0 (up to a conventional factor of two in intermediate steps of the algebra) [6].

10.5 Cross section from phase shifts

Matching the asymptotic partial-wave solution to an incident plane wave plus outgoing scattered spherical wave produces the scattering amplitude $f(\theta)$. Outside the force range the radial wave in channel ℓ may be written as a superposition of incoming and outgoing spherical waves,

$$u_\ell(r) \propto e^{-i(kr-\ell\pi/2)} - S_\ell\, e^{i(kr-\ell\pi/2)}, \tag{10.8}$$

with the unitary S-matrix element $S_\ell = e^{2i\delta_\ell}$ for a real central potential (elastic scattering). The coefficient of the outgoing scattered wave relative to the free case defines the partial-wave amplitude

$$f_\ell = \frac{S_\ell - 1}{2ik} = \frac{e^{2i\delta_\ell} - 1}{2ik} = \frac{e^{i\delta_\ell}\sin\delta_\ell}{k}. \tag{10.9}$$

Summing over partial waves with the Legendre weights of the plane-wave expansion gives

$$f(\theta) = \sum_{\ell=0}^{\infty} (2\ell+1)\, f_\ell\, P_\ell(\cos\theta) = \frac{1}{k}\sum_{\ell=0}^{\infty} (2\ell+1)\, e^{i\delta_\ell}\sin\delta_\ell\, P_\ell(\cos\theta). \tag{10.10}$$

The CM differential cross section is therefore

$$\frac{\mathrm{d}\sigma}{\mathrm{d}\Omega} = |f(\theta)|^2 = \frac{1}{k^2}\left|\sum_{\ell=0}^{\infty} (2\ell+1)\, e^{i\delta_\ell}\sin\delta_\ell\, P_\ell(\cos\theta)\right|^2. \tag{10.11}$$

(The overall phase convention for $e^{i\delta_\ell}$ varies among sources; the measurable $|f|^2$ is fixed by the δ_ℓ.) The factor $(2\ell+1)$ counts magnetic substates of a given ℓ; the Legendre polynomials build the angular pattern of each partial wave.

When only $\ell = 0$ contributes, $P_0 = 1$ and

$$\frac{\mathrm{d}\sigma}{\mathrm{d}\Omega} = \frac{\sin^2 \delta_0}{k^2}, \tag{10.12}$$

independent of angle in the CM frame. Integrating over 4π and using the orthogonality $\int P_\ell P_{\ell'} \, \mathrm{d}\Omega = 4\pi\delta_{\ell\ell'}/(2\ell+1)$ gives the total cross section

$$\sigma_{\mathrm{tot}} = \frac{4\pi}{k^2} \sum_{\ell=0}^{\infty} (2\ell+1) \sin^2 \delta_\ell = \frac{4\pi}{k^2} \sin^2 \delta_0 \quad (s\text{-wave only}). \tag{10.13}$$

Thus a single number $\delta_0(E)$ determines the entire low-energy elastic yield. The unitarity bound $\sin^2 \delta_0 \leq 1$ implies $\sigma_{\mathrm{tot}} \leq 4\pi/k^2$: at very low energy the quantum cross section can greatly exceed the geometric size of the potential well [6, 14].

For equal-mass np scattering the laboratory and CM scattering angles are related by $\theta_{\mathrm{lab}} = \theta_{\mathrm{CM}}/2$, and

$$\left(\frac{\mathrm{d}\sigma}{\mathrm{d}\Omega}\right)_{\mathrm{lab}} = 4\cos\theta_{\mathrm{lab}} \left(\frac{\mathrm{d}\sigma}{\mathrm{d}\Omega}\right)_{\mathrm{CM}}. \tag{10.14}$$

Partial-wave formulae in this lecture are always in the CM frame unless stated otherwise.

Key idea

Phase shifts δ_ℓ are the interface between potential and data. Theory: solve the radial equation for $V(r)$ and extract δ_ℓ. Experiment: measure $\mathrm{d}\sigma/\mathrm{d}\Omega$ and determine δ_ℓ.

10.6 Low energy: only s-wave scattering

Semiclassically, a projectile of momentum $p = \sqrt{2\mu E}$ that grazes the force range r_0 carries angular momentum $\ell\hbar \sim p r_0$. For nuclear $r_0 \sim 2\,\mathrm{fm}$ and $E \sim 1\,\mathrm{MeV}$ one finds $p r_0/\hbar \ll 1$: the projectile cannot bring $\ell \geq 1$ inside the nuclear force range without flying past outside the well. Only $\ell = 0$ scatters. At $E \sim 10\,\mathrm{MeV}$, $\ell = 1$ begins to contribute [6].

A sharper estimate uses the free kinetic energy scale associated with confinement in a well of size R,

$$T \sim \frac{\ell(\ell+1)\hbar^2}{2\mu R^2}.$$

For $\ell = 1$, $R \sim 1\,\mathrm{fm}$, and $\mu c^2 \sim 500\,\mathrm{MeV}$, T is tens of MeV. Incident energies far below that scale justify the s-wave truncation [6].

This is why low-energy np data are so powerful and so simple: a single phase $\delta_0(E)$ (actually one for each spin channel) carries the dynamics, and $\sigma(\theta)$ is nearly isotropic.

10.7 Square well in the continuum: matching for $E > 0$

The same square well used for the deuteron bound state can be solved for positive energy. For $\ell = 0$,

$$V(r) = \begin{cases} -V_0 & r < R, \\ 0 & r > R, \end{cases} \qquad E > 0. \tag{10.15}$$

Inside, $u(r) = A\sin(k_1 r)$ with $k_1 = \sqrt{2\mu(V_0 + E)}/\hbar$ (regularity at the origin again kills the cosine). Outside,

$$u(r) = C\sin(kr + \delta_0), \qquad k = \frac{\sqrt{2\mu E}}{\hbar}. \tag{10.16}$$

Continuity of u and u' at $r = R$ yields

$$k\cot(kR + \delta_0) = k_1 \cot(k_1 R). \tag{10.17}$$

Solving for the phase shift,

$$\delta_0 = \arctan\!\left(\frac{k}{k_1}\tan(k_1 R)\right) - kR \pmod{\pi}. \tag{10.18}$$

Given E, V_0, and R, one thus obtains $\delta_0(E)$ and then predicts σ_{tot} from (10.13) [6].

In the zero-energy limit $k \to 0$, $k_1 \to K \equiv \sqrt{2\mu V_0}/\hbar$ and the scattering length extracted from $a = -\lim(\tan\delta_0/k)$ becomes

$$a = R - \frac{\tan(KR)}{K}. \tag{10.19}$$

(If $KR = \pi/2$, $a \to \infty$: the zero-energy bound-state threshold of Lecture 7.) Then $\sigma_{\mathrm{tot}} \to 4\pi a^2$.

As $V_0 \to 0$, $\delta_0 \to 0$ and there is no scattering. For the attractive well fitted to the deuteron ($V_0 \approx 35\,\mathrm{MeV}$, $R \sim 2\,\mathrm{fm}$), low-energy δ_0 is large and σ_{tot} is tens of barns. Experiment finds the zero-energy unpolarised np cross section near 20 b, not the ~ 4–5 b that a pure triplet estimate would suggest. The resolution is that free protons and neutrons scatter in a statistical mixture of triplet and singlet spins: three triplet states and one singlet, so the spin weights are $3/4$ and $1/4$. Writing

$$\sigma = \tfrac{3}{4}\sigma_t + \tfrac{1}{4}\sigma_s, \tag{10.20}$$

and taking $\sigma_t \approx 4\pi a_t^2 \sim 4.6\,\mathrm{b}$ from the deuteron (triplet) channel leaves $\sigma_s \sim 70\,\mathrm{b}$: the singlet interaction is strong but just unbound, producing a large negative scattering length [6, 14].

10.8 Scattering length and effective range

At vanishing energy, $\delta_0 \to 0$ in such a way that

$$a = -\lim_{k\to 0}\frac{\tan\delta_0}{k} \tag{10.21}$$

defines the **scattering length** a. From $\sigma_{\text{tot}} = (4\pi/k^2)\sin^2\delta_0$ and $\sin\delta_0 \approx \tan\delta_0 \approx -ka$ one obtains

$$\sigma_{\text{tot}} \to 4\pi a^2. \tag{10.22}$$

The sign of a carries physics: a large *positive* scattering length is characteristic of a barely bound state (triplet, deuteron); a large *negative* scattering length signals a virtual state just above threshold (singlet) [6, 14].

Checked low-energy np numbers

Standard values are $a_t \approx +5.4\,\text{fm}$ (triplet) and $a_s \approx -23.7\,\text{fm}$ (singlet). The unpolarised zero-energy cross section is then

$$\begin{aligned}\sigma &= 4\pi\left(\tfrac{3}{4}a_t^2 + \tfrac{1}{4}a_s^2\right)\\ &= 4\pi\left(\tfrac{3}{4}(5.4)^2 + \tfrac{1}{4}(23.7)^2\right) \approx 4\pi(21.9 + 140.4) \approx 20\,\text{b},\end{aligned}$$

matching experiment. The huge singlet piece dominates because $|a_s|$ is so large: the singlet potential nearly binds [6, 14].

A more accurate low-energy expansion follows from matching the exterior wave to an effective-range expansion of the logarithmic derivative. Writing

$$k\cot\delta_0 = -\frac{1}{a} + \frac{1}{2}r_0k^2 + \cdots, \tag{10.23}$$

defines the effective range r_0 of fermi size. The first two terms already reproduce low-energy $\delta_0(E)$ in each spin channel without committing to a full potential at every energy [6, 14]. Fitting a and r_0 is how modern analyses encode low-energy NN physics.

Key idea

The deuteron fixes the *triplet* well near threshold. Scattering reveals a strong *singlet* interaction that fails to bind, and it maps how $\delta_\ell(E)$ evolve as higher partial waves open with energy.

10.9 Further physics: coherent scattering and spin channels

At very low energy the de Broglie wavelength of a neutron can exceed the size of a hydrogen molecule. Scattering from the two protons then interferes coherently, and the cross sections of ortho- and parahydrogen differ because the total proton spin of the molecule weights triplet and singlet np amplitudes differently. That difference is direct evidence that $\sigma_t \neq \sigma_s$ [6].

The optical analogy remains useful: an attractive well of nuclear size diffracts the incident wave much as an obstacle of size R diffracts light of wavelength $\lambda \sim 2\pi/k$. Partial-wave analysis is the quantum bookkeeping of that diffraction pattern, partial wave by partial wave.

10.10 Problems with solutions

Problem 10.1 — Cross section dimensions

From $\mathrm{d}N = \sigma\, t\, \mathrm{d}\Omega\, I\, N_t$, show that σ has dimensions of area.

Solution 10.1

$\mathrm{d}N$ is dimensionless (a count). tI has dimensions of (time)$\times$(area^{-1} time^{-1})=area^{-1}; N_t is a number; $\mathrm{d}\Omega$ is dimensionless. Hence σ must supply an area so that the product is dimensionless.

Problem 10.2 — Low-energy total cross section

At low energy only δ_0 is nonzero. Show that $\sigma_{\mathrm{tot}} = 4\pi k^{-2} \sin^2 \delta_0$. If $\delta_0 = \pi/2$, what is σ_{tot}?

Solution 10.2

From $f = (e^{i\delta_0} \sin\delta_0)/k$ one has $\mathrm{d}\sigma/\mathrm{d}\Omega = |f|^2 = \sin^2\delta_0/k^2$, isotropic in the CM frame. Integrate:

$$\sigma_{\mathrm{tot}} = \int \frac{\sin^2\delta_0}{k^2}\,\mathrm{d}\Omega = \frac{4\pi}{k^2}\sin^2\delta_0.$$

At resonance-like $\delta_0 = \pi/2$, $\sigma_{\mathrm{tot}} = 4\pi/k^2$ (unitarity limit for s-wave) [6].

Problem 10.3 — Why only s-wave at 1 MeV

Estimate $\ell_{\max} \sim pr_0/\hbar$ for $E = 1\,\mathrm{MeV}$ (lab-scale NN), $r_0 = 2\,\mathrm{fm}$, $\hbar c = 200\,\mathrm{MeV\,fm}$, $\mu c^2 \approx 500\,\mathrm{MeV}$. Argue that $\ell = 0$ dominates.

Solution 10.3

$$pc = \sqrt{2\mu c^2\, E} \approx \sqrt{1000\,\mathrm{MeV}^2} \approx 32\,\mathrm{MeV}, \qquad \frac{pr_0}{\hbar} = \frac{(pc)\,r_0}{\hbar c} \approx \frac{32\times 2}{200} \approx 0.3.$$

Values $\ell \geq 1$ require order-1 or larger; only $\ell = 0$ fits inside the nuclear range at this energy [6].

Chapter 11

Theories of Nuclear Forces

> *"Yukawa noticed that the range of nuclear forces* $r_0 \simeq 1.4\,\mathrm{fm}$ *corresponds to a particle of mass* $m_\pi c^2 \simeq 140\,\mathrm{MeV}$*."*
>
> paraphrasing H. Yukawa (1935)

Lectures 7–10 constrain the residual NN force from two sides: the deuteron multipoles and low-energy phase shifts. Both approaches are phenomenological: they fix a potential (or its phase shifts) to data. This lecture asks a deeper question: *what carries the force?* In modern quantum field theory, forces between particles arise from the exchange of virtual quanta. For electromagnetism the quantum is the massless photon and the potential is Coulomb. For the residual strong force the lightest quantum is the massive pion and the potential is Yukawa [9, 14, 5, 15, 2].

11.1 Three layers of description: from Coulomb to QED

Electromagnetism shows how the same interaction can be told at increasing depth.

Action at a distance. Two charges q_1 and q_2 exert equal and opposite forces

$$F = \frac{1}{4\pi\varepsilon_0}\frac{q_1 q_2}{r^2} \tag{11.1}$$

instantaneously across empty space. The formula works at low speeds, but instantaneous action conflicts with relativity: no influence can travel faster than light.

Classical field. Charge q_1 does not "reach out" to q_2. It produces an electric field filling space; q_2 feels a force because it sits in that field. The field is the intermediary. Changes in the field propagate at finite speed c.

Quantum field (QED). The electromagnetic field is quantized. Energy and momentum are exchanged in discrete packets (photons). The Coulomb force is the low-energy limit of exchanging *virtual* photons: off-shell quanta that mediate the interaction without appearing as free radiation. Virtual photons share the quantum numbers of real photons (massless, chargeless, spin 1); only their four-momentum differs from the on-shell condition $q^2 = 0$ [5, 15].

The same ladder applies to nucleons N_1 and N_2. Classically one might imagine a potential $V(r)$. At the quantum level the interaction is the exchange of virtual mesons. Unlike the photon, those mesons may carry mass and electric charge, and that changes the range and the selection rules of the force.

11.2 Range of a force from the uncertainty principle

A useful *heuristic* estimates the range of a force mediated by a massive quantum. Creating a virtual particle of rest energy mc^2 requires an energy fluctuation of order $\Delta E \sim mc^2$. The uncertainty principle then suggests a lifetime

$$\Delta t \lesssim \frac{\hbar}{\Delta E} \sim \frac{\hbar}{mc^2}. \tag{11.2}$$

Even if the quantum travels near the speed of light, the farthest it can go before being reabsorbed is of order

$$R \lesssim c\,\Delta t \sim \frac{\hbar c}{mc^2} = \frac{\hbar}{mc}. \tag{11.3}$$

This Compton wavelength of the mediator sets the force range. Two limits are immediate:

- **Massless mediator** ($m = 0$): $R \to \infty$. The force is long-ranged (Coulomb, gravity in the Newtonian limit).
- **Massive mediator**: R is finite. The force is short-ranged; beyond a few Compton wavelengths the exchange is exponentially suppressed.

This argument is pedagogical, not a derivation of field theory: it does not claim that energy conservation is violated. The rigorous statement is that a massive propagator $1/(q^2 + m^2c^2)$ Fourier-transforms to an exponentially screened potential, derived next from the Klein–Gordon equation [9, 14, 5, 2].

That single scale explains why nuclear forces die within a few fm while electrostatics still acts across atomic distances.

11.2.1 Predicting the pion mass from the nuclear range

Electron scattering and low-energy NN data fix the range of the residual strong force at $R \sim 1$–$2\,\mathrm{fm}$. Taking $R \approx 1.4$–$2\,\mathrm{fm}$ and $\hbar c \approx 197\,\mathrm{MeV\,fm}$,

$$mc^2 \sim \frac{\hbar c}{R} \approx \frac{197}{1.4\text{–}2} \approx 100\text{–}140\,\mathrm{MeV}. \tag{11.4}$$

Yukawa made this prediction in 1935, years before the pion was discovered. The observed mesons have

$$m_{\pi^\pm}c^2 \approx 139.6\,\mathrm{MeV}, \qquad m_{\pi^0}c^2 \approx 135\,\mathrm{MeV},$$

exactly the scale required by the nuclear force range [9, 14, 2].

Historical note: Hideki Yukawa (1907–1981)

Hideki Yukawa, working in Osaka in 1934–1935, proposed that the short-range nuclear force is mediated by the exchange of a massive boson. From the empirical range $r_0 \sim 1$–$2\,\mathrm{fm}$ he estimated a mediator mass of order $100\,\mathrm{MeV}/c^2$. The particle, the pion, was later found with $m_\pi c^2 \approx 140\,\mathrm{MeV}$, and the associated potential falls exponentially with range fixed by m_π. Yukawa received the 1949 Nobel Prize in Physics, the first Nobel awarded to a Japanese scientist. His insight is the microscopic origin of the residual NN force developed in this lecture [9, 14, 2].

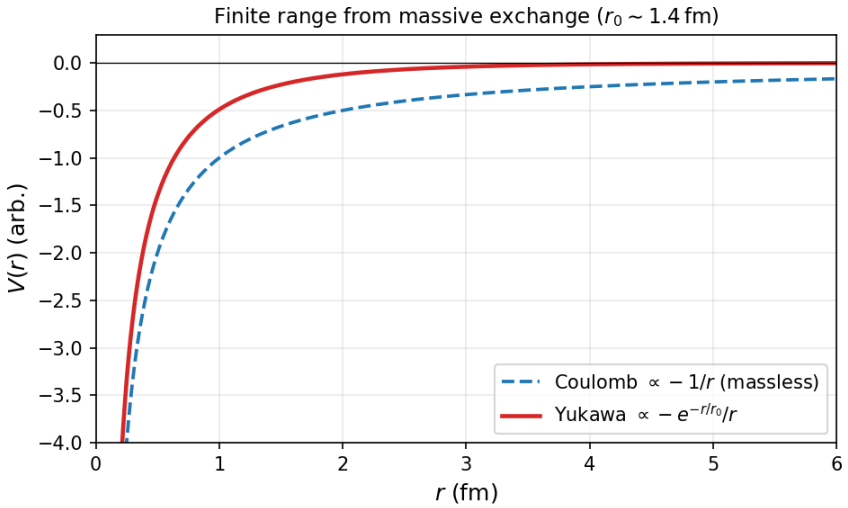

Figure 11.1: Coulomb ($-1/r$, massless exchange) versus Yukawa ($-e^{-r/r_0}/r$, massive exchange). The exponential kills the force beyond $r_0 \sim \hbar/(m_\pi c)$.

Key idea

Finite nuclear range $\Leftrightarrow$ massive exchange quantum. The pion mass and the fermi-scale range of the residual NN force are two faces of $R \sim \hbar/(m_\pi c)$.

11.3 From the Klein–Gordon equation to the Yukawa potential

The form of the potential follows from the relativistic wave equation for a spinless field of mass m. The free Klein–Gordon equation is

$$\frac{1}{c^2}\frac{\partial^2 \psi}{\partial t^2} - \nabla^2 \psi + \mu^2 \psi = 0, \qquad \mu = \frac{mc}{\hbar}. \tag{11.5}$$

For $m = 0$ this reduces to the wave equation for electromagnetic potentials. A static point source for the massless case yields Coulomb's law. With mass, a static isotropic source at the origin obeys

$$(\nabla^2 - \mu^2) V(r) = -g\,\delta^3(\boldsymbol{r}). \tag{11.6}$$

For $r \neq 0$ the radial equation is

$$\frac{1}{r}\frac{\mathrm{d}^2}{\mathrm{d}r^2}(rV) - \mu^2 V = 0,$$

so $rV = Ae^{-\mu r} + Be^{+\mu r}$. Boundedness at infinity forces $B = 0$, hence $V(r) = Ae^{-\mu r}/r$. To fix A, integrate (11.6) over a ball of radius $\varepsilon \to 0$:

$$\int_{r<\varepsilon} (\nabla^2 - \mu^2) V \, \mathrm{d}^3 r = \oint_{\partial B} \nabla V \cdot \mathrm{d}\boldsymbol{S} - \mu^2 \int V \, \mathrm{d}^3 r = -g. \tag{11.7}$$

The volume integral of $V \sim 1/r$ vanishes as $\varepsilon \to 0$, while $\nabla V \sim -A\hat{r}/r^2$ gives $\oint \nabla V \cdot \mathrm{d}\boldsymbol{S} = -4\pi A$. Therefore $A = g/(4\pi)$ (up to the overall coupling convention), and

$$V(r) = -\frac{g^2}{4\pi} \frac{\hbar c}{r} e^{-\mu r} = -\frac{g^2}{4\pi} \frac{\hbar c}{r} e^{-r/r_0}, \qquad r_0 = \frac{\hbar}{mc} \approx 1.4\,\mathrm{fm} \quad (\text{for } m = m_\pi). \tag{11.8}$$

(The overall sign and coupling convention depend on the channel; the attractive form shown here is the pedagogical scalar Yukawa well. Physical OPEP has spin–isospin structure and a tensor piece.)

Fourier-transform route. The same potential is the Fourier transform of the massive propagator. In the static Born approximation,

$$\tilde{V}(\boldsymbol{q}) = -\frac{g^2 \hbar c}{q^2 + \mu^2}, \tag{11.9}$$

and

$$\begin{aligned} V(r) &= \int \frac{\mathrm{d}^3 q}{(2\pi)^3} \tilde{V}(\boldsymbol{q}) \, e^{i\boldsymbol{q}\cdot\boldsymbol{r}} = -\frac{g^2 \hbar c}{(2\pi)^2} \int_0^\infty \frac{q^2 \, \mathrm{d}q}{q^2 + \mu^2} \frac{\sin(qr)}{qr} \\ &= -\frac{g^2 \hbar c}{4\pi} \frac{e^{-\mu r}}{r}, \end{aligned} \tag{11.10}$$

recovering (11.8). In the limit $m \to 0$ ($\mu \to 0$) one recovers the Coulomb shape $1/r$; for finite m the exponential cuts off the force beyond r_0 [14, 5].

In quantum field theory the same potential is the Fourier transform of the propagator $1/(q^2 + m^2 c^2)$ of the exchanged meson in the static Born approximation [14, 5].

11.4 Pions as mediators of the residual strong force

Real pions are copiously produced in accelerators and in cosmic-ray showers in the atmosphere. Virtual pions of the same mass and quantum numbers can be exchanged between nucleons; the associated range is their Compton wavelength $\hbar/(m_\pi c) \sim 1.4\,\mathrm{fm}$.

It is crucial to distinguish the **fundamental** strong force from the **residual** force between nucleons. Inside a nucleon, quarks exchange gluons and the interaction is extremely strong and confining. A proton or neutron as a whole is a colour singlet (“white”). When two colour-neutral nucleons approach within a fermi, residual colour forces remain, analogous to van der Waals forces between neutral atoms. Pion exchange is the longest-range piece of that residual interaction [15, 4, 14].

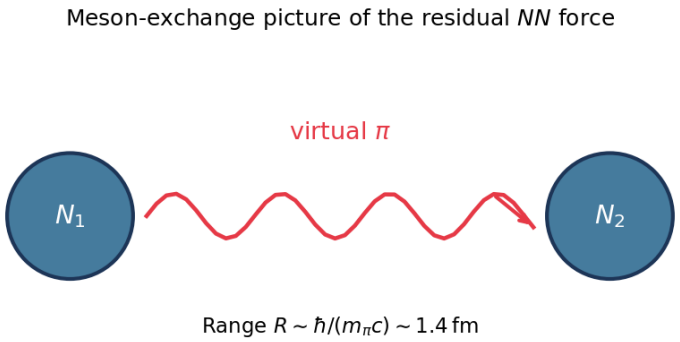

Figure 11.2: Schematic meson exchange between two nucleons. The virtual pion mediates a short-range residual force of Compton wavelength $\hbar/(m_\pi c)$.

11.4.1 Charge exchange: pp versus np

Neutral pion exchange preserves nucleon identity:

$$p \to p + \pi^0, \qquad n \to n + \pi^0. \tag{11.11}$$

Charged pion exchange converts neutron $\leftrightarrow$ proton:

$$n \to p + \pi^-, \qquad p + \pi^- \to n, \tag{11.12}$$

$$p \to n + \pi^+, \qquad n + \pi^+ \to p. \tag{11.13}$$

Consequently:

- In pp (or nn) scattering, if both nucleons keep their charges, only π^0 exchange is allowed at the one-pion level.
- In np scattering, π^0, π^+, and π^- can all contribute.

Because $m_{\pi^\pm}$ and m_{π^0} differ by only a few MeV, the pp and np forces are nearly equal once the Coulomb repulsion between protons is removed. That near-equality is the charge independence of the residual strong force, already used when arguing that only the pn triplet binds (Lecture 8) [14, 6].

11.5 One-pion exchange, tensor force, and the short-range core

Single-pion exchange (OPEP) produces not only the radial Yukawa factor (11.8) but also spin-dependent and tensor structures. The pseudoscalar πNN coupling leads, in the static limit, to a momentum-space amplitude proportional to

$$\frac{(\boldsymbol{\sigma}_1 \cdot \boldsymbol{q})(\boldsymbol{\sigma}_2 \cdot \boldsymbol{q})}{q^2 + m_\pi^2}\, \boldsymbol{\tau}_1 \cdot \boldsymbol{\tau}_2.$$

Fourier transforming and rearranging with the identity

$$(\boldsymbol{\sigma}_1 \cdot \hat{q})(\boldsymbol{\sigma}_2 \cdot \hat{q}) = \tfrac{1}{3}\boldsymbol{\sigma}_1 \cdot \boldsymbol{\sigma}_2 + \tfrac{1}{3}S_{12}(\hat{q}) \tag{11.14}$$

separates a central spin–spin piece from the tensor operator

$$S_{12} = 3(\boldsymbol{\sigma}_1 \cdot \hat{r})(\boldsymbol{\sigma}_2 \cdot \hat{r}) - \boldsymbol{\sigma}_1 \cdot \boldsymbol{\sigma}_2. \tag{11.15}$$

Differentiating the Yukawa function twice (the coordinate-space image of $q_i q_j/(q^2+m_\pi^2)$) produces the standard radial factors

$$V_C^\pi(r) \propto \frac{e^{-m_\pi r}}{r}, \tag{11.16}$$

$$V_T^\pi(r) \propto \frac{e^{-m_\pi r}}{r}\left(1 + \frac{3}{m_\pi r} + \frac{3}{(m_\pi r)^2}\right). \tag{11.17}$$

The potential piece $V_T(r)S_{12}$ is attractive in the deuteron channel and is the long-range origin of the S–D mixing, the quadrupole moment $Q_d \neq 0$, and the small correction to μ_d discussed in Lecture 9 [14, 6]. In multi-nucleon systems the tensor force largely averages out; in the two-body problem it is essential for binding.

A pure attractive Yukawa well is not enough for nuclear saturation. Phenomenological and meson-exchange potentials add a strong **repulsive core** at $r \lesssim 0.5\,\text{fm}$, often modelled as another Yukawa with a heavier mass (or as ω and multi-pion exchange). Heavier mediators have shorter Compton wavelengths, so they act only at short distance, exactly where the hard core is needed to keep nucleons from collapsing into a single blob of pion-range size [14, 4].

A realistic NN potential therefore has a hierarchy of ranges [14]:

Distance	Dominant physics	Mediators / language
$r \gtrsim 1.4\,\text{fm}$	long-range attraction, tensor	π (OPEP)
$r \sim 0.7$–$1.4\,\text{fm}$	intermediate attraction	multi-π, ρ
$r \lesssim 0.5\,\text{fm}$	short-range repulsion	ω, quark Pauli / contact terms in EFT

Modern chiral effective field theory organises the same hierarchy as an expansion in soft momenta: one-pion exchange at long range, multi-pion exchange at intermediate range, and short-range contact operators fitted to phase shifts. For this course it is enough that OPEP explains the long-range tensor force while shorter-range physics is constrained by scattering data (Lecture 10), not invented from the deuteron alone.

11.5.1 Phenomenology and mechanism

Historically, NN potentials were first fitted to deuteron properties and scattering phase shifts with adjustable strengths and ranges (phenomenology). Yukawa's insight and modern one-boson-exchange models derive the long-range form from a field-theoretic mechanism. The two approaches meet in practice: phase shifts (Lecture 10) and the deuteron multipoles (Lectures 7–9) remain the data that any mechanism-based potential must reproduce [6, 14].

Observable (L7–10)	Inferred operator	Mechanism (this lecture)
B_d, no excited states	depth/range of attraction	residual force scale
$I^\pi = 1^+$, triplet binds	spin dependence	$\boldsymbol{\sigma}_1 \cdot \boldsymbol{\sigma}_2$
$Q_d \neq 0$, μ_d deficit	tensor force S_{12}	OPEP tensor
$a_t > 0$, $a_s < 0$, $\delta_\ell(E)$	channel-dependent V	OPE + shorter range

Weak interactions provide a contrast. Exchange of the heavy Z^0 ($m_Z c^2 \approx 91\,\text{GeV}$) yields a Yukawa range $\hbar c/m_Z c^2 \sim 2\times10^{-3}\,\text{fm}$ and an effective $V_0 R^2$ five orders of magnitude smaller than the strong residual force, negligible for nuclear binding though essential for neutrino scattering [14].

Key idea

Lectures 7–11 in one line. The deuteron and phase shifts map the residual NN potential; pion exchange explains why that potential is short-ranged, spin- and tensor-dependent, and charge-independent at long distance.

11.6 Further physics: residual force and colour neutrality

Nucleons are colour singlets. The fundamental strong interaction binds quarks via gluon exchange and confines colour. The force between two nucleons is a residual, colour-van-der-Waals effect: short-ranged, saturating, and much weaker than the force inside a single nucleon [15, 4, 14]. Pion exchange is the longest piece of that residual force; heavier mesons and quark substructure dominate only at sub-fermi distances where the repulsive core appears.

11.7 Problems with solutions

Problem 11.1 — Pion mass from range

If the nuclear force range is $R = 1.4\,\text{fm}$ and $\hbar c = 197\,\text{MeV fm}$, estimate the mediator mass $mc^2 \approx \hbar c/R$. Compare with $m_\pi c^2 \approx 140\,\text{MeV}$.

Solution 11.1

The Compton relation $R = \hbar/(mc)$ rearranges to

$$mc^2 = \frac{\hbar c}{R} \approx \frac{197\,\text{MeV fm}}{1.4\,\text{fm}} \approx 141\,\text{MeV},$$

in excellent agreement with $m_\pi c^2 \approx 140\,\text{MeV}$ [9, 14].

Problem 11.2 — Photon vs pion range

Why does electromagnetism have infinite range while the residual strong force does not, in the exchange picture?

Solution 11.2

The photon is massless, so Δt can be arbitrarily long and $R \sim c\Delta t$ unbounded. The pion is massive, so $\Delta t \lesssim \hbar/(m_\pi c^2)$ and $R \sim \hbar/(m_\pi c)$ is a few fm [5, 9].

Problem 11.3 — Which pions in pp vs np?

Which pion species can mediate pp scattering if both protons remain protons? Which can mediate np?

Solution 11.3

pp: only π^0 (charged emission would turn a proton into a neutron). np: π^0, π^+, and π^- all allowed via charge-exchange and neutral channels [14].

Chapter 12

The Nuclear Shell Model

> *"The fundamental assumption of the shell model [is that] the motion of a single nucleon is governed by a potential representing the average interaction with all the other nucleons."*
>
> K. S. Krane

The liquid-drop SEMF (Lectures 4–5) describes bulk binding but cannot explain why certain proton or neutron numbers are especially stable. Just as atomic chemistry is organised by electronic shells, nuclear data show **magic numbers**

$$N, Z = 2, 8, 20, 28, 50, 82, 126 \tag{12.1}$$

at which nuclei are more tightly bound, more abundant, and more spherical than the SEMF alone predicts [6, 14, 1]. The nuclear shell model attributes those gaps to single-particle orbitals in a mean field, completed by a strong spin–orbit force.

12.1 Atomic shells as a guide

In atoms, major shells and subshells organise the periodic table. Closed shells (noble gases) are chemically inert: ionisation energies peak, radii are compact, and valence chemistry is nearly absent. Alkali metals, with a single electron outside a closed shell, share chemical behaviour because that valence electron dominates bonding.

The same logic applies to nuclei, with two important differences. First, both protons and neutrons fill independent sequences of levels (two interpenetrating Fermi seas). Second, the mean field is short-ranged and saturates, so the single-particle spectrum is not hydrogenic. Still, when N or Z reaches a magic number, separation energies jump, radii and abundances show discontinuities, and residual shell effects appear on top of the smooth SEMF [14, 6].

12.2 Empirical evidence for magic numbers

Several independent observables mark shell closures.

Binding-energy residuals. The difference between measured B/A and the SEMF shows positive peaks near magic N or Z (extra binding of closed shells). Pronounced humps appear

near $N = 28$, $N = 50$, $N = 82$ and $Z = 28, 50, 82$, among others (Fig. 12.1).

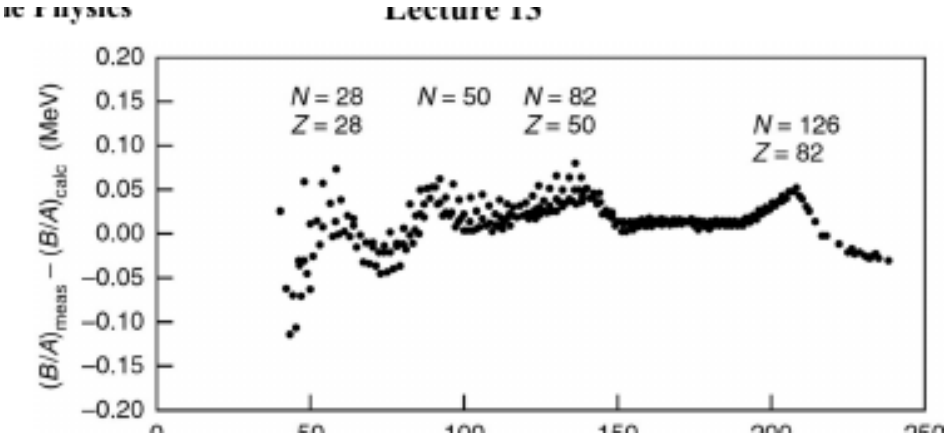

Figure 12.1: Difference between measured binding energy per nucleon and the liquid-drop (SEMF) prediction as a function of A. Peaks mark shell closures at magic N or Z (re-extracted from the full original PH5001 source page; cf. Dunlap [1] and Krane [6]).

Nuclear radii. The ratio of the measured change in nuclear radius to a smooth estimate, when N increases by two, fluctuates near $N = 20, 28, 50, 82$ (Fig. 12.2).

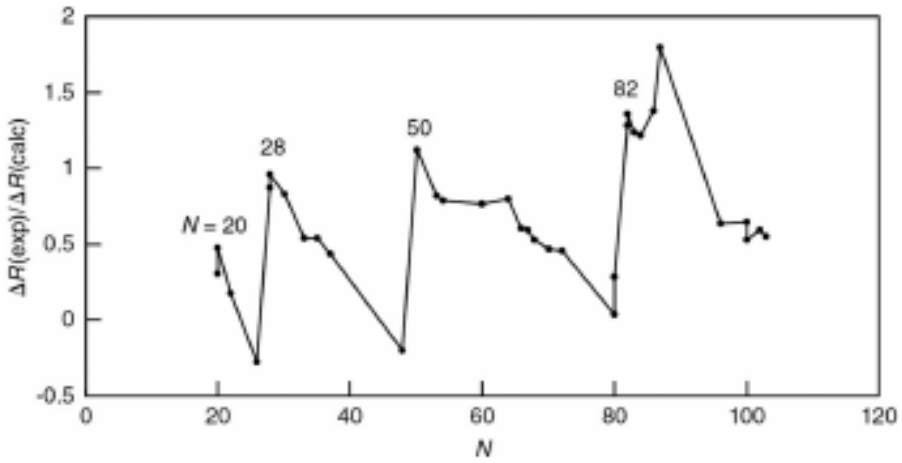

Figure 12.2: Shell effects in nuclear radii: fluctuations of $\Delta r(\text{exp})/\Delta r(\text{calc})$ near magic neutron numbers (re-extracted from the full original PH5001 source page; cf. Dunlap [1]).

Stable isotones. The number of stable isotones peaks at magic neutron numbers (Fig. 12.3): closed neutron shells favour more proton partners along the valley of stability.

Separation energies and first 2^+. S_n and S_p jump when a shell closes, analogous to atomic ionisation energies. Even–even nuclei near magic numbers also have higher-lying first 2^+ states (more rigid, spherical cores).

The experimentally identified closures are

$$2,\ 8,\ 20,\ 28,\ 50,\ 82,\ 126.$$

Beyond 126, laboratory superheavy nuclei still show evidence for further shell gaps [6, 1].

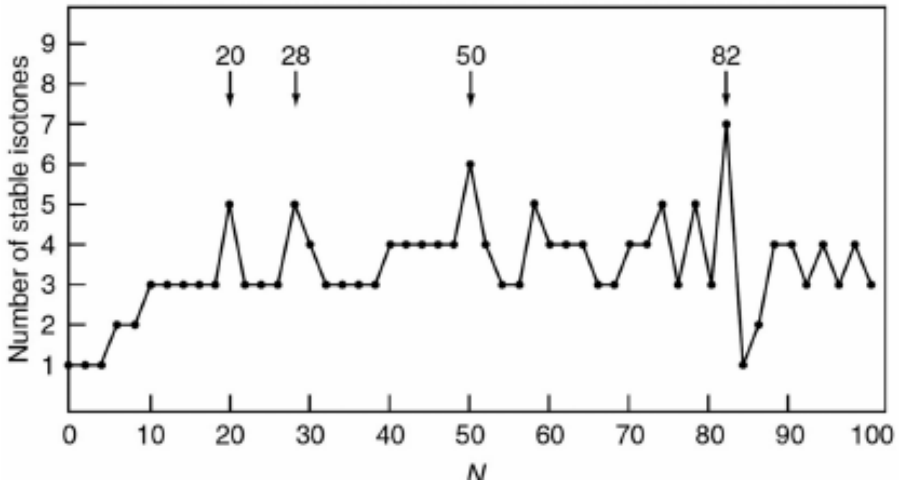

Figure 12.3: Number of stable isotones as a function of even N. Peaks at $N = 20, 28, 50, 82$ (re-extracted from the full original PH5001 source page; cf. Dunlap [1]).

Key idea

Magic numbers are experimental facts. The shell model is the mean-field theory that predicts them once a realistic single-particle potential and spin–orbit coupling are chosen.

12.3 Mean field and single-particle motion

The exact many-body Hamiltonian of A nucleons may be written schematically

$$H = \sum_{i=1}^{A} \frac{\boldsymbol{p}_i^2}{2m} + \sum_{i<j} v_{ij}, \tag{12.2}$$

where v_{ij} contains the strong interaction, Coulomb repulsion among protons, and weaker electromagnetic corrections. Solving (12.2) exactly is impossible for medium and heavy nuclei. The independent-particle approximation replaces the two-body sum by a one-body mean field $U(\boldsymbol{r})$ that represents the average interaction of one nucleon with all others:

$$H \simeq \sum_{i=1}^{A} \left[\frac{\boldsymbol{p}_i^2}{2m} + U(\boldsymbol{r}_i) \right] + V_{\mathrm{res}}. \tag{12.3}$$

Here V_{res} collects residual interactions not absorbed into U. Pairing and collective correlations live in V_{res} and become essential away from closed shells (Lectures 13–15).

The mean field is not an externally imposed force. It is generated by the nucleons themselves, so a microscopic calculation determines the occupied orbitals and U self-consistently: the orbitals produce a density, the density produces a new field, and the cycle is repeated until both agree. The Pauli principle is essential in this picture. It forces identical nucleons to occupy different quantum states and builds separate proton and neutron Fermi seas. Nuclear saturation then explains why the depth and interior density of the mean field remain roughly independent of A, while its radius grows approximately as $A^{1/3}$.

For spherical nuclei one takes a central potential $U(\boldsymbol{r}) = V(r)$. Spherical symmetry implies

that $\boldsymbol{L}^2$ and L_z commute with the single-particle Hamiltonian, so the orbital wave function separates as

$$\psi_{n\ell m}(\boldsymbol{r}) = \frac{u_{n\ell}(r)}{r}\, Y_{\ell m}(\hat{r}). \tag{12.4}$$

Substitute into the single-particle Schrödinger equation

$$-\frac{\hbar^2}{2m}\nabla^2\psi + V(r)\psi = E\psi.$$

The Laplacian in spherical coordinates yields the radial equation for $u(r)$:

$$-\frac{\hbar^2}{2m}\frac{\mathrm{d}^2 u}{\mathrm{d}r^2} + \left[V(r) + \frac{\ell(\ell+1)\hbar^2}{2mr^2}\right]u = E\,u. \tag{12.5}$$

Boundary conditions are

$$u(0) = 0 \qquad \text{(regularity at the origin)} \tag{12.6}$$

and, for a bound state in a finite well,

$$u(r) \to 0 \quad \text{as} \quad r \to \infty. \tag{12.7}$$

Protons and neutrons fill independent sequences of solutions of (12.5) (two Fermi seas). Each spatial orbital of angular momentum ℓ admits $2(2\ell+1)$ identical nucleons once spin $s = \tfrac{1}{2}$ is included, before spin–orbit coupling is turned on. Different choices of $V(r)$ change level spacings but, without spin–orbit coupling, fail to produce the full set of magic numbers [6, 1, 13].

12.4 Infinite spherical well

Take $V = 0$ for $r < R$ and $V = \infty$ for $r \geq R$. Inside the well the potential term vanishes and (12.5) becomes

$$-\frac{\hbar^2}{2m}\frac{\mathrm{d}^2 u}{\mathrm{d}r^2} + \frac{\ell(\ell+1)\hbar^2}{2mr^2}u = E\,u. \tag{12.8}$$

Define the wave number

$$k = \sqrt{\frac{2mE}{\hbar^2}}, \tag{12.9}$$

so that $E = \hbar^2 k^2/(2m)$. The regular solution of (12.8) is proportional to a spherical Bessel function,

$$u(r) = A\, r\, j_\ell(kr), \tag{12.10}$$

because $j_\ell(\rho)$ satisfies the free radial equation with $\rho = kr$. The infinite wall requires $u(R) = 0$, hence

$$j_\ell(kR) = 0. \tag{12.11}$$

Let $x_{\ell,n}$ denote the nth positive zero of j_ℓ. Then

$$k_{n\ell} = \frac{x_{\ell,n}}{R}, \qquad E_{n\ell} = \frac{\hbar^2 x_{\ell,n}^2}{2mR^2}. \tag{12.12}$$

For $\ell = 0$,

$$j_0(\rho) = \frac{\sin\rho}{\rho},$$

so the zeros are $x_{0,n} = n\pi$ with $n = 1, 2, 3, \ldots$. Higher ℓ require tabulated zeros. Ordering the resulting energies produces the sequence

$$1s,\ 1p,\ 1d,\ 2s,\ 1f,\ 2p,\ 1g,\ \ldots$$

(with $1d$ and $2s$ nearly degenerate in some realisations). Unlike the Coulomb atom, there is no prohibition on $1p$, $1d$, $1f$: the nuclear mean field is not $1/r$.

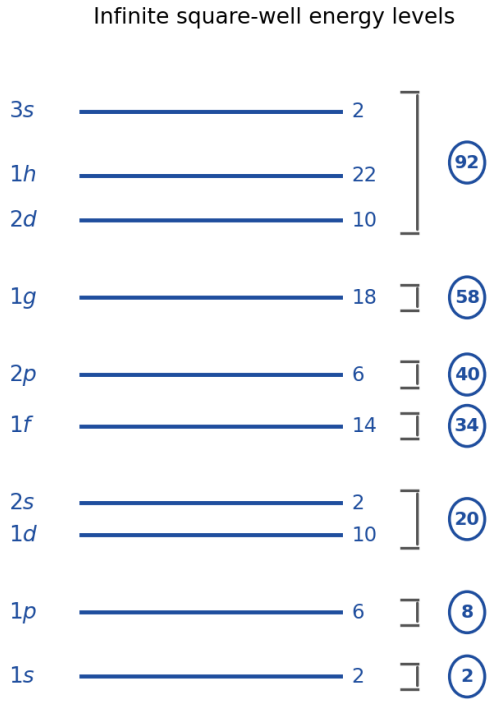

Figure 12.4: Infinite square-well single-particle levels with degeneracies and cumulative shell closures (adapted from the original PH5001 lecture figure).

Each spatial orbit of orbital angular momentum ℓ holds $2(2\ell + 1)$ identical nucleons once spin is included: $2\ell + 1$ orbital projections and two spin states. Cumulative filling therefore closes shells at

$$1s \to 2,$$
$$1s + 1p \to 2 + 6 = 8,$$
$$1s + 1p + 1d + 2s \to 8 + 10 + 2 = 20,$$

but not at 28, 50, 82, 126 [6, 1].

12.5 Isotropic harmonic oscillator

A second standard potential is the three-dimensional isotropic oscillator

$$V(r) = \tfrac{1}{2}m\omega^2 r^2. \tag{12.13}$$

In Cartesian coordinates the Hamiltonian is a sum of three independent one-dimensional oscillators,

$$H = \sum_{i=x,y,z}\left(\frac{p_i^2}{2m} + \tfrac{1}{2}m\omega^2 x_i^2\right), \tag{12.14}$$

with eigenvalues

$$E = (n_x + n_y + n_z + \tfrac{3}{2})\hbar\omega, \qquad n_x, n_y, n_z = 0, 1, 2, \ldots. \tag{12.15}$$

Define the principal oscillator quantum number

$$N = n_x + n_y + n_z = 0, 1, 2, \ldots. \tag{12.16}$$

Then

$$E_N = \left(N + \tfrac{3}{2}\right)\hbar\omega. \tag{12.17}$$

Equivalently, in spherical coordinates one writes $N = 2n_r + \ell$ with radial quantum number $n_r = 0, 1, 2, \ldots$ and orbital angular momentum ℓ. Nuclear spectroscopic labels conventionally shift the radial count so that the lowest s orbit is called $1s$ (corresponding to $n_r = 0$).

All states with the same N are degenerate. The number of Cartesian solutions with $n_x + n_y + n_z = N$ is

$$\binom{N+2}{2} = \frac{(N+1)(N+2)}{2}. \tag{12.18}$$

Including two spin projections multiplies by 2, so the occupancy of major shell N is

$$g_N = (N+1)(N+2). \tag{12.19}$$

Explicitly:

N	Orbitals (nuclear labels)	Occupancy g_N	Cumulative
0	$1s$	2	2
1	$1p$	6	8
2	$1d, 2s$	12	20
3	$1f, 2p$	20	40
4	$1g, 2d, 3s$	30	70

Cumulative magic numbers from pure oscillator filling are therefore $2, 8, 20, 40, 70, \ldots$. Again the empirical sequence beyond 20 is missed [6, 14, 13].

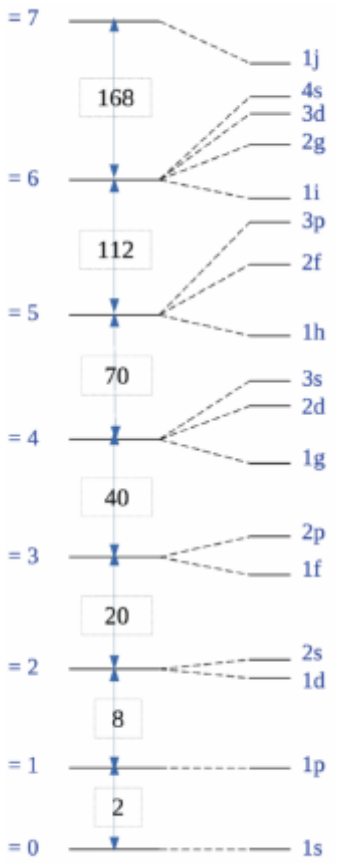

Figure 12.5: Harmonic-oscillator major shells with cumulative occupancies (adapted from the original PH5001 lecture figure).

Remark

Both the infinite well and the oscillator are unphysical as absolute walls: a particle cannot be removed by any finite energy. Real nuclei have finite separation energies $S_n, S_p \sim$ a few to tens of MeV. Finite wells (Lecture 13) fix that defect without, by themselves, fixing the magic numbers past 20.

12.6 Toward a realistic potential: Woods–Saxon shape

A finite square well allows separation but retains a discontinuous edge. Nuclear density falls smoothly over a surface thickness of order 2–3 fm. The most successful central mean field is the Woods–Saxon form

$$V(r) = -\frac{V_0}{1 + \exp\!\left[(r - R)/a\right]}, \tag{12.20}$$

with $R = r_0 A^{1/3}$ and diffuseness $a \sim 0.5\,\mathrm{fm}$ (Fig. 12.6). Even so, Woods–Saxon alone does not rearrange the magic numbers past 20; the essential missing piece is spin–orbit coupling [10, 6].

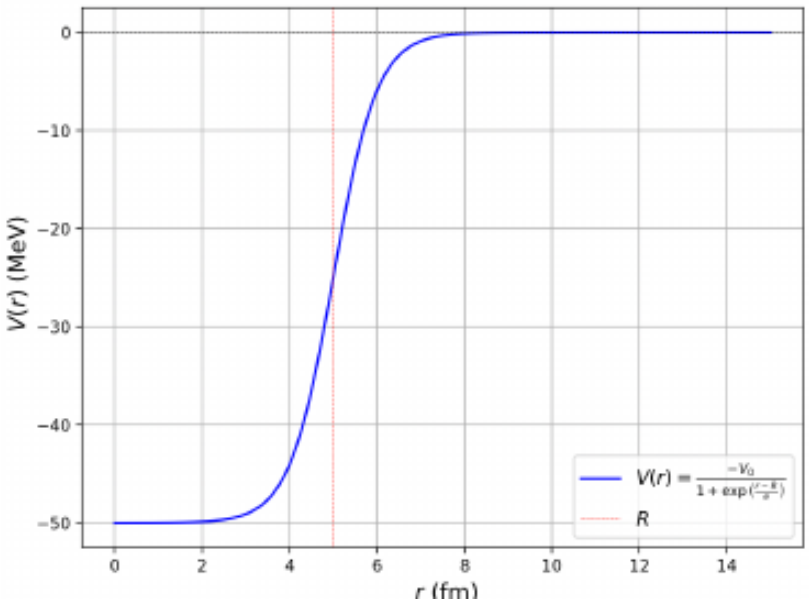

Figure 12.6: Woods–Saxon single-particle potential: flat attractive interior, diffuse surface, finite depth (adapted from the original PH5001 lecture figure; form of Woods and Saxon [10]).

12.7 Spin–orbit coupling and the correct magic numbers

Historical note: Mayer and Jensen (1949)

Maria Goeppert Mayer and, independently, **J. Hans D. Jensen** (with Haxel and Suess) showed that a strong nuclear spin–orbit force $V_{\mathrm{so}}(r)\,\boldsymbol{\ell}\cdot\boldsymbol{s}$ splits each $\ell > 0$ level into $j = \ell \pm \tfrac{1}{2}$ and rearranges the spectrum so that the empirical magic numbers appear. They shared the 1963 Nobel Prize in Physics with Wigner. The nuclear spin–orbit force is much stronger than its atomic electromagnetic counterpart and is a residual effect of the underlying NN interaction [6, 14].

Without spin–orbit coupling the single-particle Hamiltonian commutes with ℓ_z and s_z. Adding

$$H_{\rm so} = f(r)\,\boldsymbol{\ell}\cdot\boldsymbol{s} \tag{12.21}$$

is often implemented phenomenologically with a radial factor proportional to the surface derivative,

$$f(r) \propto \frac{1}{r}\frac{\mathrm{d}V_{\rm WS}}{\mathrm{d}r}. \tag{12.22}$$

Because $V_{\rm WS}$ changes most rapidly near $r \simeq R$, the nuclear spin–orbit interaction is surface peaked. High-ℓ orbits are especially sensitive: their centrifugal barrier pushes their probability density toward the surface, precisely where the derivative is largest. The proportionality constant and its sign are fitted so that the $j = \ell + \frac{1}{2}$ partner is the lower one. With this term, the good quantum numbers change: H no longer commutes with ℓ_z or s_z, but still commutes with ℓ^2, s^2, $\boldsymbol{j}^2$ and j_z, where

$$\boldsymbol{j} = \boldsymbol{\ell} + \boldsymbol{s}, \qquad j = \ell \pm \tfrac{1}{2} \quad (\ell \geq 1). \tag{12.23}$$

States are therefore labelled $n\ell_j$ (e.g. $1d_{5/2}$, $1d_{3/2}$).

12.7.1 Expectation value of the spin–orbit operator

Start from the operator identity obtained by expanding $\boldsymbol{j}^2 = (\boldsymbol{\ell}+\boldsymbol{s})^2$:

$$\boldsymbol{j}^2 = \boldsymbol{\ell}^2 + \boldsymbol{s}^2 + 2\,\boldsymbol{\ell}\cdot\boldsymbol{s}, \tag{12.24}$$

and therefore

$$\boldsymbol{\ell}\cdot\boldsymbol{s} = \frac{1}{2}(\boldsymbol{j}^2 - \boldsymbol{\ell}^2 - \boldsymbol{s}^2). \tag{12.25}$$

On a simultaneous eigenstate of $\boldsymbol{j}^2$, $\boldsymbol{\ell}^2$ and $\boldsymbol{s}^2$ with eigenvalues $j(j+1)\hbar^2$, $\ell(\ell+1)\hbar^2$ and $s(s+1)\hbar^2$,

$$\langle \boldsymbol{\ell}\cdot\boldsymbol{s}\rangle = \frac{\hbar^2}{2}\big[j(j+1) - \ell(\ell+1) - s(s+1)\big]. \tag{12.26}$$

For nucleons $s = \frac{1}{2}$, so $s(s+1) = \frac{3}{4}$.

Partner $j = \ell + \frac{1}{2}$.

$$j(j+1) = \Big(\ell+\tfrac{1}{2}\Big)\Big(\ell+\tfrac{3}{2}\Big) = \ell^2 + 2\ell + \tfrac{3}{4},$$

hence

$$j(j+1) - \ell(\ell+1) - s(s+1) = (\ell^2 + 2\ell + \tfrac{3}{4}) - (\ell^2+\ell) - \tfrac{3}{4} = \ell,$$

and

$$\langle \boldsymbol{\ell}\cdot\boldsymbol{s}\rangle_{j=\ell+1/2} = \frac{\hbar^2}{2}\,\ell. \tag{12.27}$$

Partner $j = \ell - \frac{1}{2}$.

$$j(j+1) = \Big(\ell-\tfrac{1}{2}\Big)\Big(\ell+\tfrac{1}{2}\Big) = \ell^2 - \tfrac{1}{4},$$

hence

$$j(j+1) - \ell(\ell+1) - s(s+1) = \left(\ell^2 - \tfrac{1}{4}\right) - \left(\ell^2 + \ell\right) - \tfrac{3}{4} = -(\ell+1),$$

and

$$\langle \boldsymbol{\ell} \cdot \boldsymbol{s} \rangle_{j=\ell-1/2} = -\frac{\hbar^2}{2}(\ell+1). \tag{12.28}$$

The energy shift of each partner is $\Delta E = \langle f(r) \rangle \langle \boldsymbol{\ell} \cdot \boldsymbol{s} \rangle$. With the nuclear convention $\langle f \rangle < 0$, the $j = \ell + \frac{1}{2}$ partner is lowered and the $j = \ell - \frac{1}{2}$ partner is raised. Their splitting is

$$\Delta E_{\text{so}} = E_{j=\ell-1/2} - E_{j=\ell+1/2} = -\langle f \rangle \frac{\hbar^2}{2}(2\ell+1). \tag{12.29}$$

Large-ℓ orbits therefore split most; s states ($\ell = 0$) do not split at all.

That reordering is decisive. The high-j members of each major shell ($1f_{7/2}$, $1g_{9/2}$, $1h_{11/2}$, $1i_{13/2}$) drop into lower major shells and open gaps at the observed magic numbers [16, 17, 6, 14]:

- $1f_{7/2}$ (occupancy $2j+1 = 8$) alone closes a shell at $20 + 8 = 28$;
- after 28, filling $2p_{3/2}(4) + 1f_{5/2}(6) + 2p_{1/2}(2) + 1g_{9/2}(10) = 22$ yields $28 + 22 = 50$;
- the next major regrouping, including $1h_{11/2}$ (occupancy 12), yields 82;
- including $1i_{13/2}$ (occupancy 14) yields 126.

Each j subshell holds $2j+1$ identical nucleons (protons or neutrons separately). Cumulative filling:

Orbitals filled	Cumulative N or Z
$1s_{1/2}$	2
$+1p_{3/2}, 1p_{1/2}$	8
$+1d_{5/2}, 2s_{1/2}, 1d_{3/2}$	20
$+1f_{7/2}$	28
$+2p_{3/2}, 1f_{5/2}, 2p_{1/2}, 1g_{9/2}$	50
$+1g_{7/2}, 2d_{5/2}, 2d_{3/2}, 3s_{1/2}, 1h_{11/2}$	82
$+1h_{9/2}, 2f_{7/2}, \ldots, 1i_{13/2}$	126

Key idea

Central potentials alone give $2, 8, 20$. Spin–orbit coupling is required for $28, 50, 82, 126$. Remember the mechanism, not only the list: surface-peaked spin–orbit coupling lowers the high-j ($j = \ell + \frac{1}{2}$) orbit, that orbit carries $2j+1$ nucleons, and its large occupancy creates the next shell gap.

Caution

Nuclear spin–orbit ordering is opposite to the atomic fine-structure pattern for electrons: in nuclei $j = \ell + \frac{1}{2}$ lies *below* $j = \ell - \frac{1}{2}$. The strength is also orders of magnitude larger (MeV scale vs. fractions of an eV in atoms), because the force is residual strong interaction,

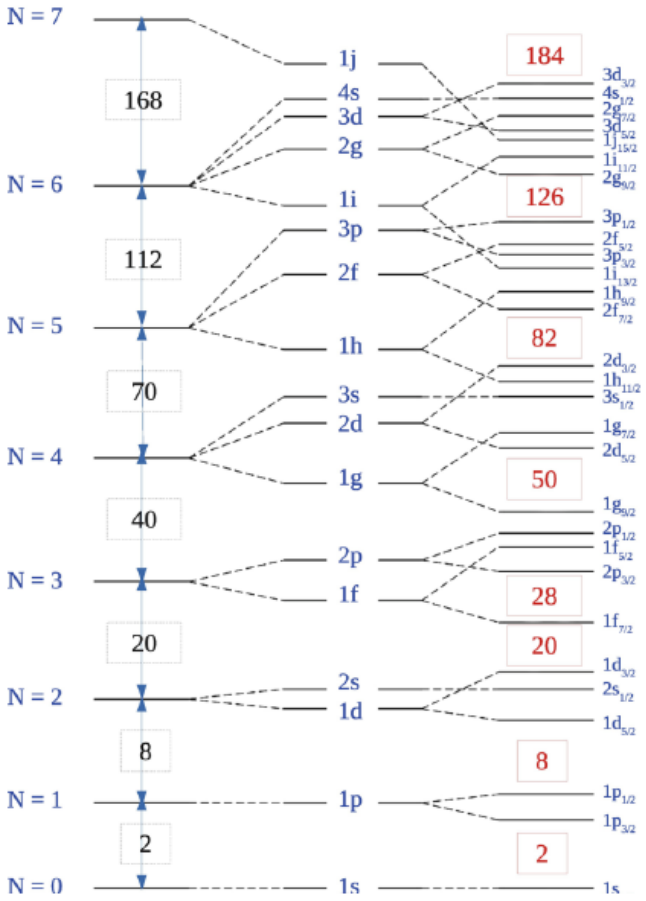

Figure 12.7: Harmonic-oscillator levels with ℓ^2 and spin–orbit splitting. Empirical magic numbers appear in red boxes (adapted from the original PH5001 lecture figure; cf. Mayer [16] and Haxel, Jensen and Suess [17]).

not electromagnetism.

12.8 Why the potential shape alone is not enough

Finite square wells, wells with rounded edges, and the Woods–Saxon form all improve separation energies and level densities relative to infinite walls. They do *not*, by themselves, produce the full magic sequence: the level order remains close to that of the oscillator or infinite well until $\boldsymbol{\ell} \cdot \boldsymbol{s}$ is added. Conversely, once a strong spin–orbit term is present, magic numbers appear for a wide class of reasonable central shapes. The empirical gaps are therefore a robust signature of spin–orbit physics, not a fine-tuned accident of one potential [6, 1].

12.9 Further physics: separation energies and double magic nuclei

Doubly magic nuclei (Z and N both magic), such as ^{4}He, ^{16}O, ^{40}Ca, ^{48}Ca, and ^{208}Pb, combine large S_n and S_p, spherical shape, and simple particle/hole spectra when one nucleon is added or removed [14, 6, 20]. They are the benchmarks against which residual interactions and ab initio methods are tested.

The one-nucleon separation energies

$$S_n(A, Z) = B(A, Z) - B(A-1, Z), \tag{12.30}$$

$$S_p(A, Z) = B(A, Z) - B(A-1, Z-1) \tag{12.31}$$

jump when a shell closes, in direct analogy with atomic ionisation energies. Two-nucleon separation energies S_{2n} and S_{2p} are often smoother against odd–even staggering and therefore especially useful for mapping shell evolution far from stability.

Magic numbers need not be universal. Far from the valley of β stability, especially in neutron-rich light and medium-mass nuclei, experimental spectroscopy shows that traditional closures such as $N = 20$ or $N = 28$ can weaken or migrate ("islands of inversion"). The next predicted closures beyond $N = 126$ (e.g. $N = 184$, $Z = 114$ or nearby) underlie the search for superheavy islands of stability [14, 1].

12.10 Problems with solutions

Problem 12.1 — Occupancy of a j subshell

How many identical nucleons can occupy a $1g_{9/2}$ orbit? What cumulative magic number is completed when $1g_{9/2}$ is filled after the $N = 28$ core and the $2p, 1f_{5/2}$ orbits?

Solution 12.1

A j subshell holds $2j+1$ identical nucleons, so

$$2j+1 = 2\cdot\tfrac{9}{2}+1 = 10.$$

After the $N=28$ core the next orbits fill as

$$\begin{aligned} 2p_{3/2}&: \ 4,\\ 1f_{5/2}&: \ 6,\\ 2p_{1/2}&: \ 2,\\ 1g_{9/2}&: \ 10, \end{aligned}$$

for a total of $4+6+2+10=22$. The cumulative closure is $28+22=50$ [6, 16].

Problem 12.2 — Why HO misses magic 28

The isotropic oscillator produces closures at $2, 8, 20, 40, \ldots$. Explain in one or two sentences how spin–orbit coupling creates a gap at 28.

Solution 12.2

In the $N=3$ oscillator shell the spin–orbit term lowers $1f_{7/2}$ ($j=\ell+\tfrac{1}{2}$, $\ell=3$) below the remaining $2p$ and $1f_{5/2}$ partners. The isolated $1f_{7/2}$ subshell holds $2j+1=8$ nucleons, so a new gap opens at $20+8=28$ [6, 14, 17].

Problem 12.3 — $\ell\cdot s$ expectation values

Using $\boldsymbol{\ell}\cdot\boldsymbol{s} = \tfrac{1}{2}(\boldsymbol{j}^2-\boldsymbol{\ell}^2-\boldsymbol{s}^2)$, show that $\langle\boldsymbol{\ell}\cdot\boldsymbol{s}\rangle = \tfrac{1}{2}\ell\hbar^2$ for $j=\ell+\tfrac{1}{2}$ and $-\tfrac{1}{2}(\ell+1)\hbar^2$ for $j=\ell-\tfrac{1}{2}$. Then show that the partner splitting is proportional to $2\ell+1$.

Solution 12.3

With $s=\tfrac{1}{2}$, $s(s+1)=\tfrac{3}{4}$. For $j=\ell+\tfrac{1}{2}$,

$$j(j+1) = \left(\ell+\tfrac{1}{2}\right)\left(\ell+\tfrac{3}{2}\right) = \ell^2+2\ell+\tfrac{3}{4},$$

so

$$j(j+1)-\ell(\ell+1)-s(s+1) = \ell$$

and $\langle\boldsymbol{\ell}\cdot\boldsymbol{s}\rangle = \tfrac{1}{2}\ell\hbar^2$. For $j=\ell-\tfrac{1}{2}$,

$$j(j+1)-\ell(\ell+1)-s(s+1) = -(\ell+1),$$

hence $-\tfrac{1}{2}(\ell+1)\hbar^2$. The difference of the two expectation values is $\tfrac{1}{2}(2\ell+1)\hbar^2$, so the energy splitting scales as $2\ell+1$ once $\langle f(r)\rangle$ is factored out [6, 13].

Problem 12.4 — Oscillator degeneracy

Derive the occupancy $g_N = (N{+}1)(N{+}2)$ of major shell N in the isotropic three-dimensional oscillator, including spin.

Solution 12.4

The number of non-negative integer solutions of $n_x{+}n_y{+}n_z = N$ is $\binom{N+2}{2} = (N{+}1)(N{+}2)/2$. Each spatial state admits two spin projections, so

$$g_N = 2 \cdot \frac{(N+1)(N+2)}{2} = (N+1)(N+2).$$

For $N = 0, 1, 2, 3$ one recovers $2, 6, 12, 20$, and the cumulative closures $2, 8, 20, 40$ [6, 1].

Chapter 13

Shell Model: Woods–Saxon Potential and Ground-State J^π

> *"For realistic calculations, more accurate potentials are preferred... Among the various models, the Woods–Saxon potential is particularly effective."*
>
> lecture notes, PH5001

Lecture 12 showed that magic numbers beyond 20 require spin–orbit coupling, and that the choice of infinite well versus harmonic oscillator does not change those magic numbers once $\boldsymbol{\ell} \cdot \boldsymbol{s}$ is strong enough. Realistic calculations still need a finite, diffuse mean field: the **Woods–Saxon** potential. With that spectrum one reads ground-state spin and parity from the extreme single-particle filling rules [6, 1, 10].

13.1 Why infinite potentials fail as absolute models

An infinite wall forbids nucleon removal: separation energies would be infinite. Real nuclei have finite S_n and S_p. A finite square well allows separation but retains a discontinuous edge. Nuclear density and the mean field fall smoothly over a surface thickness of order 2–3 fm (Lecture 2). The potential should follow that density.

13.2 Woods–Saxon single-particle potential

The standard central mean field is

$$V_{\mathrm{WS}}(r) = -\frac{V_0}{1 + \exp\big[(r - R)/a\big]}, \tag{13.1}$$

with $R = r_0 A^{1/3}$, $r_0 \approx 1.25\,\mathrm{fm}$, diffuseness $a \approx 0.5$–$0.7\,\mathrm{fm}$, and depth $V_0 \sim 50\,\mathrm{MeV}$ chosen to match separation energies [10, 6, 1]. The potential is nearly flat and attractive in the nuclear interior, then rises smoothly through the surface to zero outside. At $r = R$ one has $V = -V_0/2$. The 10%–90% surface thickness follows directly from the Woods–Saxon shape. Define

$$f(r) = \frac{-V_{\mathrm{WS}}(r)}{V_0} = \frac{1}{1 + \exp[(r - R)/a]}.$$

Solving $f(r) = p$ gives

$$\frac{1}{p} - 1 = e^{(r-R)/a}, \qquad r(p) = R + a\ln\!\left(\frac{1-p}{p}\right). \tag{13.2}$$

Thus the inner 90% point and outer 10% point are

$$r(0.9) = R - a\ln 9, \qquad r(0.1) = R + a\ln 9. \tag{13.3}$$

Their radial separation is

$$t = r(0.1) - r(0.9) = 2a\ln 9 = 4a\ln 3 \approx 4.4\,a, \tag{13.4}$$

of order 2–3 fm for realistic a.

The radial Schrödinger equation for the reduced wave function $u(r)$ is

$$-\frac{\hbar^2}{2m}\frac{\mathrm{d}^2u}{\mathrm{d}r^2} + \left[V_{\mathrm{WS}}(r) + \frac{\ell(\ell+1)\hbar^2}{2mr^2}\right]u = E\,u, \tag{13.5}$$

with $u(0) = 0$. Outside the nucleus, $V \to 0$ for a neutron. It is useful to combine the potential and centrifugal terms into

$$V_{\mathrm{eff}}(r) = V_{\mathrm{WS}}(r) + \frac{\ell(\ell+1)\hbar^2}{2mr^2}. \tag{13.6}$$

For $\ell > 0$, the positive centrifugal barrier suppresses the wave function near the origin and shifts probability toward the nuclear surface. Far outside, both terms approach zero. The radial equation then reduces to

$$\frac{\mathrm{d}^2u}{\mathrm{d}r^2} = \frac{2m|E|}{\hbar^2}\,u = \kappa^2 u \qquad (E < 0), \tag{13.7}$$

whose two solutions are $e^{+\kappa r}$ and $e^{-\kappa r}$. Normalisability eliminates the growing solution, leaving

$$u(r) \underset{r\to\infty}{\longrightarrow} C\,e^{-\kappa r}, \qquad \kappa = \sqrt{\frac{2m|E|}{\hbar^2}}. \tag{13.8}$$

Matching the interior numerical solution to this exterior exponential quantises the allowed energies. There is therefore a finite number of bound orbits, and the least-bound nucleon has a realistic separation energy of a few to tens of MeV.

The decay length $1/\kappa \propto 1/\sqrt{|E|}$ is important physics: a weakly bound neutron has a long exterior tail. Near the neutron drip line this produces diffuse skins and, for low ℓ where the centrifugal barrier is small, halo structure. A bound proton also decays, but its asymptotic tail is modified by the repulsive Coulomb potential rather than being a pure exponential at finite radius.

For protons one must add the Coulomb potential of the remaining charge distribution. A

simple estimate for a uniformly charged sphere of radius R is

$$V_{\mathrm{C}}(r) = \begin{cases} \dfrac{(Z-1)e^2}{8\pi\epsilon_0 R}\left(3 - r^2/R^2\right), & r \le R, \\ \dfrac{(Z-1)e^2}{4\pi\epsilon_0 r}, & r > R. \end{cases} \tag{13.9}$$

Consequently the proton well is shallower and slightly wider than the neutron well at the same A, which helps explain $N > Z$ for heavy stable nuclei [6, 1].

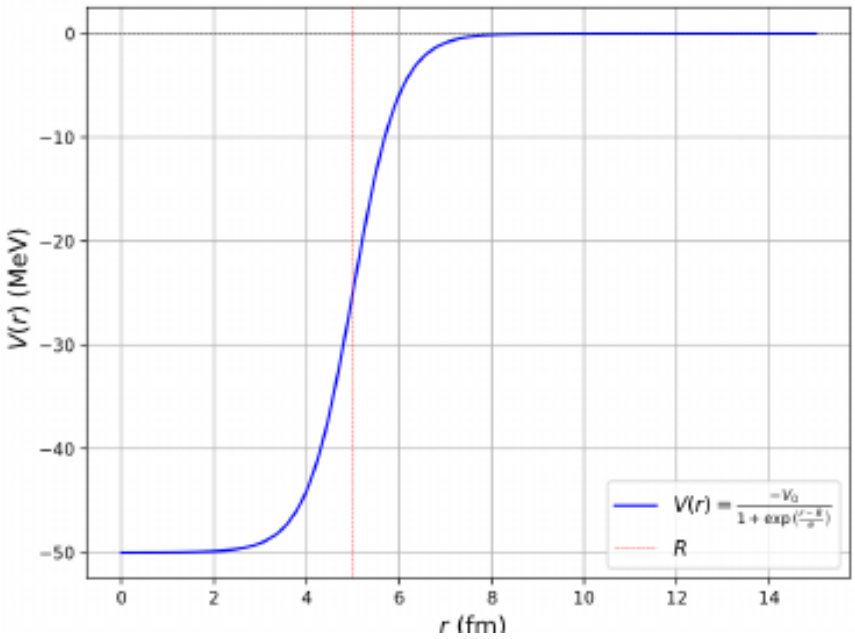

Figure 13.1: Woods–Saxon potential $V(r)$ used as the basic single-particle nuclear mean field. The red marker indicates the half-depth radius R (re-extracted with complete axes and legend from the full original PH5001 source page; Woods and Saxon [10]).

13.3 From oscillator to Woods–Saxon to spin–orbit

Compared with the oscillator, a finite diffuse well lowers high-ℓ orbitals preferentially (they live nearer the surface) and lifts accidental degeneracies such as $1d$–$2s$ and $1f$–$2p$. Typical trends when passing from oscillator (HO) to Woods–Saxon (WS) before spin–orbit:

- $1f$ drops more than $2p$;
- $1g$ drops strongly, approaching the $1f, 2p$ region;
- $1d$ and $2s$ split, with $1d$ usually lower;
- $2d$ and $3s$ descend; the uppermost level becomes $1h$.

Adding $\boldsymbol{\ell} \cdot \boldsymbol{s}$ then splits each $\ell > 0$ level: $1p \to p_{3/2}, p_{1/2}$; $1d \to d_{5/2}, d_{3/2}$; $1f \to f_{7/2}, f_{5/2}$; $1g \to g_{9/2}, g_{7/2}$; $1h \to h_{11/2}, h_{9/2}$. The magic numbers remain $2, 8, 20, 28, 50, 82, 126$, but the detailed spacings become realistic (Fig. 13.2).

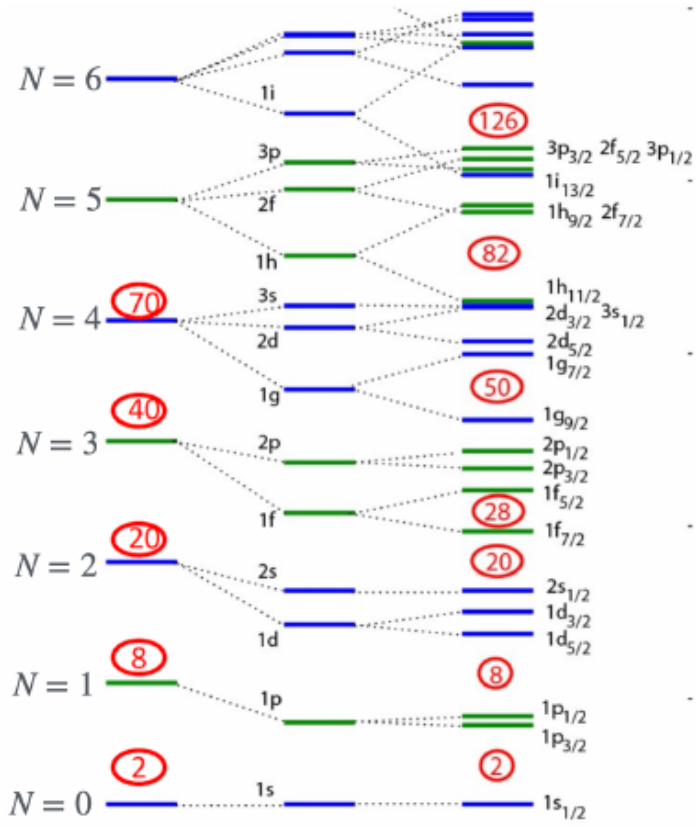

Figure 13.2: Single-particle spectrum: harmonic oscillator (HO), Woods–Saxon (WS), and Woods–Saxon plus spin–orbit (WS+LS). Red circles mark shell closures (adapted from the original PH5001 lecture figure; cf. Dunlap [1] and Krane [6]).

Key idea

Magic numbers are robust once spin–orbit is present. Energy values and intra-shell ordering depend on the central potential; Woods–Saxon is the standard realistic choice. The finite depth controls separation energies, the diffuseness controls surface physics, the centrifugal term separates different ℓ, and spin–orbit coupling separates $j = \ell \pm \frac{1}{2}$.

13.4 Extreme single-particle model

In the **extreme single-particle** (or independent-particle) limit one assumes:

1. nucleons fill the lowest available single-particle orbits;
2. residual interactions are dominated by pairing of like nucleons into $J = 0$ pairs;
3. ground-state properties of odd-A nuclei (spin, parity, magnetic moment) are carried by the last unpaired nucleon.

Even–even nuclei then have all nucleons paired. The model is most reliable near closed shells; mid-shell, configuration mixing and collective motion become essential (Lecture 15).

13.5 Spin and parity: notation

Nuclear "spin" means total angular momentum $\boldsymbol{I}$ (often written J). For a single nucleon,

$$\boldsymbol{j} = \boldsymbol{\ell} + \boldsymbol{s}, \qquad |j| = \sqrt{j(j+1)}\,\hbar, \qquad \pi = (-1)^{\ell}. \tag{13.10}$$

The spectroscopic label is I^π (or J^π). Example: a nucleon in $d_{5/2}$ ($\ell = 2$, $j = \frac{5}{2}$) has $I^\pi = \frac{5}{2}^+$.

13.6 Even–even nuclei: always 0^+

Every proton and every neutron can pair to total angular momentum zero. Consider two identical nucleons in the same $n\ell_j$ orbit. The Pauli principle restricts the allowed total angular momenta of the pair to the even values

$$I = 0, 2, \ldots, 2j - 1 \tag{13.11}$$

(odd multipoles are excluded for two identical fermions in one j shell). Among these, the residual short-range attraction favours the maximum spatial overlap, which occurs for the $I = 0$ pair. That pair has positive parity regardless of whether ℓ is even or odd, because

$$\pi_{\text{pair}} = (-1)^{\ell}\,(-1)^{\ell} = +1. \tag{13.12}$$

With all nucleons paired,

$$I^\pi = 0^+, \tag{13.13}$$

independent of which orbits are filled. That is a robust success of the model and of experiment for essentially all even–even ground states [6, 1, 20]. The magnetic moment vanishes as well (Lecture 14).

13.7 Odd-A nuclei: last nucleon rules

Either Z or N is odd. All but one nucleon form $J = 0$ pairs; the unpaired nucleon occupies the last partially filled orbit $n\ell_j$ and determines

$$I = j, \qquad \pi = (-1)^\ell. \tag{13.14}$$

13.7.1 Example: ^{15}N

Nitrogen-15 has $Z = 7$, $N = 8$. Neutrons fill a closed shell through $1p_{1/2}$. The proton occupation is

$$(1s_{1/2})^2(1p_{3/2})^4(1p_{1/2})^1. \tag{13.15}$$

The unpaired proton is in $1p_{1/2}$ ($\ell = 1$, $j = \frac{1}{2}$), so

$$I^\pi = \tfrac{1}{2}^-, \tag{13.16}$$

in agreement with experiment.

13.7.2 Pairing can reorder occupations: ^{61}Ni

Nickel-61 has $Z = 28$, $N = 33$. The protons fill the closed $Z = 28$ shell. Above the $N = 28$ neutron core one must place five valence neutrons in the $2p_{3/2}$, $1f_{5/2}$ and $2p_{1/2}$ sequence. Two competing occupations illustrate the role of residual pairing:

$$(2p_{3/2})^4(1f_{5/2})^1 \quad \Rightarrow \quad I^\pi = \tfrac{5}{2}^-, \tag{13.17}$$

$$(2p_{3/2})^3(1f_{5/2})^2 \quad \Rightarrow \quad I^\pi = \tfrac{3}{2}^-. \tag{13.18}$$

In the second configuration the two $1f_{5/2}$ neutrons form a $J = 0$ pair, and the unpaired neutron remains in $2p_{3/2}$. Experiment finds $I^\pi = \frac{3}{2}^-$ for the ground state of ^{61}Ni [20, 21, 6], so the paired $(1f_{5/2})^2$ occupation is preferred (Fig. 13.3).

The lesson is not a universal rule that "pairing is always stronger in high-ℓ orbits", but rather that residual pairing can reorder nearby configurations when single-particle spacings are small. The extreme model still applies once the correct odd orbit is identified [6, 1].

13.7.3 Example: ^{17}O

Oxygen-17 ($Z = 8$, $N = 9$) has closed proton shells and neutrons $(1s_{1/2})^2(1p_{3/2})^4(1p_{1/2})^2(1d_{5/2})^1$ (Fig. 13.4). The valence neutron is $1d_{5/2}$, so

$$I^\pi = \tfrac{5}{2}^+. \tag{13.19}$$

Evaluated data confirm the ground state $5/2^+$ and a first excited $1/2^+$ state at 871 keV, corresponding to promotion of the valence neutron to $2s_{1/2}$ [20, 21]. Negative-parity states involve p-shell holes. Excited states of ^{17}O are treated systematically in Lecture 15.

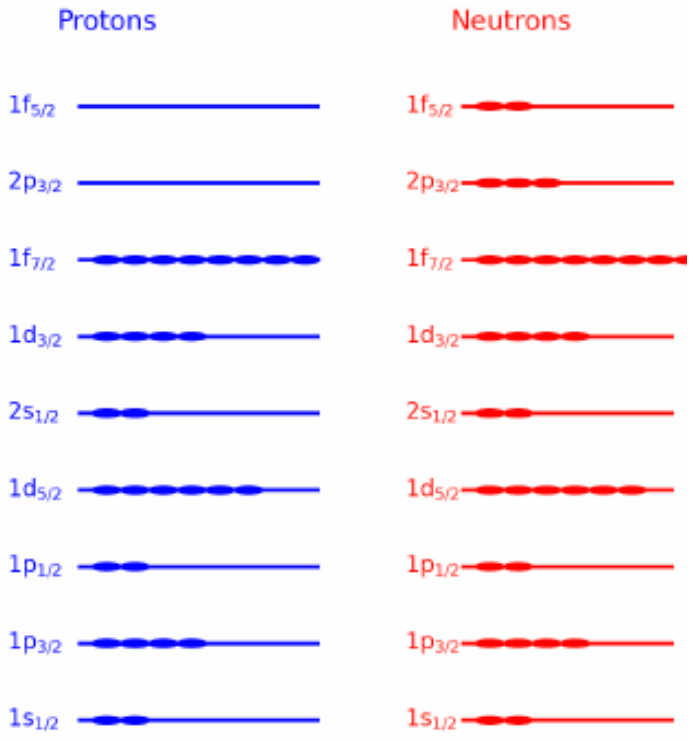

Figure 13.3: Single-particle filling for $^{61}\mathrm{Ni}_{33}$: protons (blue) and neutrons (red). The odd neutron occupies $2p_{3/2}$ rather than $1f_{5/2}$ because residual pairing of two neutrons in $1f_{5/2}$ lowers the total energy. The displayed valence occupations are $(2p_{3/2})^3(1f_{5/2})^2$ (re-extracted from the full original PH5001 source page).

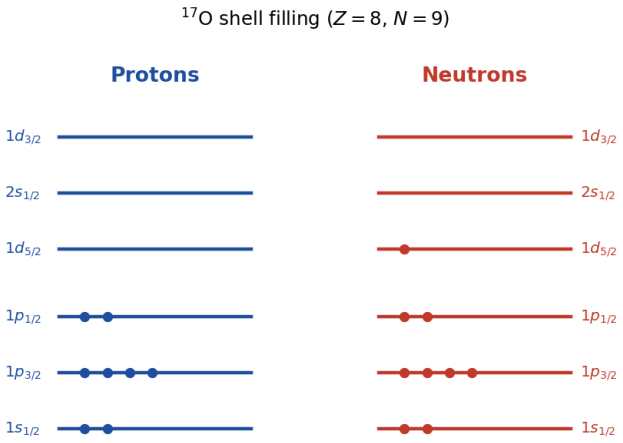

Figure 13.4: Shell-model level occupation for $^{17}\mathrm{O}$: closed proton shell and unpaired $1d_{5/2}$ neutron (adapted from the original PH5001 lecture figure).

13.8 Odd–odd nuclei

Both an unpaired proton and an unpaired neutron contribute. Their angular momenta $\boldsymbol{j}_p$ and $\boldsymbol{j}_n$ couple to a multiplet of total angular momentum

$$|j_p - j_n| \le I \le j_p + j_n, \tag{13.20}$$

in integer steps, with parity

$$\pi = (-1)^{\ell_p + \ell_n}. \tag{13.21}$$

The triangle rule alone does *not* select the ground-state member of the multiplet: residual proton–neutron interactions decide the ordering. Nordheim's empirical rules provide a first guide [19, 6], but they are not rigorous theorems. Few odd–odd nuclei are stable (Lecture 5); ^{14}N ($I^\pi = 1^+$) is a classic light example [20].

Key idea

Even–even: 0^+. Odd A: I^π of the last unpaired nucleon (subject to pairing reordering near closely spaced levels). Odd–odd: an allowed multiplet $|j_p - j_n| \le I \le j_p + j_n$, with the ground member fixed by residual pn interactions.

13.9 Pairing and the SEMF

Two nucleons in the same j orbit prefer $I_{\text{pair}} = 0$. That pairing energy is the microscopic origin of the SEMF pairing term δ (Lecture 4) and of the even–even preference for stability. Breaking a pair costs $\sim$ 1–2 MeV and is the first step toward many low-lying even–even excitations (two-quasiparticle states), while odd-A spectra often show the pure single-particle sequence until core excitations set in [6].

13.10 Further physics: proton versus neutron potentials

Because protons feel Coulomb repulsion in addition to the nuclear mean field, the proton single-particle spectrum is not identical to the neutron spectrum at the same A. Relative to neutrons, proton orbits are pushed upward, and the least-bound proton typically has a smaller separation energy near the proton drip line than the analogous neutron near the neutron drip line [6, 1].

In transfer and knockout reactions one therefore maps proton and neutron spectroscopic factors separately. Near closed shells the extreme single-particle assignments for I^π remain robust; far from stability the same residual interactions that reorder ^{61}Ni can rearrange whole sequences of levels and even dissolve traditional magic numbers. Modern shell-model and density-functional calculations keep the Woods–Saxon (or Hartree–Fock) mean field as the starting point and diagonalise a residual interaction in a truncated valence space.

13.11 Problems with solutions

Problem 13.1 — Woods–Saxon radius

For ^{208}Pb with $r_0 = 1.25\,\mathrm{fm}$, compute $R = r_0 A^{1/3}$. If $a = 0.65\,\mathrm{fm}$, estimate the 10%–90% surface thickness $t = 4a\ln 3$.

Solution 13.1

$$A^{1/3} = 208^{1/3} \approx 5.924, \qquad R = 1.25 \times 5.924 \approx 7.40\,\mathrm{fm}.$$

The surface thickness is

$$t = 4a\ln 3 = 4 \times 0.65 \times \ln 3 \approx 2.86\,\mathrm{fm},$$

consistent with electron-scattering skins [1, 6, 10].

Problem 13.2 — Ground-state J^π

Predict I^π for ^{17}O and for ^{40}Ca in the extreme single-particle model.

Solution 13.2

^{17}O: unpaired neutron in $1d_{5/2}$ ($\ell = 2$, $j = \frac{5}{2}$) $\Rightarrow \frac{5}{2}^+$. ^{40}Ca: doubly magic even–even $\Rightarrow 0^+$ [6, 20].

Problem 13.3 — ^{15}N configuration

Write the proton and neutron occupations of ^{15}N and deduce I^π.

Solution 13.3

Neutrons: closed through $1p_{1/2}$ ($N = 8$). Protons: $(1s_{1/2})^2(1p_{3/2})^4(1p_{1/2})^1$. Unpaired proton in $1p_{1/2} \Rightarrow I^\pi = \frac{1}{2}^-$ [6, 20].

Problem 13.4 — Odd–odd multiplet

An unpaired $d_{5/2}$ proton and an unpaired $p_{1/2}$ neutron form an odd–odd configuration. List the allowed I^π values and state what additional physics is needed to choose the ground member.

Solution 13.4

$$|j_p - j_n| = 2, \qquad j_p + j_n = 3,$$

so $I = 2, 3$. Parity $\pi = (-1)^{2+1} = -$, hence 2^- and 3^-. Residual proton–neutron interactions (guided empirically by Nordheim rules) select which of these is the ground state [19, 6].

Chapter 14

Schmidt Magnetic Moments

> *"In the extreme single-particle model the magnetic moment of an odd-A nucleus is attributed to the last unpaired nucleon."*
>
> standard shell-model statement

Lecture 8 treated the deuteron as a two-body magnetic moment. For heavier odd-A nuclei the extreme shell model makes a parallel claim: paired nucleons cancel, and μ is that of the valence nucleon in orbit $n\ell_j$. Plotting the resulting $\mu(j)$ gives the **Schmidt lines** [6, 1, 2].

14.1 Even–even nuclei: vanishing moment

In an even–even ground state every nucleon is paired to $I = 0$. Orbital and spin magnetism cancel within each pair, so

$$\mu = 0 \qquad (I^\pi = 0^+). \tag{14.1}$$

Experiment confirms that even–even ground states carry no static magnetic dipole (consistent with $I = 0$).

14.2 Nuclear magneton and g-factors

Magnetic moments of nuclei are measured in units of the nuclear magneton

$$\mu_N = \frac{e\hbar}{2m_p} \approx 5.05 \times 10^{-27}\,\mathrm{J\,T^{-1}}, \tag{14.2}$$

about 1/1836 of the Bohr magneton $\mu_B = e\hbar/(2m_e)$ because $m_p \gg m_e$. The z-component of the magnetic-moment operator for a single nucleon is

$$\mu_z = \left(g_\ell\, \ell_z + g_s\, s_z\right)\frac{\mu_N}{\hbar}, \tag{14.3}$$

with free-nucleon g-factors

$$\begin{aligned} g_\ell^{(p)} &= 1, \quad g_s^{(p)} = 5.5857, \\ g_\ell^{(n)} &= 0, \quad g_s^{(n)} = -3.8260. \end{aligned} \tag{14.4}$$

A useful way to remember the orbital factors is to begin with the magnetic moment of a particle of charge q and mass m:

$$\boldsymbol{\mu}_\ell = \frac{q}{2m}\,\boldsymbol{\ell} = \frac{q}{e}\frac{m_p}{m}\,\frac{\mu_N}{\hbar}\,\boldsymbol{\ell}. \tag{14.5}$$

For a proton, $q = e$ and $m \simeq m_p$, giving $g_\ell^{(p)} = 1$; for a neutron, $q = 0$, giving $g_\ell^{(n)} = 0$ in the free one-body operator. The spin factors follow from the measured intrinsic moments:

$$\mu_p = g_s^{(p)}\frac{\mu_N}{\hbar}\left(\frac{\hbar}{2}\right) = 2.7928\,\mu_N, \qquad \mu_n = \frac{g_s^{(n)}}{2}\mu_N = -1.9130\,\mu_N. \tag{14.6}$$

A structureless Dirac fermion would have $g_s = 2$. The large anomalous moments of the proton and neutron reflect their quark substructure: the proton (uud) and neutron (udd) carry internal charge currents even though the neutron is neutral overall. The neutron therefore has no orbital g_ℓ from net charge, yet a large spin moment [6, 5].

Because of the strong spin–orbit force, the good single-particle angular momentum is $\boldsymbol{j} = \boldsymbol{\ell} + \boldsymbol{s}$. The spectroscopic moment is the expectation value of μ_z in the stretched state $m_j = j$:

$$\mu = \langle j, m_j = j |\, g_\ell \ell_z + g_s s_z \,| j, m_j = j\rangle \frac{\mu_N}{\hbar}. \tag{14.7}$$

14.3 Case $j = \ell + \frac{1}{2}$: unique m_ℓ, m_s

For $j = \ell + \frac{1}{2}$ and $m_j = j = \ell + \frac{1}{2}$, the only combination consistent with $m_\ell + m_s = m_j$ is

$$m_\ell = \ell, \qquad m_s = +\tfrac{1}{2}. \tag{14.8}$$

The coupled state is therefore a single uncoupled basis vector,

$$|j = \ell + \tfrac{1}{2}, m_j = j\rangle = |\ell, m_\ell = \ell\rangle |\tfrac{1}{2}, m_s = \tfrac{1}{2}\rangle. \tag{14.9}$$

Consequently

$$\langle \ell_z \rangle = \ell\hbar, \qquad\qquad \langle s_z \rangle = \tfrac{1}{2}\hbar, \tag{14.10}$$

$$\begin{aligned} \frac{\mu}{\mu_N} &= \frac{1}{\hbar}\left(g_\ell \ell\hbar + g_s \frac{\hbar}{2}\right) \\ &= g_\ell \ell + \tfrac{1}{2} g_s. \end{aligned} \tag{14.11}$$

Using $\ell = j - \frac{1}{2}$ gives, one algebraic step at a time,

$$\frac{\mu}{\mu_N} = g_\ell\left(j - \tfrac{1}{2}\right) + \tfrac{1}{2} g_s = j\, g_\ell + \tfrac{1}{2}(g_s - g_\ell). \tag{14.12}$$

Specialising to free g-factors gives the first Schmidt formula

$$\frac{\mu}{\mu_N} = \begin{cases} j + 2.293 & \text{odd proton } (g_\ell = 1,\ g_s = 5.586), \\ -1.913 & \text{odd neutron } (g_\ell = 0,\ g_s = -3.826). \end{cases} \tag{14.13}$$

For a $d_{5/2}$ proton ($\ell = 2$, $j = \frac{5}{2}$), $\mu \approx 4.79\,\mu_N$ on the Schmidt line. For any odd neutron with $j = \ell + \frac{1}{2}$, the moment is simply half the free-neutron moment (independent of j), because only spin contributes.

14.4 Case $j = \ell - \frac{1}{2}$: two mixed components

For $j = \ell - \frac{1}{2}$ and $m_j = j$, two (m_ℓ, m_s) pairs contribute:

$$\begin{aligned} |1\rangle &= |m_\ell = \ell,\ m_s = -\tfrac{1}{2}\rangle, \\ |2\rangle &= |m_\ell = \ell - 1,\ m_s = +\tfrac{1}{2}\rangle. \end{aligned} \tag{14.14}$$

The stretched state is the normalised combination

$$|j, m_j = j\rangle = a|1\rangle + b|2\rangle. \tag{14.15}$$

14.4.1 Coefficients from $J_+|j,j\rangle = 0$

The raising operator $J_+ = L_+ + S_+$ annihilates the highest-weight state. The two ladder operators act according to

$$L_+|\ell, m_\ell\rangle = \hbar\sqrt{\ell(\ell+1) - m_\ell(m_\ell+1)}\,|\ell, m_\ell + 1\rangle, \tag{14.16}$$

$$S_+|\tfrac{1}{2}, m_s\rangle = \hbar\sqrt{\tfrac{1}{2}(\tfrac{1}{2}+1) - m_s(m_s+1)}\,|\tfrac{1}{2}, m_s + 1\rangle. \tag{14.17}$$

Therefore

$$J_+|1\rangle = (L_+ + S_+)|\ell, -\tfrac{1}{2}\rangle = \hbar|\ell, +\tfrac{1}{2}\rangle, \tag{14.18}$$

$$J_+|2\rangle = (L_+ + S_+)|\ell - 1, +\tfrac{1}{2}\rangle = \hbar\sqrt{2\ell}\,|\ell, +\tfrac{1}{2}\rangle. \tag{14.19}$$

Here the compact ket on the right denotes $|m_\ell = \ell, m_s = +\frac{1}{2}\rangle$. Acting on the mixture now gives

$$\begin{aligned} 0 = J_+|j,j\rangle &= aJ_+|1\rangle + bJ_+|2\rangle \\ &= \hbar(a + b\sqrt{2\ell})|\ell, +\tfrac{1}{2}\rangle. \end{aligned} \tag{14.20}$$

Since the ket and $\hbar$ are nonzero, the coefficient must vanish:

$$a + b\sqrt{2\ell} = 0 \qquad \Rightarrow \qquad a = -b\sqrt{2\ell}, \tag{14.21}$$

together with normalisation $|a|^2 + |b|^2 = 1$. Therefore

$$|a|^2 = \frac{2\ell}{2\ell+1}, \qquad |b|^2 = \frac{1}{2\ell+1}. \tag{14.22}$$

Choosing an irrelevant overall phase so that $b > 0$, the normalized state can be written explicitly as

$$|j = \ell - \tfrac{1}{2}, j\rangle = -\sqrt{\frac{2\ell}{2\ell+1}}\,|1\rangle + \sqrt{\frac{1}{2\ell+1}}\,|2\rangle. \tag{14.23}$$

These are precisely the Clebsch–Gordan coefficients for coupling ℓ and $s = \frac{1}{2}$ to $j = \ell - \frac{1}{2}$.

14.4.2 Expectation value of μ_z

Diagonal matrix elements of the magnetic operator are

$$\begin{aligned} \langle 1|\mu_z/\mu_N|1\rangle &= g_\ell \ell - \tfrac{1}{2} g_s, \\ \langle 2|\mu_z/\mu_N|2\rangle &= g_\ell(\ell-1) + \tfrac{1}{2} g_s, \end{aligned} \tag{14.24}$$

and cross terms vanish by orthogonality of the $|m_\ell m_s\rangle$ basis. More explicitly, ℓ_z and s_z are diagonal in this basis, so

$$\langle 1|\ell_z|2\rangle = \langle 1|s_z|2\rangle = 0. \tag{14.25}$$

This diagonality, not orthogonality alone for an arbitrary operator, is the reason the interference terms vanish. Expanding the full matrix element,

$$\begin{aligned} \frac{\mu}{\mu_N} &= (a^*\langle 1| + b^*\langle 2|)\frac{g_\ell \ell_z + g_s s_z}{\hbar}(a|1\rangle + b|2\rangle) \\ &= |a|^2\langle 1|\mu_z/\mu_N|1\rangle + |b|^2\langle 2|\mu_z/\mu_N|2\rangle \\ &\quad + a^*b\langle 1|\mu_z/\mu_N|2\rangle + b^*a\langle 2|\mu_z/\mu_N|1\rangle. \end{aligned} \tag{14.26}$$

The last line is zero, and the weighted average is therefore

$$\frac{\mu}{\mu_N} = |a|^2\big(g_\ell \ell - \tfrac{1}{2} g_s\big) + |b|^2\big(g_\ell(\ell-1) + \tfrac{1}{2} g_s\big). \tag{14.27}$$

Insert $|a|^2 = 2\ell/(2\ell+1)$ and $|b|^2 = 1/(2\ell+1)$:

$$\begin{aligned} \frac{\mu}{\mu_N} &= \frac{2\ell}{2\ell+1}\big(g_\ell \ell - \tfrac{1}{2} g_s\big) + \frac{1}{2\ell+1}\big(g_\ell(\ell-1) + \tfrac{1}{2} g_s\big) \\ &= \frac{1}{2\ell+1}\Big[2\ell^2 g_\ell - \ell g_s + (\ell-1)g_\ell + \tfrac{1}{2} g_s\Big] \\ &= \frac{1}{2\ell+1}\Big[(2\ell^2 + \ell - 1)g_\ell - \big(\ell - \tfrac{1}{2}\big)g_s\Big]. \end{aligned} \tag{14.28}$$

Now set $j = \ell - \frac{1}{2}$, so $\ell = j + \frac{1}{2}$ and $2\ell + 1 = 2j + 2$. The two coefficients in the numerator become

$$2\ell^2 + \ell - 1 = 2\big(j + \tfrac{1}{2}\big)^2 + \big(j + \tfrac{1}{2}\big) - 1 = 2j^2 + 3j = j(2j+3), \tag{14.29}$$

$$\ell - \tfrac{1}{2} = j. \tag{14.30}$$

Thus

$$\begin{aligned} \frac{\mu}{\mu_N} &= \frac{j(2j+3)g_\ell - j g_s}{2(j+1)} \\ &= \frac{j}{2(j+1)}\big[(2j+3)g_\ell - g_s\big]. \end{aligned} \tag{14.31}$$

Adding and subtracting $jg_\ell/[2(j+1)]$ in the last expression gives the equivalent standard Schmidt form

$$\frac{\mu}{\mu_N} = \frac{j}{2(j+1)}[(2j+3)g_\ell - g_s] = j\,g_\ell - \frac{j}{2(j+1)}(g_s - g_\ell). \tag{14.32}$$

Specialising to free g-factors:

$$\frac{\mu}{\mu_N} = \begin{cases} \dfrac{j}{j+1}\,(j - \frac{1}{2}g_s^{(p)} + \frac{3}{2}) = \dfrac{j(j-1.293)}{j+1} & \text{odd proton,} \\ -\dfrac{j}{2(j+1)}\,g_s^{(n)} = +1.913\,\dfrac{j}{j+1} & \text{odd neutron.} \end{cases} \tag{14.33}$$

For an odd neutron in $p_{1/2}$ ($j = \frac{1}{2}$), $\mu/\mu_N = 1.913 \times \frac{1}{2}/\frac{3}{2} = 0.638$. These limiting curves are the Schmidt lines first discussed by Schmidt in 1937 [18, 6, 1].

14.4.3 Independent check: the projection theorem

The same result follows without writing Clebsch–Gordan coefficients. Rotational symmetry requires the expectation value of any vector operator in $|jm_j\rangle$ to point along $\boldsymbol{j}$. Hence

$$\langle \ell_z \rangle = \frac{\langle \boldsymbol{\ell}\cdot\boldsymbol{j}\rangle}{j(j+1)\hbar^2}\,m_j\hbar, \qquad \langle s_z \rangle = \frac{\langle \boldsymbol{s}\cdot\boldsymbol{j}\rangle}{j(j+1)\hbar^2}\,m_j\hbar. \tag{14.34}$$

Using $\boldsymbol{j} = \boldsymbol{\ell} + \boldsymbol{s}$,

$$2\boldsymbol{\ell}\cdot\boldsymbol{j} = \boldsymbol{j}^2 + \boldsymbol{\ell}^2 - \boldsymbol{s}^2, \tag{14.35}$$

$$2\boldsymbol{s}\cdot\boldsymbol{j} = \boldsymbol{j}^2 - \boldsymbol{\ell}^2 + \boldsymbol{s}^2. \tag{14.36}$$

For the spectroscopic state $m_j = j$, division by $\hbar$ gives

$$\frac{\langle \ell_z \rangle}{\hbar} = \frac{j(j+1) + \ell(\ell+1) - s(s+1)}{2(j+1)}, \tag{14.37}$$

$$\frac{\langle s_z \rangle}{\hbar} = \frac{j(j+1) - \ell(\ell+1) + s(s+1)}{2(j+1)}. \tag{14.38}$$

Substitution into $\mu/\mu_N = g_\ell\langle\ell_z\rangle/\hbar + g_s\langle s_z\rangle/\hbar$, with $s = \frac{1}{2}$, reproduces Eqs. (14.13) and (14.32). This is the same projection theorem used for the deuteron in Lecture 8; it is a valuable check because it keeps every orbital and spin term visible.

14.4.4 Why a one-hole state has the same Schmidt value

A filled j subshell has zero total moment because the contributions from m and $-m$ cancel. To construct a hole state with total $M = +j$, remove the particle with $m = -j$. The remaining shell therefore has

$$\mu_{\text{hole}}(M = +j) = 0 - \mu_{\text{particle}}(m = -j) = \mu_{\text{particle}}(m = +j), \tag{14.39}$$

because a vector moment changes sign under $m \to -m$. Thus a particle and a hole in the same j orbit have the same Schmidt moment in the extreme model, even though their many-body

occupations are complementary.

14.5 Schmidt lines and experiment

Plotting μ against j for odd-proton nuclei gives two rising lines ($j = \ell \pm \frac{1}{2}$). For odd-neutron nuclei the $j = \ell + \frac{1}{2}$ line is flat at $-1.913\,\mu_N$ and the $j = \ell - \frac{1}{2}$ line is positive and slowly rising. Experimental ground-state moments of odd-A nuclei typically fall *between* the two Schmidt lines for the assigned j (Fig. 14.1) [18, 6, 2, 22]. The Schmidt curves are theoretical single-particle limits, not rigorous mathematical bounds; they organise the data and diagnose configuration purity.

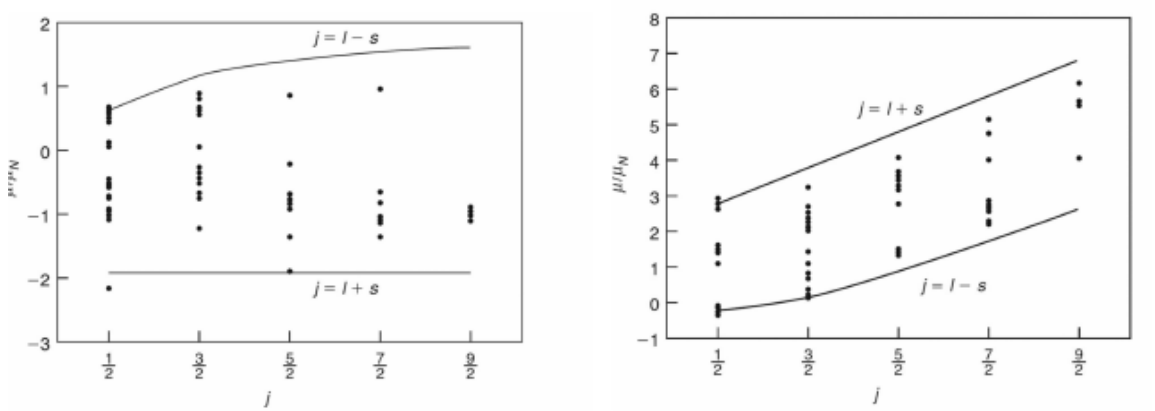

Figure 14.1: Schmidt lines and data: left, odd-N (neutron) moments; right, odd-Z (proton) moments (re-extracted from the full-resolution original PH5001 lecture source page; cf. Dunlap [1], Krane [6], and Stone [22]).

14.6 Why real nuclei lie between the Schmidt lines

The extreme single-particle picture is too simple:

- configuration mixing admixes other orbitals with the same I^π;
- meson-exchange currents modify the free one-body magnetic operator inside the nucleus;
- collective core polarisation contributes for soft nuclei far from closed shells;
- effective spin g-factors are often reduced from free values. A common phenomenological estimate is $g_s^{\text{eff}} \approx 0.7\, g_s^{\text{free}}$, but this is not a universal law and should be fitted orbit by orbit [6, 1].

Near doubly magic cores (e.g. ^{17}O, ^{41}Ca) agreement with Schmidt values is better; mid-shell nuclei deviate more [6, 2, 1, 22]. When a measured μ lies close to one Schmidt line, the valence assignment $j = \ell \pm \frac{1}{2}$ is strongly supported; intermediate values tag mixing.

Key idea

Schmidt lines are the shell-model baseline for μ. They fix the single-particle g-factors and $j = \ell \pm \frac{1}{2}$ assignment; deviations measure correlations beyond the extreme model.

14.7 Further physics: magnetic moments as configuration tags

Measured magnetic moments are among the most sensitive tests of the valence configuration near closed shells. If μ lies close to one Schmidt line, the extreme single-particle assignment $j = \ell \pm \frac{1}{2}$ is strongly supported. Intermediate values signal configuration mixing or collective admixtures [6, 2, 22].

Effective g_s factors reduced from the free nucleon values are a compact way to summarise medium modifications, but they absorb several distinct mechanisms: core polarisation, meson-exchange currents, and truncated model spaces. For that reason one should not treat a single quenching factor as fundamental. Near doubly magic cores such as ^{16}O and ^{40}Ca, moments of neighbouring odd-A nuclei remain comparatively close to Schmidt predictions; far from magic numbers, collective contributions dominate and the Schmidt picture is only a reference baseline.

14.8 Problems with solutions

Problem 14.1 — Schmidt value for $d_{5/2}$ proton

Compute the Schmidt moment for an odd proton in $j = \ell + \frac{1}{2} = \frac{5}{2}$.

Solution 14.1

For $j = \ell + \frac{1}{2}$ and free proton g-factors,

$$\frac{\mu}{\mu_N} = j\, g_\ell + \tfrac{1}{2}(g_s - g_\ell) = \tfrac{5}{2} \cdot 1 + \tfrac{1}{2}(5.586 - 1) = 2.5 + 2.293 = 4.793.$$

Equivalently, $\mu/\mu_N = j + 2.293$ [18, 6].

Problem 14.2 — Neutron $p_{1/2}$ Schmidt moment

For an odd neutron with $j = \ell - \frac{1}{2} = \frac{1}{2}$ ($\ell = 1$), compute the Schmidt moment in nuclear magnetons.

Solution 14.2

For an odd neutron with $j = \ell - \frac{1}{2}$,

$$\frac{\mu}{\mu_N} = +1.913\,\frac{j}{j+1} = 1.913 \times \frac{1/2}{3/2} = \frac{1.913}{3} \approx 0.638.$$

Equivalently, $\mu/\mu_N = -g_s^{(n)} j/(2(j+1))$ with $g_s^{(n)} = -3.826$ yields the same result [6, 18].

Problem 14.3 — Neutron $j = \ell + \frac{1}{2}$

Show that any odd neutron with $j = \ell + \frac{1}{2}$ has Schmidt moment $\mu = -1.913\,\mu_N$, independent of j.

Solution 14.3

With $g_\ell^{(n)} = 0$ and $g_s^{(n)} = -3.826$, the $j = \ell + \tfrac{1}{2}$ formula collapses to

$$\frac{\mu}{\mu_N} = \tfrac{1}{2} g_s = -1.913,$$

for every such orbit. Only the spin moment contributes [6, 1].

Problem 14.4 — Coefficients a and b

For $j = \ell - \tfrac{1}{2}$ and $m_j = j$, derive $|a|^2 = 2\ell/(2\ell+1)$ and $|b|^2 = 1/(2\ell+1)$ from $J_+|j,j\rangle = 0$.

Solution 14.4

Write $|j,j\rangle = a|1\rangle + b|2\rangle$ with $|1\rangle = |\ell, -\tfrac{1}{2}\rangle$ and $|2\rangle = |\ell-1, +\tfrac{1}{2}\rangle$. Acting with $J_+ = L_+ + S_+$ and using $L_+|\ell,m\rangle = \hbar\sqrt{\ell(\ell+1) - m(m+1)}\,|\ell, m+1\rangle$ gives the condition $a + b\sqrt{2\ell} = 0$. Together with $|a|^2 + |b|^2 = 1$ one obtains

$$|a|^2 = \frac{2\ell}{2\ell+1}, \qquad |b|^2 = \frac{1}{2\ell+1},$$

as in the main text [6].

Chapter 15

Shell-Model Excited States and Collective Motion

> *"Experimentally, it is observed that nuclei can have several excited states... The nuclear shell model is instrumental in explaining these excited states."*
>
> lecture notes, PH5001

Ground-state I^π and Schmidt moments test the filling of the mean field. Excited states test whether the same orbitals, with particle promotions and pair breaking, organise the low-lying spectrum. Near closed shells the extreme shell model works well (classic example: ^{17}O). In mid-shell even–even nuclei the first 2^+ state is collective, and vibrational or rotational models are required [6, 1, 14].

15.1 Ground state of ^{17}O

Oxygen-17 has $Z = 8$, $N = 9$. Protons fill the closed shell through $1p_{1/2}$ (magic $Z = 8$) and contribute $I = 0$. Neutrons fill

$$(1s_{1/2})^2\,(1p_{3/2})^4\,(1p_{1/2})^2\,(1d_{5/2})^1. \tag{15.1}$$

The unpaired neutron is in $1d_{5/2}$ ($\ell = 2$, $j = \frac{5}{2}$), so

$$I^\pi = \tfrac{5}{2}^+, \tag{15.2}$$

matching experiment. The closed proton shell and nearly closed neutron p shell make ^{17}O a textbook single-particle nucleus: the core is ^{16}O and the valence neutron is weakly coupled to it.

15.2 Single-particle excitations of ^{17}O

Promoting the valence neutron to a higher empty orbit changes I^π without breaking the ^{16}O core:

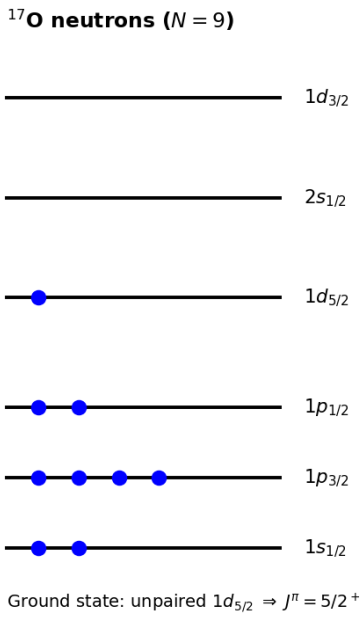

Figure 15.1: Neutron filling for ^{17}O. The ground state is fixed by the unpaired $1d_{5/2}$ neutron (adapted from the original PH5001 lecture figure).

Configuration (valence n)	I^π	Character
$1d_{5/2}$	$\frac{5}{2}^+$	ground state
$2s_{1/2}$	$\frac{1}{2}^+$	first s-wave excitation
$1d_{3/2}$	$\frac{3}{2}^+$	spin–orbit partner of $d_{5/2}$

These positive-parity states appear in the low-lying spectrum and carry large single-particle strength in one-neutron transfer. Evaluated levels place the $1/2^+$ state at 871 keV and show additional positive- and negative-parity excitations consistent with *sd* and *p*-shell rearrangements [20, 21, 6].

15.3 Particle–hole excitations in ^{17}O

Higher states involve exciting a nucleon from a filled orbit, leaving a hole.

Hole in $1p_{3/2}$. Promote one neutron from $1p_{3/2}$ into $1d_{5/2}$. After the transition one has three neutrons in $1p_{3/2}$ (odd occupancy) and two in $1d_{5/2}$. The unpaired hole in $1p_{3/2}$ yields

$$I^\pi = \tfrac{3}{2}^- \tag{15.3}$$

($\ell = 1 \Rightarrow \pi = -$).

Hole in $1p_{1/2}$. Promote from $1p_{1/2}$ into $1d_{5/2}$: one unpaired neutron remains in $1p_{1/2}$, giving

$$I^\pi = \tfrac{1}{2}^-. \tag{15.4}$$

Multi-particle couplings. When three unpaired neutrons sit in different orbits (e.g. $1p_{1/2}$, $1d_{5/2}$, $2s_{1/2}$), their angular momenta couple to several total I. Parity of a multi-particle configuration is the product of single-particle parities,

$$\pi = \prod_i (-1)^{\ell_i}. \tag{15.5}$$

A state such as $\frac{5}{2}^-$ can arise from coupling three unequal j values with overall negative parity. The extreme model still provides the language of orbits and parities even when residual interactions fix the detailed multiplet ordering.

15.4 Even–even example: ^{38}Ar

Argon-38 has $Z = 18$, $N = 20$. Neutrons fill the magic $N = 20$ shell; protons sit two holes below $Z = 20$. The ground state is even–even, so

$$I^\pi = 0^+. \tag{15.6}$$

Because $N = 20$ is closed, low-lying excitations often rearrange protons.

Proton $1d_{3/2} \to 1f_{7/2}$. Leaving one proton in $1d_{3/2}$ and one in $1f_{7/2}$ produces two unequal j values. Allowed total angular momenta run from $|7/2 - 3/2| = 2$ to $7/2 + 3/2 = 5$:

$$I = 2, 3, 4, 5, \qquad \pi = (-1)^2(-1)^3 = -. \tag{15.7}$$

States $2^-, 3^-, 4^-, 5^-$ are therefore expected; the observed 3^- is naturally associated with this particle–hole (or two-proton) excitation across the *sd*–*pf* interface [6].

Proton $2s_{1/2} \to 1d_{3/2}$. Breaking a $2s_{1/2}$ pair and promoting one proton toward $1d_{3/2}$ yields $I = 1, 2$ with positive parity ($\pi = (-1)^{0+2} = +$). Forming such a state costs both pair-breaking energy ($\sim 2\,\text{MeV}$) and single-particle promotion energy, so the associated 2^+ tends to lie near $\sim 4\,\text{MeV}$, higher than the first collective 2^+.

15.5 Systematics of the lowest 2^+ in even–even nuclei

In the great majority of even–even nuclei the lowest excited state is 2^+. Important exceptions occur near doubly closed shells, where a 0^+ or 3^- state may intervene; globally, however, a low-lying 2^+ cannot be explained by single-particle counting alone: the same pattern appears for hundreds of nuclei over a wide range of A (Fig. 15.2).

Empirical systematics of the lowest $E(2^+)$ show three regimes [6, 1, 14]:

1. **Magic and near-magic nuclei:** $E(2^+)$ is large (several MeV), reflecting rigid spherical cores.

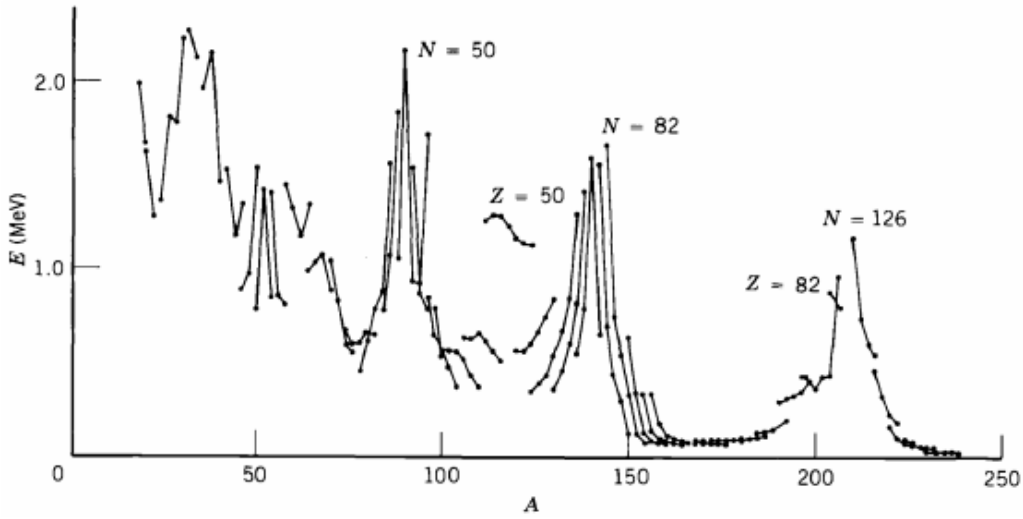

Figure 15.2: Energies of the lowest 2^+ states of even-Z, even-N nuclei versus A. Peaks occur at shell closures; mid-shell regions show much lower $E(2^+)$ (re-extracted with complete axes from the full original PH5001 source page; cf. Krane [6]).

2. **Spherical and weakly collective regions:** typical $E(2^+)$ values are of order 1 MeV. An approximately harmonic quadrupole vibrator has $E(4^+)/E(2^+) \approx 2$, while transitional nuclei need not obey this ideal ratio.

3. **Deformed regions $A \sim 150$–190 and $A \gtrsim 230$:** $E(2^+)$ drops to tens of keV, with $E(4^+)/E(2^+) \approx 10/3 \approx 3.33$, the rigid-rotor ratio.

Peaks of $E(2^+)$ at magic N or Z reconnect these collective trends to shell structure: closed shells stiffen the nucleus against deformation.

Key idea

Odd-A neighbours of closed shells: single-particle and particle–hole excitations. Even–even mid-shell nuclei: collective 2^+ (vibration or rotation). The shell model alone is incomplete for the latter.

15.6 Vibrational model

For spherical even–even nuclei ($A \lesssim 150$) the equilibrium shape is spherical. Small excess energy can excite volume-conserving surface oscillations. The nuclear radius is expanded in spherical harmonics,

$$R(\theta,\phi,t) = \bar{R}\left[1 + \sum_{\lambda=0}^{\infty}\sum_{\mu=-\lambda}^{\lambda} \alpha_{\lambda\mu}(t)\, Y_{\lambda\mu}(\theta,\phi)\right], \tag{15.8}$$

with multipolarity λ and deformation amplitudes $\alpha_{\lambda\mu}(t)$. To derive the volume constraint, write the volume enclosed by the surface as

$$\mathcal{V} = \frac{1}{3}\int R^3(\theta,\phi,t)\,\mathrm{d}\Omega. \tag{15.9}$$

For small amplitudes, $(1+\epsilon)^3 = 1 + 3\epsilon + \mathcal{O}(\epsilon^2)$, so Eq. (15.8) gives

$$\begin{aligned}\mathcal{V} &= \frac{\bar{R}^3}{3}\int\left[1 + 3\sum_{\lambda\mu}\alpha_{\lambda\mu}Y_{\lambda\mu}\right]\mathrm{d}\Omega + \mathcal{O}(\alpha^2)\\ &= \frac{4\pi\bar{R}^3}{3}\left(1 + \frac{3\alpha_{00}}{\sqrt{4\pi}}\right) + \mathcal{O}(\alpha^2),\end{aligned} \tag{15.10}$$

where $\int Y_{\lambda\mu}\mathrm{d}\Omega = \sqrt{4\pi}\,\delta_{\lambda 0}\delta_{\mu 0}$. Keeping $\mathcal{V} = 4\pi\bar{R}^3/3$ therefore requires

$$\alpha_{00} = 0 \qquad \text{to first order.} \tag{15.11}$$

At second order a small monopole correction compensates the volume change from $|\alpha_{\lambda\mu}|^2$. The intrinsic parity of a one-phonon excitation of multipolarity λ is $(-1)^\lambda$, because $Y_{\lambda\mu}(-\hat{r}) = (-1)^\lambda Y_{\lambda\mu}(\hat{r})$.

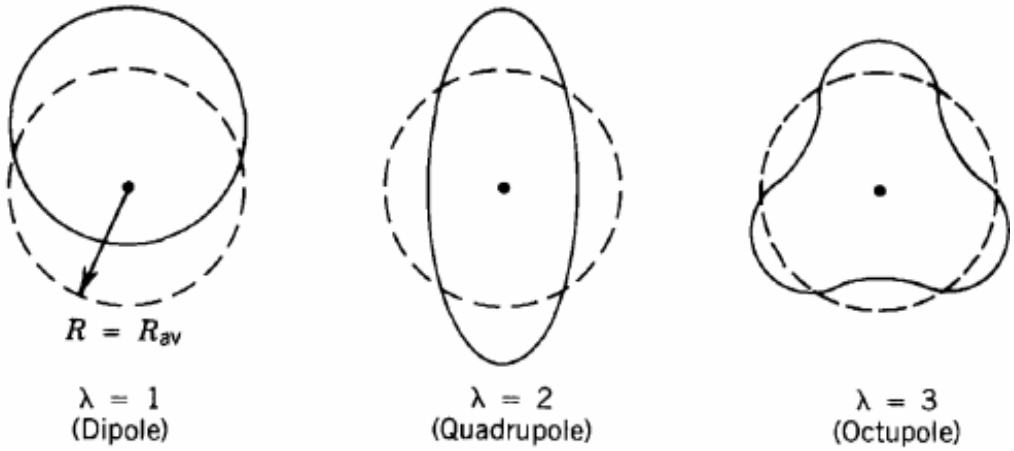

Figure 15.3: Lowest vibrational modes of a nucleus: dipole ($\lambda = 1$), quadrupole ($\lambda = 2$), octupole ($\lambda = 3$) (re-extracted from the full original PH5001 source page; cf. Krane [6]).

Breathing mode ($\lambda = 0$). With $Y_{00} = 1/\sqrt{4\pi}$,

$$R(\theta,\phi,t) = \bar{R}\big(1 + \alpha_{00}(t)\big). \tag{15.12}$$

The nucleus expands and contracts uniformly without changing shape. This isoscalar monopole mode lies at high excitation energy and does not produce the low-lying quantized shape spectrum of interest here.

Dipole mode ($\lambda = 1$). A pure $\lambda = 1$ surface deformation is equivalent to a displacement of the nuclear centre of mass. To see this explicitly, translate a sphere by a small vector $\boldsymbol{d}$. Along direction $\hat{r}$, its new surface is

$$R'(\hat{r}) = \bar{R} + \boldsymbol{d}\cdot\hat{r} + \mathcal{O}(d^2/\bar{R}). \tag{15.13}$$

The angular function $\boldsymbol{d}\cdot\hat{r}$ is a linear combination of the three $Y_{1\mu}$. Thus a $\lambda = 1$ deformation merely moves the whole sphere and can be removed by choosing the centre-of-mass origin. It is

not an intrinsic excitation. Low-lying shape phonons begin at quadrupole order. (Giant dipole resonances are a different, high-energy isovector phenomenon in which protons and neutrons oscillate against each other.)

Quadrupole mode ($\lambda = 2$). The nucleus oscillates between prolate and oblate ellipsoidal shapes. This mode produces the dominant low-lying vibrational spectrum of spherical even–even nuclei.

Octupole mode ($\lambda = 3$). More complex pear-shaped surface oscillations; the one-phonon state is 3^-.

15.6.1 Phonons and the vibrational spectrum

Each multipole amplitude $\alpha_{\lambda\mu}$ behaves as a harmonic oscillator coordinate. For one normal coordinate the Hamiltonian has the form

$$H_{\lambda\mu} = \frac{\pi_{\lambda\mu}^2}{2B_\lambda} + \frac{1}{2}C_\lambda \alpha_{\lambda\mu}^2, \qquad \omega_\lambda = \sqrt{\frac{C_\lambda}{B_\lambda}}, \tag{15.14}$$

where B_λ is the collective inertia and C_λ the restoring-force constant. Canonical quantisation gives

$$E_{n_\lambda} = \left(n_\lambda + \tfrac{1}{2}\right)\hbar\omega_\lambda. \tag{15.15}$$

Only excitation energies are observed, so the common zero-point term is subtracted and n_λ quanta cost $n_\lambda \hbar\omega_\lambda$. These quanta are called **phonons**. The lowest vibrational excitation is one quadrupole phonon:

$$E = \hbar\omega_2, \qquad I^\pi = 2^+, \tag{15.16}$$

because the phonon carries angular momentum $\lambda = 2$ and parity $(-1)^\lambda = +$. For even–even nuclei the ground state is 0^+ and this 2^+ is the first excited state of the vibrational model.

Two quadrupole phonons have energy $2\hbar\omega_2$. Coupling two identical $I = 2$ bosons allows only the totally symmetric states $I = 0, 2, 4$ (the odd values $1, 3$ are forbidden for identical phonons), all with positive parity: the two-phonon triplet $0^+, 2^+, 4^+$.

Three quadrupole phonons give energy $3\hbar\omega_2$ and allowed $I^\pi = 0^+, 2^+, 3^+, 4^+, 6^+$. One octupole phonon gives

$$E = \hbar\omega_3, \qquad I^\pi = 3^-. \tag{15.17}$$

In the harmonic limit the two-phonon 4^+ and the one-phonon 2^+ satisfy

$$\frac{E(4^+)}{E(2^+)} = \frac{2\hbar\omega_2}{\hbar\omega_2} = 2, \tag{15.18}$$

matching the empirical ratio for many nuclei with $A \sim 30$–150. The equality is an ideal harmonic limit, not an exact universal rule: anharmonicities split the two-phonon multiplet and shift the ratio away from 2. For an incompressible liquid drop with surface tension σ and density ρ, the

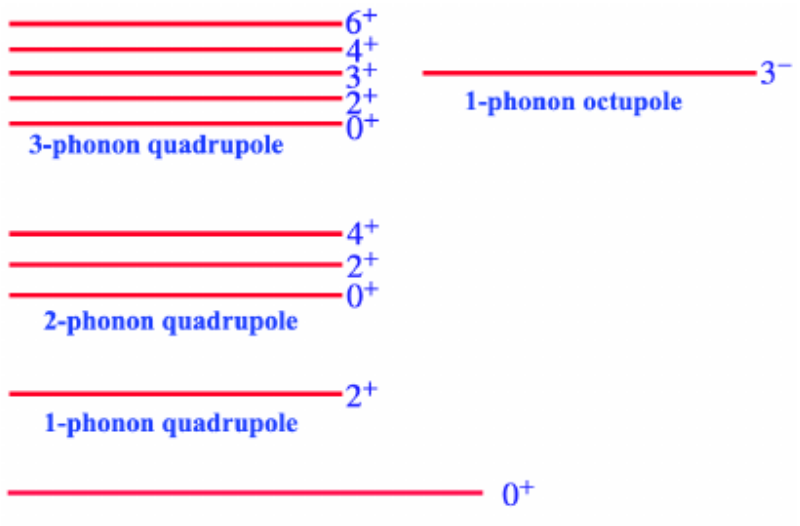

Figure 15.4: Schematic vibrational spectrum of an even–even nucleus: one-, two- and three-phonon quadrupole multiplets and the one-phonon octupole 3^- (re-extracted from the full original PH5001 source page).

classical surface-mode frequencies scale as

$$\omega_\lambda = \sqrt{\frac{\sigma(\lambda-1)(\lambda+2)\lambda}{\rho\,\bar{R}^3}}, \tag{15.19}$$

so higher multipoles are stiffer and lie higher in energy [6, 1, 14].

15.7 Rotational model

Nuclei with large static quadrupole moments (notably $A \sim 150$–190 and $A \gtrsim 230$) are permanently deformed (Fig. 15.5). For an axially symmetric rotor the intrinsic deformation may be parametrised by a quadrupole parameter β_2 through

$$R(\theta) = \bar{R}\bigl(1 + \beta_2 Y_{20}(\theta) + \cdots\bigr). \tag{15.20}$$

Rotation about an axis perpendicular to the symmetry axis produces a quantized rotational band.

Classically $E = \tfrac{1}{2}\mathcal{I}\omega^2 = L^2/(2\mathcal{I})$. In quantum mechanics the squared angular momentum of the rotor is replaced by $I(I+1)\hbar^2$, so

$$E_I = \frac{\hbar^2}{2\mathcal{I}}\, I(I+1). \tag{15.21}$$

For the ground band of an even–even axial nucleus the projection of angular momentum on the symmetry axis vanishes ($K = 0$). Symmetry under a rotation by π about an axis perpendicular to the symmetry axis then admits only even I with positive parity:

$$I^\pi = 0^+, 2^+, 4^+, 6^+, \ldots \tag{15.22}$$

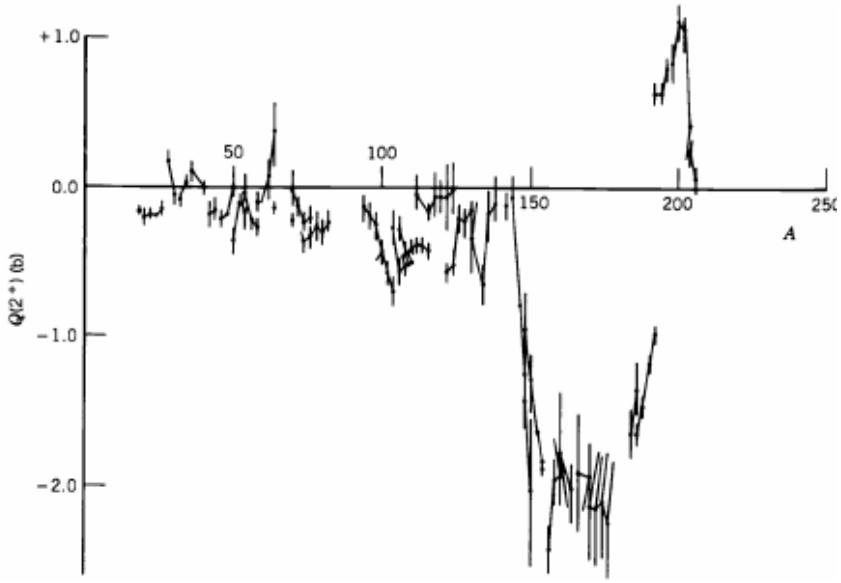

Figure 15.5: Electric quadrupole moments of the lowest 2^+ states of even–even nuclei. Large $|Q|$ in deformed regions signals permanent deformation (re-extracted with complete axes from the full original PH5001 source page; cf. Krane [6]).

(odd-I members are excluded). Using $E(2^+) = 6\hbar^2/(2\mathcal{I})$ and $E(4^+) = 20\hbar^2/(2\mathcal{I})$ one finds

$$\frac{E(4^+)}{E(2^+)} = \frac{20}{6} = \frac{10}{3} \approx 3.33, \tag{15.23}$$

the classic rotor ratio. Rotational 2^+ energies are typically of order 10–100 keV, much lower than vibrational ~ 1 MeV levels [6, 14, 1].

The same deformation that produces the rotational band also generates a large intrinsic quadrupole moment Q_0. For a uniformly charged, slightly deformed nucleus,

$$Q_0 \simeq \frac{3}{\sqrt{5\pi}}\, Ze\bar{R}^2\beta_2 \qquad \text{(to first order in } \beta_2\text{)}. \tag{15.24}$$

The laboratory spectroscopic quadrupole moment of a band member is

$$Q_s(I,K) = \frac{3K^2 - I(I+1)}{(I+1)(2I+3)}\, Q_0. \tag{15.25}$$

For the $K = 0$ ground-state band this is negative when $Q_0 > 0$: a prolate intrinsic shape does not imply a positive laboratory Q_s. The reduced transition probability is

$$B(E2; IK \to I-2, K) = \frac{5}{16\pi} Q_0^2 \left|\langle IK\, 2\, 0 | I-2, K\rangle\right|^2 . \tag{15.26}$$

Thus Q_s is linear in Q_0, whereas $B(E2)$ is quadratic in Q_0. Enhanced $B(E2)$ values (many Weisskopf units) are a hallmark of collective rotation, in contrast to single-particle estimates near closed shells [6, 1].

15.8 Limitations of the extreme shell model

The extreme single-particle picture fails when:

- several valence nucleons occupy an open shell (need configuration mixing and residual two-body matrix elements);
- the nucleus is soft or deformed far from magic numbers (collective rotational/vibrational degrees of freedom);
- continuum and cluster structures appear near drip lines.

Modern shell-model calculations keep the mean-field orbitals but diagonalise a residual interaction in a truncated valence space. Collective models build on the same single-particle structure: magic numbers still mark where sphericity is preferred.

Key idea

Near closed shells, excited states are particle promotions and particle–hole excitations on top of a magic core. ^{17}O is the cleanest example. Mid-shell even–even spectra demand collective vibration ($E(4^+)/E(2^+) \approx 2$) or rotation ($E(4^+)/E(2^+) \approx 3.33$).

15.9 Further physics: spectroscopic factors

One-nucleon transfer reactions such as (d, p) or (p, d) measure how much of a pure single-particle orbital is present in a nuclear state. The spectroscopic factor S quantifies that overlap: $S = 1$ for an ideal single-particle state on an inert closed core, while $S < 1$ signals fragmentation of the single-particle strength among several eigenstates [6, 1].

Near doubly magic cores, low-lying odd-A states often carry large spectroscopic factors, consistent with the extreme shell model. As one moves away from closed shells, residual interactions spread the strength and S decreases. Sum rules constrain the total strength available in a given orbit: the summed spectroscopic factors for adding or removing a nucleon from a closed shell cannot exceed the orbit's degeneracy. Fragmentation of spectroscopic strength is therefore direct experimental evidence for the limitations of the extreme independent-particle picture and for the need for configuration mixing or collective degrees of freedom.

15.10 Problems with solutions

Problem 15.1 — First excited state of ^{17}O

In the extreme single-particle model, what is I^π if the valence neutron of ^{17}O is promoted from $1d_{5/2}$ to $2s_{1/2}$? Compare with the evaluated excitation energy.

Solution 15.1

$2s_{1/2}$ has $\ell = 0$, $j = \frac{1}{2}$, so $I^\pi = \frac{1}{2}^+$. ENSDF places this state at 871 keV, matching the observed first excited state [20, 21, 6].

Problem 15.2 — ^{38}Ar multiplet

A proton is excited from $1d_{3/2}$ to $1f_{7/2}$ in ^{38}Ar. List the allowed I^π values for the two unpaired protons.

Solution 15.2

$j_1 = \frac{3}{2}$, $j_2 = \frac{7}{2}$ give

$$|j_1 - j_2| \le I \le j_1 + j_2 \quad \Rightarrow \quad I = 2, 3, 4, 5.$$

Parity $(-1)^{2+3} = -$, so $2^-, 3^-, 4^-, 5^-$ [6].

Problem 15.3 — Rotor vs vibrator ratio

Compute $E(4^+)/E(2^+)$ for a pure axial rotor with $E(I) \propto I(I+1)$. Compare with the ideal harmonic vibrator value.

Solution 15.3

For the rotor,

$$E(2) \propto 2 \cdot 3 = 6, \qquad E(4) \propto 4 \cdot 5 = 20,$$

so the ratio is $20/6 = 10/3 \approx 3.33$. For a harmonic quadrupole vibrator, $E(4^+) = 2\hbar\omega_2$ while $E(2^+) = \hbar\omega_2$, so the ratio is 2 [6, 14].

Problem 15.4 — Why $\lambda = 1$ is not a shape phonon

Explain why a pure $\lambda = 1$ term in the surface expansion does not generate an intrinsic low-lying vibrational excitation.

Solution 15.4

A $\lambda = 1$ deformation displaces the nuclear surface in a way that is equivalent to a shift of the centre of mass. Transforming to the CM frame removes the amplitude, so there is no intrinsic shape excitation. Low-lying surface phonons therefore begin at quadrupole order ($\lambda = 2$) [6, 1].

Chapter 16

Radioactivity and Alpha Decay

"A factor of 2 in energy means a factor of 10^{24} *in half-life! The theoretical explanation of this Geiger–Nuttall rule in 1928 was one of the first triumphs of quantum mechanics."*

K. S. Krane [6]

The semi-empirical mass formula and the β-stability parabolas (earlier chapters) predict which nuclei are energetically favoured against nucleon rearrangement. Experiment organises itself differently: on the chart of nuclides, every known species is plotted by neutron number N and proton number Z, and the dominant decay mode in each region is read directly from the map [6, 1, 14, 2]. Heavy nuclei predominantly emit α particles; nuclei far from the valley of β stability adjust N/Z by β decay. This chapter develops the phenomenology of radioactivity and α decay: the chart, the decay Q-value, two-body kinematics, the exponential decay law, the Geiger–Nuttall systematics, and the potential-barrier picture that Gamow used to explain the extreme sensitivity of the half-life to Q.

16.1 Chart of nuclides and where α decay lives

Figure 16.1 shows the chart of nuclides: each point is a known nuclide, with Z on the horizontal axis and N on the vertical axis. Stable species form a narrow band called the *valley of stability*. Away from that band, characteristic decay modes dominate: β^- emission on the neutron-rich side, β^+ emission and/or electron capture on the proton-rich side, and α decay in the upper-right corner where both Z and N are large.

Why heavy nuclei emit α particles. The red-shaded region in Fig. 16.1 corresponds to very heavy nuclei, typically $Z \gtrsim 82$ (lead, bismuth, and the actinides). An α particle is a ^{4}He nucleus ($Z = 2$, $N = 2$). Emitting it reduces both Z and N by 2, moving the system diagonally down and to the left on the chart toward more stable configurations [6, 1].

Three physical reasons combine to favour α emission in this region:

(i) **Coulomb repulsion.** The SEMF Coulomb term grows as $Z(Z-1)/A^{1/3}$. For large Z, the electrostatic energy of packing many protons into a finite volume makes the parent less bound than lighter fragments would be.

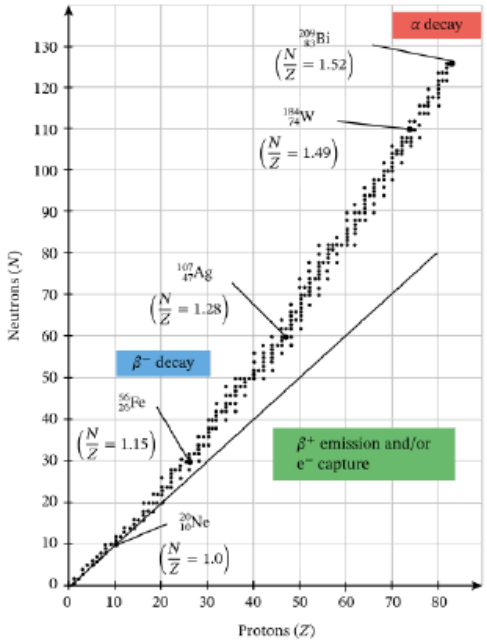

Figure 16.1: Chart of nuclides showing regions of dominant decay mode: α decay, β^- decay, and β^+/electron capture. Re-extracted from the original PH5001 lecture source pages (Prof. Bharat Kumar, PH5001).

(ii) **Declining B/A.** Beyond the iron peak, the average binding energy per nucleon decreases for very heavy nuclei, so releasing a tightly bound cluster can lower the total rest mass.

(iii) **The anomalously large binding of ^{4}He.** Helium-4 is doubly magic ($Z = N = 2$) with experimental binding energy $B_\alpha \approx 28.3\,\text{MeV}$ (about 7 MeV per nucleon). That large B_α enters the Q-value with a positive sign and makes α emission energetically preferred over most other light clusters [6, 1, 14].

Stable versus long-lived nuclei. Around $A \sim 200$ to 210 one finds the last stable combinations of N and Z on Earth. Beyond that point no stable species exist; heavy nuclides decay by α and/or β chains toward lead. Many nuclides with $150 < A < 210$ are not strictly stable but are *long-lived*: their α half-lives exceed the age of the Earth, so they persist in natural samples (^{238}U, ^{232}Th, ^{235}U, and others). The chart therefore distinguishes three categories: stable nuclei in the valley, long-lived radioactive nuclei with human-scale or geological half-lives, and short-lived nuclei studied in the laboratory.

Key idea

On the chart of nuclides, α decay occupies the upper-right corner ($Z \gtrsim 82$). Each emission step moves $(N, Z) \to (N-2, Z-2)$. The last stable nuclides lie near $A \sim 209$; beyond that, all heavy species are radioactive.

16.2 Particle emission versus fission

When a heavy nucleus breaks apart, the process is classified by the size of the fragments:

- **Particle emission:** one fragment is much smaller than the other (proton, neutron, deuteron, α, or a slightly heavier cluster).
- **Fission:** the nucleus splits into two fragments of comparable mass (treated later in the course).

Among light ejectiles, α emission is usually dominant because $B_\alpha \approx 28.3\,\mathrm{MeV}$ is exceptionally large. Dunlap illustrates this for ^{235}U: emission of a neutron, proton, or ^{3}He has $Q < 0$, while α emission has $Q \approx +4.7\,\mathrm{MeV}$ [1]. Heavier clusters such as ^{12}C or ^{14}C can be emitted in rare instances, but the thicker Coulomb barrier and small preformation probability suppress those channels by many orders of magnitude relative to α decay [6].

16.3 The α decay scheme and Q-value

The basic process is

$$ {}^{A}_{Z}X \;\rightarrow\; {}^{A-4}_{Z-2}Y + {}^{4}_{2}\mathrm{He} + Q. \tag{16.1}$$

The decay is spontaneous only if $Q > 0$: the total rest mass of the products is less than that of the parent, and the excess appears as kinetic energy of the daughter and the α particle.

16.3.1 Q from nuclear masses

Let m_{N} denote nuclear masses (masses of the bare nuclei, without electrons). Then

$$ Q = \Big[m_{\mathrm{N}}({}^{A}_{Z}X) - m_{\mathrm{N}}({}^{A-4}_{Z-2}Y) - m_{\mathrm{N}}({}^{4}\mathrm{He}) \Big] c^2. \tag{16.2}$$

A positive Q means the parent nucleus is heavier than the sum of the daughter and α masses.

16.3.2 Q from atomic masses: cancellation of electrons

In the laboratory one uses atomic masses m_{atom}, which include Z electrons for a neutral atom. Write the relation between atomic and nuclear masses as

$$ m_{\mathrm{atom}}({}^{A}_{Z}X) = m_{\mathrm{N}}({}^{A}_{Z}X) + Z m_e - B_e(Z), \tag{16.3}$$

where m_e is the electron mass and $B_e(Z)$ is the total electronic binding energy of the neutral atom (a few keV per electron, negligible on the MeV scale of nuclear decays).

For the three bodies in Eq. (16.1):

$$ m_{\mathrm{atom}}({}^{A}_{Z}X) = m_{\mathrm{N}}({}^{A}_{Z}X) + Z m_e - B_e(Z), \tag{16.4}$$

$$ m_{\mathrm{atom}}({}^{A-4}_{Z-2}Y) = m_{\mathrm{N}}({}^{A-4}_{Z-2}Y) + (Z-2) m_e - B_e(Z-2), \tag{16.5}$$

$$ m_{\mathrm{atom}}({}^{4}\mathrm{He}) = m_{\mathrm{N}}({}^{4}\mathrm{He}) + 2 m_e - B_e(2). \tag{16.6}$$

Subtract Eq. (16.5) and Eq. (16.6) from Eq. (16.4):

$$\begin{aligned} m_{\mathrm{atom}}({}^{A}_{Z}X) - m_{\mathrm{atom}}({}^{A-4}_{Z-2}Y) - m_{\mathrm{atom}}({}^{4}\mathrm{He}) \\ = \Big[m_{\mathrm{N}}({}^{A}_{Z}X) - m_{\mathrm{N}}({}^{A-4}_{Z-2}Y) - m_{\mathrm{N}}({}^{4}\mathrm{He})\Big] \\ + \underbrace{\big[Zm_e - (Z-2)m_e - 2m_e\big]}_{=0} \\ - \big[B_e(Z) - B_e(Z-2) - B_e(2)\big]. \end{aligned} \tag{16.7}$$

The electron-mass term vanishes identically because the parent atom has Z electrons, the daughter has $Z-2$, and the helium atom has 2, so $Z = (Z-2)+2$. The remaining electronic binding-energy difference is of order 10 keV and is neglected in nuclear energetics [1, 6]. Therefore

$$Q \approx \Big[m_{\mathrm{atom}}({}^{A}_{Z}X) - m_{\mathrm{atom}}({}^{A-4}_{Z-2}Y) - m_{\mathrm{atom}}({}^{4}\mathrm{He})\Big]c^2. \tag{16.8}$$

Caution

In Eq. (16.8), $m_{\mathrm{atom}}({}^{4}\mathrm{He})$ is the mass of a *neutral helium atom*, not the mass of the bare α particle. Using the wrong mass tabulation entry is a common source of error of several MeV.

16.3.3 Q from binding energies

The binding energy of a nucleus is defined by $m_{\mathrm{N}}c^2 = Zm_pc^2 + Nm_nc^2 - B$. For the decay (16.1), the mass difference can be rewritten entirely in terms of binding energies:

$$\begin{aligned} Q &= \Big[m_{\mathrm{N}}(X) - m_{\mathrm{N}}(Y) - m_{\mathrm{N}}(\alpha)\Big]c^2 \\ &= \Big[(Zm_p + Nm_n - B_X) - \big((Z-2)m_p + (N-2)m_n - B_Y\big) - \big(2m_p + 2m_n - B_\alpha\big)\Big]c^2. \end{aligned} \tag{16.9}$$

The nucleon mass terms cancel because $A = (A-4)+4$ and $Z = (Z-2)+2$:

$$Q = B_Y + B_\alpha - B_X. \tag{16.10}$$

Thus α decay is exothermic when the combined binding of the daughter plus the α exceeds the binding of the parent.

Numerical value of B_α

Evaluated data give $B_\alpha = B({}^{4}\mathrm{He}) \approx 28.296\,\mathrm{MeV}$ [20, 21, 1]. This value should be taken from experiment: the SEMF significantly underbinds the doubly magic ^{4}He and must not be used for B_α.

16.3.4 SEMF estimates and the $A \sim 150$ puzzle

Parent and daughter binding energies can be estimated with the semi-empirical mass formula (pairing term δ often omitted for a first trend):

$$B = a_v A - a_s A^{2/3} - a_c \frac{Z(Z-1)}{A^{1/3}} - a_{\mathrm{sym}} \frac{(N-Z)^2}{A} + \delta. \tag{16.11}$$

Along the β-stable line for fixed A, the atomic number is approximately

$$Z \approx \frac{A/2}{1 + 0.0078\, A^{2/3}}. \tag{16.12}$$

Inserting Eqs. (16.11) and (16.12) into Eq. (16.10) with $B_\alpha = 28.3\,\mathrm{MeV}$ gives $Q_\alpha > 0$ for $A \gtrsim 145$–150.

Yet the chart shows many stable or long-lived nuclides up to $A \sim 209$ (^{208}Pb is the heaviest stable nucleus). Only beyond $A \approx 210$ does one find no stable species at all. Two complementary explanations resolve the apparent contradiction:

(i) **Shell and pairing effects.** The SEMF is a smooth average. Individual nuclides can have Q_α shifted by several MeV by shell closures (notably $N = 126$) and odd-even pairing, so some isotopes with SEMF $Q > 0$ are actually sub-threshold or have very small Q [6, 1].

(ii) $Q > 0$ **is necessary but not sufficient.** Even when $Q_\alpha > 0$, the half-life depends exponentially on Q through Coulomb-barrier tunneling (Lecture 17). For $Q \lesssim 4\,\mathrm{MeV}$, lifetimes can exceed $10^{17}\,\mathrm{s}$ and the decay is effectively unobservable in ordinary laboratory times [1, 6]. A nucleus can therefore have positive α decay energy yet appear stable on human timescales.

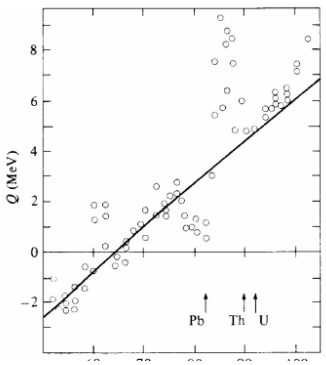

Figure 16.2: Experimental α-decay Q-values (circles) versus proton number Z, compared with the SEMF estimate (solid line). Multiple circles at the same Z correspond to different neutron numbers. Adapted from Cottingham and Greenwood [23]; axes restored from the original PH5001 source page.

Figure 16.2 shows that Q becomes positive for heavy Z near the actinides, with scatter at fixed Z from different N. Adding neutrons to a heavy isotope generally lowers Q_α and lengthens the half-life.

16.4 Kinematics: sharing of Q between α and daughter

The Q-value is the total kinetic energy released. If the parent nucleus is initially at rest, momentum conservation requires the daughter and α to recoil in opposite directions with equal magnitude of linear momentum.

Step 1: Momentum conservation.

$$\boldsymbol{p}_d + \boldsymbol{p}_\alpha = 0 \quad \Rightarrow \quad |\boldsymbol{p}_d| = |\boldsymbol{p}_\alpha| = p. \tag{16.13}$$

Step 2: Kinetic energies in terms of p.

$$K_d = \frac{p^2}{2M_d}, \qquad K_\alpha = \frac{p^2}{2M_\alpha}, \tag{16.14}$$

where M_d and M_α are the nuclear masses of the daughter and the α particle.

Step 3: Energy conservation.

$$K_d + K_\alpha = Q. \tag{16.15}$$

Step 4: Eliminate p. Substitute the kinetic-energy expressions:

$$\frac{p^2}{2M_d} + \frac{p^2}{2M_\alpha} = Q. \tag{16.16}$$

Factor out $p^2/2$:

$$\frac{p^2}{2}\left(\frac{1}{M_d} + \frac{1}{M_\alpha}\right) = Q. \tag{16.17}$$

Combine the fractions:

$$\frac{1}{M_d} + \frac{1}{M_\alpha} = \frac{M_d + M_\alpha}{M_d M_\alpha}. \tag{16.18}$$

Hence

$$p^2 = \frac{2QM_dM_\alpha}{M_d + M_\alpha}. \tag{16.19}$$

Step 5: Solve for K_α and K_d.

$$K_\alpha = \frac{p^2}{2M_\alpha} = \frac{2QM_dM_\alpha}{M_d + M_\alpha} \cdot \frac{1}{2M_\alpha} = Q\,\frac{M_d}{M_d + M_\alpha}. \tag{16.20}$$

Similarly,

$$K_d = Q\,\frac{M_\alpha}{M_d + M_\alpha}. \tag{16.21}$$

Step 6: Approximate for heavy nuclei. For $A \gg 4$, $M_d \approx (A-4)u$ and $M_\alpha \approx 4u$, so $M_d + M_\alpha \approx Au$. Therefore

$$K_\alpha \approx Q\left(1 - \frac{4}{A}\right), \qquad K_d \approx Q\,\frac{4}{A}. \tag{16.22}$$

For $A = 200$, $K_\alpha/Q = 1 - 4/200 = 0.98$: about 98% of the energy is carried by the α particle and about 2% by the recoiling daughter [6, 1]. Detectors measure K_α; from it one reconstructs $Q = K_\alpha(M_d + M_\alpha)/M_d$.

Remark

The recoiling daughter ($\sim 100\,\text{keV}$ for $Q \sim 5\,\text{MeV}$) has enough energy to break chemical bonds, so α sources must be thin coatings if one wishes to avoid recoil losses from the active layer [6].

16.5 Exponential decay law, activity, mean life, and half-life

Radioactive decay is a Poisson process: for a single nucleus that has not yet decayed at time t, the probability to decay in the next interval $\mathrm{d}t$ is $\lambda\,\mathrm{d}t$, where λ is the decay constant (probability per unit time).

Step 1: Differential equation for $N(t)$. For a large sample, the rate of change of the number of undecayed nuclei is proportional to the number present:

$$\frac{\mathrm{d}N}{\mathrm{d}t} = -\lambda N(t). \tag{16.23}$$

Step 2: Solve the equation. Separate variables and integrate from $t = 0$ (when $N = N_0$):

$$\int_{N_0}^{N(t)} \frac{\mathrm{d}N}{N} = -\lambda \int_0^t \mathrm{d}t \quad \Rightarrow \quad \ln\frac{N(t)}{N_0} = -\lambda t \quad \Rightarrow \quad N(t) = N_0\, e^{-\lambda t}. \tag{16.24}$$

Step 3: Mean life. The mean (average) lifetime of a nucleus in the sample is

$$\tau = \int_0^\infty t\,\lambda e^{-\lambda t}\,\mathrm{d}t = \frac{1}{\lambda}. \tag{16.25}$$

(One integration by parts gives $\tau = 1/\lambda$.)

Step 4: Half-life. The half-life $t_{1/2}$ is defined by $N(t_{1/2}) = N_0/2$:

$$\frac{N_0}{2} = N_0\, e^{-\lambda t_{1/2}} \quad \Rightarrow \quad e^{-\lambda t_{1/2}} = \frac{1}{2} \quad \Rightarrow \quad \lambda t_{1/2} = \ln 2. \tag{16.26}$$

Therefore

$$t_{1/2} = \frac{\ln 2}{\lambda} = \frac{0.693}{\lambda}, \qquad \tau = \frac{t_{1/2}}{\ln 2} \approx 1.443\, t_{1/2}. \tag{16.27}$$

Step 5: Activity. The activity (decay rate) is

$$\mathcal{A}(t) = -\frac{\mathrm{d}N}{\mathrm{d}t} = \lambda N(t) = \lambda N_0\, e^{-\lambda t}. \tag{16.28}$$

Activity also falls by a factor of two in one half-life. In SI units, $\mathcal{A}$ is measured in becquerels (Bq = decays per second); the curie ($1\,\text{Ci} = 3.7 \times 10^{10}\,\text{Bq}$) remains common in nuclear medicine [13, 6].

Key idea

Two laboratory observables characterise α decay: Q (from K_α and kinematics) and $t_{1/2}$ (from the time dependence of activity). They are related by the Geiger–Nuttall rule, explained by Gamow tunneling in Lecture 17.

16.6 Geiger–Nuttall rule

In 1911, Geiger and Nuttall discovered empirically that α emitters with large disintegration energy have short half-lives, and conversely [6, 2]. For known α emitters, Q spans roughly 4–9.5 MeV while $t_{1/2}$ spans from microseconds to $\sim 10^9$ years. The empirical relation is

$$\log_{10}(t_{1/2}/\mathrm{s}) = a\,Q^{-1/2} + b, \tag{16.29}$$

where a and b depend primarily on Z. Different isotopic chains (e.g. thorium, uranium) form parallel lines on the plot.

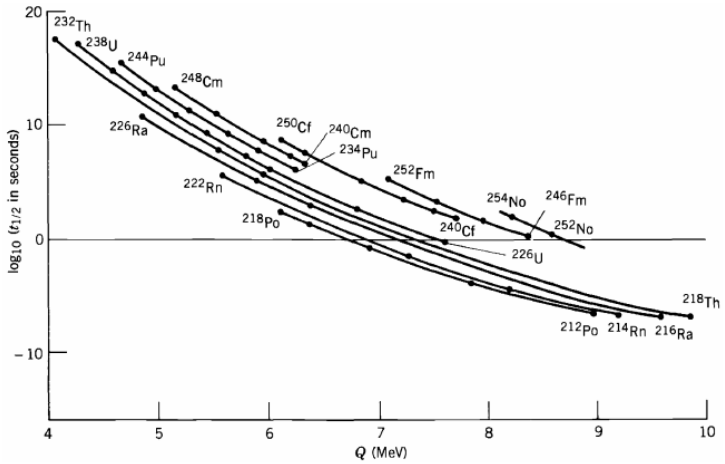

Figure 16.3: Geiger–Nuttall systematics: $\log_{10}(t_{1/2}/\mathrm{s})$ versus α-decay energy Q (MeV). Even–even nuclei form smooth curves for fixed Z [24, 6]. Axes restored from the original PH5001 source page.

Even–even versus odd-A nuclei. When all α emitters are plotted together, there is scatter about the average trend. Restricting to fixed Z and even–even (Z, N) yields smooth curves. Odd-A and odd–odd nuclei follow the same inverse trend but lie *above* the even–even lines: their half-lives are longer by factors of 2 to 10^3 at comparable Q [6]. The prominent example is ^{235}U (even Z, odd N): its long half-life ($t_{1/2} \approx 7 \times 10^8$ y) allows natural uranium to persist and thermal-neutron fission reactors to operate.

Orders of magnitude. ^{232}Th ($Q \approx 4.08$ MeV, $t_{1/2} \approx 1.4 \times 10^{10}$ y) and ^{218}Th ($Q \approx 9.85$ MeV, $t_{1/2} \approx 10^{-7}$ s) illustrate that a factor of about 2 in Q corresponds to roughly 10^{24} in $t_{1/2}$ [1, 6]. This extreme sensitivity is the central puzzle solved by Gamow's tunneling theory.

16.7 Toward Gamow's theory: preformation and the potential

Historical note: Gamow, Gurney, and Condon (1928)

George Gamow (1904–1968), together with Gurney and Condon, explained Geiger–Nuttall systematics by quantum tunneling of a preformed α through the Coulomb barrier [25, 26, 6, 14, 2]. The success of the one-body model does not prove that α clusters exist permanently inside heavy nuclei; it shows that decay rates behave *as if* an α were preformed at the nuclear surface.

In the Gamow model one assumes that two protons and two neutrons are already correlated as an α cluster inside the parent nucleus. The cluster moves in a potential energy $V(r)$ due to the residual nucleus, where r is the distance between their centres:

- **Nuclear well ($r < R$).** The strong force dominates. The potential is approximated by a square well of depth $V_0 \sim 30$–$40\,\mathrm{MeV}$. The Coulomb repulsion is small inside the nuclear volume and is neglected in this first approximation.
- **Coulomb barrier ($r > R$).** The nuclear force has short range; outside the surface the repulsive Coulomb potential remains:

$$V_{\mathrm{C}}(r) = \frac{(Z-2)\cdot 2e^2}{4\pi\varepsilon_0\, r} = \frac{Z_1 Z_2 e^2}{4\pi\varepsilon_0\, r}, \tag{16.30}$$

  with $Z_1 = Z - 2$ (charge of the daughter) and $Z_2 = 2$ (charge of the α).

For $\ell = 0$ the centrifugal term vanishes; $\ell \neq 0$ adds $\hbar^2\ell(\ell+1)/(2\mu r^2)$ to the barrier (Lecture 17).

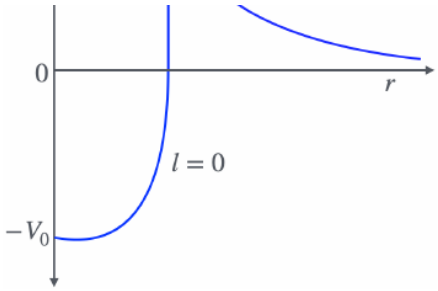

Figure 16.4: Nuclear square well joined to the Coulomb barrier $V_{\mathrm{C}}(r)$ for $\ell = 0$. The horizontal line marks the available energy $E = Q$. The classically forbidden region lies between the inner radius R and the outer turning point b where $V_{\mathrm{C}}(b) = Q$. Re-extracted from the original PH5001 lecture source pages.

Barrier height: numerical example. The Coulomb barrier height is the value of V_{C} at the effective contact distance. For $Z = 72$ and $A \approx 216$, the daughter radius is

$$R_d \approx 1.25\, A^{1/3}\,\mathrm{fm} \approx 1.25 \times 216^{1/3}\,\mathrm{fm} \approx 1.25 \times 6\,\mathrm{fm} \approx 7.5\,\mathrm{fm}. \tag{16.31}$$

Including the α-particle radius $R_\alpha \approx 1.5\,\mathrm{fm}$, the centre-to-centre distance at contact is

$$R \approx R_d + R_\alpha \approx 9\,\mathrm{fm}. \tag{16.32}$$

At this separation,

$$V_{\mathrm{C}} \approx \frac{2 \times (Z-2) \times e^2/(4\pi\varepsilon_0)}{R} \approx \frac{2 \times 70 \times 1.44\,\mathrm{MeV\,fm}}{9\,\mathrm{fm}} \approx 22.4\,\mathrm{MeV}. \tag{16.33}$$

Typical α-decay Q values are only 4–9 MeV, so $Q \ll V_{\mathrm{C}}(R)$: classically the α cannot escape. Quantum mechanics permits tunneling through the barrier between R and b; the calculation of the penetration probability is the subject of Lecture 17.

Takeaway

α decay in heavy nuclei is favoured by large B_α and Coulomb energy considerations ($Q > 0$ from roughly $A \sim 150$ onward in the SEMF). Observed stability up to $A \sim 209$ requires tunneling: $Q > 0$ is necessary but not sufficient. The Geiger–Nuttall correlation and the potential-barrier picture set the stage for the Gamow factor derived in the next chapter.

16.8 Further physics from the literature

Even–even systematics and hindrance. Krane emphasises that Geiger–Nuttall plots restricted to fixed Z and even–even (Z, N) form smooth curves, while odd-A and odd–odd nuclei lie systematically above those curves (longer lifetimes at the same Q) [6]. The deviation is quantified by the *hindrance factor* $F = \lambda_{\mathrm{theory}}/\lambda_{\mathrm{exp}}$: values near unity indicate a normal Gamow transition; $F \gg 1$ signals poor parent-daughter overlap or selection-rule suppression.

Neutron number and shell effects. Adding neutrons to a heavy isotope generally lowers Q_α and lengthens $t_{1/2}$. A pronounced discontinuity near $N = 126$ appears in $Q(A)$ plots because the daughter from α emission often sits near that closed neutron shell [6, 1]. The SEMF captures the average trend but not these local kinks; evaluated masses from [20, 21] are required for quantitative work.

Competition with other channels. For very heavy nuclei, spontaneous fission competes with α decay; the dominant mode depends on Z, A, and shell structure. Cluster radioactivity (^{14}C, ^{24}Ne, and heavier ejectiles) and proton radioactivity near the proton drip line are rare variants of the same barrier penetration physics with different charge, mass, and preformation factors [6, 1, 14].

Historical context. Rutherford's 1911 interpretation of Geiger–Marsden scattering established the nuclear atom; the same α particles from natural sources later provided discrete energy spectra that confirmed energy quantisation in nuclear decays [2, 14]. Modern silicon detectors resolve α groups to keV precision, enabling branching-ratio studies (Lecture 17).

Reading guide

Krane [6] Ch. 8 (systematics and potential model); Dunlap [1] Ch. 8 (energetics and atomic-mass conventions); Basdevant [14] Sect. 2.6 (Gamow model overview); Demtröder [2] Sect. 3.3 (historical Geiger–Nuttall plot and kinematics).

16.9 Problems with solutions

Problem 16.1 — K_α fraction for $A = 220$

For α decay of a nucleus with $A = 220$, estimate the fraction of Q carried by the α particle using Eq. (16.22).

Solution 16.1

Step 1. Write the kinematic ratio from momentum conservation:

$$\frac{K_\alpha}{Q} = \frac{M_d}{M_d + M_\alpha}.$$

Step 2. Approximate masses by nucleon count: $M_d \approx (A-4)u$ and $M_\alpha \approx 4u$, so $M_d + M_\alpha \approx Au$.

Step 3. Substitute $A = 220$:

$$\frac{K_\alpha}{Q} \approx 1 - \frac{4}{A} = 1 - \frac{4}{220} = 1 - 0.01818 = 0.982.$$

The α particle carries about 98.2% of Q; the daughter recoil is about 1.8% [6, 1].

Problem 16.2 — Half-life and mean life from λ

A sample has decay constant $\lambda = 1.0 \times 10^{-6}\,\mathrm{s}^{-1}$. Find (a) the half-life $t_{1/2}$ in days, and (b) the mean life τ.

Solution 16.2

Step 1 (half-life). From Eq. (16.27):

$$t_{1/2} = \frac{\ln 2}{\lambda} = \frac{0.693}{1.0 \times 10^{-6}\,\mathrm{s}^{-1}} = 6.93 \times 10^{5}\,\mathrm{s}.$$

Step 2 (convert to days).

$$t_{1/2} = \frac{6.93 \times 10^{5}}{86400\,\mathrm{s/day}} \approx 8.0\,\mathrm{days}.$$

Step 3 (mean life).

$$\tau = \frac{1}{\lambda} = \frac{1}{1.0 \times 10^{-6}} = 1.0 \times 10^{6}\,\mathrm{s} \approx 11.6\,\mathrm{days}.$$

Note $\tau = t_{1/2}/\ln 2 \approx 1.443\, t_{1/2}$.

Problem 16.3 — Activity decay over three half-lives

At $t = 0$ a source has activity $\mathcal{A}_0 = 3.7 \times 10^{4}\,\mathrm{Bq}$ (1 mCi). What is the activity after $3\,t_{1/2}$?

Solution 16.3

Step 1. Activity follows Eq. (16.28): $\mathcal{A}(t) = \mathcal{A}_0\, e^{-\lambda t}$.

Step 2. After one half-life, $\mathcal{A}$ falls by a factor of 2. After three half-lives:

$$\mathcal{A}(3t_{1/2}) = \frac{\mathcal{A}_0}{2^3} = \frac{\mathcal{A}_0}{8}.$$

Step 3. Numerical value:

$$\mathcal{A}(3t_{1/2}) = \frac{3.7 \times 10^4}{8} = 4.6 \times 10^3\,\text{Bq}.$$

Problem 16.4 — Coulomb barrier height for $Z = 92$

Estimate the Coulomb barrier height for α decay of ^{238}U ($Z = 92$, $A = 238$) using $R_d = 1.25A^{1/3}$ fm and $R_\alpha = 1.5$ fm. Compare with typical $Q \approx 4.3$ MeV.

Solution 16.4

Step 1 (daughter radius).

$$R_d = 1.25 \times 238^{1/3}\,\text{fm} \approx 1.25 \times 6.20\,\text{fm} \approx 7.75\,\text{fm}.$$

Step 2 (contact distance).

$$R = R_d + R_\alpha \approx 7.75 + 1.5 = 9.25\,\text{fm}.$$

Step 3 (barrier height). With $Z_1 = Z - 2 = 90$:

$$V_C(R) = \frac{2 \times 90 \times 1.44\,\text{MeV fm}}{9.25\,\text{fm}} \approx 28\,\text{MeV}.$$

Step 4 (comparison). $Q \approx 4.3\,\text{MeV} \ll 28\,\text{MeV}$, so the decay proceeds only by quantum tunneling. The ratio $Q/V_C \sim 0.15$ explains the enormous half-life ($\sim 4.5 \times 10^9$ y) [6, 20].

Problem 16.5 — Geiger–Nuttall estimate

Two even–even isotopes of the same element have α energies $Q_1 = 5.0$ MeV and $Q_2 = 6.0$ MeV. If the first has $t_{1/2}^{(1)} = 10^6$ s, estimate $t_{1/2}^{(2)}$ using $\log_{10} t_{1/2} = aQ^{-1/2} + b$ with the same a, b.

Solution 16.5

Step 1. Subtract the two Geiger–Nuttall equations:

$$\log_{10} t_{1/2}^{(2)} - \log_{10} t_{1/2}^{(1)} = a\left(Q_2^{-1/2} - Q_1^{-1/2}\right).$$

Step 2. For a rough estimate, use the typical slope from Krane's plots: $a \approx -1.4\,\mathrm{MeV}^{1/2}$ (magnitude depends on Z).

$$Q_2^{-1/2} - Q_1^{-1/2} = \frac{1}{\sqrt{6.0}} - \frac{1}{\sqrt{5.0}} = 0.4082 - 0.4472 = -0.039.$$

$$\log_{10} \frac{t_{1/2}^{(2)}}{t_{1/2}^{(1)}} \approx (-1.4) \times (-0.039) \approx 0.055.$$

Step 3.

$$t_{1/2}^{(2)} \approx 10^6 \times 10^{0.055} \approx 1.1 \times 10^6\,\mathrm{s}.$$

A 20% increase in Q shortens the half-life modestly on a log scale; over larger Q intervals the effect becomes enormous ($\sim 10^{24}$ for a factor of 2 in Q over the full actinide range) [6, 1].

Chapter 17

Alpha Decay: Tunneling and the Gamow Factor

> *"The central feature of this one-body model is that the α particle is preformed inside the parent nucleus… the theory works quite well, especially for even–even nuclei."*
> K. S. Krane [6]

Lecture 16 established the observables Q and $t_{1/2}$, the Geiger–Nuttall correlation, and the nuclear-well plus Coulomb-barrier potential. This chapter derives the Gamow tunneling factor in full: rectangular-barrier warm-up with the *reduced mass* μ, the Coulomb-barrier integral evaluated without skipped steps, the assault frequency, the decay rate $\lambda = S_\alpha\, f\, P$, and the fine structure of α spectra from angular-momentum and parity selection rules [6, 1, 14, 2].

17.1 Classically forbidden region

The available energy $E = Q$ of an emitted α particle is typically 4–9 MeV, much less than the Coulomb barrier height $B \sim 20$–$30\,\mathrm{MeV}$ at the nuclear surface. Three regions of the radial potential are distinguished (Fig. 17.1):

(i) **Well ($r < R$).** The α moves inside the attractive nuclear potential (depth $V_0 \sim 35\,\mathrm{MeV}$) with kinetic energy approximately $Q + V_0$.

(ii) **Barrier ($R < r < b$).** The Coulomb potential exceeds the total energy Q. Classically the particle cannot enter this region: its kinetic energy would have to be negative.

(iii) **Asymptotic ($r > b$).** The Coulomb potential falls below Q; the α escapes with kinetic energy Q.

The outer *classical turning point* b is defined by

$$V_{\mathrm{C}}(b) = Q, \qquad b = \frac{Z_1 Z_2 e^2}{4\pi\varepsilon_0\, Q}, \tag{17.1}$$

with $Z_1 = Z - 2$ (daughter charge) and $Z_2 = 2$ (α charge).

Quantum mechanics permits a non-zero probability for the α to traverse the classically forbidden interval $R \le r \le b$. Dunlap expresses the lifetime as $\tau = \tau_0 / P$, where P is the escape

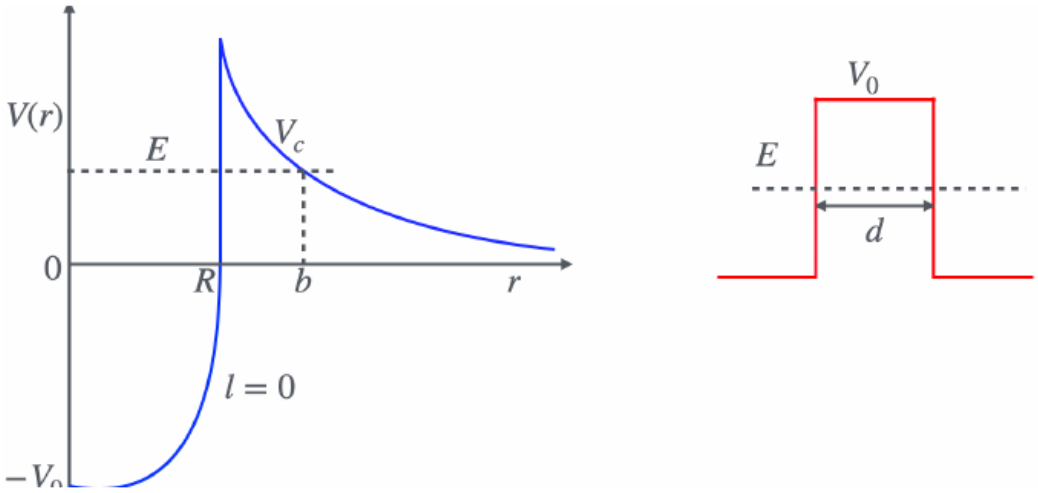

Figure 17.1: Left: nuclear well plus Coulomb barrier with total energy $E = Q$, inner radius R, and outer turning point b. Right: rectangular barrier of height V_0 and width d used as a warm-up for tunneling theory. Re-extracted from the original PH5001 lecture source pages.

probability and τ_0 is a formation time scale; the course uses the equivalent form $\lambda = S_\alpha\, f\, P$ with assault frequency f and preformation factor S_α [1, 6].

17.2 Rectangular barrier and the reduced mass

For a one-dimensional rectangular barrier of height $V_0 > E$ and width d, the Schrödinger equation in the forbidden region gives an evanescent wavefunction $\psi \propto e^{-\gamma r}$ with

$$\gamma = \frac{\sqrt{2\mu(V_0 - E)}}{\hbar}, \tag{17.2}$$

where μ is the *reduced mass* of the α-daughter system:

$$\mu = \frac{m_\alpha\, M_d}{m_\alpha + M_d}. \tag{17.3}$$

For heavy nuclei $M_d \gg m_\alpha$, so $\mu \approx m_\alpha$ to good approximation, but all barrier formulas must be written with μ for consistency with the two-body Coulomb problem [1].

Matching the wavefunction and its derivative at the barrier boundaries yields the standard WKB result for the transmission probability:

$$P \approx e^{-2\gamma d} = \exp\!\left[-\frac{2d}{\hbar}\sqrt{2\mu(V_0 - E)}\right]. \tag{17.4}$$

The factor $(V_0 - E)$ is the amount by which the potential exceeds the particle energy inside the barrier.

17.3 Coulomb barrier and the Gamow integral

For a non-rectangular barrier, one divides the interval into slices of width $\mathrm{d}r$ and multiplies the elementary penetration factors. This WKB approximation gives

$$P \approx \exp\left[-2\int_R^b \gamma(r)\,\mathrm{d}r\right] = e^{-2G}, \tag{17.5}$$

where

$$\gamma(r) = \frac{\sqrt{2\mu[V(r)-Q]}}{\hbar}, \qquad G = \int_R^b \gamma(r)\,\mathrm{d}r. \tag{17.6}$$

Coulomb potential measured from the turning point. It is convenient to write the Coulomb potential for $R \le r \le b$ as

$$V(r) = \frac{Z_1 Z_2 e^2}{4\pi\varepsilon_0}\left(\frac{1}{r} - \frac{1}{b}\right), \tag{17.7}$$

so that $V(b) = 0$ and $V(r) - Q = V(r)$ in the forbidden region (since $Q = Z_1 Z_2 e^2/(4\pi\varepsilon_0 b)$). Substituting into Eq. (17.6):

$$G = \frac{\sqrt{2\mu}}{\hbar}\sqrt{\frac{Z_1 Z_2 e^2}{4\pi\varepsilon_0}}\int_R^b \sqrt{\frac{1}{r} - \frac{1}{b}}\,\mathrm{d}r. \tag{17.8}$$

17.4 Evaluating the integral: every step

Define

$$I = \int_R^b \sqrt{\frac{1}{r} - \frac{1}{b}}\,\mathrm{d}r = \int_R^b \sqrt{\frac{b-r}{br}}\,\mathrm{d}r. \tag{17.9}$$

Step 1: Trigonometric substitution. Set

$$r = b\sin^2\theta. \tag{17.10}$$

Differentiate:

$$\mathrm{d}r = 2b\sin\theta\cos\theta\,\mathrm{d}\theta. \tag{17.11}$$

Express $1/r$:

$$\frac{1}{r} = \frac{1}{b\sin^2\theta}. \tag{17.12}$$

Form the combination under the square root:

$$\frac{1}{r} - \frac{1}{b} = \frac{1}{b\sin^2\theta} - \frac{1}{b} = \frac{1-\sin^2\theta}{b\sin^2\theta} = \frac{\cos^2\theta}{b\sin^2\theta}. \tag{17.13}$$

Take the square root (positive in the interval of interest):

$$\sqrt{\frac{1}{r} - \frac{1}{b}} = \sqrt{\frac{\cos^2\theta}{b\sin^2\theta}} = \frac{\cos\theta}{\sqrt{b}\,\sin\theta} = \frac{\cot\theta}{\sqrt{b}}. \tag{17.14}$$

Step 2: Rewrite the integral in θ.

$$I = \int \frac{\cot\theta}{\sqrt{b}} \cdot 2b \sin\theta \cos\theta \, \mathrm{d}\theta. \tag{17.15}$$

Simplify the integrand:

$$\frac{\cot\theta}{\sqrt{b}} \cdot 2b \sin\theta \cos\theta = \frac{\cos\theta}{\sin\theta\sqrt{b}} \cdot 2b \sin\theta \cos\theta = \frac{2b\cos^2\theta}{\sqrt{b}} = 2\sqrt{b}\cos^2\theta. \tag{17.16}$$

Hence

$$I = 2\sqrt{b} \int \cos^2\theta \, \mathrm{d}\theta. \tag{17.17}$$

Step 3: Integrate $\cos^2\theta$. Use $\cos^2\theta = \frac{1}{2}(1+\cos 2\theta)$:

$$I = 2\sqrt{b} \int \frac{1+\cos 2\theta}{2} \, \mathrm{d}\theta = \sqrt{b} \int (1+\cos 2\theta) \, \mathrm{d}\theta = \sqrt{b}\left(\theta + \frac{\sin 2\theta}{2}\right). \tag{17.18}$$

Step 4: Limits of integration. When $r = R$:

$$\sin^2\theta_R = \frac{R}{b} \quad \Rightarrow \quad \theta_R = \arcsin\sqrt{\frac{R}{b}}. \tag{17.19}$$

When $r = b$:

$$\sin^2\theta_b = 1 \quad \Rightarrow \quad \theta_b = \frac{\pi}{2}. \tag{17.20}$$

Step 5: Evaluate at the limits.

$$I = \sqrt{b}\left[\frac{\pi}{2} + \frac{\sin\pi}{2}\right] - \sqrt{b}\left[\arcsin\sqrt{\frac{R}{b}} + \frac{\sin(2\theta_R)}{2}\right]. \tag{17.21}$$

Since $\sin\pi = 0$:

$$I = \sqrt{b}\left[\frac{\pi}{2} - \arcsin\sqrt{\frac{R}{b}} - \frac{\sin(2\theta_R)}{2}\right]. \tag{17.22}$$

Step 6: Simplify $\sin(2\theta_R)$. Use $\sin(2\theta_R) = 2\sin\theta_R\cos\theta_R$ with $\sin\theta_R = \sqrt{R/b}$ and $\cos\theta_R = \sqrt{1-R/b}$:

$$\sin(2\theta_R) = 2\sqrt{\frac{R}{b}}\sqrt{1-\frac{R}{b}} = 2\sqrt{\frac{R}{b}\left(1-\frac{R}{b}\right)}. \tag{17.23}$$

Therefore

$$\frac{\sin(2\theta_R)}{2} = \sqrt{\frac{R}{b}\left(1-\frac{R}{b}\right)}. \tag{17.24}$$

Step 7: Use $\arccos$ form. Since $\arccos x + \arcsin x = \pi/2$,

$$\frac{\pi}{2} - \arcsin\sqrt{\frac{R}{b}} = \arccos\sqrt{\frac{R}{b}}. \tag{17.25}$$

The final result is

$$I = \sqrt{b}\left[\arccos\sqrt{\frac{R}{b}} - \sqrt{\frac{R}{b}\left(1-\frac{R}{b}\right)}\right]. \tag{17.26}$$

Step 8: Assemble G and P. Substituting Eq. (17.26) into Eq. (17.8):

$$G = \frac{\sqrt{2\mu}\,Z_1 Z_2 e^2}{4\pi\varepsilon_0\,\hbar}\sqrt{\frac{b}{Q}}\left[\arccos\sqrt{\frac{R}{b}} - \sqrt{\frac{R}{b}\left(1-\frac{R}{b}\right)}\right], \tag{17.27}$$

where we used $Q = Z_1 Z_2 e^2/(4\pi\varepsilon_0 b)$ to write $\sqrt{Z_1 Z_2 e^2/(4\pi\varepsilon_0)} = \sqrt{Qb}$. The tunneling probability is

$$P = e^{-2G}. \tag{17.28}$$

17.5 Barrier height B and the small Q/B limit

The Coulomb barrier height at $r = R$ is

$$B = \frac{Z_1 Z_2 e^2}{4\pi\varepsilon_0\,R}, \qquad \frac{R}{b} = \frac{Q}{B}. \tag{17.29}$$

In terms of B and Q, Eq. (17.27) becomes

$$G = \frac{Z_1 Z_2 e^2}{4\pi\varepsilon_0\,\hbar}\sqrt{\frac{2\mu}{Q}}\left[\arccos\sqrt{\frac{Q}{B}} - \sqrt{\frac{Q}{B}\left(1-\frac{Q}{B}\right)}\right]. \tag{17.30}$$

Small Q/B expansion. For typical α decays, $Q/B \sim 0.1$–0.2. Expand for $Q/B \ll 1$:

$$\arccos\sqrt{\frac{Q}{B}} \approx \frac{\pi}{2} - \sqrt{\frac{Q}{B}}, \qquad \sqrt{\frac{Q}{B}\left(1-\frac{Q}{B}\right)} \approx \sqrt{\frac{Q}{B}}. \tag{17.31}$$

The bracket becomes $\pi/2 - 2\sqrt{Q/B}$. Keeping the leading term $\pi/2$ and using $Q = \tfrac{1}{2}\mu v^2$ for the asymptotic α speed v:

$$G \approx \frac{\pi Z_1 Z_2 e^2}{4\pi\varepsilon_0\,\hbar v} = \frac{Z_1 Z_2 e^2}{4\varepsilon_0\,\hbar v}, \qquad v = \sqrt{\frac{2Q}{\mu}}. \tag{17.32}$$

Thus $P \sim \exp(-2G)$ depends exponentially on $1/v \propto Q^{-1/2}$, which is the Geiger–Nuttall rule [6, 1, 14].

Key idea

Because $P \sim \exp(-c/\sqrt{Q})$, a small increase in Q reduces G and multiplies the decay rate by many orders of magnitude. The Geiger–Nuttall rule is a direct consequence of Coulomb-barrier tunneling.

17.6 Assault frequency, preformation, and $\lambda = S_\alpha f P$

The tunneling probability P is the escape probability *per attempt*. The α bounces inside the well, presenting itself at the barrier with characteristic frequency f. The decay constant is

$$\lambda = S_\alpha \, f \, P, \tag{17.33}$$

where S_α is the *preformation factor* (probability that nucleons are clustered as an α at the barrier surface). For normal even–even transitions $S_\alpha \approx 1$; suppressed transitions have $S_\alpha \ll 1$ and are called *hindered* [6].

Assault frequency. If the α travels back and forth across diameter $2R$ at interior speed v_0, the time for one round trip is $2R/v_0$, so

$$f = \frac{v_0}{2R}. \tag{17.34}$$

Inside the well the kinetic energy is $Q + V_0$ (where V_0 is the well depth, typically $\sim 35\,\text{MeV}$):

$$\frac{1}{2}\mu v_0^2 = Q + V_0 \quad \Rightarrow \quad v_0 = \sqrt{\frac{2(Q+V_0)}{\mu}}. \tag{17.35}$$

Hence

$$f = \frac{1}{2R}\sqrt{\frac{2(Q+V_0)}{\mu}} = \sqrt{\frac{Q+V_0}{2\mu R^2}}. \tag{17.36}$$

Combining with Eq. (17.28):

$$\lambda = S_\alpha \sqrt{\frac{Q+V_0}{2\mu R^2}}\, e^{-2G}, \qquad t_{1/2} = \frac{\ln 2}{\lambda}. \tag{17.37}$$

Caution

Absolute half-life calculations are extremely sensitive to the assumed radius: Krane notes that a 4% change in R can change calculated $t_{1/2}$ by a factor of about five. Measured lifetimes are therefore sometimes used to infer an effective sum of nuclear and α radii [6].

17.7 Fine structure, branching, and selection rules

When the daughter is left in an excited state, each branch has its own $Q_i = Q_{\text{gs}} - E_i^*$ and its own required orbital angular momentum ℓ carried by the α. The centrifugal barrier adds $\hbar^2\ell(\ell+1)/(2\mu r^2)$ to $V(r)$, raising G and suppressing high-ℓ branches [6, 1].

Selection rules. The α particle has intrinsic spin 0 and negative parity ($\pi_\alpha = -1$). Angular momentum and parity conservation require

$$\boldsymbol{J}_i = \boldsymbol{J}_f + \boldsymbol{\ell}, \qquad \pi_i = \pi_f \times (-1)^\ell. \tag{17.38}$$

Allowed ℓ values satisfy $|J_i - J_f| \le \ell \le J_i + J_f$ with the parity condition. In practice, the lowest allowed ℓ dominates because it minimises the barrier.

17.7.1 Even–even example: $^{244}\mathrm{Cm} \to {}^{240}\mathrm{Pu}$

Both parent and daughter ground states are 0^+. The daughter rotational band begins at 2^+ (43 keV), 4^+ (142 keV), 6^+ (296 keV) [20, 21]. Evaluated branching ratios from the LNHB/ENSDF database are approximately [20, 21, 28]:

Daughter state	E^* (keV)	ℓ	Branch (%)
0^+ (gs)	0	0	≈ 76.7
2^+	43	2	≈ 23.3
4^+	142	4	≈ 0.22
6^+	296	6	≈ 0.036

The ground-state branch ($\ell = 0$) dominates. The 2^+ branch is reduced because the centrifugal barrier raises the effective G by roughly 0.5 MeV and the smaller Q_i further increases G [6]. Higher members of the rotational band are strongly suppressed.

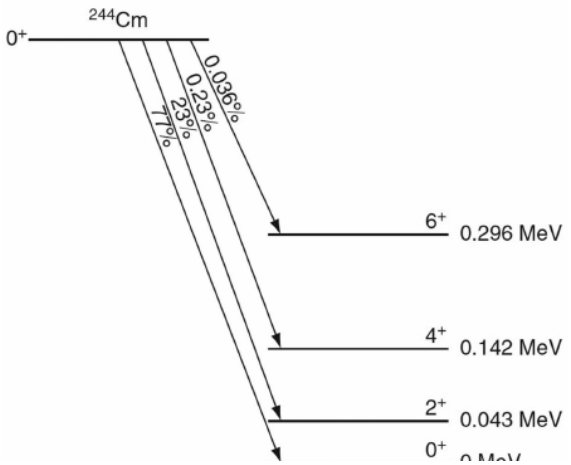

Figure 17.2: Branching ratios for α decay of ^{244}Cm to levels of ^{240}Pu. Re-extracted from the original PH5001 lecture source pages; branching fractions from evaluated data [20, 21, 28].

17.7.2 Odd-A example: $^{243}\mathrm{Am} \to {}^{239}\mathrm{Np}$

Remark

The original lecture slides incorrectly labelled this case as ^{249}Am. The correct parent is ^{243}Am ($J^\pi = \frac{5}{2}^-$), which α-decays to ^{239}Np ($J^\pi = \frac{5}{2}^+$ ground state) [20, 21, 6].

Ground-state branch. Parent $\frac{5}{2}^-$ to daughter $\frac{5}{2}^+$ requires a change of parity, so ℓ must be odd. The lowest allowed value is $\ell = 1$. The centrifugal barrier makes this branch highly hindered: evaluated data give a branching ratio of only $\approx 0.16\%$ [20, 21].

Dominant branch to $\frac{5}{2}^-$ at 75 keV. The daughter level at $E^* = 75\,\text{keV}$ has $J^\pi = \frac{5}{2}^-$, matching the parent parity. An $\ell = 0$ transition is therefore allowed. Although Q_i is reduced by 75 keV, the much thinner $\ell = 0$ barrier dominates, and this branch carries $\approx 88\%$ of the α intensity [20, 21, 6].

Other branches. The first excited state $\frac{7}{2}^+$ at low energy requires $\ell \geq 2$ (angular momentum change from $\frac{5}{2}$ to $\frac{7}{2}$ with parity match). Higher-ℓ branches are further suppressed. Figure 17.3 summarises the scheme.

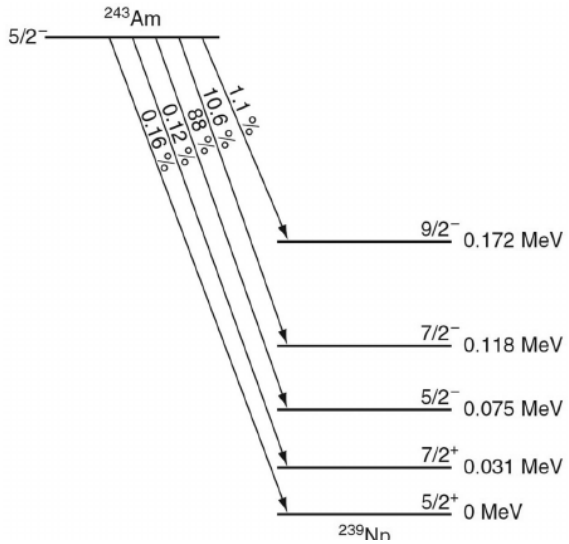

Figure 17.3: Branching ratios for α decay of ^{243}Am to levels of ^{239}Np. Re-extracted from the original PH5001 lecture source pages; isotope corrected from ^{249}Am to ^{243}Am [20, 21, 28].

Hindrance factors. The hindrance factor $F = \lambda_{\text{theory}}/\lambda_{\text{exp}}$ (or equivalently the ratio of predicted to observed branch intensity) quantifies deviations from the Gamow estimate. Large F indicates poor parent-daughter overlap or selection-rule suppression beyond the centrifugal barrier [6].

17.8 Why many nuclei with $Q > 0$ still appear stable

The SEMF gives $Q_\alpha > 0$ already near $A \sim 150$, yet many nuclides up to ^{208}Pb are stable or long-lived. If G is large, e^{-2G} is extraordinarily small and $t_{1/2}$ can exceed $10^{17}\,\text{s}$ ($\sim 10^{10}$ years). Only when Q rises into the actinide range do laboratory half-lives become short. This is precisely the Geiger–Nuttall message encoded in $P = e^{-2G}$: $Q > 0$ is necessary for spontaneous α decay, but the half-life is fixed by tunneling.

Takeaway

The Gamow theory explains (i) why $Q > 0$ does not imply short lifetimes, (ii) the Geiger–Nuttall $Q^{-1/2}$ correlation, and (iii) the fine structure of α spectra through ℓ-dependent barriers and selection rules. Use reduced mass μ throughout, and remember $\lambda = S_\alpha f P$.

17.9 Further physics from the literature

Radius sensitivity and effective sizes. Absolute Gamow half-lives depend exponentially on R through both G and f. Krane reports that a 4% change in the radius parameter can shift calculated $t_{1/2}$ by a factor of about five; practitioners sometimes invert the problem and infer an effective R-sum from measured lifetimes [6]. Deformed nuclei ($A \gtrsim 230$) further modify the barrier because the Coulomb potential is not spherically symmetric at the surface.

Preformation and cluster decay. The preformation factor S_α accounts for the probability that four nucleons are correlated as an α at the nuclear surface. Heavier cluster emissions (^{14}C, ^{24}Ne, and others) use the same $P = e^{-2G}$ framework but with larger reduced mass, higher Coulomb barrier, and vastly smaller S_α [6, 1, 14]. The first observed ^{14}C branch from ^{223}Ra had relative intensity $\sim 10^{-9}$ compared with α decay.

Proton radioactivity. Near the proton drip line, one-proton emission becomes the $Z_2 = 1$ analogue of Gamow theory when $Q_p > 0$. The same WKB integral applies with $Z_1 = Z - 1$, $Z_2 = 1$, and μ replaced by the proton-daughter reduced mass [6, 1].

Alignment experiments. When neither parent nor daughter has spin 0, several ℓ values may contribute to the same transition. Measuring the angular distribution of α particles relative to a spin-aligned source disentangles the ℓ-components; Krane Fig. 8.8 shows such an analysis for aligned ^{253}Es [6].

Reading guide

Krane [6] Sects. 8.4–8.6 (Gamow factor, fine structure, hindrance); Dunlap [1] Sect. 8.2 (WKB derivation with μ); Demtröder [2] Sect. 3.3 (historical context and Gamow peak notation); Basdevant [14] Sect. 2.6 (model and half-life systematics).

17.10 Problems with solutions

Problem 17.1 — Turning point b

For α decay with $Z_1 = 90$, $Z_2 = 2$, and $Q = 5.0\,\mathrm{MeV}$, calculate the classical turning point b. Use $e^2/(4\pi\varepsilon_0) = 1.44\,\mathrm{MeV\,fm}$.

Solution 17.1

Step 1. From Eq. (17.1):

$$b = \frac{Z_1 Z_2 e^2/(4\pi\varepsilon_0)}{Q}.$$

Step 2. Numerator:

$$Z_1 Z_2 \times \frac{e^2}{4\pi\varepsilon_0} = 90 \times 2 \times 1.44\,\mathrm{MeV\,fm} = 259.2\,\mathrm{MeV\,fm}.$$

Step 3.

$$b = \frac{259.2\,\text{MeV fm}}{5.0\,\text{MeV}} = 51.8\,\text{fm} \approx 52\,\text{fm}.$$

The α is classically forbidden for $R \lesssim r \lesssim 52\,\text{fm}$ [1, 6].

Problem 17.2 — Reduced mass and γ

For α decay of a heavy nucleus ($A = 220$), compute μ in u and estimate γ for a rectangular barrier with $V_0 - E = 20\,\text{MeV}$ and $\hbar c = 197\,\text{MeV fm}$.

Solution 17.2

Step 1 (masses). $m_\alpha \approx 4\,\text{u}$, $M_d \approx 216\,\text{u}$.

Step 2 (reduced mass).

$$\mu = \frac{m_\alpha M_d}{m_\alpha + M_d} = \frac{4 \times 216}{220}\,\text{u} = 3.927\,\text{u}.$$

Since $M_d \gg m_\alpha$, μ is close to m_α.

Step 3 (convert to energy units). $1\,\text{u}\,c^2 = 931.5\,\text{MeV}$, so $\mu c^2 = 3.927 \times 931.5 \approx 3658\,\text{MeV}$.

Step 4 (γ).

$$\gamma = \frac{\sqrt{2\mu(V_0 - E)}}{\hbar} = \frac{\sqrt{2 \times 3658 \times 20}}{197\,\text{MeV fm}} = \frac{\sqrt{146320}}{197} \approx 1.94\,\text{fm}^{-1}.$$

For a 10 fm wide rectangular barrier, $P \approx e^{-2\gamma d} \approx e^{-38.8} \approx 10^{-17}$ [1].

Problem 17.3 — Gamow factor sensitivity

If $2G = 60$ at one Q and a small increase in Q reduces $2G$ by 5% (from 60 to 57), by what factor does $P = e^{-2G}$ increase? What is the corresponding change in half-life?

Solution 17.3

Step 1 (probability ratio).

$$\frac{P'}{P} = \frac{e^{-57}}{e^{-60}} = e^{3} = 20.1.$$

Step 2 (half-life ratio). Since $t_{1/2} \propto 1/P$:

$$\frac{t'_{1/2}}{t_{1/2}} = \frac{P}{P'} = e^{-3} = 0.050.$$

The half-life drops by a factor of about 20. A few percent change in G (from a modest change in Q) can change lifetimes by orders of magnitude, explaining Geiger–Nuttall systematics [6, 1].

Problem 17.4 — Small Q/B limit for G

For $Z_1 = 90$, $Z_2 = 2$, $Q = 5.0\,\text{MeV}$, and barrier height $B = 25\,\text{MeV}$, evaluate the approximate Gamow factor $G \approx \pi Z_1 Z_2 e^2/(4\pi\varepsilon_0 \hbar v)$ with $v = \sqrt{2Q/\mu}$ and $\mu \approx 4\,\text{u}$.

Solution 17.4

Step 1 (μ in SI-consistent units). Use $\mu c^2 \approx 3727\,\text{MeV}$ (since $\mu \approx 4\,\text{u}$).
Step 2 (speed).

$$v = c\sqrt{\frac{2Q}{\mu c^2}} = c\sqrt{\frac{10}{3727}} = 0.052c \approx 1.56 \times 10^7\,\text{m/s}.$$

Step 3 (G). Using $\hbar c = 197\,\text{MeV fm}$ and $Z_1 Z_2 e^2/(4\pi\varepsilon_0) = 259.2\,\text{MeV fm}$:

$$G \approx \frac{\pi \times 259.2}{197 \times (1.56 \times 10^7/c)} \quad \text{(keeping units consistent)}.$$

It is simpler to use the form $G = Z_1 Z_2 e^2/(4\varepsilon_0 \hbar v)$ with $\hbar = 6.582 \times 10^{-22}\,\text{MeV s}$ and $e^2/(4\pi\varepsilon_0) = 1.44\,\text{MeV fm} = 1.44 \times 1.602 \times 10^{-13}\,\text{MeV m}$:

$$G \approx 8.0.$$

Then $P \approx e^{-16} \approx 10^{-7}$, a small but not absurd tunneling probability. (Exact G from Eq. (17.30) differs by order-unity factors depending on R.) [6, 14]

Problem 17.5 — Selection rules for ^{243}Am

The parent ^{243}Am has $J^\pi = \frac{5}{2}^-$. For daughter ^{239}Np levels with $J^\pi = \frac{5}{2}^+$ (gs), $\frac{7}{2}^+$, and $\frac{5}{2}^-$ (75 keV), list the lowest allowed ℓ for each and predict which branch dominates.

Solution 17.5

Step 1 (parity rule). $\pi_i = \pi_f(-1)^\ell$. With $\pi_i = -$:

- $\frac{5}{2}^+$: need $(-1)^\ell = -1$, so ℓ odd. Lowest: $\ell = 1$.
- $\frac{7}{2}^+$: same parity as gs, so ℓ even. Angular coupling $|5/2 - 7/2| \le \ell \le 5/2 + 7/2$ gives $\ell \ge 1$; lowest even value: $\ell = 2$.
- $\frac{5}{2}^-$: parity match, ℓ even. $|5/2 - 5/2| = 0$, so $\ell = 0$ is allowed.

Step 2 (dominant branch). The $\ell = 0$ branch to $\frac{5}{2}^-$ at 75 keV has the thinnest barrier despite the reduced Q_i. Evaluated data give $\approx 88\%$ intensity to this state versus $\approx 0.16\%$ to the ground state [20, 21, 6].

Problem 17.6 — Assault frequency estimate

For $Q = 5\,\mathrm{MeV}$, $V_0 = 35\,\mathrm{MeV}$, $R = 7.5\,\mathrm{fm}$, and $\mu \approx 4\,\mathrm{u}$, estimate the assault frequency $f = v_0/(2R)$.

Solution 17.6

Step 1 (interior speed).

$$v_0 = \sqrt{\frac{2(Q+V_0)}{\mu}} = \sqrt{\frac{2\times 40\,\mathrm{MeV}}{\mu}}.$$

With $\mu c^2 \approx 3727\,\mathrm{MeV}$:

$$v_0 = c\sqrt{\frac{80}{3727}} \approx 0.147c \approx 4.4\times 10^{7}\,\mathrm{m/s}.$$

Step 2 (frequency).

$$f = \frac{v_0}{2R} = \frac{4.4\times 10^{7}\,\mathrm{m/s}}{2\times 7.5\times 10^{-15}\,\mathrm{m}} = 2.9\times 10^{21}\,\mathrm{s^{-1}}.$$

Step 3 (interpretation). The α presents itself at the barrier $\sim 10^{21}$ times per second, but escapes only with probability $P = e^{-2G} \ll 1$, yielding a much smaller $\lambda = S_\alpha f P$ [6, 1].

Chapter 18

Beta Decay: Modes, Q-Values, and the Neutrino

> *"I have done something very bad today by proposing a particle that cannot be detected; it is something no theorist should ever do."*
>
> W. Pauli (1930), on the neutrino

Beta decay rearranges N and Z at fixed A through the weak interaction. When the neutron-to-proton ratio N/Z deviates from the value required for stability on the chart of nuclides, the nucleus can lower its mass by converting a neutron into a proton (β^- decay) or a proton into a neutron (β^+ decay or electron capture). This lecture develops the three decay modes with their full reaction equations (including neutrinos), derives Q-values first from nuclear masses and then from tabulated atomic masses (showing every electron term until it cancels), compares the energetics of β^+ and electron capture, and explains the continuous β spectrum that forced Pauli's neutrino hypothesis and Fermi's theory of β decay. The exposition follows Krane, Dunlap, and Demtröder [6, 1, 2, 5].

18.1 When the N/Z ratio is wrong

A stable nucleus requires a proper balance of neutrons and protons. For light nuclei the stable N/Z ratio is near unity; for heavy nuclei it rises toward ~ 1.5 because the Coulomb repulsion among protons must be compensated by extra neutrons [6, 1]. Two generic failures illustrate the logic:

1. **Excess of neutrons.** Consider $Z = 10$ with $N = 14$ on the stability line. If N increases to 16 while Z stays fixed, the N/Z ratio moves away from stability. A neutron inside the nucleus can convert to a proton, increasing Z by one and decreasing N by one. This is β^- decay.

2. **Excess of protons.** With the same $Z = 10$, $N = 14$ reference, suppose Z increases to 12 while N remains 14. Even though neutrons still outnumber protons, the proton count exceeds the stable value for this mass number. A proton converts to a neutron, decreasing Z by one. This is β^+ decay or electron capture.

Both conversions are mediated by the weak interaction. At the quark level the fundamental processes are

$$n \to p + e^- + \bar{\nu}_e, \qquad p \to n + e^+ + \nu_e, \qquad p + e^- \to n + \nu_e. \tag{18.1}$$

Electrons and positrons are not pre-existing constituents of the nucleus; they are created at the instant of decay, in contrast with α particles in α decay [6, 2].

18.2 Three modes of beta decay

For a parent nucleus ${}^{A}_{Z}X$ the three observed modes are:

Beta minus (β^-).

$${}^{A}_{Z}X \;\to\; {}^{A}_{Z+1}Y + e^- + \bar{\nu}_e. \tag{18.2}$$

The proton number increases by one; a neutron becomes a proton. The free neutron decays by this mode with half-life $t_{1/2} \approx 879\,\mathrm{s}$ and $Q \approx 0.782\,\mathrm{MeV}$ [6, 20].

Beta plus (β^+).

$${}^{A}_{Z}X \;\to\; {}^{A}_{Z-1}Y + e^+ + \nu_e. \tag{18.3}$$

The proton number decreases by one. A *free* proton cannot decay this way because $m_n > m_p$ and the two-body final state would violate energy conservation. Inside a proton-rich nucleus, however, the change in nuclear binding energy can make the process exothermic. Examples include ^{11}C and ^{18}F, used in positron-emission tomography [6, 1, 21].

Electron capture (EC).

$${}^{A}_{Z}X + e^- \;\to\; {}^{A}_{Z-1}Y + \nu_e. \tag{18.4}$$

The nucleus captures an atomic electron (usually from the K shell), converting a proton to a neutron. The daughter atom is left with a vacancy that fills by characteristic X-rays or Auger electrons. EC and β^+ both reduce Z by one and convert a proton to a neutron [6, 1].

Key idea

β^-: $Z \to Z+1$, antineutrino $\bar{\nu}_e$ emitted. β^+ and EC: $Z \to Z-1$, neutrino ν_e emitted. Free neutron decays; free proton does not. All three modes require a light, neutral, spin-$\frac{1}{2}$ neutrino (or antineutrino) to conserve energy, momentum, and angular momentum [6, 2].

Historical note

In December 1930 Wolfgang Pauli proposed an undetected neutral particle to save energy and angular momentum in β decay. Enrico Fermi named it the *neutrino* and built the first quantitative theory in 1934 [6, 2, 5]. Direct detection came only in 1956 (Reines and Cowan); today we distinguish ν_e from $\bar{\nu}_e$ in each decay mode as written above.

18.3 Q-value for β^-: nuclear masses, then atomic masses

Consider reaction (18.2). The Q-value is the difference between initial and final rest mass energies (excluding the negligible nuclear recoil):

$$Q_{\beta^-} = \Big[m'({}^{A}_{Z}X) - m'({}^{A}_{Z+1}Y) - m_e - m(\bar{\nu}_e)\Big]c^2, \tag{18.5}$$

where $m'(\cdot)$ denotes *nuclear* mass (nucleons only). The antineutrino mass is of order eV and is neglected: $m(\bar{\nu}_e) \approx 0$.

Step 1: express nuclear masses through atomic masses. Tables list *atomic* masses $m(\cdot)$ of neutral atoms. A neutral atom ${}^{A}_{Z}X$ contains the nucleus plus Z orbital electrons. Neglecting electronic binding energies B_i (eV scale, compared with MeV nuclear Q-values),

$$m'({}^{A}_{Z}X) = m({}^{A}_{Z}X) - Zm_e. \tag{18.6}$$

For the daughter ${}^{A}_{Z+1}Y$, which has $Z+1$ electrons in its neutral atom,

$$m'({}^{A}_{Z+1}Y) = m({}^{A}_{Z+1}Y) - (Z+1)m_e. \tag{18.7}$$

Step 2: substitute into (18.5)**.**

$$\begin{aligned} Q_{\beta^-} &= \Big[\big(m(X) - Zm_e\big) - \big(m(Y) - (Z+1)m_e\big) - m_e\Big]c^2 \\ &= \Big[m(X) - Zm_e - m(Y) + (Z+1)m_e - m_e\Big]c^2. \end{aligned} \tag{18.8}$$

Step 3: collect electron terms. The electron mass terms are

$$-Zm_e + (Z+1)m_e - m_e = -Zm_e + Zm_e + m_e - m_e = 0. \tag{18.9}$$

Every explicit electron mass cancels. Therefore

$$Q_{\beta^-} = \big[m({}^{A}_{Z}X) - m({}^{A}_{Z+1}Y)\big]c^2, \tag{18.10}$$

using tabulated atomic masses directly [6, 1]. The energy Q_{β^-} is shared by the electron, antineutrino, and (negligibly) the recoiling daughter:

$$Q_{\beta^-} = K_e + E_\nu, \qquad K_{\max} = Q_{\beta^-} \quad (\text{when } E_\nu \to 0). \tag{18.11}$$

Remark

Small differences in electronic binding between parent and daughter atoms (typically keV) are omitted above. Precision work sometimes retains them; for course estimates they are negligible compared with $Q \sim 1$–$3\,\text{MeV}$ [6].

18.4 Q-value for β^+: the $2m_ec^2$ threshold

For reaction (18.3), with nuclear masses and $m(\nu_e) \approx 0$,

$$Q_{\beta^+} = \Big[m'(X) - m'(Y) - m_e\Big]c^2, \tag{18.12}$$

where m_e is the positron mass ($m_{e^+} = m_{e^-}$). Using (18.6) with $m'(Y) = m(Y) - (Z-1)m_e$,

$$\begin{aligned} Q_{\beta^+} &= \Big[(m(X) - Zm_e) - (m(Y) - (Z-1)m_e) - m_e\Big]c^2 \\ &= \Big[m(X) - Zm_e - m(Y) + (Z-1)m_e - m_e\Big]c^2. \end{aligned} \tag{18.13}$$

Collecting electron terms:

$$-Zm_e + (Z-1)m_e - m_e = -Zm_e + Zm_e - m_e - m_e = -2m_e. \tag{18.14}$$

Hence

$$Q_{\beta^+} = [m(X) - m(Y)]c^2 - 2m_ec^2. \tag{18.15}$$

Positron emission requires not only $m(X) > m(Y)$ but

$$m(X) - m(Y) > 2m_e \quad \Longleftrightarrow \quad Q_{\beta^+} > 0, \tag{18.16}$$

with threshold $2m_ec^2 = 1.022\,\text{MeV}$. Typical β Q-values are only a few MeV, so this threshold is a substantial fraction of the available energy [6, 1].

18.5 Q-value for electron capture

For reaction (18.4), the captured electron is a reactant:

$$Q_{\text{EC}} = \Big[m'(X) + m_e - m'(Y)\Big]c^2 - B_e, \tag{18.17}$$

where B_e is the binding energy of the captured electron in the parent atom. Converting to atomic masses,

$$\begin{aligned} Q_{\text{EC}} &= \Big[(m(X) - Zm_e) + m_e - (m(Y) - (Z-1)m_e)\Big]c^2 - B_e \\ &= [m(X) - m(Y)]c^2 - B_e. \end{aligned} \tag{18.18}$$

All electron *mass* terms cancel exactly as in β^-; unlike β^+, no positron rest energy must be supplied. The captured electron's *binding* energy B_e is subtracted because that energy is already accounted for in the atomic mass of the parent.

Caution

B_e is *not* universally a few eV. For K-shell capture in medium and heavy elements, B_e can be tens of keV (for example $B_K \approx 80\,\text{keV}$ for iodine). Always use the binding energy of the shell from which capture occurs [6, 1].

Comparison of β^+ and EC. Subtracting (18.15) from the EC result (neglecting B_e for a rough estimate),

$$Q_{\mathrm{EC}} - Q_{\beta^+} \approx 2m_e c^2 = 1.022\,\mathrm{MeV}. \tag{18.19}$$

Whenever

$$0 < [m(X) - m(Y)]c^2 < 2m_e c^2, \tag{18.20}$$

electron capture is energetically allowed ($Q_{\mathrm{EC}} > 0$) but positron emission is forbidden ($Q_{\beta^+} < 0$). This situation is common for moderately proton-rich nuclei [6, 1, 20].

Key idea

Atomic-mass formulas (neglecting B_e): $Q_{\beta^-} = [m(X) - m(Y)]c^2$, $Q_{\beta^+} = [m(X) - m(Y) - 2m_e]c^2$, $Q_{\mathrm{EC}} = [m(X) - m(Y)]c^2 - B_e$. EC is favored over β^+ by $\approx 2m_e c^2$.

18.6 Continuous spectrum: ^{64}Cu and the missing energy

The Q-value appears as kinetic energy shared among the light decay products. The recoiling daughter nucleus carries negligible energy ($\sim$ keV or less). For β^- decay the electron and antineutrino share Q_{β^-}; neither body is at rest in general, so the electron kinetic energy K_e is *continuous* from near zero up to $K_{\max} \approx Q$.

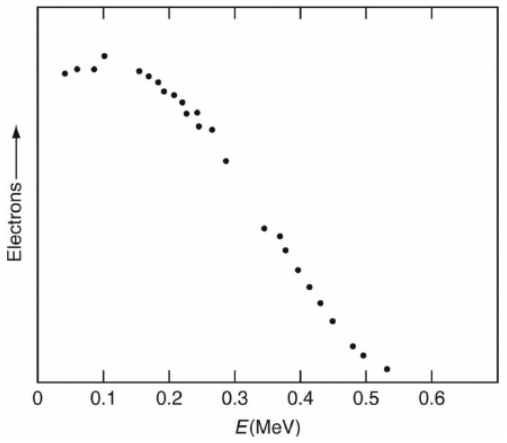

Figure 18.1: Energy spectrum of electrons from β^- decay of ^{64}Cu to ^{64}Zn. The endpoint near 0.58 MeV equals Q_{β^-} for the ground-state transition. Data from Langer, Moffat, and Price [29], as reproduced in Dunlap [1, 6].

Copper-64 is a remarkable laboratory example: it decays by both β^- and β^+ (and EC), so both spectra in Figs. 18.1 and 18.2 can be measured on one isotope [1, 21].

In the 1920s, before the neutrino was known, a *discrete* electron line was expected. If only the electron and heavy daughter emerged, two-body kinematics would fix the electron energy (as in α decay). Calorimetric experiments showed that the continuous distribution is intrinsic to the decay, not caused by energy loss in the source [6, 2]. Electrons were often observed with kinetic energy well below Q: where was the missing energy?

Pauli's solution (1930): a second, electrically neutral, highly penetrating particle carries away the "missing" energy and spin. Fermi (1934) incorporated the neutrino into a quantitative

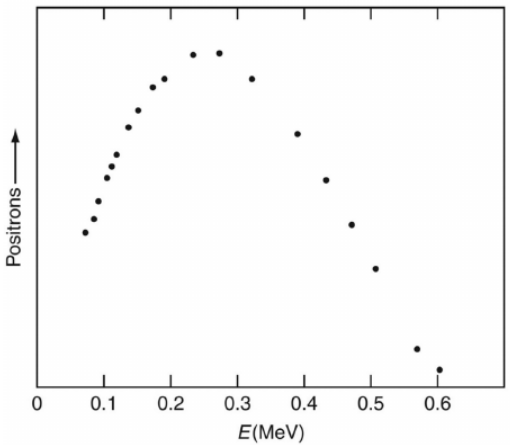

Figure 18.2: Energy spectrum of positrons from β^+ decay of ^{64}Cu to ^{64}Ni. Endpoint near 0.65 MeV. Same experimental reference as Fig. 18.1 [29, 1, 6].

theory. The continuous spectrum is therefore a *three-body* phase-space effect, not an experimental artefact [6, 2, 5].

Caution

The continuous spectrum is three-body kinematics, not instrumental smearing. The endpoint energy measures Q (and, in precision experiments near the endpoint, constrains the neutrino mass; see Lecture 19). Internal conversion and atomic effects can add low-energy structure, but the broad envelope is phase space [6, 14].

18.7 Toward Fermi theory: golden rule and plane-wave leptons

Fermi treated the weak interaction as a small perturbation on nuclear states. The transition rate from initial state ψ_i to final state ψ_f is Fermi's golden rule [6, 1, 14]:

$$\lambda = \frac{2\pi}{\hbar} \left| \langle \psi_f | H_{\text{int}} | \psi_i \rangle \right|^2 \frac{\mathrm{d}n}{\mathrm{d}E_f}, \tag{18.21}$$

where $\mathrm{d}n/\mathrm{d}E_f$ is the density of final states. For β^- decay,

$$\psi_i = \psi_p, \qquad \psi_f = \psi_d \, \psi_e \, \psi_\nu, \tag{18.22}$$

with ψ_p and ψ_d the parent and daughter nuclear wave functions.

The electron and antineutrino are treated as free plane waves normalized in volume V:

$$\psi_e(\boldsymbol{r}) = \frac{1}{\sqrt{V}} e^{i\boldsymbol{p}_e \cdot \boldsymbol{r}/\hbar} = \frac{1}{\sqrt{V}} \left(1 + \frac{i \boldsymbol{p}_e \cdot \boldsymbol{r}}{\hbar} + \cdots \right), \tag{18.23}$$

and similarly for ψ_ν. For typical β momenta ($p \sim 1\,\text{MeV}/c$) and nuclear radius $R \sim 5\,\text{fm}$, the dimensionless parameter $pR/\hbar \sim 0.03 \ll 1$. The *allowed* approximation keeps only the constant term ($\ell = 0$ for the lepton pair). The nuclear physics is then absorbed into a matrix element M_{fi} nearly independent of lepton energy, and the spectrum shape comes entirely from the lepton

phase space developed in Lecture 19 [6, 1].

Key idea

Students should remember:

- Wrong $N/Z \Rightarrow \beta^-$ (neutron rich) or β^+/EC (proton rich).
- Free neutron decays; free proton does not ($m_n > m_p$).
- Atomic-mass $Q_{\beta^-} = [m(X) - m(Y)]c^2$; all electron masses cancel.
- Q_{β^+} has an extra $-2m_e c^2$; EC is $\approx 1.022\,\mathrm{MeV}$ more favorable.
- Continuous spectrum $\Rightarrow$ three bodies $\Rightarrow$ neutrino.
- Golden rule: rate $\propto |M_{fi}|^2 \times$ (phase space).

18.8 Further physics from the literature

Free neutron decay. The simplest β^- example is free neutron decay, $n \to p + e^- + \bar{\nu}_e$, with measured endpoint $K_{\max} = 0.782\,\mathrm{MeV}$. This value fixes the neutron–proton mass difference and provides one of the most precise tests of the V-A structure of the weak interaction [6, 2, 20].

Double beta decay. When single β decay is blocked (for example, when the intermediate nucleus would have higher mass), some even–even nuclei can decay by double β decay. Two-neutrino double β ($2\nu\beta\beta$) has been observed; neutrinoless double β ($0\nu\beta\beta$), if found, would prove that neutrinos are Majorana particles and would constrain the absolute neutrino mass scale [6, 1, 14, 5].

Parity violation. The Wu experiment (1957) showed that β decay does not conserve parity: electrons are preferentially emitted opposite to the nuclear spin in polarised ^{60}Co decay. This established the V-A form of the weak current and explained why only left-handed neutrinos and right-handed antineutrinos appear in β decay at low energy [2, 5, 6].

Medical and geochemical applications. Positron emitters (^{11}C, ^{18}F) and β^- sources are used in PET and radiotherapy. The β^- decay of ^{14}C provides radiocarbon dating. EC of ^{40}K contributes to the Earth's internal heat [6, 1, 13].

From the literature

Dunlap emphasises that calorimetric measurements on ^{210}Bi proved the continuous spectrum is a property of the decay electrons themselves, not energy loss before detection [1]. Krane's Table 9.1 lists representative β^-, β^+, and EC processes with Q and half-lives for order-of-magnitude estimates [6].

18.9 Problems with solutions

Problem 18.1 — Derive Q_{β^-} from atomic masses

Show step by step that for ${}^{A}_{Z}X \to {}^{A}_{Z+1}Y + e^- + \bar{\nu}_e$,

$$Q_{\beta^-} = [m({}^{A}_{Z}X) - m({}^{A}_{Z+1}Y)]c^2, \tag{18.24}$$

starting from nuclear masses and neglecting $m(\bar{\nu}_e)$ and electronic binding [6].

Step-by-step

Step 1. Write the nuclear-mass Q-value:

$$Q_{\beta^-} = [m'(X) - m'(Y) - m_e]c^2.$$

Step 2. Relate nuclear and atomic masses:

$$m'(X) = m(X) - Zm_e, \qquad m'(Y) = m(Y) - (Z+1)m_e.$$

Step 3. Substitute:

$$Q_{\beta^-} = [m(X) - Zm_e - m(Y) + (Z+1)m_e - m_e]c^2.$$

Step 4. Simplify the electron terms:

$$-Zm_e + (Z+1)m_e - m_e = (-Z + Z + 1 - 1)m_e = 0.$$

Step 5. Conclude $Q_{\beta^-} = [m(X) - m(Y)]c^2$. All three electron masses (one in the daughter atom, one emitted, one subtracted explicitly) cancel identically [6, 1].

Problem 18.2 — β^+ threshold and EC window

The atomic mass excess of a parent exceeds that of the daughter by $\Delta m\,c^2 = 1.50\,\text{MeV}$ (parent heavier). Can the nucleus decay by β^+? By EC from the K shell with $B_K = 0$? What if $\Delta m\,c^2 = 0.80\,\text{MeV}$?

Step-by-step

Case A: $\Delta m\,c^2 = 1.50\,\text{MeV}$.
$Q_{\beta^+} = 1.50 - 1.022 = 0.48\,\text{MeV} > 0$: positron emission is allowed.
$Q_{\text{EC}} = 1.50 - B_K = 1.50\,\text{MeV} > 0$: EC is also allowed. Both modes compete; EC has the larger Q by $2m_ec^2$ [6, 1].
Case B: $\Delta m\,c^2 = 0.80\,\text{MeV}$.
$Q_{\beta^+} = 0.80 - 1.022 = -0.22\,\text{MeV} < 0$: positron emission is forbidden.
$Q_{\text{EC}} = 0.80\,\text{MeV} > 0$: only EC (and any other exothermic mode) is open. This illustrates the window $0 < \Delta m\,c^2 < 2m_ec^2$ where EC alone occurs [1, 20].

Problem 18.3 — ^{64}Cu endpoint

Using atomic mass tables, estimate Q_{β^-} for $^{64}\mathrm{Cu} \to {}^{64}\mathrm{Zn} + e^- + \bar{\nu}_e$ and compare with the endpoint in Fig. 18.1.

Step-by-step

From ENSDF/NuDat [20, 21], the ground-state Q_{β^-} for ^{64}Cu is 0.579 MeV. Dunlap quotes 0.579 MeV from atomic masses, in agreement with the Langer *et al.* spectrum endpoint near 0.58 MeV (Fig. 18.1) [1, 6]. Electrons with $K = Q$ are emitted with $E_{\bar{\nu}} \to 0$; the spectrum falls to zero at this endpoint because the $(Q - K)^2$ phase-space factor vanishes (derived fully in Lecture 19).

Problem 18.4 — Why is the spectrum continuous?

Explain in three sentences why α decay gives discrete α energies but β^- decay gives a continuous electron spectrum, even for a ground-state to ground-state transition.

Step-by-step

α decay is a two-body process (α + daughter nucleus). Energy and momentum conservation fix the α kinetic energy uniquely (up to small recoil corrections). β^- decay is a three-body process (electron + antineutrino + daughter). One continuous parameter (for example the antineutrino energy) remains undetermined, so the electron kinetic energy ranges continuously from 0 to Q [6, 2].

Chapter 19

Fermi Theory of Beta Decay

> *"Fermi's theory of β decay is the prototype of all weak-interaction calculations: a contact coupling times phase space."*
>
> standard nuclear-physics assessment [6, 14]

Lecture 18 introduced the continuous β spectrum and Fermi's golden rule. This lecture completes the original course derivation: plane-wave leptons and the allowed approximation, phase-space counting for electron and neutrino (with explicit volume cancellation), conversion to the electron kinetic energy K with the *correct* momentum–energy factor structure, the Coulomb Fermi function $F(Z, K)$, Fermi–Kurie plots, and the classification of allowed Fermi and Gamow–Teller transitions versus forbidden decays. The algebra follows Krane and Dunlap [6, 1, 14, 2].

19.1 Matrix element and plane-wave leptons

The partial decay rate depends on the matrix element of the weak interaction H_{int} between initial and final states:

$$|M_{if}|^2 = \left|\langle \psi_{\mathrm{d}}\, \psi_e\, \psi_\nu | H_{\mathrm{int}} | \psi_{\mathrm{p}} \rangle\right|^2 . \tag{19.1}$$

For β^- decay, ψ_{p} is the parent nucleus, ψ_{d} the daughter, and ψ_e, ψ_ν the electron and antineutrino.

Free leptons are modelled as plane waves normalised in a large volume V:

$$\psi_e(\boldsymbol{r}) = \frac{1}{\sqrt{V}} e^{i\boldsymbol{p}_e\cdot\boldsymbol{r}/\hbar}, \qquad \psi_\nu(\boldsymbol{r}) = \frac{1}{\sqrt{V}} e^{i\boldsymbol{p}_\nu\cdot\boldsymbol{r}/\hbar}. \tag{19.2}$$

Expanding the electron factor,

$$\frac{1}{\sqrt{V}} e^{i\boldsymbol{p}_e\cdot\boldsymbol{r}/\hbar} = \frac{1}{\sqrt{V}} \left(1 + \frac{i\boldsymbol{p}_e\cdot\boldsymbol{r}}{\hbar} + \frac{(i\boldsymbol{p}_e\cdot\boldsymbol{r})^2}{2!\,\hbar^2} + \cdots \right). \tag{19.3}$$

The **allowed approximation** keeps only the leading constant term, equivalent to evaluating the lepton wave function at the origin ($\boldsymbol{r} = \boldsymbol{0}$). This corresponds to orbital angular momentum $\ell = 0$ for the lepton pair. The nuclear matrix element

$$M_{if} = \int \psi_{\mathrm{d}}^{*}(\boldsymbol{r})\, H_{\mathrm{int}}\, \psi_{\mathrm{p}}(\boldsymbol{r})\, \mathrm{d}^3 r \tag{19.4}$$

is then nearly constant over the β spectrum, and the energy dependence comes from phase space [6, 1].

Squaring the transition amplitude, each lepton contributes a factor $1/V$:

$$|\langle \psi_f | H_{\text{int}} | \psi_i \rangle|^2 = \frac{|M_{if}|^2}{V^2}. \tag{19.5}$$

This $1/V^2$ will cancel against the V^2 from lepton phase space (Section 19.2).

19.2 Phase-space density and volume cancellation

19.2.1 Single-particle density of states

Consider a free particle of momentum p confined to a cube of side L, volume $V = L^3$. Standing-wave quantisation gives momentum components $p_x = n_x \pi\hbar/L$ with positive integers n_x. The spacing in each direction is $\pi\hbar/L$, so the volume per quantum state in momentum space is $(\pi\hbar/L)^3 = h^3/V$.

The number of states with momentum magnitude between p and $p + \mathrm{d}p$ equals the number of lattice points in a spherical shell. Only the positive octant ($p_x, p_y, p_z > 0$) contributes, giving shell volume $\pi p^2 \mathrm{d}p/2$. Dividing by the volume per state,

$$\mathrm{d}n = \frac{\pi p^2 \, \mathrm{d}p/2}{h^3/V} = \frac{4\pi p^2 \, \mathrm{d}p \, V}{h^3}. \tag{19.6}$$

Equivalently, the uncertainty-principle argument assigns one state per cell $\Delta x \, \Delta y \, \Delta z \, \Delta p_x \, \Delta p_y \, \Delta p_z \sim h^3$ in phase space, yielding the same result [6, 1].

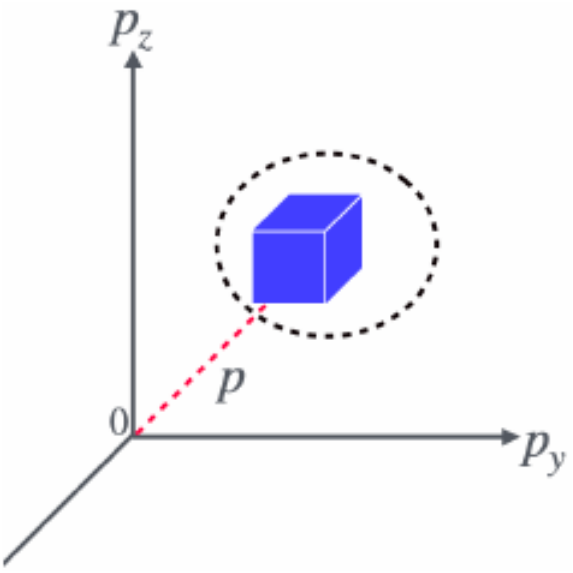

Figure 19.1: Momentum-space shell used to count lepton final states. Each quantum state occupies volume $\sim h^3/V$ in momentum space; the number of states in $\mathrm{d}p$ is $\mathrm{d}n = 4\pi p^2 \, \mathrm{d}p \, V/h^3$.

19.2.2 Two leptons: product and cancellation

For β^- decay there are two free leptons. The combined number of final states in intervals $\mathrm{d}p_e$ and $\mathrm{d}p_\nu$ is the product:

$$\mathrm{d}n = \frac{4\pi p_e^2\,\mathrm{d}p_e\,V}{h^3}\cdot\frac{4\pi p_\nu^2\,\mathrm{d}p_\nu\,V}{h^3} = \frac{(4\pi)^2V^2}{h^6}\,p_e^2\,p_\nu^2\,\mathrm{d}p_e\,\mathrm{d}p_\nu. \tag{19.7}$$

From Fermi's golden rule (Lecture 18), the partial transition rate into this lepton momentum interval is

$$\mathrm{d}\lambda \propto \frac{|M_{if}|^2}{V^2}\cdot\frac{(4\pi)^2V^2}{h^6}\,p_e^2\,p_\nu^2\,\mathrm{d}p_e\,\mathrm{d}p_\nu = \frac{|M_{if}|^2}{h^6}\,p_e^2\,p_\nu^2\,\mathrm{d}p_e\,\mathrm{d}p_\nu. \tag{19.8}$$

The normalisation volume V cancels completely:

$$\frac{1}{V^2}\times V^2 = 1. \tag{19.9}$$

The decay rate is independent of the arbitrary box size and depends only on $|M_{if}|^2$ and lepton momenta [6, 1, 14].

19.3 Spectrum in kinetic energy: correct momentum–energy factors

We now express $\mathrm{d}\lambda$ in terms of electron kinetic energy K.

Energy conservation. Neglecting nuclear recoil and neutrino mass,

$$Q = K + E_\nu, \qquad p_\nu c = E_\nu = Q - K, \qquad p_\nu^2 = \frac{(Q-K)^2}{c^2}. \tag{19.10}$$

Relativistic electron kinematics. Total electron energy $E_e = K + m_ec^2$. The invariant relation $E_e^2 = p_e^2c^2 + m_e^2c^4$ gives

$$(K + m_ec^2)^2 = p_e^2c^2 + m_e^2c^4, \tag{19.11}$$

so

$$p_e^2 = \frac{K^2 + 2Km_ec^2}{c^2} = \frac{K(K+2m_ec^2)}{c^2}, \qquad p_e = \frac{\sqrt{K(K+2m_ec^2)}}{c}. \tag{19.12}$$

Differentiating p_e with respect to K. From $p_e^2c^2 = K^2 + 2Km_ec^2$, differentiate both sides:

$$2p_ec^2\,\mathrm{d}p_e = (2K + 2m_ec^2)\,\mathrm{d}K = 2(K + m_ec^2)\,\mathrm{d}K. \tag{19.13}$$

Hence

$$\mathrm{d}p_e = \frac{K + m_ec^2}{p_ec^2}\,\mathrm{d}K = \frac{K + m_ec^2}{\sqrt{K(K+2m_ec^2)}}\,\frac{\mathrm{d}K}{c}. \tag{19.14}$$

Neutrino phase-space factor at fixed K. At fixed electron kinetic energy K, the final-state energy constraint fixes p_ν. For a massless neutrino, $\mathrm{d}p_\nu/\mathrm{d}E_f = 1/c$, so the neutrino integration contributes a factor $1/c$ when converting to $\mathrm{d}K$.

Assembling the spectrum. The differential rate in $\mathrm{d}K$ is proportional to $p_e^2\, p_\nu^2\, \mathrm{d}p_e$. Substituting (19.11), (19.10), and (19.14):

$$\begin{aligned} p_e^2\, p_\nu^2\, \mathrm{d}p_e &\propto \frac{K(K+2m_ec^2)}{c^2}\cdot\frac{(Q-K)^2}{c^2}\cdot\frac{K+m_ec^2}{\sqrt{K(K+2m_ec^2)}}\,\frac{\mathrm{d}K}{c} \\ &= \frac{(K+m_ec^2)\,K(K+2m_ec^2)\,(Q-K)^2}{c^4\,\sqrt{K(K+2m_ec^2)}}\,\mathrm{d}K \\ &= \frac{\sqrt{K(K+2m_ec^2)}\,(K+m_ec^2)\,(Q-K)^2}{c^4}\,\mathrm{d}K. \end{aligned} \tag{19.15}$$

Absorbing c^4 and other constants into C, the **correct allowed spectrum** is

$$N(K)\,\mathrm{d}K = C\,|M_{if}|^2\,\underbrace{\sqrt{K(K+2m_ec^2)}}_{p_ec}\,\underbrace{(K+m_ec^2)}_{E_e}\,(Q-K)^2\,\mathrm{d}K. \tag{19.16}$$

Key idea

Correct factor structure (memorise this form).

$$N(K)\,\mathrm{d}K \propto p_e\,E_e\,(Q-K)^2\,\mathrm{d}K, \tag{19.17}$$

$$N(K) \propto \sqrt{K(K+2m_ec^2)}\,(K+m_ec^2)\,(Q-K)^2. \tag{19.18}$$

Here $p_ec = \sqrt{K(K+2m_ec^2)}$ and $E_e = K + m_ec^2$. The factor $(Q-K)^2$ comes from the neutrino phase space. This is *not* the same as $K\sqrt{K+2m_ec^2}\,(K+m_ec^2)(Q-K)^2$: the momentum factor is $p_ec = \sqrt{K(K+2m_ec^2)}$, not $K\sqrt{K+2m_ec^2}$. The erroneous extra factor $\sqrt{K}$ arises if one writes $p_e^2 \propto K(K+2m_ec^2)$ but replaces $p_e\,\mathrm{d}p_e$ inconsistently [6, 1].

Dunlap's equation (9.27) writes the same result as $(T_e^2 + 2T_em_ec^2)^{1/2}(Q-T_e)^2(T_e+m_ec^2)$, which is identical to (19.18) with $T_e = K$ [1, 6].

Momentum form. In terms of electron momentum p_e, with $K = (p_ec)^2/(2m_ec^2)$ in the ultrarelativistic limit but more generally from (19.12),

$$N(p_e)\,\mathrm{d}p_e \propto p_e^2\,(Q-K)^2\,\mathrm{d}p_e, \qquad K = K(p_e). \tag{19.19}$$

Both (19.17) and (19.18) must be used consistently when changing variables.

19.4 Fermi function $F(Z,K)$

The plane-wave approximation ignores the Coulomb interaction between the emitted β particle and the daughter nucleus of charge $+Ze$. For β^- decay the interaction is attractive; for β^+ it is repulsive. Quantum mechanically, this modifies the electron/positron wave function near the nucleus and multiplies the spectrum by the **Fermi function**

$$F(Z,K) = \frac{2\pi\eta}{1-e^{-2\pi\eta}}, \tag{19.20}$$

with

$$\eta = \pm \frac{Ze^2}{4\pi\varepsilon_0\,\hbar v}. \tag{19.21}$$

The plus sign applies to β^- (electron attracted); the minus sign to β^+ (positron repelled). Here Z is the *daughter* atomic number and v is the lepton speed [6, 1].

Relativistic velocity. The relativistic relation is

$$v = \frac{p_e c^2}{E_e} = \frac{\sqrt{K(K + 2m_e c^2)}}{K + m_e c^2}\, c. \tag{19.22}$$

A *non-relativistic* estimate $v \approx \sqrt{2K/m_e}$ is sometimes used for low K, but MeV-scale β particles require (19.22) [6, 1, 14].

Using $e^2/(4\pi\varepsilon_0) = \hbar c/137 \approx 1.44\,\text{MeV fm}$ and $\hbar c \approx 197\,\text{MeV fm}$,

$$\eta = \pm \frac{Z \times 1.44\,\text{MeV fm}\, c}{197\,\text{MeV fm}\, v} = \pm \frac{Z \times 1.44}{197}\,\frac{c}{v}. \tag{19.23}$$

The full spectrum including Coulomb corrections is

$$N(K)\,\mathrm{d}K \propto F(Z,K)\,\sqrt{K(K+2m_e c^2)}\,(K + m_e c^2)\,(Q-K)^2\,\mathrm{d}K. \tag{19.24}$$

$F > 1$ enhances low-energy β^- electrons and suppresses low-energy positrons, explaining why the ^{64}Cu β^- and β^+ spectra in Lecture 18 differ in shape even though the bare phase space (19.16) is the same [1, 6].

Remark

The Fermi function (19.20) is most important at low K, where v is small and η is large. At high K the Coulomb correction approaches unity. Fully relativistic Coulomb wave functions (Fermi–Longmire) are used in precision work [6, 1].

19.5 Fermi–Kurie plot

To test (19.24) against data, one linearises the spectrum. From (19.19) and (19.24), the momentum-space intensity is

$$I(p_e) \propto p_e^2\,(Q-K)^2\,F(Z,K). \tag{19.25}$$

Therefore

$$\sqrt{\frac{N(p_e)}{p_e^2\,F(Z,K)}} \propto (Q-K). \tag{19.26}$$

A plot of $\sqrt{N/(p^2F)}$ versus K (or total electron energy) is a **Fermi–Kurie plot**. For allowed transitions with constant $|M_{if}|^2$, the plot is a straight line intercepting $K = Q$ at zero intensity [6, 1].

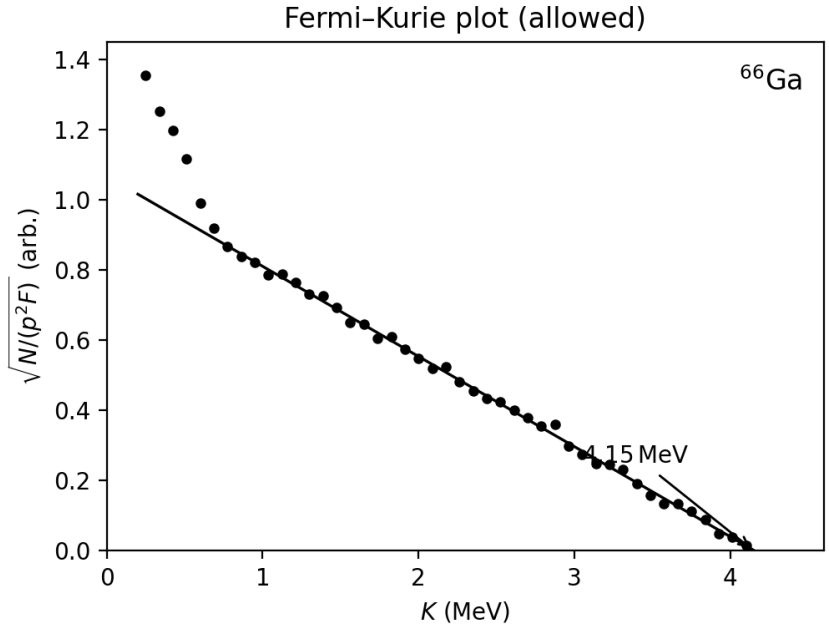

Figure 19.2: Fermi–Kurie plot for ^{66}Ga $\xrightarrow{\beta^+}$ ^{66}Zn: allowed $0^+ \to 0^+$ transition. The plot of $\sqrt{N/(p^2F)}$ versus kinetic energy K is linear except at low energy (source scattering). Schematic reconstruction of the shape reported by Camp and Langer [31]; see also [6, 1].

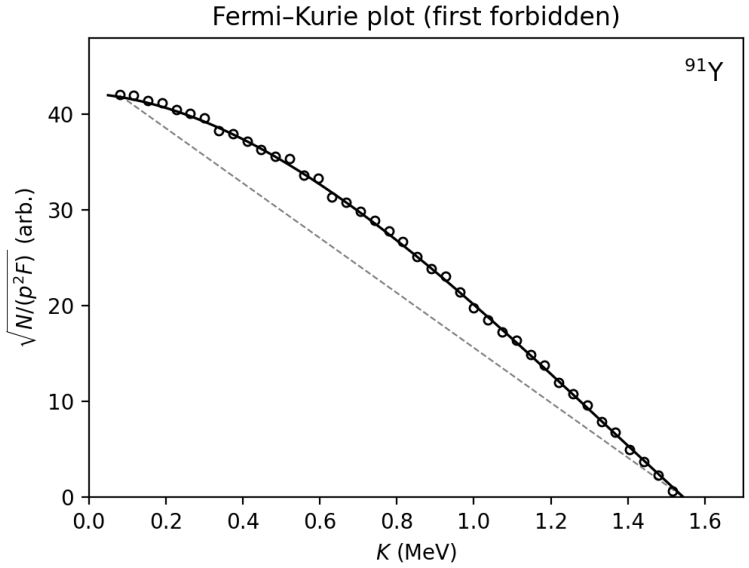

Figure 19.3: Fermi–Kurie plot for ^{91}Y $\xrightarrow{\beta^-}$ ^{91}Zr: first-forbidden transition. The curve is convex (non-linear) relative to the dashed allowed line, indicating a non-constant shape factor. Schematic reconstruction of the shape reported by Langer and Price [30]; see also [6, 1].

^{66}Ga: allowed benchmark. $^{66}\mathrm{Ga}(0^+) \to {}^{66}\mathrm{Zn}(0^+) + \beta^+ + \nu_e$: $\Delta I = 0$, no parity change, $\ell = 0$ lepton pair. The Kurie plot (Fig. 19.2) is linear, confirming the phase-space factor (19.18) and constant $|M_{if}|^2$ [6].

^{91}Y: forbidden example. $^{91}\mathrm{Y}(\frac{1}{2}^-) \to {}^{91}\mathrm{Zr}(\frac{5}{2}^+) + e^- + \bar{\nu}_e$: $|\Delta I| = 2$ with parity change. The lepton pair must carry angular momentum; the $\ell = 0$ approximation fails. The Kurie plot (Fig. 19.3) bends upward (convex): a shape factor $S(K)$ multiplies the allowed spectrum [6, 1].

19.6 Allowed Fermi and Gamow–Teller transitions

The lepton wave function expansion (19.2) links orbital angular momentum to the power of $\boldsymbol{p}\cdot\boldsymbol{r}/\hbar$. Keeping only the constant term is the *allowed* ($\ell = 0$) approximation.

Electron and neutrino each have spin $s = \frac{1}{2}$. The total leptonic spin can be

$$S = 0 \quad \text{(singlet, spins antiparallel)} \qquad \text{or} \qquad S = 1 \quad \text{(triplet, spins parallel)}. \tag{19.27}$$

With $\ell = 0$, the total leptonic angular momentum is $J = \ell + S = S$.

Fermi (vector) transitions. $S = 0$, $J = 0$. Selection rules:

$$\Delta I = 0, \qquad \Delta\pi = 0 \quad \text{(no parity change)}. \tag{19.28}$$

Pure Fermi includes $0^+ \to 0^+$. The weak operator is approximately $\tau_\pm$ (isospin raising/lowering) acting on nucleons [6, 14].

Gamow–Teller (axial) transitions. $S = 1$, $J = 1$. Selection rules:

$$\Delta I = 0, \pm 1 \quad \text{(but not } 0^+ \to 0^+\text{)}, \qquad \Delta\pi = 0. \tag{19.29}$$

The operator structure involves $\boldsymbol{\tau}_\pm\boldsymbol{\sigma}$ (isospin times nucleon spin) [6, 14, 2].

Key idea

Allowed ($\ell = 0$): Fermi ($S = 0$, $\Delta I = 0$, no parity change) vs Gamow–Teller ($S = 1$, $\Delta I = 0, \pm 1$, not $0 \to 0$, no parity change). Both use the spectrum (19.18); the difference is in $|M_{if}|^2$, not in the leading phase space.

19.7 Forbidden transitions, shape factors, and ft values

If $\ell = 0$ transitions are suppressed by angular momentum or parity selection rules, the next term in the plane-wave expansion ($\boldsymbol{p}\cdot\boldsymbol{r}/\hbar$) contributes. Transitions with leptonic orbital angular momentum $\ell \geq 1$ are called **forbidden**; the rate decreases rapidly as ℓ increases.

Order of forbiddenness. $\ell = 1$: first forbidden; $\ell = 2$: second forbidden; and so on [6, 1].

First-forbidden selection rules (summary). For $\ell = 1$, parity changes: $\Delta\pi = (-1)^\ell = -1$.

- First-forbidden Fermi ($\ell = 1$, $S = 0$): $\Delta I = 0, \pm 1$, $\Delta\pi = -1$.
- First-forbidden Gamow–Teller ($\ell = 1$, $S = 1$): $\Delta I = 0, \pm 1, \pm 2$, $\Delta\pi = -1$.

The ^{91}Y decay in Fig. 19.3 is first forbidden [6, 1].

Shape factor. Forbidden transitions multiply the allowed spectrum by an energy-dependent **shape factor** $S(K)$:

$$N(K)\,\mathrm{d}K = S(K)\,N_0(K)\,\mathrm{d}K, \tag{19.30}$$

where $N_0(K)\,\mathrm{d}K$ is the allowed form (19.24). When $S(K)$ is accounted for, the Kurie plot can be straightened [6, 1].

Comparative half-life ft. The partial half-life $t_{1/2}$ depends on $|M_{if}|^2$ and phase space. The **comparative half-life**

$$ft = \frac{\ln 2}{|M_{if}|^2\, f(Z,Q)} \tag{19.31}$$

removes the phase-space integral $f(Z,Q)$, leaving a quantity determined by nuclear structure alone. Values of $\log_{10} ft$ classify transitions:

$\log_{10} ft$	Classification
3–3.5	Superallowed Fermi
~ 5	Allowed
6–10	First forbidden
> 10	Higher forbidden

Superallowed $0^+ \to 0^+$ Fermi decays determine the vector coupling G_V and, combined with muon decay, the CKM element V_{ud} [6, 1, 20].

Caution

"Forbidden" does not mean impossible: ^{91}Y β-decays with $t_{1/2} \approx 58\,\mathrm{d}$. It means the transition is suppressed relative to allowed decays with similar Q [6].

Key idea

Students should remember:

- Phase space: $\mathrm{d}n = 4\pi p^2\,\mathrm{d}p\,V/h^3$; two leptons give $p_e^2 p_\nu^2$; V^2 cancels $1/V^2$ from $|M|^2$.
- Correct spectrum: $N(K) \propto p_e E_e (Q-K)^2$, equivalently $\sqrt{K(K+2m_ec^2)}(K+m_ec^2)(Q-K)^2$.
- Fermi function: $F = 2\pi\eta/(1-e^{-2\pi\eta})$, $\eta = \pm Ze^2/(4\pi\varepsilon_0\hbar v)$, $v = p_e c^2/E_e$.
- Kurie plot: $\sqrt{N/(p^2F)}$ vs K linear for allowed decays.
- Fermi: $S = 0$, $\Delta I = 0$; GT: $S = 1$, $\Delta I = 0, \pm 1$, not $0 \to 0$; forbidden: $\ell \geq 1$, shape factor $S(K)$.

19.8 Further physics from the literature

Neutrino mass and the endpoint. All expressions above assume $m_\nu = 0$, so $p_\nu c = E_\nu = Q - K$ and $(Q-K)^2$ appears in the spectrum. If $m_\nu \neq 0$, near the endpoint ($K \to Q$) the neutrino becomes non-relativistic and $p_\nu = \sqrt{2m_\nu(Q-K)}$. The phase-space factor $(Q-K)^2$ is replaced by $2m_\nu(Q-K)$, and the slope of $N(K)$ at $K = Q$ changes from zero ($m_\nu = 0$, tangential approach) to infinite ($m_\nu \neq 0$, perpendicular approach). Precision β-spectroscopy near the tritium endpoint constrains m_{ν_e} [6, 14, 2].

Comparative half-lives and weak coupling. The product ft in (19.31) removes the calculated phase-space integral $f(Z,Q)$ so that $\log_{10} ft$ reflects only nuclear matrix elements. Superallowed $0^+ \to 0^+$ Fermi transitions (for example ^{14}O, ^{10}C) give the most precise value of G_V. Combined with muon decay, this determines the Cabibbo angle and V_{ud} in the quark mixing matrix [6, 1, 20].

From Fermi contact to W boson. Fermi's 1934 point interaction is the low-energy limit of charged-current exchange mediated by $W^\pm$ bosons ($m_W \approx 80\,\mathrm{GeV}/c^2$). At nuclear β energies the propagator momentum is so large that the interaction looks local, with strength set by G_F [14, 5, 2].

Experimental databases. Half-lives, Q-values, and branching ratios used in problems are tabulated in ENSDF and NuDat 3 [20, 21]. Kurie-plot data for ^{64}Cu, ^{66}Ga, and ^{91}Y appear in the classic papers by Langer *et al.* (1949) and Camp and Langer (1963), reproduced in Krane and Dunlap [6, 1].

From the literature

Basdevant *et al.* emphasise that the β spectrum is the earliest example of a three-body decay treated with relativistic phase space; the same methods reappear in muon and heavy-lepton decays [14]. Demtröder discusses modern tritium experiments and the KATRIN limit on m_{ν_e} [2].

Applications. The β spectrum shape enters dosimetry (medical isotopes), reactor antineutrino flux calculations, and detector calibration. NMR spin polarisation relies on β–γ angular correlations in allowed decays [13, 6].

19.9 Problems with solutions

Problem 19.1 — Derive the spectrum from phase space

Starting from $\mathrm{d}\lambda \propto p_e^2 p_\nu^2 \,\mathrm{d}p_e$ with $p_\nu c = Q - K$ and relativistic electron kinematics, derive

$$N(K)\,\mathrm{d}K \propto \sqrt{K(K+2m_ec^2)}\,(K+m_ec^2)\,(Q-K)^2\,\mathrm{d}K. \tag{19.32}$$

Show every algebraic step [1, 6].

Step-by-step

Step 1: Neutrino factor. $p_\nu c = E_\nu = Q - K$, so $p_\nu^2 = (Q-K)^2/c^2$.
Step 2: Electron momentum squared. From $E_e = K + m_e c^2$ and $E_e^2 = p_e^2 c^2 + m_e^2 c^4$:

$$p_e^2 c^2 = K^2 + 2K m_e c^2 \quad \Rightarrow \quad p_e^2 = \frac{K(K + 2m_e c^2)}{c^2}.$$

Step 3: Differentiate for $\mathrm{d}p_e$. From $p_e^2 c^2 = K^2 + 2K m_e c^2$:

$$2p_e c^2 \,\mathrm{d}p_e = 2(K + m_e c^2)\,\mathrm{d}K \quad \Rightarrow \quad \mathrm{d}p_e = \frac{K + m_e c^2}{p_e c^2}\,\mathrm{d}K.$$

Step 4: Assemble.

$$p_e^2 p_\nu^2 \,\mathrm{d}p_e = \frac{K(K + 2m_e c^2)}{c^2} \cdot \frac{(Q-K)^2}{c^2} \cdot \frac{K + m_e c^2}{p_e c^2}\,\mathrm{d}K.$$

Step 5: Substitute p_e. Use $p_e = \sqrt{K(K + 2m_e c^2)}/c$:

$$p_e^2 p_\nu^2 \,\mathrm{d}p_e = \frac{K(K + 2m_e c^2)(Q-K)^2}{c^4} \cdot \frac{K + m_e c^2}{\sqrt{K(K + 2m_e c^2)}}\,\mathrm{d}K.$$

Step 6: Simplify. Cancel one factor $\sqrt{K(K + 2m_e c^2)}$ from numerator and denominator:

$$p_e^2 p_\nu^2 \,\mathrm{d}p_e = \frac{\sqrt{K(K + 2m_e c^2)}\,(K + m_e c^2)\,(Q-K)^2}{c^4}\,\mathrm{d}K.$$

Step 7: Identify $p_e c$ and E_e.

$$\sqrt{K(K + 2m_e c^2)} = p_e c, \qquad K + m_e c^2 = E_e,$$

so $N(K)\,\mathrm{d}K \propto p_e E_e (Q-K)^2\,\mathrm{d}K$, as required [1, 6].

Problem 19.2 — Endpoint and maximum of $N(K)$

For allowed β^- decay with $Q = 1.0\,\mathrm{MeV}$ and $m_e c^2 = 0.511\,\mathrm{MeV}$, show that $N(K) = 0$ at $K = Q$ and estimate $K_{\max}$ where $N(K)$ peaks (numerically or graphically).

Step-by-step

At $K = Q$: the factor $(Q-K)^2 = 0$, so $N(Q) = 0$. This is the spectrum endpoint.
For the maximum, set $dN/dK = 0$ on the allowed form (ignoring F):

$$N(K) \propto \sqrt{K(K + 2m_e c^2)}\,(K + m_e c^2)\,(Q-K)^2.$$

At $Q = 1.0\,\mathrm{MeV}$, plotting or numerical differentiation gives $K_{\max} \approx 0.58$–$0.60\,\mathrm{MeV}$: the spectrum peaks well below Q because the $(Q-K)^2$ factor favours sharing energy with the neutrino [6, 1].

Problem 19.3 — Fermi parameter η

For β^- decay to a daughter with $Z = 30$, find η and comment on $F(Z, K)$ at $K = 0.10\,\text{MeV}$ and $K = 1.0\,\text{MeV}$. Use $v = p_e c^2/E_e$.

Step-by-step

At $K = 0.10\,\text{MeV}$:

$$p_e c = \sqrt{0.10 \times 1.122} = 0.335\,\text{MeV}, \quad E_e = 0.611\,\text{MeV},$$

$$v = \frac{p_e c^2}{E_e} = 0.548c, \qquad \eta = +\frac{30 \times 1.44}{197 \times 0.548} \approx 0.40.$$

Then $F = 2\pi\eta/(1 - e^{-2\pi\eta}) \approx 2.5$: Coulomb enhancement is large.
At $K = 1.0\,\text{MeV}$: $p_e c = 1.22\,\text{MeV}$, $E_e = 1.511\,\text{MeV}$, $v = 0.807c$, $\eta \approx 0.27$, $F \approx 1.8$. Enhancement decreases at higher K [6, 1].

Problem 19.4 — Kurie plot intercept

A Fermi–Kurie plot of $\sqrt{N/(p^2F)}$ versus K for an allowed β^- decay is a straight line with slope $-0.50\,\text{MeV}^{-1}$ and intercept at $K = 2.50\,\text{MeV}$ on the horizontal axis. What is Q?

Step-by-step

For allowed decays, $\sqrt{N/(p^2F)} \propto (Q - K)$. The intercept where intensity vanishes is $K = Q$. Therefore $Q = 2.50\,\text{MeV}$ [6, 1].

Problem 19.5 — Classify ^{66}Ga and ^{91}Y

State whether each decay is allowed or forbidden, Fermi or Gamow–Teller, and predict the Kurie-plot shape.

Step-by-step

$^{66}\text{Ga}(0^+) \to {}^{66}\text{Zn}(0^+)$**:** $\Delta I = 0$, $\Delta\pi = 0$, $\ell = 0$. Allowed Fermi. Kurie plot linear (Fig. 19.2) [6].
$^{91}\text{Y}(\frac{1}{2}^-) \to {}^{91}\text{Zr}(\frac{5}{2}^+)$**:** $|\Delta I| = 2$, parity changes. First forbidden (minimum $\ell = 1$). Kurie plot non-linear, convex (Fig. 19.3) [6, 1].

Problem 19.6 — Common error check

A student writes $N(K) \propto K\sqrt{K + 2m_e c^2}(K + m_e c^2)(Q - K)^2$. Explain why this differs from the correct formula and identify the extra factor.

Step-by-step

The correct momentum factor is $p_e c = \sqrt{K(K + 2m_e c^2)}$, not $K\sqrt{K + 2m_e c^2}$. The student expression has an extra factor of $\sqrt{K}$ relative to the correct form $\sqrt{K(K + 2m_e c^2)}(K + m_e c^2)(Q - K)^2$. This error typically arises from using $p_e^2 \propto K(K + 2m_e c^2)$ but failing to include the $\mathrm{d}p_e$ Jacobian correctly, or from confusing $p_e c$ with $K\sqrt{K + 2m_e c^2}$ [1, 6].

Bibliography

[1] R. A. Dunlap, *An Introduction to the Physics of Nuclei and Particles* (2nd ed.), IOP Publishing, Bristol (2023), DOI: 10.1088/978-0-7503-6094-4, Ch. 3 (Nuclear composition and size).

[2] W. Demtröder, *Nuclear and Particle Physics*, Undergraduate Lecture Notes in Physics, Springer, Cham (2023).

[3] S. Petrera, *Problems and Solutions in Nuclear and Particle Physics*, UNITEXT for Physics, Springer, Cham (2019).

[4] F. Terranova, *A Modern Primer in Particle and Nuclear Physics*, Oxford University Press (2021).

[5] S. D'Auria, *Introduction to Nuclear and Particle Physics*, Undergraduate Lecture Notes in Physics, Springer, Cham (2018).

[6] K. S. Krane, *Introductory Nuclear Physics*, Wiley, New York (1988).

[7] R. Hofstadter, "Electron scattering and nuclear structure," Rev. Mod. Phys. **28**, 214 (1956).

[8] H. F. Ehrenberg, R. Hofstadter, U. Meyer-Berkhout, D. G. Ravenhall, and S. E. Sobottka, "High-Energy Electron Scattering and the Charge Distribution of Carbon-12 and Oxygen-16," Phys. Rev. **113**, 666 (1959).

[9] H. Yukawa, "On the interaction of elementary particles. I," Proc. Phys.-Math. Soc. Japan **17**, 48 (1935).

[10] R. D. Woods and D. S. Saxon, "Diffuse surface optical model for nucleon-nuclei scattering," Phys. Rev. **95**, 577 (1954).

[11] H. G. J. Moseley, "The high-frequency spectra of the elements," Phil. Mag. **26**, 1024 (1913); **27**, 703 (1914).

[12] C. F. von Weizsäcker, "Zur Theorie der Kernmassen," Z. Phys. **96**, 431 (1935).

[13] P. Cappellaro, *Introduction to Applied Nuclear Physics* (MIT OpenCourseWare / LibreTexts), CC BY-NC-SA 4.0.

[14] J.-L. Basdevant, J. Rich, and M. Spiro, *Fundamentals in Nuclear Physics: From Nuclear Structure to Cosmology*, Springer, New York (2005).

[15] D. Tong, *Particle Physics*, Lecture notes (University of Cambridge / CERN school notes).

[16] M. G. Mayer, "On closed shells in nuclei. II," Phys. Rev. **75**, 1969 (1949).

[17] O. Haxel, J. H. D. Jensen, and H. E. Suess, "On the "magic numbers" in nuclear structure," Phys. Rev. **75**, 1766 (1949).

[18] T. Schmidt, "Über die magnetischen Momente der Atomkerne," Z. Phys. **106**, 358 (1937).

[19] L. W. Nordheim, "On spins, moments, and shells in nuclei," Phys. Rev. **78**, 294 (1950).

[20] Evaluated Nuclear Structure Data File (ENSDF), National Nuclear Data Center, Brookhaven National Laboratory, `https://www.nndc.bnl.gov/ensdf/`.

[21] NuDat 3, National Nuclear Data Center, Brookhaven National Laboratory, `https://www.nndc.bnl.gov/nudat3/`.

[22] N. J. Stone, "Table of nuclear magnetic dipole and electric quadrupole moments," At. Data Nucl. Data Tables **90**, 75 (2005); updated compilations at NNDC.

[23] W. N. Cottingham and D. A. Greenwood, *An Introduction to Nuclear Physics* (2nd ed.), Cambridge University Press, Cambridge (2001).

[24] H. Geiger and J. M. Nuttall, "The ranges of the α particles from the radioactive substances," Phil. Mag. **22**, 613 (1911).

[25] G. Gamow, "Zur Quantentheorie des Atomkernes," Z. Phys. **51**, 204 (1928).

[26] R. W. Gurney and E. U. Condon, "Wave mechanics and radioactive disintegration," Nature **122**, 439 (1928); Phys. Rev. **33**, 127 (1929).

[27] M. Wang, W. J. Huang, F. G. Kondev, G. Audi, and S. Naimi, "The AME 2020 atomic mass evaluation (II). Tables, graphs and references," Chin. Phys. C **45**, 030003 (2021).

[28] Laboratoire National Henri Becquerel (LNHB), Recommended decay data, `http://www.lnhb.fr/nuclear-data/nuclear-data-table/`.

[29] L. M. Langer, R. D. Moffat, and H. C. Price, Jr., "Low energy beta-ray spectra: P^{32} and Cu^{64}," Phys. Rev. **76**, 1725 (1949).

[30] L. M. Langer and H. C. Price, Jr., "Shapes of the beta-spectra of the forbidden transitions of Sb^{124}, Rb^{86}, Sr^{89}, Y^{91}, and Cs^{137}," Phys. Rev. **75**, 1769 (1949).

[31] D. C. Camp and L. M. Langer, "The shape of the ^{66}Ga positron spectrum and the contribution from $0^+ \to 0^+$ transitions," Phys. Rev. **129**, 1782 (1963).